DOCTORAL THESIS

# Concepts for Hot Sheet Metal Forming of Titanium Alloys

Eva-Lis Odenberger

LULEÅ UNIVERSITY OF TECHNOLOGY

# Concepts for Hot Sheet Metal Forming of Titanium Alloys

**Eva-Lis Odenberger**

Division of Solid Mechanics
Department of Applied Physics and Mechanical Engineering
Luleå University of Technology
SE-971 87 Luleå, Sweden

**Doctoral Thesis**

Printed by Universitetstryckeriet, Luleå 2009

ISSN: 1402-1544
ISBN 978-91-7439-046-9

Luleå 2009

www.ltu.se

*To my family*

# Preface

This work has been carried out partly at the Division of Solid Mechanics, Department of Applied Physics and Mechanical Engineering at Luleå University of Technology and partly at Industrial Development Centre in Olofström AB, Sweden.

I am very grateful to my supervisor, Professor Mats Oldenburg for his initiation of this research project and for his support and guidance during this work. I would like to thank my former co-supervisor, Dr Bengt Wikman, for his advice, guidance and help. Thank you colleagues and friends at the division of Solid Mechanics and at Industrial Development Centre, for contributing to such pleasant research and development work.

My co-workers in the appended papers deserve very special thanks. Dr Mikael Jansson at Engineering Research AB for your invaluable dedication, guidance and contribution. Also, Dr Robert Pedersen at Volvo Aero Corporation and Luleå University of Technology, Mr Jörgen Hertzman at Industrial Development Centre and colleagues at the LFT in Erlangen Nuremberg, Germany, for contributing to the research work regarding titanium metallurgy and material testing.

I am especially grateful to research assistant Mr Jan Granström for his help during the performance of the sheet metal forming tests presented in Paper B. Also, to my co-workers at Industrial Development Centre for their help in the manufacturing and test procedure of the hot forming tools presented in paper C to F, Mr Peter Axelsson, Mr Jukka Rajalampi and Mr Per Thilderkvist, among others. Your help has been invaluable. I would also like to acknowledge co-workers at Volvo Aero Corporation, for their contribution to my work and for the fruitful discussions we have had.

Finally, I would like to express my deepest and dearest gratitude to my beloved family, my husband Torbjörn and my wonderful children Alva and Sixten, for always being there. Also to my mother, Maj-Lis. I wouldn't have made it without your support.

Luleå, December, 2009
Eva-Lis Odenberger

# Acknowledgements

The research founding by VINNOVA (Swedish Agency for Innovation Systems), grant P22122-1A and 2007-00288 are gratefully acknowledged.

# Abstract

To increase the competitiveness of the Swedish aero engine industry alternative manufacturing methods for load carrying aero engine structures are desired, in order to reduce product cost and enable weight reduction and thereby fuel consumption. Traditionally, these structures mainly consist of large-scaled single castings of e.g. titanium- and nickel based super alloys. By fabrication, the structures are instead built from sheet metal parts, small ingots and simple forgings which are welded together and heat treated. The alternative approach implies the need for time and cost efficient evaluations of candidate manufacturing techniques, early in the product development process. One challenge in producing complete structures within shape tolerance lies in accurate predictions of springback and compensation for shape deviation which occurs in the different processes of the manufacturing chain.

Finite Element (FE) simulations are used extensively in e.g. the sheet metal stamping industry where the technology has contributed to a better understanding of chosen sheet metal forming processes and where the prediction capabilities has significantly reduced the time consuming, inexact and costly die tryouts. However, the reliability of the numerical simulations depends not only on the models and methods used but also on the accuracy and applicability of the input data. The material model and related property data must be consistent with the conditions of the material in the process of interest. In addition, creating as little deviance as possible between the FE model and the experimental setup is a prerequisite for the correlation between predicted and measured values. Naturally, difficulties regarding e.g. modelling and estimations of friction arise, among others.

The objective of this thesis is to suggest possible hot and cold forming concepts based on FE analyses for the production of sheet metal prototype components in the titanium alloys Ti-6Al-4V and Ti-6242 together with the nickel based super alloy Inconel 718, respectively. The research activities are focused on material characterisation, evaluation of suitable constitutive models and its calibration, virtual tool design and manufacturing of sheet metal forming tools together with production of prototype components. The aim is to perform a direct-hit research and development work in which the lead time is short and the need for the manual die tryout can be kept at a minimum. The forming tests functions as validation tests in which predicted responses of global forming force, draw-in, temperature, strain localisation and shape deviation are correlated with predicted responses. Different yield criteria which include the anisotropy and strength differential (asymmetry in yielding between tension and compression) of the titanium alloy Ti-6Al-4V are

compared with an isotropic assumption. Special emphasises are made to models and methods suitable for analyses in the medium temperature range, for evaluations early in the product development process.

In paper A, compression tests on Ti-6Al-4V were performed at different temperatures in order to study the mechanical behaviour and create experimental reference data for identification of material model parameters of constitutive equations. Inverse modelling was used as a method for the parameter identification, in which three different equations were studied. At a temperature of 500°C, none of the studied constitutive equations were found able to satisfactory describe the flow behaviour. However, the method was found suitable for the purpose of identifying model parameters. Later on, the physically based constitutive equation developed by Nemat-Nasser et al. (2001) [1] was found able to describe the flow behaviour of Ti-6242. In the work by Nemat-Nasser et al. (2001) the model has been shown able to describe the flow behaviour of Ti-6Al-4V at different temperatures and strain rates accurately.

The equation was applied in FE analyses of a hot forming test, a U-bend test, of Ti-6242. The experimental study of Ti-6242, including U-bend tests, at different thermo-mechanical conditions performed in Paper B, revealed that the formability is increased and that the springback can be decreased with increasing temperature. However, it was also found that an increased temperature alone does not necessary imply a reduced shape deviation.

In paper C, a short lead time methodology for the design, compensation and manufacturing of deep drawing tools in the nickel based alloy Inconel 718 is suggested. Rather than stating a new methodology, the work contributes to the idea that it is possible to perform a virtual direct-hit development work for the production of five different double-curved components within tolerance at an extremely short lead time. Compensation for the predicted shape deviation was performed for one of the components in which the tool surfaces were over compensated by means of FE analyses.

In paper D and F, the short lead time methodology was applied for the development of hot forming concepts to produce two different Ti-6Al-4V sheet metal components. The material characterisation, presented in paper E, provides with experimental reference data for calibration of three different yield criteria. Predicted responses such as punch force, draw-in and shape deviation show promising agreement with experimental observations when applying anisotropic yield formulations. The shape of the yield surface was found important for the prediction of shape deviation and the occurrence of

strain localisation. Some issues of the FE-model suggest areas for further development. An interesting extension to the present work would be to include models for phase transformation and creep or stress relaxation and include the effect of strain rate for sheet metal forming in the higher temperature range. Further on, it is of interest to extent anisotropic yield criteria to function in coupled thermo-mechanical analyses and to include orthotropic elasticity. This, in order to increase the possibility to perform detailed studies of the temperature as an important process parameter for the prediction of shape deviation and studies of strain localisation limits.

# Thesis

The thesis consists of a summary and the following appended papers:

**Paper A**

E.-L. Westman, R. Pederson, B. Wikman, M. Oldenburg, Numerical and Microstructural Evaluation of Elevated Temperature Compression Tests on Ti-6Al-4V, *Ti-2003 Science and Technology, 10th World Conference on Titanium, Hamburg, Germany, 13-18 July 2003*, Volume III, pages 1461-1468.

**Paper B**

E.-L. Odenberger, R. Pederson, M. Oldenburg, Thermo-mechanical material response and hot sheet metal forming of Ti-6242. Materials Science and Engineering: A, Volume 489, Issues 1-2, pp158-168, 2008.

**Paper C**

E.-L. Odenberger, M. Jansson, P. Thilderkvist, H. Gustavsson, M. Oldenburg, A short lead time methodology for design, compensation and manufacturing of deep drawing tools for Inconel 718, IDDRG 2008 Conference, Best in Class Stamping, pp 697-708.

**Paper D**

E.-L. Odenberger, M. Oldenburg, P. Thilderkvist, T. Stoehr, J. Lechler, M. Merklein, Tool development based on modelling and simulation of hot sheet metal forming in titanium Ti-6Al-4V, Submitted for publication.

**Paper E**

E.-L. Odenberger, J. Hertzman, P. Thilderkvist, M. Merklein, A. Kuppert, T. Stoehr, J. Lechler, M. Oldenburg, Thermo-mechanical sheet metal forming of aero engine components in Ti-6Al-4V – PART 1: Material characterisation. To be submitted.

**Paper F**

E.-L. Odenberger, M. Jansson, M. Oldenburg, Thermo-mechanical sheet metal forming of aero engine components in Ti-6Al-4V – PART 2: Constitutive modelling and validation. To be submitted.

# Contents

# Appended papers

**Paper A.** *Numerical and Microstructural Evaluation of Elevated Temperature Compression Tests on Ti-6Al-4V*

**Paper B.** *Thermo-mechanical Material Response and Hot Sheet Metal Forming of Ti-6242*

**Paper C.** *A short lead time methodology for design, compensation and manufacturing of deep drawing tools for Inconel 718*

**Paper D.** *Tool development based on modelling and simulation of hot sheet metal forming in titanium Ti-6Al-4V*

**Paper E.** *Thermo-mechanical sheet metal forming of aero engine components in Ti-6Al-4V – PART 1: Material characterisation*

**Paper F.** *Thermo-mechanical sheet metal forming of aero engine components in Ti-6Al-4V – PART 2: Constitutive modelling and validation*

# 1. Introduction

## 1.1 Background

To preserve or increase the competitiveness of companies in the modern industry, a prerequisite is to perform a direct-hit product development process in which the lead time is short and the outcome is accurate. One key feature, in the production industry, is to develop suitable manufacturing processes where the tryout can be kept at a minimum. The industry of today has to decrease its negative impact on the environment. Considering the vehicle industry such as for transportation on the road, railway or in air, high performance and light weight materials are desirable to reduce weight and thereby fuel consumption yet with maintained performance.

The advanced numerical finite element (FE) technology and CAE-tools in combination with existing computer capacity makes a completely virtual process development possible. FE simulations are used extensively in e.g. the sheet metal stamping industry where the technology has contributed to a better understanding of chosen forming processes and where the prediction capabilities has significantly reduced the time consuming and costly die tryouts. Complex geometries in industrial applications with large deformations, nonlinear materials and contacts can be treated effectively and quickly [2-6]. However, the reliability of the numerical simulations depends not only on the models and methods used but also on the accuracy and applicability of the input data. The material model and related property data must be consistent with the conditions of the material in the process of interest.

To increase the competitiveness of the Swedish aero engine industry alternative manufacturing methods for static load carrying aero engine structures are desired, in order to reduce product cost and enable weight reduction and thereby fuel consumption. Traditionally, these structures mainly consist of large-scaled single castings of e.g. titanium- and nickel based super alloys. By fabrication, the structures are instead built from sheet metal parts, small ingots and simple forgings which are welded together and heat treated. This alternative approach implies the need for time and cost efficient evaluations of candidate manufacturing techniques, early in the product development process. One challenge in producing such complete structures within shape tolerance lies in accurate predictions of springback and compensation for shape deviation which occurs in the different processes of the manufacturing chain.

The aerodynamic geometries of included sheet metal parts are generally smoothly double-curved and the resultant geometry, thickness, residual stress state and mechanical properties obtained in the forming process influence the shape deviation of the complete structure upon welding and heat treatment. Accurate predictions of and compensation for the springback obtained in the sheet metal forming process by means of finite element (FE) analyses, may therefore be considered as a key subject in fabrication of complete titanium structures. A schematic illustration of load carrying aero engine structures are shown in figure 1, consisting of titanium and nickel based alloys.

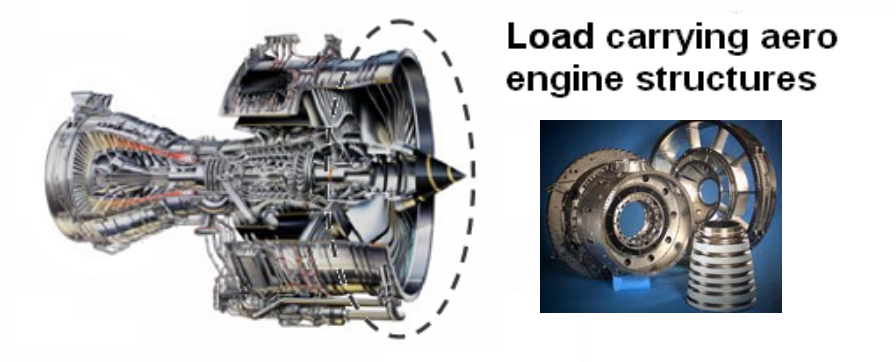


Figure 1. Schematic illustration of load carrying aero engine structures consisting of titanium and nickel based alloys.

## 1.2 Research question and aim

The research question which has been formulated within this thesis is:

*To which extent can accurate and validated material descriptions be obtained, in an optimal sense, by innovative methods for material testing and characterisation and how is such material descriptions applied in virtual product and process development?*

The purpose of this thesis is to suggest concepts for hot sheet metal forming of foremost the titanium alloy Ti-6Al-4V but also Ti-6242. Two prototype components are studied within the research work, which functions as demonstrators to evaluate the applicability of chosen methods and models in the virtual tool development process. The thesis comprise studies of the mechanical properties of Ti-6Al-4V and Ti-6242, identification of suitable material models and methods for calibration and suggestions for concepts of hot sheet metal forming based on FE analyses in which predicted values are compared with measured by performing validation experiments.

The focus has been on different levels of model complexity for numerical predictions which are able to yield acceptable accuracy of hot titanium sheet metal forming, in the concept phase of the product development process. The research work is limited to studies of FE-models for conventional sheet metal forming techniques in the medium temperature range. The computed resultant springback obtained in a hot sheet metal forming process depend on the produced level and condition of stress. The accuracy in the prediction of the residual stress condition depends of a variety of factors. For example the temperature, the material model, i.e. the description of the elasticity, yield surface and hardening law along with the distribution and magnitude of friction, stiffness of the forming tool and the ability to obtain equal conditions in the numerical model as in the experiment.

This work includes the influence of the yield criterion and determination of flow behaviour assuming isotropic hardening. In addition the elastic anisotropy and the influence of plastic straining are studied. Considerable efforts have been made to ensure the equality between the FE-model and the experimental setups, as far as possible. Features such as tool geometries, draw depth, blank holder forces, blank positioning, draw-in and temperature have been controlled and measured.

The basic strategy within this research work has been to create an experimental foundation, consisting of initial material and hot forming tests from which observations are made and conclusions are drawn regarding formability and springback behaviour. Models with a low level of complexity are studied and compared with more advanced, e.g. in which the anisotropy of the studied alloys are included. Tool concepts for the production of two sheet metal geometries are developed and manufactured. FE analyses are used in the development process, and the hot forming procedures functions as validation tests. The aim has been to perform a direct-hit development work with short lead times, in which the research activities are considered the basic driving force.

The alternative fabrication process of interest for the aero engine industry requires development of new manufacturing technologies and relations with new sub-suppliers. It is desirable that sub-suppliers are able to deliver not only sheet metal parts within shape and thickness tolerances, but also results from FE analyses of the forming procedure for use in subsequent analyses of welding and heat treatment. The scope of the research project was therefore also to identify a few SMEs within the titanium or advanced material industry with potentials to develop into future sub-suppliers of titanium sheet metal

parts for the aero engine industry. The research project gather competence from research centres within numerical analyses of sheet metal forming, SMEs with practical experiences of titanium forming and the aero engine industry. With the support of academic research activities the aim was to perform an effective development work of the companies by introducing advanced tools for numerical analyses and material characterisation, in order for the companies to take necessary technology steps. A process which has been initiated within the project.

## 1.3 A brief literature review

### 1.3.1 The titanium alloys Ti-6Al-4V and Ti-6242

Titanium alloys are often used in aerospace applications such as for turbine engines, airframe applications and space applications, mainly because of their superior strength to weigh ratio. Ti-6Al-4V is the most widely used titanium alloy and other applications can be found in medical prostheses and to some extent in the automotive, marine and chemical industry. Ti-6Al-4V is a two phase ($\alpha+\beta$) alloy implying a variety of possible microstructures and property combinations depending on different factors such as the thermo-mechanical processing, chemical composition, interstitials (mainly oxygen) and impurities [7-10]. The $\alpha$ phase has a crystal *hcp*-structure and the softer $\beta$ phase a *bcc*-structure. A variation in Young's modulus is present mainly considered to be due to the heat treatment, alloy concentration, interstitials/substitutional, impurity levels and in case of textured sheets, the angle between the rolling direction and specimen axis (anisotropy).

Titanium Ti-6Al-2Sn-4Zr-2Mo-0.08Si or Ti-6242 was developed in the late 1960's. It is a titanium alloy with high temperature stability for long-term applications (up to 425°C) and is one of the most creep-resistant, often used when the temperature range do not permit usage of Ti-6Al-4V. The alloy is a near-alpha, alpha-beta alloy and the structures are typically equiaxed $\alpha$ in a transformed $\beta$ matrix or a fully transformed micro structure. The $\alpha$ phase has a crystal *hcp*-structure and the $\beta$ phase a *bcc* crystal structure, as of Ti-6Al-4V.

Typical flow behaviours of the alloys at elevated temperatures are illustrated in figure 2, obtained from compressive testing on cylindrical specimens. The well observed peak stress is followed by flow softening in the higher temperature range. In published work by e.g. Ding et al. [10-11] and [12] with included references, this behaviour is suggested to originate from temperature increases, microstructural changes, break up of the grain structure, recrystallisation, phased changes, shear band formation and damage during deformation.

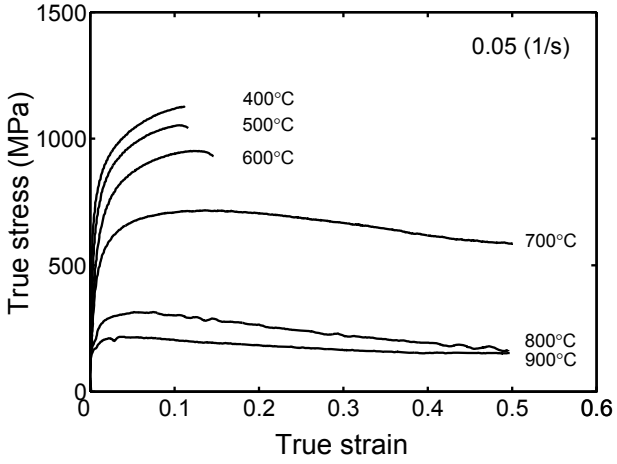


Figure 2. True stress-strain relations for Ti-6242 at indicated strain rate and temperatures.

Both alloys have excellent corrosion resistance compared to other metallic alloys and at low temperatures a very thin oxide film protects the surface. However, at higher temperatures oxygen begins to dissolve from the oxide into the underlying metal forming a so called alpha case, which causes embrittlement. The oxide film grows inwards by diffusion of oxygen and the corrosion velocity is strongly dependent on the temperature [7, 8].
Typical physical properties of Ti-6Al-4V and Ti-6242 can be found in table 1 and further information on the both titanium alloys in e.g. [7, 8, 12-14].

Table 1.
Summary of typical physical properties [7, 8, 13]

| **Property** | **Ti-6AL-4V** | **Ti-6242** |
|---|---|---|
| Beta transus temperature | 995°C | 990°C |
| Melting point | ~1655 ± 20°C | ~1705°C |
| Density (a) | 4.428 g/cm$^3$ | 4.540 g/cm$^3$ |
| Young's modulus (a) | 115 ± 15 GPa | 113 GPa |
| Poisson's ratio (a) | 0.26-0.36 | 0.325 |
| Thermal conductivity (a) | 7 W/m*K | 7 W/m*K |
| Specific heat capacity (a) | 580 J/kg*K | 460 J/kg*K |
| Thermal coefficient of linear expansion (b) | 9.0*10$^{-6}$/°C | 7.7*10$^{-6}$/°C |

(a) Typical values at room temperature. (b) Mean coefficient from 0 to 100°C

### 1.3.2 Sheet metal forming of titanium

Generally, titanium alloys are considered more difficult to form and often have less predictable forming characteristics than other metallic alloys such as steel and aluminium. The literature states that titanium alloys can be formed in room temperature or at lower elevated temperatures to some extent, yet also that the obtained springback upon forming thin sheets are scattering and thus difficult to predict. A high degree of springback is common in cold and hot forming processes due to the high yield stress in combination with a low elastic modulus. Further, the hexagonal crystal structure (*hcp*) of the α-phase has anisotropic characteristics which implying consequences to the elastic properties [7, 8]. Considering this, titanium components are commonly formed at elevated temperatures often by overcompensating tool geometries and performing multi stage forming with intermediate annealing or by applying a second "hot sizing" operation. In the hot sizing process the part is allowed to be creep formed into the final desired shape.

The formability of titanium and its alloys are fairly low depending on the material grade. By increasing the forming temperature an increased formability is obtained in which the springback and the scatter in yield stress can be reduced. However, such techniques require heat resistant forming tools and the commonly slow forming velocities with subsequent holding times implying long exposure times at high temperatures and additional costs. As the temperature exposure increases a higher degree of contamination occurs. Hot forming should generally not be performed at temperatures higher than ~815°C without a protective atmosphere to avoid deterioration of the mechanical properties. When oxygen enrichment of titanium occurs, the material becomes more brittle.

At even higher temperatures some titanium alloys exhibit super plastic properties which make super plastic forming (SPF) applicable. The process was originally developed due to the difficulties associated with conventional sheet metal forming of titanium alloys. The super plastic forming procedure is performed under high temperatures in the range of 870 - 925°C, still below the β-transus temperature, and at very low strain rates (often at about $10^{-4}$ $s^{-1}$). Due to the low flow stress, springback is not an issue. Initially, parts manufactured by SPF were considerably expensive, but with experience the SPF setup has become quite common and inexpensive. However, SPF is often used for components with a high degree of complexity or when a substantial degree of material stretching is necessary [7, 8, 15-17]. Due to the presented difficulties, the lowest possible forming temperature that allow for the desired geometry is normally chosen.

Titanium alloys are sensitive to the strain rate and a higher formability is generally obtained when forming titanium alloys at lower strain rates in room temperature. However, at elevated temperatures the profit of a decreased or increased strain rate is determined by the alloy of interest. Titanium alloys are also sensitive to the Bauschinger effect, which is reported to be most pronounced in room temperature. Further information on sheet metal forming in titanium can be found in e.g. [7, 8, 18-24]

# 2. Finite element modelling

Nonlinear analysis based on the finite element method (FEM) is one essential component of computer-aided design (CAD/CAE). Manufacturing and testing of prototypes is increasingly being replaced by the use of nonlinear FE simulations because it provides a more rapid and less expensive way to evaluate manufacturing and design concepts. However, the use of nonlinear finite element technique requires an understanding of the fundamental concepts which confronts the user with many choices and pitfalls. The intent of this section is to shortly review some of the methods and features related to nonlinear finite element analysis, without being complete in any sense.

## 2.1 Explicit time integration

Sheet metal forming includes nonlinearities due to material behaviour, instabilities and contact constrains. Explicit solvers are widely used in forming simulations with advantages such as convergence stability and fewer computations per time step along with a less storage requirement compared to implicit methods. This makes explicit solvers suitable for large scale problems. However, the time integration is conditionally stable and thus requires a small time step to guarantee stability. In this thesis, the explicit FE solver in LS-DYNA [25] has been used. For a more extensive discussion on time integration, see e.g. Belytschko et al. [2, 3].

The FE discretisation in space, based on the weak form of the equation of motion results in

$$[M]\{a\} = \{f\} \tag{2.1}$$

where

$$\{f\} = \{f^{ext}\} - \{f^{\text{int}}\} \tag{2.2}$$

In which $[M]$ is the mass matrix, $\{a\}$ is the acceleration vector and $\{f^{ext}\}$ and $\{f^{int}\}$ are the external and internal force vectors, respectively. The mass matrix is

$$[M] = \sum_e \int_V \rho [N]^T [N] dV \tag{2.3}$$

where $\rho$ is the density and [$N$] is the shape function matrix. The integral is taken over the domain $V$ and is summarised for all elements $e$. The internal force vector is

$$\left\{f^{\text{int}}\right\} = \sum_e \int_V [B]^T \{\sigma\} dV \tag{2.4}$$

where [$B$] is the strain-velocity matrix and {σ} is the Voigt vector of the Cauchy stress components. The external force vector includes body forces and resulting forces from boundary conditions according to

$$\left\{f^{ext}\right\} = \sum_e \int_V [N]^T \{b\} dV + \sum_e \int_S [N]^T \{\bar{t}\} dS \tag{2.5}$$

Where $\{b\}$ is the body force vector and $\{\bar{t}\}$ is the traction vector acting on the boundary $S$. The discretisation in time is accomplished using the central difference scheme. In the current state $n$, the internal and external forces, velocities $\{v\}_n$ and displacements $\{d\}_n$ are known. The acceleration in Equation 2.1 and 2.2 becomes

$$\{a\}_n = [M]^{-1}\left(\left\{f^{ext}\right\}_n - \left\{f^{\text{int}}\right\}_n\right) \tag{2.6}$$

The velocity $\{v\}_{n+\frac{1}{2}}$ is evaluated at time $t_{n+\frac{1}{2}}$ using the time step $\Delta t_n$

$$t_{n+\frac{1}{2}} = t_n + \frac{\Delta t_n}{2} \tag{2.7}$$

and

$$\{v\}_{n+\frac{1}{2}} = \{v\}_{n-\frac{1}{2}} + \Delta t_n \{a\}_n \tag{2.8}$$

The displacements $\{d\}_{n+1}$ at time $t_{n+1}$ is found from

$$\{d\}_{n+1} = \{d\}_n + \Delta t_n \{v\}_{n+\frac{1}{2}} \tag{2.9}$$

The stress state of the material is updated to find the internal forces, see e.g. Belytschko et al. [2]. The largest allowable time step $\Delta t$, is determined by the highest natural frequency of the system according to Equation 2.10 which is related to the density and stiffness of the material.

$$\Delta t \leq \frac{2}{\omega_{\max}} \tag{2.10}$$

where

$$\omega_{\max} \approx 2\frac{c}{L_e} \tag{2.11}$$

which yields the Courant's stability criteria

$$\Delta t \leq \frac{L_e}{c} \tag{2.12}$$

where $c$ is the wave propagation velocity and $L_e$ is a characteristic length in the structure such as the minimum distance between two nodes.

The shell element type used in this work is fully integrated. With this element type it is assumed that the stress through the thickness in the blank is negligible compared to the in-plane stress. The use of fully integrated shell elements is CPU costly, but recommended when springback predictions are of interest. In the performed FE analyses of this work, 9 integration points through the thickness are applied in order to preserve high accuracy.

The contact modelling is defined by a master and slave formulation. The nodes on the slave surface are checked to determine if penetration with a master segment occur. If penetration occurs, contact forces are used to keep the surfaces apart which depend on the penetration depth. The contact algorithm can be based on a penalty formulation or a constraint algorithm.

## 2.2 Thermo-mechanical coupling

Considering hot sheet metal forming under isothermal conditions, the mechanical properties at the desired temperature and the thermal expansion occurring upon heating and cooling can be taken into account by performing thermo-mechanical analyses. In specific, the cooling to room temperature yields thermal stresses which has an impact on the springback.

In simulations of thermo-mechanical forming procedures, the ability to use the same geometric description in both the mechanical and thermal analysis is desirable. In hot forming of titanium, the blank and the tool parts can posses different temperatures. The blank may then be subjected to contact with the tools on one side first and subsequently on both sides i.e. one-sided and double-sided contact. To accurately capture the heat transfer, the thermal element proposed by Bergman and Oldenburg [26] is applied. The thermal shell element has a linear in-plane temperature approximation with a quadratic approximation in the thickness direction.

The temperature dependant mechanical properties of the alloy are defined trough the mechanical and thermal material definitions. Examples of temperature dependant mechanical properties which can be included in commercial available material models are e.g. initial yield stress and hardening, Young's modulus, Poisons ratio and the thermal expansion coefficient. Examples of temperature dependant thermal properties are the heat capacity and thermal conductivity.

In the thermal contact the heat transfer coefficient is defined, which generally vary with pressure and temperature interval. A contact gap is defined, for which the thermal contact is considered. If convection and radiation exchange (including the emissivity) is assumed to be of importance, this has to be included.

If a speed up factor is applied in the explicit analysis the thermal properties such as the thermal conductivity, heat transfer coefficient and radiation factor have to be scaled in order to yield the correct response. For further reading in the area the reader is referred to e.g. [27 - 29].

# 3. Constitutive modelling

The ability of the material model in combination with the model input to describe the material behaviour in a process of interest is decisive to the accuracy of predicted responses. Some of the features that constitute the material model are the definition of elasticity, constitutive models for the material hardening and criterion for yielding, the hardening law and e.g. models for phase transformation, microstructural evolution and creep or stress relaxation. In processes where the temperature is included, the material model includes both the temperature dependant mechanical and thermal properties of the material.

Among the various features that constitute the FE material model the elasticity, hardening law and the shape of the yield surface are of major importance for the accuracy in the predictions of strain localisation and springback [30, 31]. For more details, the reader is referred to e.g. Lubliner [32], Betytschko [2], Ottosen and Ristinmaa [33] and Lewis et al. [27].

In order to delimit the scope of the research, constitutive models for the hardening and yield surface are studied in which isotropic hardening is assumed. This section presents the constitutive equation proposed by Nemat-Nasser et al. [1] and the anisotropic yield criteria developed by Barlat et al. (2003) [34] and Cazacu et al. (2006) [35]. These models are of interest for the FE modelling of sheet metal forming processes of titanium alloys. Thus, the used methods for and results of model calibration with applications to Ti-6242 and Ti-6Al-4V is presented. Finally, plastic instability in sheet metal forming is most briefly discussed.

## 3.1 Elasticity

The basic behaviour of an elasto-plastic material upon loading can be described by a linear elastic behaviour with a stiffness E, up to the initial yield stress $\sigma_y$ in which elastic strains, $\varepsilon^e$, are developed. When the loading exceeds the point of initial yield stress, plastic straining occurs, $\varepsilon^p$, cf. figure 3.

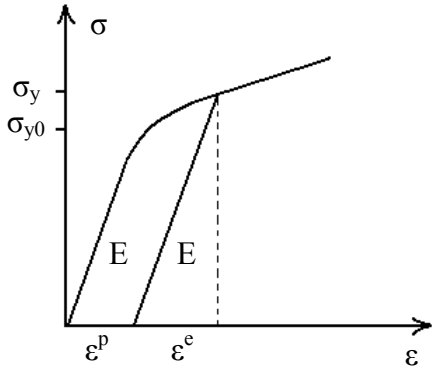


Figure 3. Basic uni-axial response of an elastic-plastic material.

A basic assumption is that metals behave linearly isotropic according to Hooke's law in Equation 3.1, in one dimension

$$\sigma = E\varepsilon \tag{3.1}$$

where Young's modulus, E, is dependant on the specific material and temperature. Furthermore, the elastic modulus is independent of the rate of loading (for non extreme values of the loading rate). A material that behaves according to this in the elastic range is fully described by the two stiffness parameters E and υ (Poisson's ratio). Hooke's generalised law for isotropic materials in Cartesian tensor form may be written according to Equations 3.2-3.5 where $\lambda$ and $\mu$ are the so called Lamé parameters, $\sigma_{ij}$ is the stress tensor and $\varepsilon_{ij}$ is the Cauchy infinitesimal strain tensor.

$$\sigma_{ij} = \lambda\varepsilon_{kk}\delta_{ij} + 2\mu\varepsilon_{ij} \tag{3.2}$$

where

$$\lambda = \frac{\nu E}{(1+\nu)(1-2\nu)} \quad ; \quad \mu = \frac{E}{2(1+\nu)} \tag{3.3}$$

and

$$G = \frac{E}{2(1+\nu)} \tag{3.4}$$

which yields

$$\sigma_{ij} = 2G\left[\varepsilon_{ij} + \frac{\nu}{1-2\nu}\varepsilon_{kk}\delta_{ij}\right] \tag{3.5}$$

However, several experimental studies have observed that the elastic modulus decrease with the level of plastic straining and that the stress-strain relation during unloading is slightly non linear, see e.g. [31] with references there in. Titanium alloys such as Ti-6Al-4V have also been observed, as mentioned earlier, to posses anisotropic elastic properties [7, 8]. A test in room temperature was performed to evaluate the change of elastic modulus with plastic straining in room temperature, see paper E. The study indicated a slight decrease with plastic straining. The description of the elastic behaviour upon unloading is one important feature in predictions of the amount of springback in sheet metal forming procedures.

## 3.2 Material characterisation and model calibration

Material characterisation and related model development and calibration are areas in which considerable research efforts are made. This originates from the fact that the reliability of the numerical simulations depends on the models and methods used together with the accuracy and applicability of the input data.

The material characterisation performed in this thesis revealed many interesting characteristics of the alloy. Based on these observations, necessary model requirements are determined and a few selected models were chosen for model calibration and evaluation.

### 3.2.1 Constitutive equation

The initial Gleeble compression tests on both Ti-6Al-4V and Ti-6242 revealed a quite low formability at low temperatures and a flow softening behaviour at high temperatures, see figure 2. Also, the plastic properties were found to depend on the rolling direction and strain rate, which indicated plastic anisotropy and strain rate sensitivity. See figure 4.

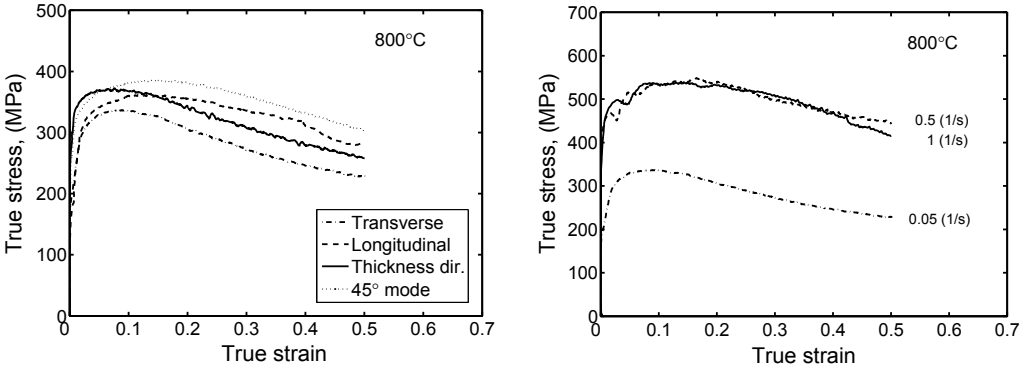


Figure 4. True stress-strain relations for Ti-6242 at indicated temperature, extraction direction of tested specimens and strain rate. The strain rate in the first figure is 0.05 $s^{-1}$.

A constitutive equation of interest to describe the hardening is the model developed by Nemat-Nasser et al. (2001) [1], cf. Equation 3.6-3.9. The physically based model comprises eight model parameters that have to be determined experimentally.

In the work by Nemat-Nasser et al. the model has successfully been applied to Ti-6Al-4V compressed at high temperatures and various strain rates. The model is a function of temperature and strain rate and is also able to describe a flow softening behaviour in which the temperature rise due to deformation and strain rate is included. The model was originally developed for metals with *bcc* and *fcc* crystal structure, in the absence of dynamic strain aging, defined for commercially pure tantalum and oxygen free and high conductivity (OHFC) copper [36]. The flow stress, $\tau$, is divided into two parts, one athermal and one thermally activated part according to

$$\tau = \tau^* + \tau_a \tag{3.6}$$

The first part, $\tau^*$, is associated with the thermally activated crossing of obstacles by dislocations and the other part, $\tau_a$, due to the athermal resistance to the motion of dislocations. The model was modified and $\tau^*$ is assumed to depend on both strain rate and temperature as well as on the dislocation density, $\rho$, while $\tau_a$ only depends on $\rho$.

$$\tau\left(\gamma,\dot{\gamma},T\right)=\tau^{0}\left(1-\left(-\frac{k}{G_0}T\left(\ln\frac{\dot{\gamma}\,f\left(\gamma,T\right)}{\dot{\gamma}_0}\right)\right)^{\frac{1}{2}}\right)f\left(\gamma,T\right)+\tau_a^0\gamma^n \qquad (3.7)$$

where

$$f\left(\gamma,T\right)=1+a_0\left(1-\left(\frac{T}{T_m}\right)^2\right)\gamma \qquad (3.8)$$

and where the temperature is calculated from

$$T=T_0+\Delta T,$$

$$\Delta T=\int_0^{\gamma}\frac{\tau}{4.39C_V}d\gamma, \qquad (3.9)$$

$$C_V=0.56\exp(T/2000)$$

Above, $\gamma$ denotes the effective plastic strain; $\dot{\gamma}$ is the effective strain rate; $T$ is the temperature; $\tau^0$ is an effective stress to be determined empirically; $k$ is Boltzmann's constant; $G_0$ is the total energy barrier that a dislocation must overcome by its thermal activation in the absence of an applied stress; $\gamma_0$ is a reference strain rate related to the density of mobile dislocations, initial (or some reference) average dislocation spacing and attempt frequency of a dislocation to overcome its energy barrier; $T_m$ is the melting temperature and $a_0$ is a constant depending on the initial (or reference) dislocation density.

The function $f(\gamma,T)$ is defined for *hcp* Ti-6Al-4V where the parameters, $p$ and $q$ are suggested equal to 1 and 2 respectively. The $p$ and $q$ parameters define the shape of the energy barrier.

The eight constitutive parameters ($P_i$) that have to be determined are: $P_1=\tau_a^0$, $P_2=\tau^0$, $P_3=n$, $P_4=p$, $P_5=q$, $P_6=k/G_0$, $P_7=\gamma_0$, $P_8=a_0$. However, Nemat-Nasser et al. [1] applied the constitutive equation for Ti-6Al-4V with three

different microstructures by adjusting only the three parameters $P_{1\text{-}3}$. The model predictions were found to be in good agreement with experimental results and the initial microstructure (including grain size and their distribution) only affects the athermal part of the flow stress.

In the present work, the term calculating the adiabatic temperature increase in Equation 3.9 is neglected due to the rather low strain rate used in the experiments. No adiabatic temperature increase was measured during the Gleeble compression tests. Inverse modelling is used as a method to estimate the three material model parameters for Ti-6242.

An in-house programming system designed for analysis of inverse problems are used, INVSYS [37]. In this work, the experimental reference data consists of the experimentally determined flow curve at 400°C. An error measure i.e. an objective function, $f(x_k)$, is defined in a least square sense describing the discrepancies between the experimental reference data, $y$, and the predicted data, i.e. the flow curve generated by the constitutive equation upon different parameter values $z(x_k)$. The objective is to minimise the error between the model prediction and the experimental reference data according to Equation 3.10.

$$\min f(x) = \min \frac{1}{2} \sum_{j=1}^{M} (y_j - z(x_k))^2 \tag{3.10}$$

where $j$ = 1,…M is the selected number of experimental data points. The optimisation algorithm used is the unconstrained subspace-searching simplex method (SUBPLEX) [38] which is based on direct search of zero order to find the minimum of Equation 3.10. The calculation of the gradient of $f(x_i)$ is not required. The method is suitable for minimising very noisy and non-smooth objective functions suitable in which numerical responses from FE analyses are applied due to robustness rather than computational efficiency, see e.g. [39]. A schematic illustration of the inverse modelling procedure is presented in figure 5, in which a set of sub-programs are used. The sub-programs consist, in this case of fortran routines and Linux shell scripts to control, handle and manage the data flow and data communication.

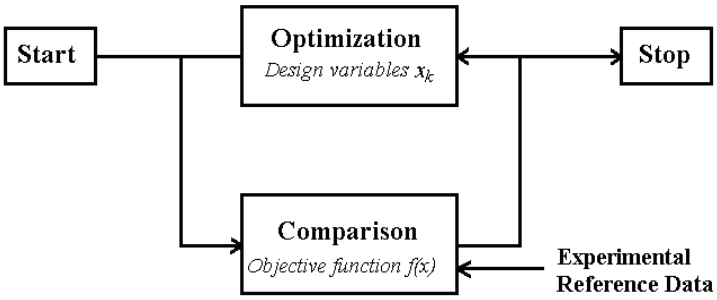


Figure 5. Schematic illustration of inverse modelling.

The determined material model parameters yield the flow curve presented in figure 6, in which the experimentally determined curve obtained by the Gleeble test at 400°C also is presented.

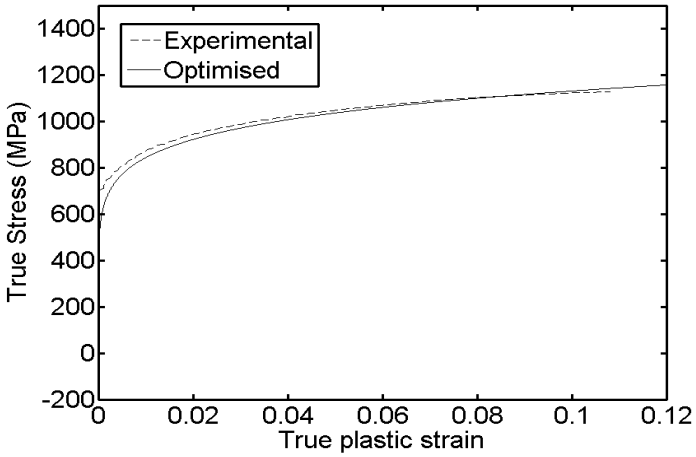


Figure 6. Experimental and optimised flow curve for Ti-6242 for the Nemat-Nasser et al. (2001) constitutive equation.

### 3.2.2 Yield criteria

The Ti-6Al-4V alloy has different elastic and inelastic properties depending on the choice of axis. The material is in other words anisotropic, as opposed to isotropic in which the properties is equal in all directions. Typically, the material becomes orthotropic in the cold rolling procedure to produce thin sheets. The principal material directions are the rolling, transversal and through-thickness directions. The difference in properties is characterised by different yield strength and plastic flow for each direction. To determine the anisotropy of thin sheets, material testing is performed in different in-plane directions.

The plastic anisotropy is often characterised by a difference in yield stress and true plastic flow relative to the rolling direction, defined by the Lankford coefficient, $R_\alpha$, assuming plastic incompressibility:

$$R_\alpha = \frac{\varepsilon_w^p}{\varepsilon_t^p} = plastic\ incomp. = -\frac{\varepsilon_w^p}{\varepsilon_w^p - \varepsilon_l^p} \tag{3.11}$$

where α is the angle from the rolling direction, *w* denotes the plastic strain in the width direction, *t* the thickness and, *l* longitudinal direction. In the isotropic case, the Lankford coefficients become equal to unity.

Numerous anisotropic yield formulations which can account for plastic anisotropy have been formulated the past decades. E.g. Hill's yield criterion (1950) [40], which contains four anisotropy coefficients in the plane stress condition that have to be determined experimentally. Since only four parameters are available, the criterion is not able to capture together the observed anisotropy in yield stress and Lankford coefficients [41, 42]. Barlat and Lian's (1989) tri-component criterion, [43], presented a yield criterion for plane stress conditions in which, as for the Hill's criterion, four anisotropy parameters are used to describe the yield surface. In this model the material parameter *m*, is proposed. If a value of 2 is applied, the yield surface reduces to the Hill yield surface, i.e. to the von Mises yield surface in the isotropic case. With an increasing value of *m*, in the isotropic case, the shape of the Barlat tri-component yield surface adopts the shape of the Tresca yield surface.

The anisotropic yield criteria developed for cubic metals by e.g. Hosford [44] and Barlat and co-workers (2003, 2005) [34, 45] accounts for plastic anisotropy with an increased number of parameters. The anisotropy coefficients are determined from experimental reference data in order to calibrate the yield criteria with respect to both yield stress and Lankford coefficients. These models assume symmetry in tension and compression. The physically based macroscopic formulation by Cazacu et al. (2006) [35] describes both the anisotropy and the known asymmetry in yielding exhibited by *hcp* materials.

In this thesis, an isotropic assumption is compared with the anisotropic yield criteria proposed by Barlat et al. (2003) and Cazacu et al. (2006). The shape of the yield surfaces are determined using a material testing and an identification programme which minimise the objective function in a least square sense.

The experimental reference data at different temperatures ranging from room temperature up to 560°C consist of data obtained from uniaxial tension tests performed in the 00 (along), 45 and 90 (transverse) in-plane directions, see figure 7. The evaluation area, using ARAMIS$^{TM}$ strain measurement system [46], is the facets where necking occurs in order to obtain true stress – true strain values even after the occurrence of necking.

The uniaxial tensile test can be considered a useful test since it is simple, cheap and robust, at least when performed in room temperature. It is also a standard test, which make material data easy to obtain if not available. The drawback with the occurrence of necking in the specimen, which traditionally makes large strain data difficult to evaluate can be overcome by using the ARAMIS$^{TM}$ system.

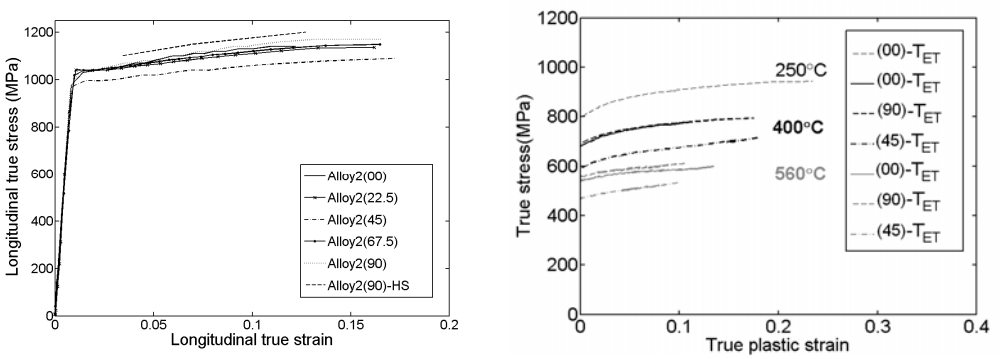


Figure 7. Flow curves at room temperature and at elevated temperatures, respectively.

The initial yield stresses for uniaxial compression is determined to evaluate the asymmetry in yielding between tension and compression. Further, the initial yield stress for a balanced biaxial stress state ($\sigma_{xx} = \sigma_{yy}$) is also determined by performing a viscous bulge test in room temperature. The ARAMIS$^{TM}$ strain measurement system is used to continuously measure surface strains and geometry (radius of the dome) during the test. The test setup is illustrated in figure 8 where the pressure is continuously measured by a sensor in the bottom of the silicone rubber punch to determine the biaxial stress according to Equation 3.12.

$$\sigma_b = \frac{p \cdot r_b}{2t_b} \tag{3.12}$$

where $p$ is the pressure, $r_b$ is the radius of the curvature and $t_b$ is the thickness at the top of the dome. After the test is performed, the biaxial stress-strain curve is determined using software as part of the ARAMIS$^{TM}$ system.
The balanced biaxial yield stress, $\sigma_b$, is obtained using the experimental biaxial reference point measured during biaxial tension in the viscous bulge test according to

$$REF(\sigma, -\varepsilon_t) = (1136.0, 0.075) \tag{3.13}$$

where the biaxial R-value was determined to 1.02. The biaxial yield stress, $\sigma_b$, is determined by calibrating the considered yield criteria to obtain the experimental reference point response in Equation 3.13 in a biaxial tension of an element using FE analyses. The compressive and biaxial data are transformed to 400°C assuming the same behaviour as in room temperature. This, since no possibility existed to perform the tests at elevated temperatures within the project.

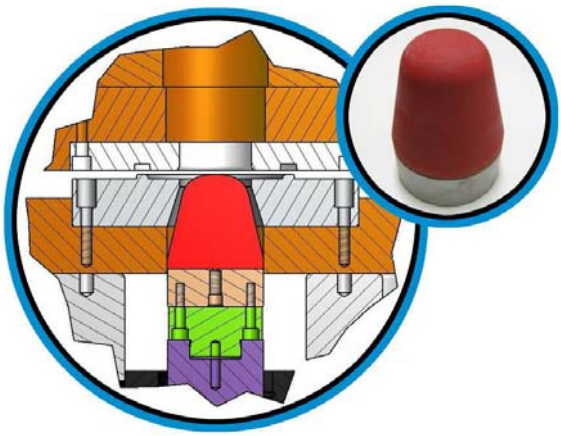

Figure 8. Illustration of the test setup for the viscous bulge test.

Barlat et al. (2003) propose an anisotropic yield criterion which is composed of two convex functions formulated as

$$f = \Phi' + \Phi'' - 2\bar{\sigma}_f^{\,m} = 0 \tag{3.14}$$

where

$$\Phi' = \left| X_1' - X_2' \right|^m \tag{3.15}$$

and

$$\Phi'' = \left|2X_2'' - X_1''\right|^m + \left|2X_1'' + X_2''\right|^m \tag{3.16}$$

in which $X'_{1,2}$ and $X''_{1,2}$ are the principal values of the linearly transformed stress deviator matrices {s},

$$\left\{X'\right\} = \left[C'\right]\left\{s\right\} \tag{3.17}$$

$$\left\{X''\right\} = \left[C''\right]\left\{s\right\} \tag{3.18}$$

The exponent *m* is the same parameter as in the Barlat's tri-component criterion, [43], which can be seen as a material parameter of its own. For an *m*-value equal to two, the yield surface reduces to Hill yield surface, i.e. von Mises yield surface in the isotropic case. With increasing value of *m* in the isotropic case, the Barlat et al. (2003) yield surface adopts the shape of the Tresca yield surface. The matrices C' and C'' can be expressed in terms of eight anisotropy coefficients $\alpha_i$, which all reduces to unity in the isotropic case.

To determine the eight anisotropy coefficients $\alpha_1$ to $\alpha_8$, eight material tests need to be performed. In this work, the initial yield stresses $\sigma_{00}$, $\sigma_{45}$, $\sigma_{90}$, and the Lankford coefficients $R_{00}$, $R_{45}$, $R_{90}$ are determined from uniaxial tension tests. The viscous bulge test is used to determine the biaxial yield stress, $\sigma_b$, and biaxial R-value, $R_b$. The yield stress data and Lankford coefficients used in the calibration are presented in table 2 and the resulting anisotropy coefficients in table 3. The rolling direction (00) of the Ti-6Al-4V blank is used as reference in the calibrations.

The resulting yield surfaces at room temperature and at 400°C are shown in figure 9 for different amount of shear stress $\sigma_{12}/\bar{\sigma}$. In figure 10 the predicted initial yield stress $\sigma_Y$ and R are compared with measured values, assuming an *m*-value of 8 for different angle directions (α) referenced the rolling direction (0).

Table 2.
Calibration data for Ti-6Al-4V at different temperatures. Initial yield stress, $\sigma_\alpha$, in [MPa].

| | $\sigma_{00}$ | $\sigma_{45}$ | $\sigma_{90}$ | $\sigma_b$ | $R_{00}$ | $R_{45}$ | $R_{90}$ | $R_b$ |
|---|---|---|---|---|---|---|---|---|
| RT | 1000.0 | 972.0 | 1020.0 | 1093.8 | 0.4 | 1.19 | 0.61 | 1.02 |
| 400°C | 681.0 | 591.0 | 691.0 | 744.9 | 0.6 | 1.26 | 0.512 | 1.02 |
| 560°C | 545.0 | 461.0 | 560.0 | 596.1 | 0.65 | 1.325 | 0.63 | 1.02 |

Table 3.
Barlat et al. parameter values for Ti-6Al-4V at different temperatures and $m = 8$.

| | $\alpha_1$ | $A_2$ | $\alpha_3$ | $\alpha_4$ | $\alpha_5$ | $\alpha_6$ | $\alpha_7$ | $\alpha_8$ |
|---|---|---|---|---|---|---|---|---|
| RT | 0.7713 | 1.021 | 0.8272 | 0.9666 | 0.9889 | 0.7464 | 1.024 | 1.151 |
| 400°C | 0.9828 | 0.8534 | 0.7874 | 0.9764 | 0.986 | 0.7878 | 1.132 | 1.426 |
| 560°C | 0.9748 | 0.8883 | 0.8199 | 0.9647 | 0.9756 | 0.7851 | 1.162 | 1.486 |

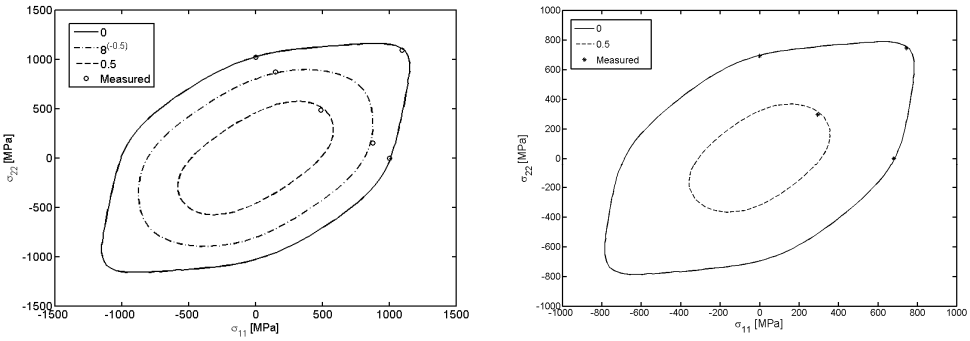


Figure 9. Titanium alloy Ti-6Al-4V yield surface at room temperature and 400°C determined with 8 parameters for equal amounts of shear stress $\sigma_{12}/\bar{\sigma}$, respectively.

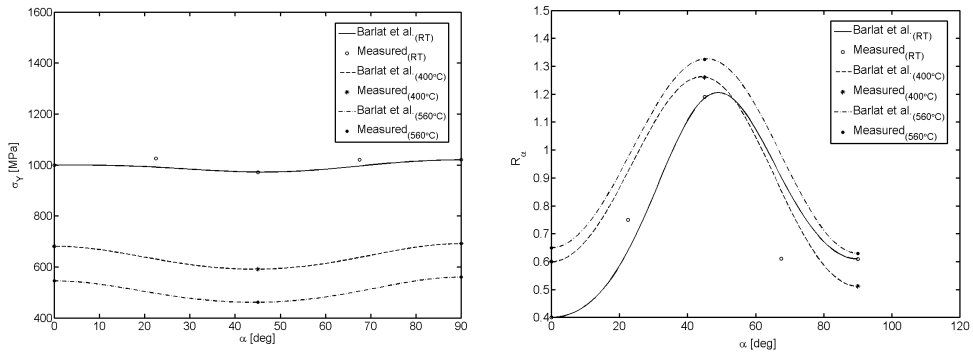


Figure 10. $\sigma_Y$ and $R_\alpha$ predicted and measured with eight parameters at indicated temperatures, respectively.

The orthotropic yield criterion proposed by Cazacu et al. (2006), consider both the tension/compression asymmetry and the anisotropic behaviour of hcp

metals and alloys. The authors introduced an isotropic yield criterion of the form

$$\left(|S_1| - kS_1\right)^a + \left(|S_2| - kS_2\right)^a + \left(|S_3| - kS_3\right)^a = F \tag{3.19}$$

where $S_i$, $I$ =1,…,3 are the principal values of the stress deviator. The exponent $a$, is a positive integer and $k$ is a material constant. The ratio of tensile to compressive uniaxial yield stress is given by

$$\frac{\sigma_T}{\sigma_C} = \left\{ \frac{\left(\frac{2}{3}(1+k)\right)^a + 2\left(\frac{1}{3}(1-k)\right)^a}{\left(\frac{2}{3}(1-k)\right)^a + 2\left(\frac{1}{3}(1+k)\right)^a} \right\}^{\frac{1}{a}} \tag{3.20}$$

or

$$k = \frac{1 - h\left(\frac{\sigma_T}{\sigma_C}\right)}{1 + h\left(\frac{\sigma_T}{\sigma_C}\right)} \tag{3.21a}$$

with

$$h\left(\frac{\sigma_T}{\sigma_C}\right) = \left[ \frac{2^a - 2\left(\frac{\sigma_T}{\sigma_C}\right)^a}{\left(2\frac{\sigma_T}{\sigma_C}\right)^a - 2} \right]^{\frac{1}{2}} \tag{3.21b}$$

If $k$ = 0 and $a$ = 2, the criterion reduces to the von Mises yield criterion. From Equation 3.21b, it follows that for different values of the exponent $a$, $k$ is restricted in order to be real [35]. The isotropic formulation is extended to orthotropy by a linear transformation on the deviatoric stress tensor, S:

$$\Sigma = C[S] \tag{3.22}$$

where C is a constant 4$^{th}$-order tensor. Thus, the orthotropic criterion is

$$\left(\left|\Sigma_1\right| - k\Sigma_1\right)^a + \left(\left|\Sigma_2\right| - k\Sigma_2\right)^a + \left(\left|\Sigma_3\right| - k\Sigma_3\right)^a = F \qquad (3.23)$$

For the 3-D stress condition the orthotropic criterion involves 9 independent anisotropy coefficients together with *a* and *k*. For $k \in [-1,1]$ and any integers *a* $\geq$ 1, the anisotropic yield function is convex in the variables $\Sigma_1$, $\Sigma_2$, $\Sigma_3$ (principal transformed stresses).

The yield stress data in tension, compression and for the balanced biaxial stress state together with Lankford coefficients used in the calibration are presented in table 5. The seven identified anisotropy parameters along with *a* and *k*, for the plane stress condition, are presented in table 6. The resulting yield surfaces at 400°C are shown in figure 11, for different values of *a* and amount of shear stress $\sigma_{12}/\bar{\sigma}$. In figure 12 the predicted initial yield stress $\sigma_Y$ and R-values are compared with measured values, for different angle directions with referenced to the rolling direction (α).

Table 5.
Calibration data for Ti-6Al-4V at different temperatures. Initial yield stress, $\sigma_\alpha$, in [MPa]

| | $\sigma_{00}$ | $\sigma_{45}$ | $\sigma_{90}$ | $\sigma_b$ | $\sigma_{C00}$ | $R_{00}$ | $R_{45}$ | $R_{90}$ | $R_b$ |
|---|---|---|---|---|---|---|---|---|---|
| RT | 1000.0 | 972.0 | 1020.0 | 1093.8 | 1106.3 | 0.4 | 1.19 | 0.61 | 1.0 |
| 400°C | 681.0 | 591.0 | 691.0 | 744.9 | 753.4 | 0.6 | 1.26 | 0.512 | 1.0 |

Table 6.
Cazacu et al. parameter values for Ti-6Al-4V at 400°C.

| | $C_{11}$ | $C_{22}$ | $C_{33}$ | $C_{12}$ | $C_{13}$ | $C_{23}$ | $C_{44}$ | *a* | *k* |
|---|---|---|---|---|---|---|---|---|---|
| 400°C | 1.7268 | 1.74 | 1.849 | 0.762 | 0.653 | 0.663 | 1.321 | 2 | -0.255 |
| 400°C | 1.959 | 1.837 | 1.955 | 0.684 | 0.48 | 0.451 | 1.88 | 8 | -0.085 |

The elastic degradation i.e. the decreasing elastic modulus with plastic straining, is accounted for according to table 7 when applying the Cazacu et al. yield criterion in the FE analyses of the validation test at 400°C, presented in section 4.3.

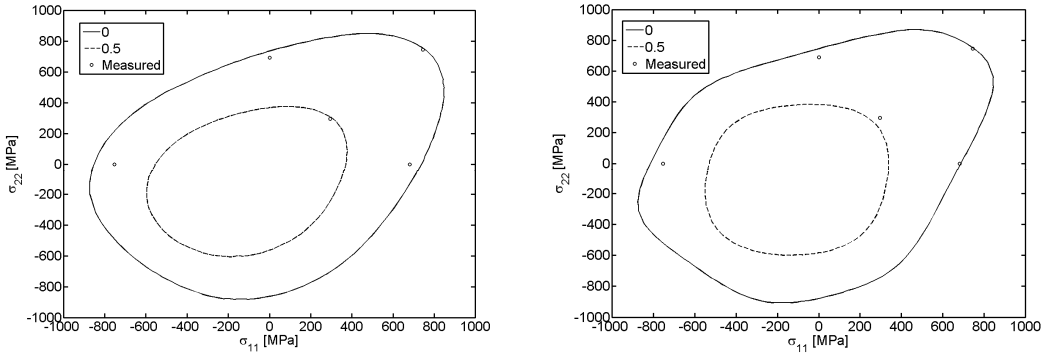


Figure 11. Titanium alloy Ti-6Al-4V yield surface at 400°C determined with seven anisotropy parameters together with $k$ and $a$ = 2 and 8, respectively. The Cazacu et al. criterion, for equal amounts of shear stress $\sigma_{12}/\bar{\sigma}$ .

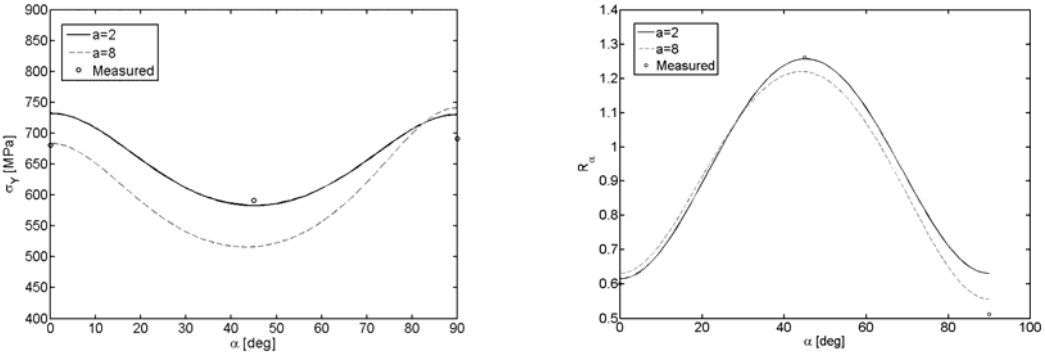


Figure 12. $\sigma_Y$ and $R_\alpha$ predicted and measured with seven parameters and indicated values of $a$.

Table 7.
Elastic degradation of Ti-6Al-4V in the (90) direction, determined at different true plastic strain levels in room temperature.*Scaled from room temperature data.

| *Alloy* | *Temperature [°C]* | *Direction* | *Young's modulus [GPa] at true plastic strain level [%]* | | | | |
|---|---|---|---|---|---|---|---|
| | | | *0* | *0.71* | *1.21* | *2.2* | *3.1* |
| 2 | RT | (90) | 120.8 | 120.7 | 119.3 | 116.7 | 114.2 |
| 2 | 400* | (00) | 98.30 | 98.22 | 97.08 | 94.96 | 92.93 |

For the isotropic assumption, the Barlat et al. (2003) yield criterion is applied, using the initial yield stress in the (00)-direction along with R-values equal to 1. The *m*-parameter is chosen to 2 and 8 obtaining the von Mises yield surface and a more Tresca-like yield surface, see figure 13.

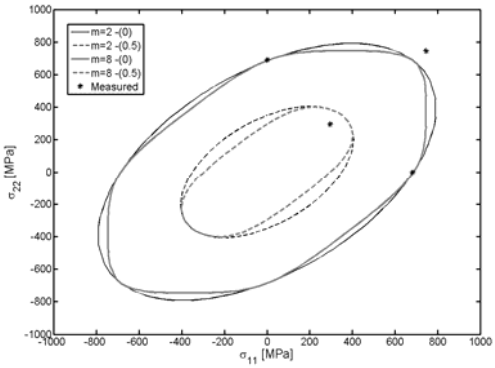


Figure 13. Titanium alloy Ti-6Al-4V yield surface at 400°C determined with an isotropic assumption for different values of the parameter *m* and equal amounts of shear stress $\left(\sigma_{12} / \bar{\sigma}\right)$.

## 3.3 Plastic instability

In sheet metal forming several failure modes exists, such as

1. Strain localisation
2. Fracture
3. Wrinkling
4. Shape distortion

In this work, the failure modes that have been the main topics are strain localisation and shape distortion.

When the force increases and it can not be compensated by hardening of the material, this leads to strain localisation and fracture. Several studies have been performed in which the phenomenon is described by plastic instability theory, e.g. Hora et al. [47]. In material failure caused by plastic instability, diffuse necking is followed by localised necking.

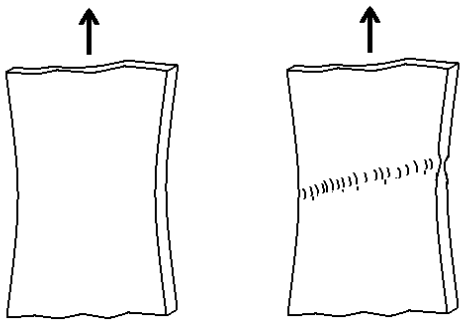

Figure 14. Schematic illustration on the development of diffuse and localised necking upon tension, respectively.

Diffuse necking is accompanied by strain localisation and a contraction of the specimen width which is generally not visible. This can however be identified trough an engineering measure, in which the force reaches a maximum value. In the local instability, the strains localise in the thickness of the sheet referred to localised necking. Beyond this point, the deformation is concentrated to this area and the strain increases rapidly until rupture, see illustration in figure 14.

The yield criterion is one important part of the material model, considering accurate predictions of the onset of strain localisation [30].

# 4. Virtual tool development

Before sophisticated tools for construction and numerical methods in combination with adequate computer capacity were available, the development of products and manufacturing techniques were time consuming, expensive and inexact processes. The tryout of new manufacturing processes was, and still is to some extent, complicated in which the trial and error process are performed using physical prototype tools. Considering sheet metal forming, new components, new materials or even a different sheet thickness, often resulted in that a loop of changes had to be made. In order to change responses obtained in a forming process such as problems regarding springback, wrinkling, strain localisation or even formation of cracks, major changes in the tool concept are often required. In worst case, completely new tools are necessary. It is obvious that a large amount of failed components and tools are produced in such procedures. At the same time, modifications in already manufactured tools are not always easy to perform.

Today, virtual product and process design is common in modern industries with a developed technology level. Problem areas are identified and improvements are made in an early stage. In e.g. the automotive industry, the FE technique for analyses of product functionality and sheet metal forming procedures is a valuable tool, for studies of crashworthiness and passenger safety but also to improve tool designs for the production of car body components and load carrying features. Further on, CAE tools for construction, component assembling and machining are most useful tools.

In the aero engine industry, numerical analyses are applied in e.g. the field of aerodynamics, life time analyses, fatigue and simulation of manufacturing processes such as welding. The benefit of performing virtual development is obvious, where the try out can be kept minimal and ideally the development process should be of a direct-hit character. That is, a new component in a previously not experienced material can be produced within tolerances and where the need for any changes to be made in the manufactured tools or techniques is minimal.

The direct-hit vision can be considered a long term goal. The predicted behaviour or outcome considering sheet metal forming processes is a direct result of used methods and models and their capability to describe the reality such as, the material behaviour, tool geometries, contacts and friction, boundary conditions and heat transfer, among others. At the same time there always exists a deviation between the virtual FE model and the reality.

Nevertheless, it has been shown in work by many, that accurate correlations between calculated and measured responses can be obtained. The usage of proper methods and models along with accurate model calibration, in combination with the maintenance of similar conditions in the analysis and experimental setup can be considered key features. Material characterisation and constitutive modelling is an area of research focus, in order to include the observed behaviour for different materials to increase the accuracy of predicted responses. The temperature adds an extra dimension to the problem.

In the following sections some of the experimental observations and numerical prediction of hot sheet metal forming of titanium and Inconel 718 are presented. The initial U-bend tests on Ti-6242 are followed by a presentation of the proposed short lead time methodology for tool design, compensation and validation. The previously presented yield criteria are applied in two different hot forming applications where two Ti-6Al-4V prototype components are produced. The predicted punch force, draw-in, shape deviation and also strain localisation is compared with experimental observations. Finally, some benefits and aspects of performing coupled thermo-mechanical FE analyses in the design of hot forming procedures for titanium are illustrated and discussed.

## 4.1 Experimental foundation and initial studies

To experimentally study the influence of process parameters, such as temperature, punch speed and friction along with rolling direction on the response during sheet metal forming of titanium, U-bend tests were performed. The setup consists of heated punch and die geometries, designed with respect to the minimum bend radius in room temperature [8]. Forming tests are performed, with different starting temperatures and holding times where rectangular sheet metal specimens are formed into a hat profile. Figure 15, presents a forming case in which a room tempered sheet specimen of Ti-6242 is cold formed. Fracture occurred when forming was performed in room temperature or when the blank had been exposed to temperatures over the beta transus temperature.

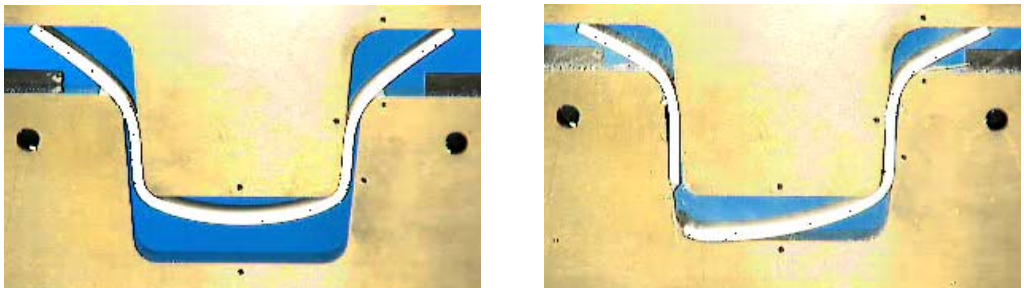

Figure 15. Fracture characteristics during forming sequence for the test with forming velocity 5 mm/s, (L). Loading and first fracture, respectively.

The forming procedure was successful at elevated temperatures. Generally, an increased deformation rate had a negative influence on the formability, likewise for blanks extracted along (00) the rolling direction. Examples of the measured forming force are presented in figure 16.

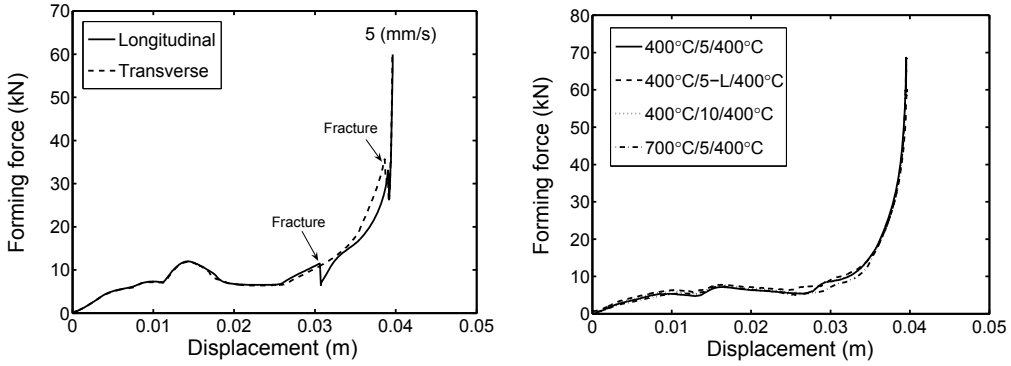


Figure 16. Punch force vs. stroke displacement at indicated forming velocities and extraction directions of sheet specimens. In the first figure forming take place in room temperature and in the second figure at indicated initial temperatures (sheet specimen start temperature/forming velocity/tool temperature).

The springback behaviour alters when the sheets are formed with a starting temperature of about 700ºC, compared to forming with a blank starting temperature of about 400ºC, cf. figure 17. The minimum springback was obtained by hot isothermal forming at 400°C applying a subsequent holding time of 15 minutes in heated forming tools (400°C).

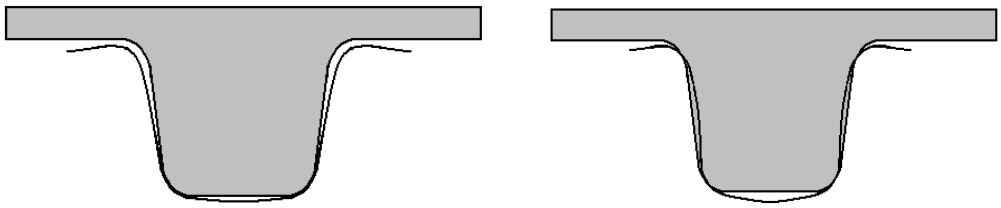

Figure 17. Schematic illustration of final shapes of formed sheet specimens with a starting temperature of approximately 400ºC and with a starting temperature of approximately 700ºC, respectively.

An FE analysis of the isothermal test performed at 400°C is conducted. The FE-model and predicted punch force are presented in figure 18 and 19, which show quite good correlations with measured values. The Nemat-Nasser et al. (2001) constitutive equation is used to describe the material hardening, assuming an isotropic von Mises yield surface and isotropic hardening. The specimen in the Gleeble test and in the U-bend test is extracted transverse (90) the rolling direction. Predictions of the springback, is presented in figure 20.

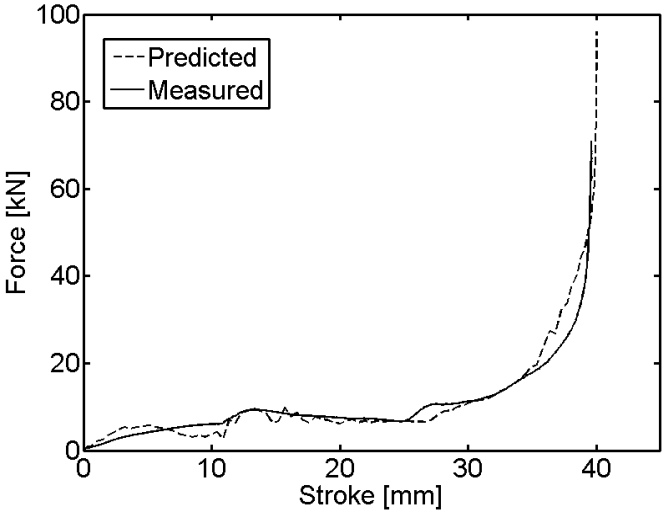


Figure 18. Measured and predicted punch force assuming a friction coefficient of 0.3 and the Nemat –Nasser model.

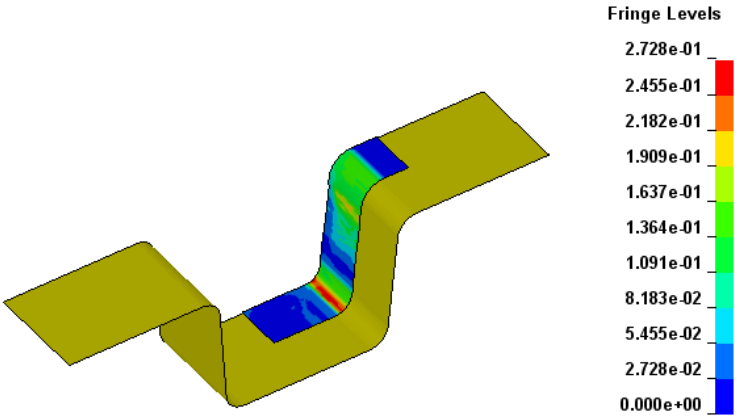


Figure 19. FE model of the U-bend tests performed isothermally at 400ºC, effective plastic strain distribution.

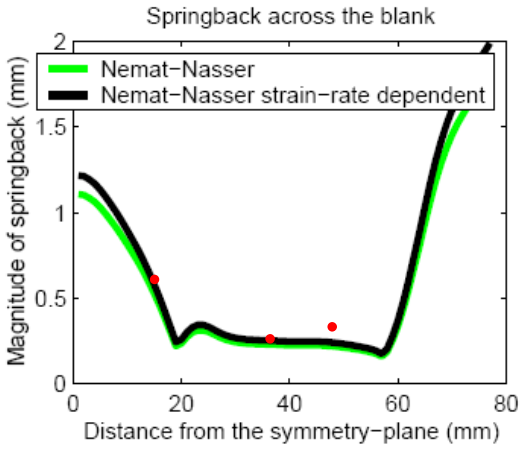


Figure 20. Measured (red dots) and predicted springback for the isothermal forming at 400ºC [48].

## 4.2 A short lead time methodology

As discussed before, a successful development of forming techniques for new materials in the modern industry must be time and cost effective, yet accurate. The ability to realize successful projects with short lead times has become increasingly important for the forming industry today. By chance of performing a commercial development project, a systematic way of working with the design, compensation and manufacturing of deep drawing prototype tools generating high quality components at an extremely short lead time was

suggested. Tool development for five different sheet metal components in the nickel based alloy Inconel 718, were initiated by Volvo Aero Corporation.

The aerospace industry demands extremely high safety and reliability. Thus, good knowledge is required regarding the effects of the manufacturing process on the material and the influence on the resultant properties through the complete manufacturing chain of the fabrication process. Analyses of sheet metal forming can provide with information on formability, shape deviation, resultant mechanical properties and residual stress state. Information which is important input to analyses of subsequent manufacturing processes such as welding and heat treatment.

When the lead time is of significant importance, finding time efficient and functional solutions applicable to the process of interest is crucial. Concerning sheet metal forming and prototype deep drawing tools, the design, manufacturing and the test stamping procedure are the main time-consuming activities. In order to keep the lead time short, the die tryout needs to be kept at a minimum. Through material testing and virtual tool design, in which CAD generated forming concepts are evaluated, secured and optimized by means of FE analyses, the best starting position for the tool manufacturing were obtained. Based on the chosen methods and models, the virtual components are within shape and thickness tolerances. In contrast to the U-bend tests, geometries of included sheet metal parts of complete load carrying aero engine structures are commonly smooth and double-curved. In combination with the anisotropic and high strength plastic properties of Inconel 718 in room temperature, a different forming setup had to be considered. Hot forming was not an option in the commercial project. See figure 21 for a schematic illustration of the tool setup.

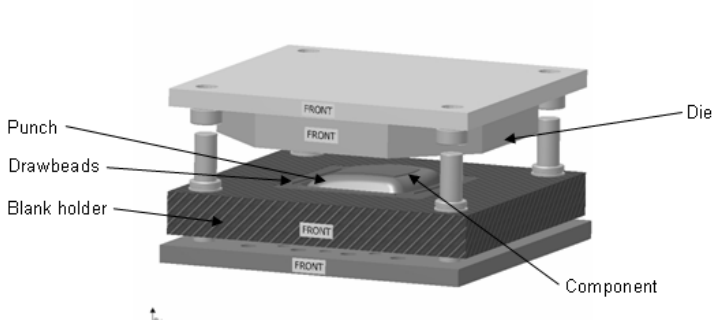


Figure 21. Schematic illustration of the tool setup.

The suggested forming concepts were secured and optimized with respect to sheet metal formability, material thinning and shape deviation. The springback of each component were reduced by performing changes in the virtual tool

concepts, such as in the geometry of the punch and die, punch radii, draw bead geometry and location, draw radii, draw depth and blank holder force. Remaining shape deviation was compensated for, if necessary, with the FE-tool using the *INTERFACE_COMPENSATED_NEW capability in LS-DYNA v971. The BARLAT_YLD2000 material model [34] was used with eight model parameters to describe the yield surface, accounting for the anisotropy of the alloy. The yield stress, the hardening and the Lankford parameters were determined by uniaxial tensile tests and a silicon rubber bulge test for the balanced biaxial stress state together with non-destructive dynamic tests on the Young's modulus. Forming limit tests (FLC) were performed to study strain localization limits. The m-parameter was set to a value of 8, which is a typical value for materials with an *fcc* crystal structure [34].

The design phase was divided into four main steps:

i. *Drafting stage* - generation of preliminary forming concepts.
ii. *Evaluation stage* - securing the forming concepts with respect to strain distribution and strain localization limits.
iii. *Improvement stage* - improving the forming concepts to minimize springback and shape deviation. The target is virtual components within thickness tolerance and if possible, also within shape tolerance.
iv. *Compensation stage* - compensating for the remaining shape deviation, if necessary. The target is virtual components within shape and thickness tolerances.

Schematic flow charts of the complete design phase and compensation stage are presented in figure 22 and 23.

The lead time associated with tool manufacturing is another important activity to consider. The choice of tool material and aspects such as delivery time, the need for subsequent through-hardening and the machinability is of importance. Concurrently, the manufacturing phase was initiated parallel with the design phase, in which certain dimensions were frozen early in the project to gain time. During the tool manufacturing and assembly, certain check points were included. Thus, features which were of special importance for the forming procedure were checked and approved during the specific manufacturing process or assembly stage associated to it.

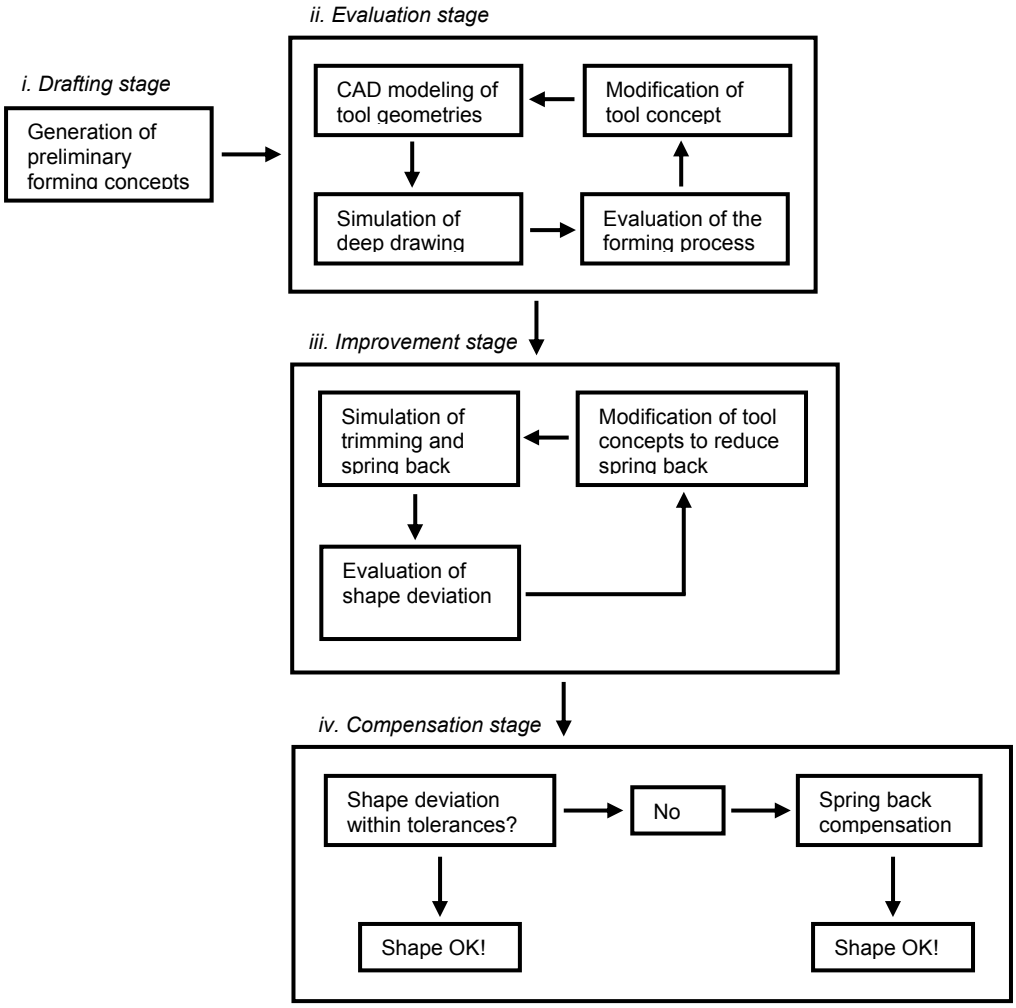


Figure 22. Schematic flow chart of the design phase.

The methodology comprises material characterization, tool design and tool material selection, analyses of sheet metal forming (FE-analyses), springback compensation, tool manufacturing, choice of lubricant, prototype stamping, laser cutting and laser scanning for shape deviation determination. The procedure is a completely CAE-controlled process, in which time consuming and inexact manual die tryout could be kept at a minimum.

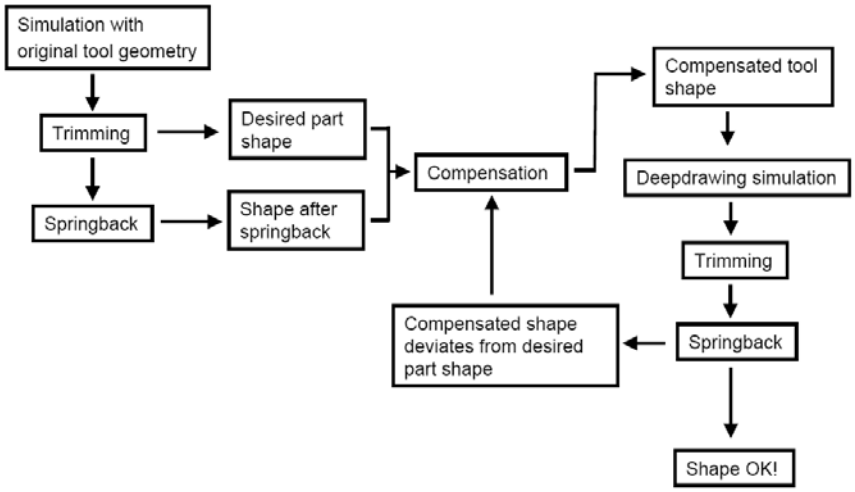


Figure 23. Schematic flow chart of the compensation stage, the springback compensation.

By working according to the presented methodology and paying special attention to obtaining equal conditions in the analyses and the test stamping procedure, all five sheet metal components were produced successfully in 15 weeks. No or minor modifications of the manufactured tools were required in order to produce components within tolerance. The predicted and measured shape deviations for a section of two of the five components (A and B) are presented in figure 24 and 25. The tool surfaces for component B, were compensated for spring back in which the shape deviation was predicted within the sheet thickness. A value of 1.0 corresponds to 100% of the original sheet thickness.

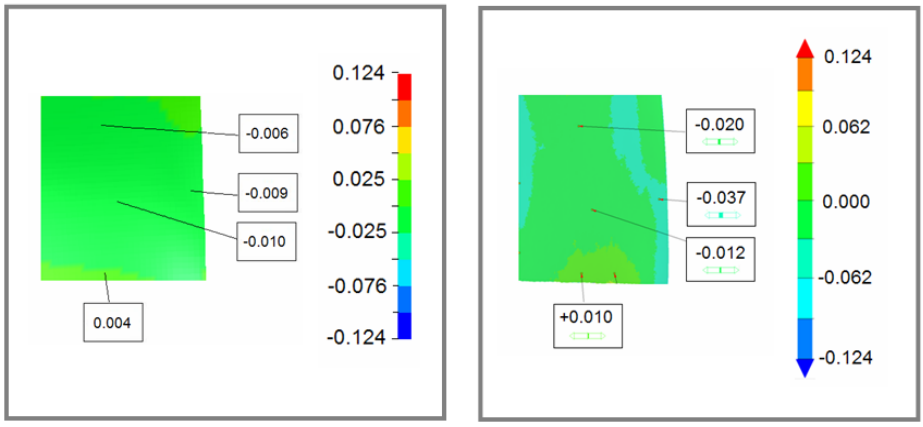


Figure 24. Shape deviation generated by FE-analysis and laser scanning with best fit CAD evaluation for a section of (A), respectively.

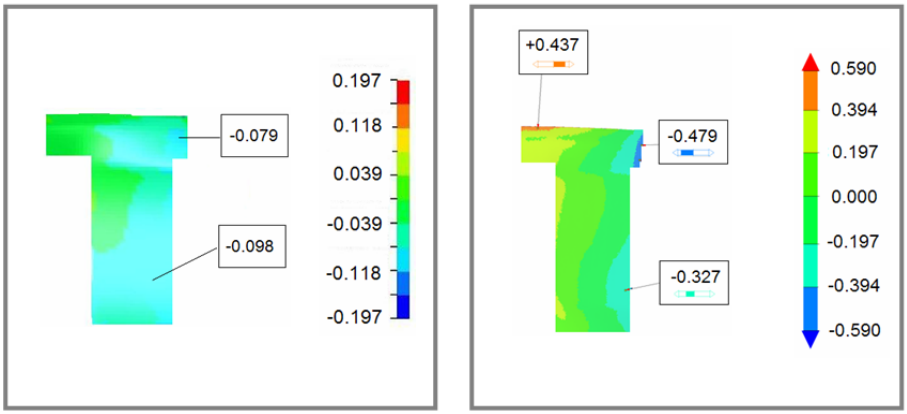


Figure 25. Shape deviation generated by FE-analysis and laser scanning with best fit CAD evaluation for a section of (B), respectively.

## 4.3 Tool development based on FE analyses

Based on the short lead time methodology, tool concepts for the two titanium prototype components are presented. The material characterisation and yield surface calibration of Ti-6Al-4V previously presented are used in the development process in order to evaluate the applicability of chosen models.

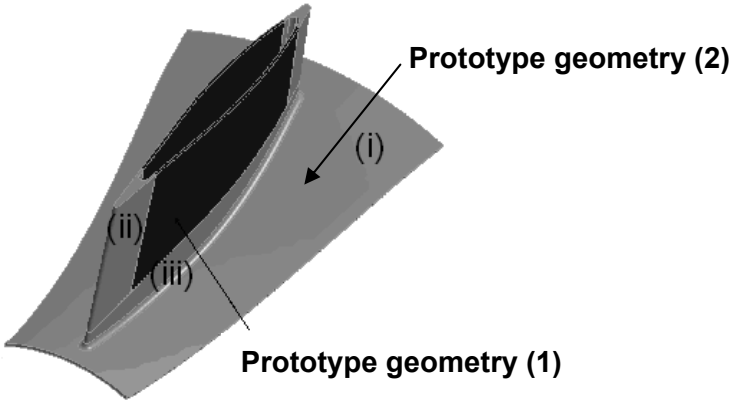


Figure 26. Schematic illustration of the Ti-6Al-4V subcomponent with sheet metal parts.

The geometry of the components can be found in figure 26 and paper D and F, respectively. The suggested hot forming concepts are based on hot inner tool parts, with the capability of controlling the temperatures of the individual parts, according to figure 27 and 28. Both forming procedures can be designated stretch forming operations in which a minimal draw-in is desired. Flat binder surfaces are compared with edge bending features. A large binder area, i.e. a

large blank size, is chosen for both components due to limitations in available blank holder force. The prototype tools are manufactured partly to investigate the functionality of chosen materials and tool features, (including tool and insulation material, regulation and temperature distribution) and partly to compare predicted values of punch force, draw-in, shape deviation and the occurrence of strain localisation with measured values. Further on, the titanium sheet metal components functions as parts of a subcomponent in which the sheet metal parts are welded together with small ingots and simple forgings at Volvo Aero Corporation. The tool functionality was found satisfactory for research and prototype applications.

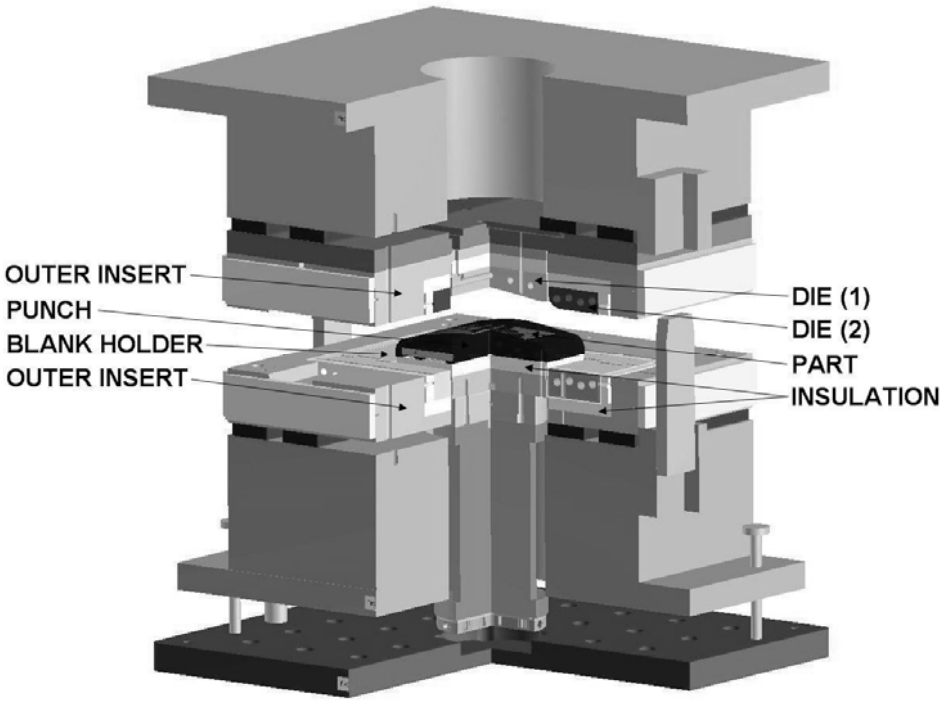


Figure 27. CAD-illustration of the tool concept for hot forming of Ti-6Al-4V.

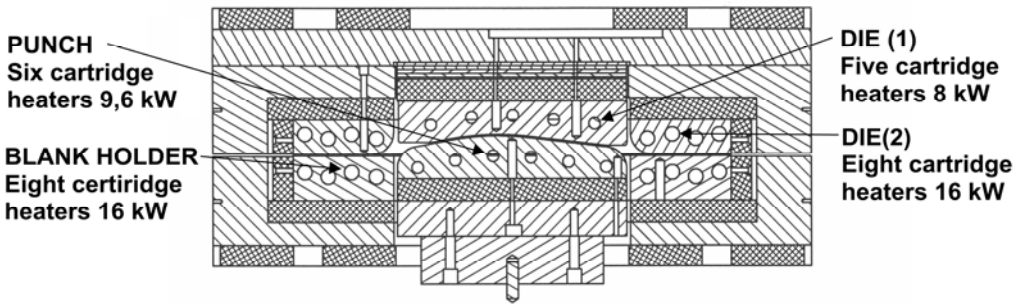


Figure 28. Location of cartridge heaters and total power output in one of the hot forming tools.

The shape of the yield surface was found important to the ability to predict strain localisation and shape deviation accurately. Considering component (1), the predicted punch force and shaped deviation correlates with acceptable accuracy with measured values when the anisotropy is considered, cf. figure 29 to 31. The Barlat et al. (2003) yield criterion was applied with six anisotropy coefficients and assuming isotropic hardening.

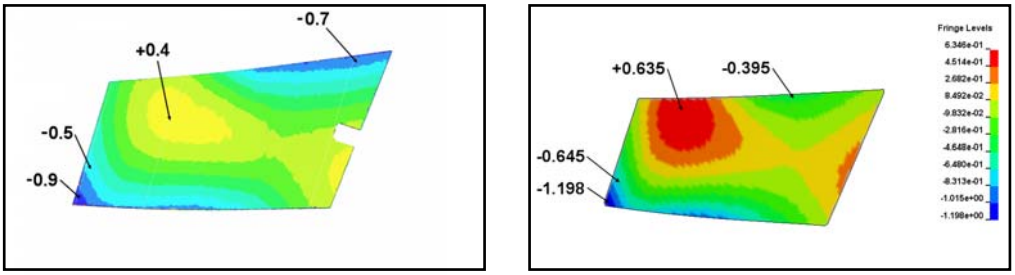


Figure 29. Measured and predicted shape deviation [mm] of the prototype component (1) formed at 400°C, using anisotropic data.

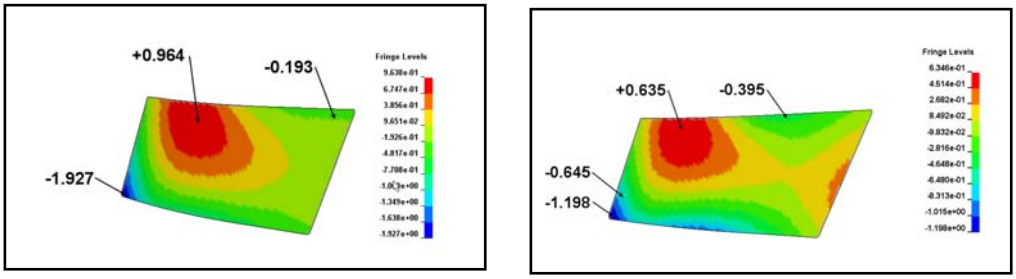


Figure 30. Predicted shape deviation [mm] at 400°C of the prototype component, using isotropic (90) or anisotropic data.

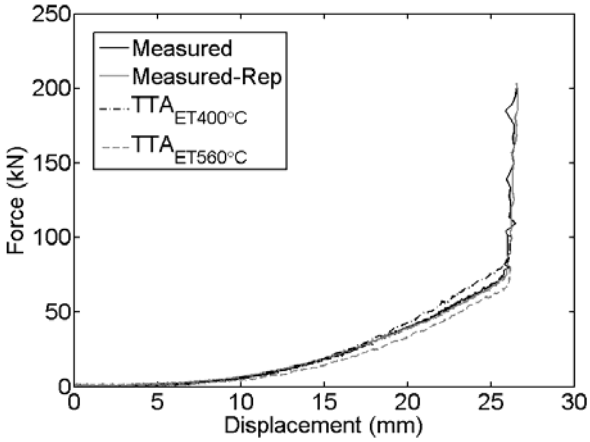


Figure 31. Measured and calculated punch force at 400°C isothermal hot forming of component (1).

During the hot forming of the double-curved prototype component (2) in alloy 2, strain localisation occurred, see figure 32.

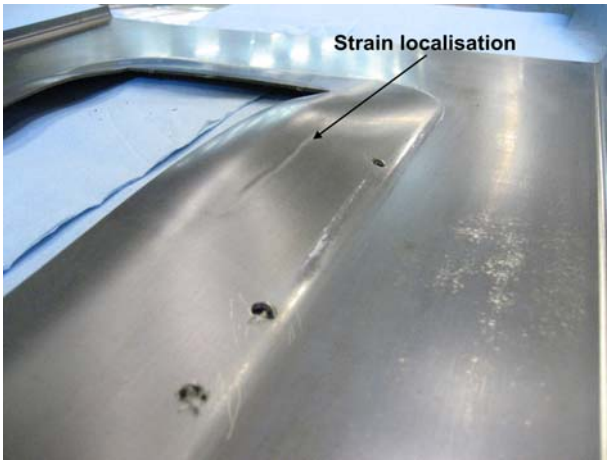


Figure 32. Photograph of the strain localisation which occurred in the hot forming of the Ti-6Al-4V sheet metal component (2).

The Barlat et al. (2003) yield criterion is applied for different values of the *m*-parameter. FE-analyses applying the Barlat et al. yield criterion do not fully capture the strain localisation observed in the validation test.

Applying the Cazacu et al (2006) yield criterion with a low *a*-value ($a = 2$) gives a close prediction of the occurrence and location of the observed strain localisation. A high value of the *a*-parameter does not result in any strain

localisation. The predicted draw-in with a value of the *a*-parameter equal to 2 gives the closest match see table 8. Hence, a value of the *a*-parameter equal to 2 is assumed to be suitable cf. figure 33.

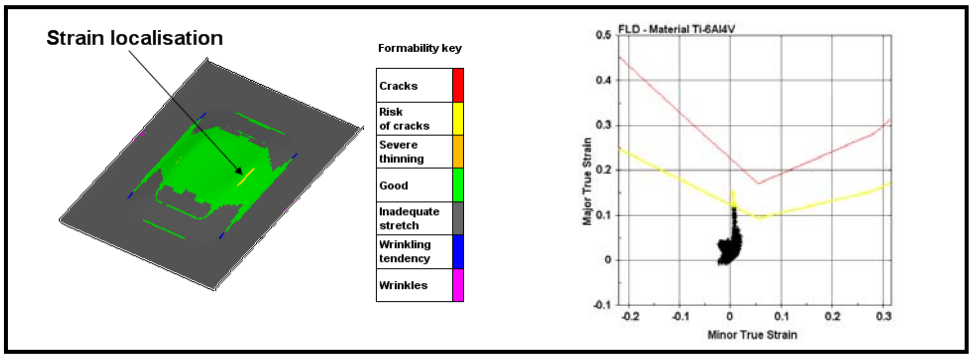


Figure 33. Formability and FLC plot for the forming test performed isothermally at 400°C, with the Cazacu et al. yield criterion assuming a value of *a* equal to 2.

Table 8.
Measured and predicted draw-in [mm] for the validation tests (VT) at 400°C. The applied yield criteria with different values of the *m*- and *a*-parameters, assuming a friction coefficient of 0.25.

| *Yield criterion* | *Parameter* | *Predicted draw-in* | *Measured draw-in* |
|---|---|---|---|
| Barlat et al. | $m = 2$ | 1.61 | 2.0 |
| Barlat et al. | $m = 8$ | 1.63 | 2.0 |
| Cazacu et al. | $a = 2$ | 1.97 | 2.0 |
| Cazacu et al. | $a = 8$ | 2.39 | 2.0 |

Assuming an isotropic yield surface, strain localisation occurs much too early leading to fracture, see figure 34. This was not experimentally observed.

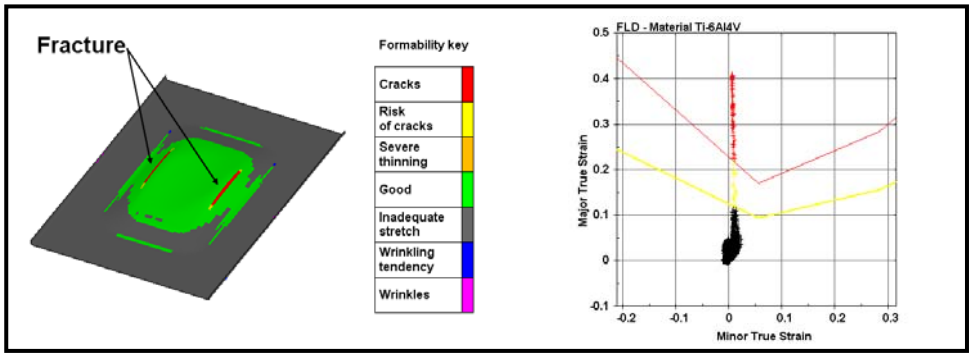


Figure 34. FLC plot for the forming test performed isothermally at 400°C, with an isotropic yield surface assumption and an *m*-value of 8.

The measured and predicted punch force is presented in figure 35, using the different yield criteria with the *a*- or *m*-parameter equal to 2.

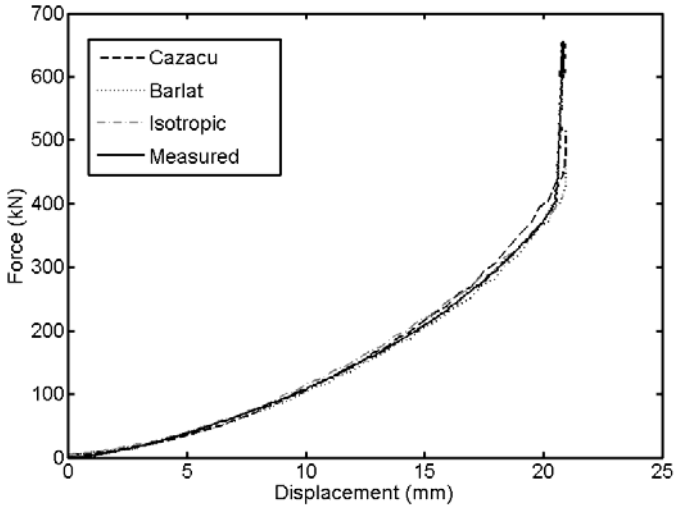


Figure 35. Measured and predicted punch force for the studied yield criteria, *m* and *a* equal to 2.

The measured shape deviations of the hot validation test (VT) for component (2) and of a hot sizing test (HST) are presented in figure 36, respectively. The measured maximum shape deviation is determined to (-0.626/+0.2) mm, excluding the corner at the upper left hand side of +0.75 mm for the validation test and to (-1.85/+1.74) mm for the hot sizing test. It is obvious that relaxation occur with time during the elastic deformation in the HST performed at 560°C with a holding time of 15 minutes. The shape deviation is however significant compared to the nominal geometry.

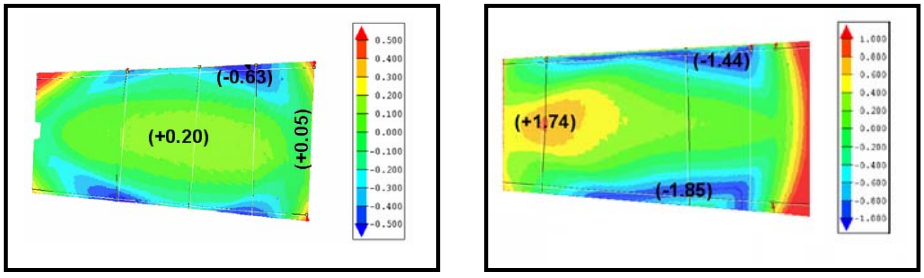


Figure 36. Measured shape deviation [mm] of the prototype component (2) formed at 400°C (VT) and crash formed at 560°C including a holding time of 15 minutes (HST), respectively.

The corresponding predicted shape deviations for the validation test (VT), depending on the used yield criterion and values of the *m*- or *a*- parameters, are presented in table 9. The effect of the cooling procedure in which the development of thermal stresses is included in the FE analysis, was found of importance for the magnitude of the shape deviation.

Table 9.
Predicted and measured shape deviation [mm] of the prototype component, neglecting or including the effect of the cooling procedure. The applied yield criteria with different values of the *m*- and *a*-parameters.

| *Yield criterion* | *Parameter* | *Predicted shape deviation* | *Predicted shape deviation including the cooling procedure* | *Measured shape deviation* |
|---|---|---|---|---|
| Barlat et al. | $m = 2$ | +0.15/-0.55/-0.13 | +0.30/-0.54/-0.05 | +0.20/-0.63/+0.05 |
| Barlat et al. | $m = 8$ | +0.07/-0.53/+0.15 | +0.16/-0.52/+0.24 | +0.20/-0.63/+0.05 |
| Cazacu et al. | $a = 2$ | +0.09/-0.63/-0.18 | +0.17/-0.62/-0.10 | +0.20/-0.63/+0.05 |
| Cazacu et al. | $a = 8$ | +0.20/-0.63/+0.00 | +0.26/-0.60/-0.19 | +0.20/-0.63/+0.05 |

The predicted shape deviation are comparative to the measured values, considering the Barlat et al. (2003) yield criterion, with the exception of the measured deviating corner on the upper left hand corner, see figure 37. The predicted shape deviation is in close match with the measured values, using the Cazacu et al. (2005) yield criterion, see figure 38. Note that the shape deviation distribution correlates well with the measured, again with the exception of the upper left hand corner.

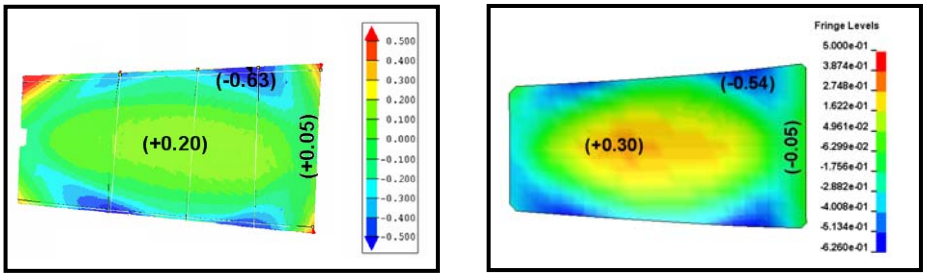


Figure 37. Measured and predicted shape deviation [mm], respectively. Barlat et al. (2003) yield criterion (*m*=2).

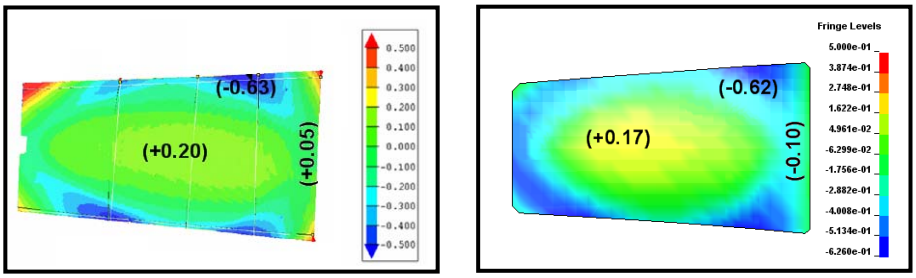


Figure 38. Measured and predicted shape deviation [mm] , respectively. Cazacu et al. (2006) yield criterion ($a$=2).

## 4.4 Anisotropic elasticity – a parametric study

The elastic properties of Ti-6Al-4V were studied using the non destructive excitation technique using the Resultant Frequency and Damping Analyser (RFDA) system 23 by IMCE [49, 50]. The tests show different pronounced elastic anisotropy in room temperature depending on the material batch of Ti-6Al-4V, purchased from different suppliers, as presented in table 10.

Table 10.
Elastic properties of Ti-6Al-4V. Temperature in [°C] and Young's modulus in [GPa].

| *Alloy* | *Test method* | *Temperature* | *Young's modulus* | | |
|---|---|---|---|---|---|
| | | | *(00)* | *(90)* | *(45)* |
| 1 | RFDA | RT | 109 | 130 | 116 |
| 2 | RFDA | RT | 118.8 | 119.9 | 117.2 |
| 2 | $T_{RT}$ | RT | 118.6 | 120.8 | 119.9 |
| 2 | RFDA | 250 | 106.7 | 109.0 | 105.9 |
| 1 | RFDA | 400 | - | 97 | - |
| 2 | RFDA | 400 | 98.3 | 101.0 | 97.3 |
| 2 | RFDA | 560 | 90.0 | 92.5 | 89.0 |

For the weak elastic anisotropy of alloy 2, isotropic elasticity may be considered as a valid assumption. However, the pronounced anisotropic behaviour of alloy 1 may be important to consider. To evaluate the influence of the elasticity on predictions of shape deviation, a rather straight forward parametric study is performed. Isotropic elasticity with different values of Young's modulus is assumed. That is, Young's modulus is altered with the values of alloy 1 in the (00), (45) and (90) direction during the simulations of the sheet metal forming and springback, respectively. The plastic behaviour is held constant according to the properties of alloy 2 at 400°C. The parametric

study is performed using the Barlat et al. (2003) yield criterion, using six anisotropy coefficients for the hot forming concept of component (2).

The parametric study indicates that a pronounced anisotropy in Young's modulus has a clear impact on the predicted shape deviation. The predicted maximum shape deviation is presented in table 11. The elastic part of the total strain over the component area is quite large, see examples in figure 39. An orthotropic description of the elastic properties may be justified when considering alloys with pronounced elastic anisotropy.

Table 11.

Parametric study of the influence of anisotropic elasticity (alloy 1) on predicted maximum shape deviation [mm].

| *Forming analysis, E (dir)* | *Analysis of trim and springback, E (dir)* | *Maximum shape deviation* | *Deviation from reference (90-90)* |
|---|---|---|---|
| (00) | (00) | 0.7302 | 0.944 |
| (00) | (45) | 0.6862 | 0.887 |
| (00) | (90) | 0.6116 | 0.791 |
| (45) | (00) | 0.8662 | 1.120 |
| (45) | (45) | 0.8135 | 1.052 |
| (45) | (90) | 0.7251 | 0.938 |
| (90) | (00) | 0.9253 | 1.197 |
| (90) | (45) | 0.8684 | 1.123 |
| (90) | (90) | 0.7732 | 1.000 |

## 4.5 The temperature as a process parameter

The mechanical properties of Ti-6Al-4V is characterised by anisotropic low elasticity in combination with high strength anisotropic plasticity. This, in addition with the asymmetry in yielding between tension/compression and the quite low formability in room temperature imply difficulties considering sheet metal forming of double-curved geometries. Conventional forming techniques of such components often imply concentration of plastic straining within the blank, such as over draw bead geometries, in draw radius and over the punch geometry, see figure 39 for a couple examples.

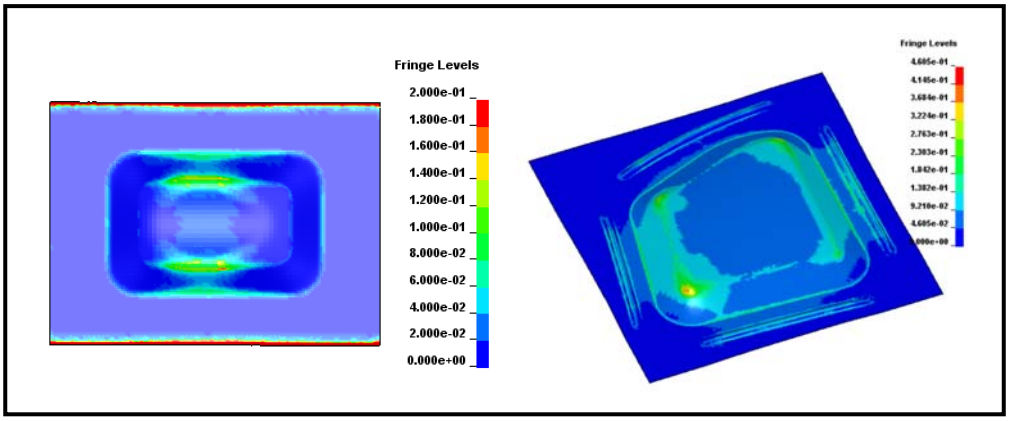


Figure 39. Illustration of the effective plastic strain distribution obtained by sheet metal forming of smoothly double-curved components in titanium and aluminium, respectively.

By increasing the temperature, the formability can be improved and the yield stress decreased. However, in the higher temperature range the flow softening behaviour may add to the strain concentration effect upon increasing temperature. To be able to model such material behaviours in an accurate manner, it is necessary to include models such as for phase transformation and creep/stress relaxation including the effects of strain rate.

However, suppose that the possibility to control the temperature within the forming tool are utilised. Then the global material responses caused by e.g. flow softening which is initiated at certain strain levels, may be prevented by applying a tailored cooling. Cooling in desired regions, such as in blank holding areas or in other areas where concentration of plastic straining naturally occur ought to be beneficial in combination with modifications of the tool geometries and blank holding features. Likewise, the decrease in yield stress and altered mechanical properties due to temperature and phase changes may be taken advantage of. For example, by controlling the temperature, the deformation can be directed to desirable regions such as in the component area, see the first picture in figure 41, in order to obtain sufficient plastic straining and thereby reduce the springback and its scattering characteristics of titanium alloys.

Some of these features are illustrated using a forming procedure similar to that of component (1), as described previously. See figure 40. By performing coupled thermo-mechanical analyses and using a blank geometry which naturally concentrate plastic straining in the component area, the desired and directed strain distribution effect can be enhanced by applying a comparatively

higher forming temperature of the punch. An increased level of plastic straining, or an increased area which is plastically deformed, can be obtained (Case I and II) in table 12.

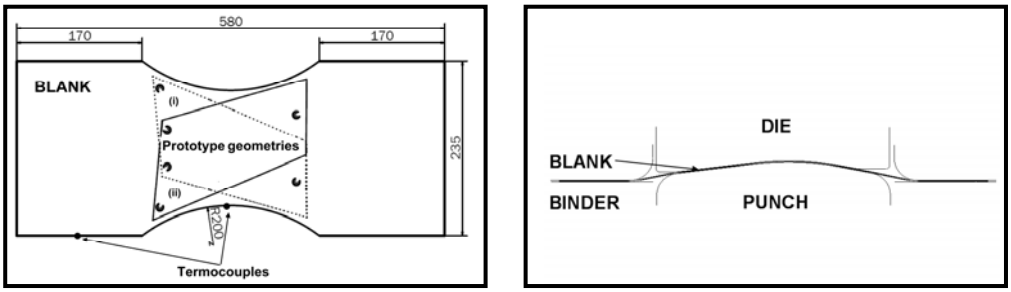


Figure 40. Illustration of blank size with locations of the prototype geometries (1) in Ti-6Al-4V and set up for the hot forming concept.

The initial blank and tool part temperatures are defined for four cases, I-IV, presented in table 12 with reference to figure 27 and 40. The tool part temperatures are considered homogeneous and constant during the forming procedure due to the feedback control system in which the temperatures are regulated with respect to desired temperature values. In the coupled thermo-mechanical analyses the von Mises yield criterion assuming isotropic hardening is applied. Young's modulus, the yield stress and hardening used in the temperature range of 20-560°C are the same as applied in the (00)-direction of paper F. For higher temperatures, compressive flow data of Ti-6Al-4V presented in [12] are applied. Thermal properties of Ti-6Al-4V regarding Poisson's ratio, coefficient of thermal expansion, specific heat and thermal conductivity are found in the literature [7]. Extrapolated data are used for temperatures out of range of those presented. A heat transfer coefficient of 2000 $Wm^{-2}K^{-1}$ is applied for the tool-blank interface, according to the performed heat transfer test described in paper E.

Table 12.
Definition of temperature [°C] cases for coupled thermo-mechanical analyses.

| *Case* | *Initial blank temperature* | *Tool part temperature* | | | |
|---|---|---|---|---|---|
| | | *DIE 1* | *DIE 2* | *PUNCH* | *BINDER* |
| I | 560 | 560 | 400 | 560 | 400 |
| II | 800 | 800 | 400 | 800 | 400 |
| III | 400 | 800 | 400 | 800 | 400 |
| IV | 400 | 400 | 800 | 400 | 800 |

The predicted final temperatures and effective plastic strain distribution, respectively for the different cases are shown in figure 41 and 42. The calculated response shows that the shape deviation is reduced by locally increasing the temperature over the component area, cf. figure 44 and 45. In contrast to applying comparatively high temperatures in binder regions causing strain localisation which lead to fracture (Case IV), a medium range temperature in the binder area is found beneficial. Locking features would be possible to form due to an increased formability compared to at room temperature, and a reduction of the required holder force is obtained due to the comparatively lower force requirement for plastic yielding to occur in the component area. This would imply that the blank size geometry can be optimised with respect to the available blank holder force, strain localisation and resultant shape deviation.

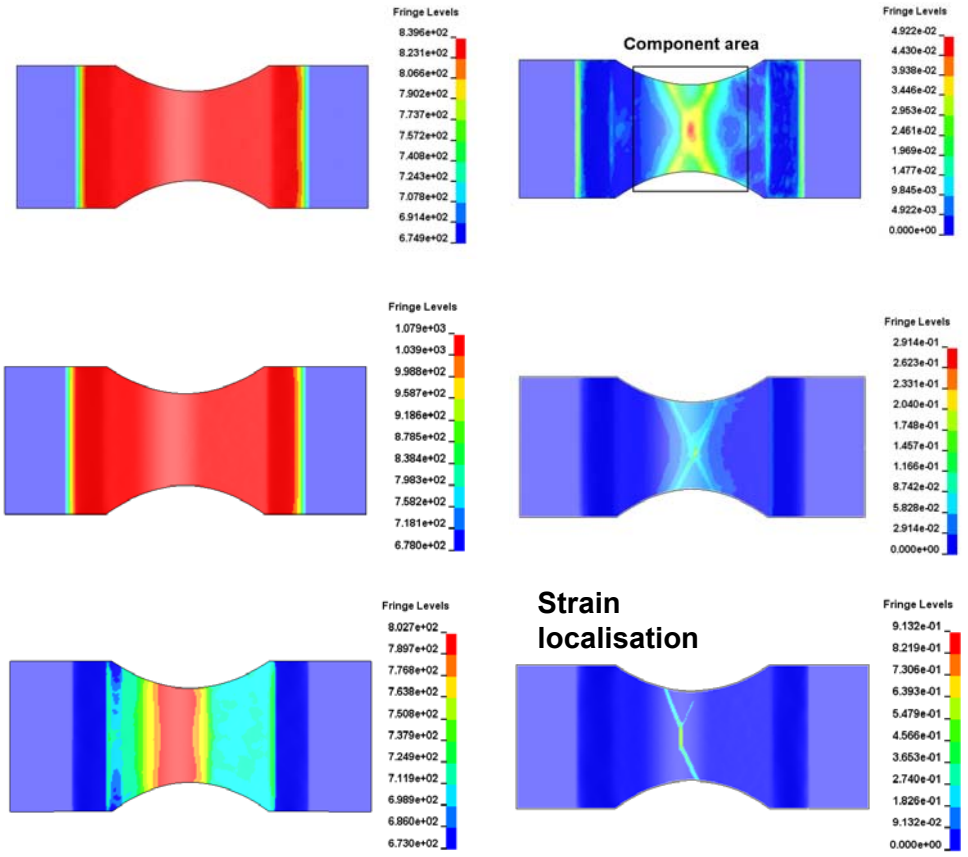


Figure 41. Predicted temperature [K] and effective plastic strain distribution at the end of the forming procedure of the prototype component (1), formed with different starting temperatures according to case I-III, respectively.

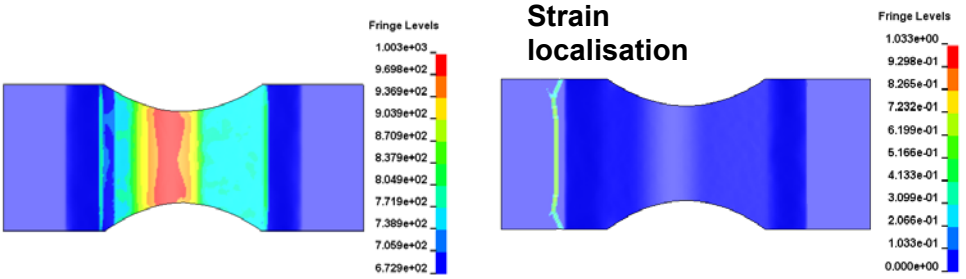


Figure 42. Predicted temperature [K] and effective plastic strain distribution at the end of the forming procedure of the prototype component (1), formed with different starting temperatures according to case IV, respectively.

The corresponding FLC plots for case II and III are presented in figure 43.

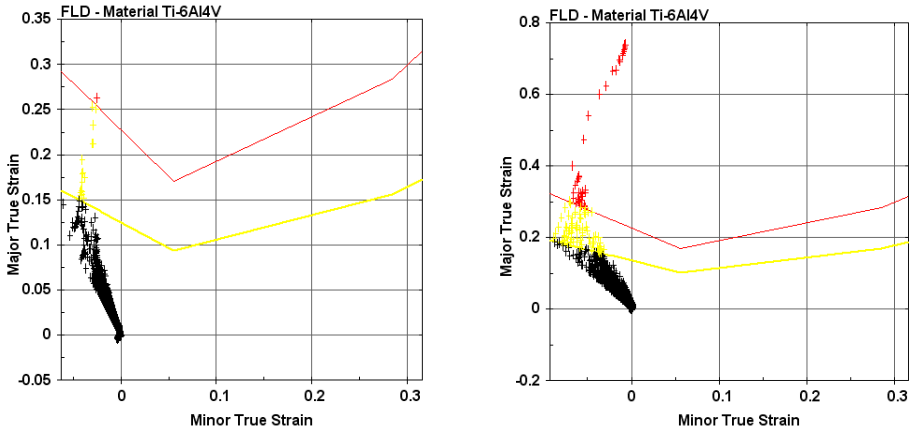


Figure 43. FLC plots for case II and III, respectively.

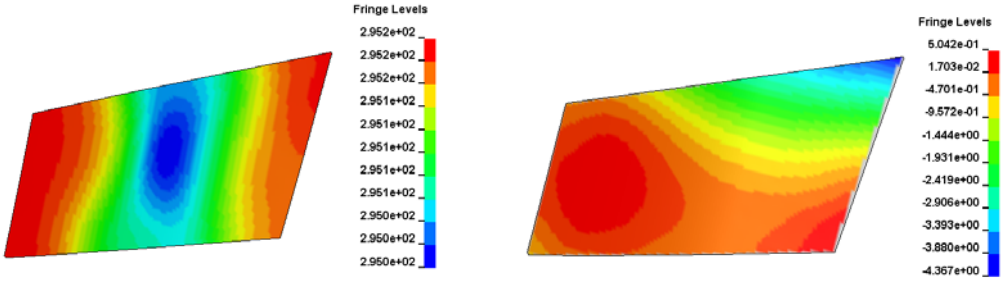


Figure 44. Predicted temperature and shape deviation after forming, cooling and trimming of the prototype component (1) formed according to case I, respectively.

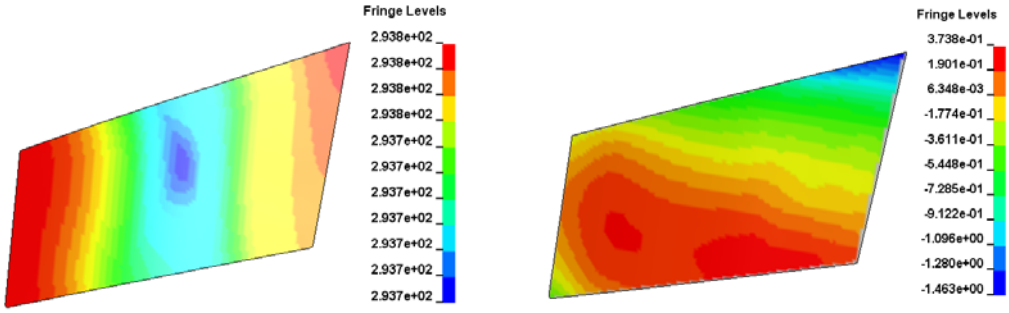


Figure 45. Predicted temperature and shape deviation after forming, cooling and trimming of the prototype component (1) formed according to case II, respectively.

When applying an elastic or plastic deformation to Ti-6Al-4V at elevated temperatures, stress relaxation or creep occur. By considering models for anisotropy, phase transformation and relaxation in coupled thermo-mechanical analyses the benefit of studying the temperature – and time as process parameters, would be most valuable.

In this section, the isotropic von Mises yield surface with isotropic hardening was assumed in the performed coupled thermo-mechanical analyses. The assumption was shown to predict failure too early in the forming procedure of component (2).

# 5. Summary of appended papers

## 5.1 Paper A

In this paper, an investigation of the use of inverse modelling for estimation of material model parameters is presented. The compression tests are performed on cylindrical specimens of forged Ti-6Al-4V, using the Gleeble test method. The results indicated that initial material hardening was followed by specimen cracking at lower temperatures while at 700˚C and 900˚C material hardening was followed by flow softening. The alloy was also found to be strain rate sensitive. The ability of three different constitutive equations to describe the inelastic thermo mechanical hardening behaviour of Ti-6Al-4V has been examined but none of them were found able to describe it satisfactorily. However, it was shown that inverse modelling is a viable way to determine relevant material parameters, if suitable functions are chosen. Changes in the microstructure as a consequence of heat treatment and deformation were also investigated. In general, it was found in cross sections parallel to the loading direction, that the deformation was non-uniform and concentrated in bands going diagonally from one corner to the other. The alpha platelets in the Widmanstätten structure were increasingly broken up going from the less deformed anvil contact region into the more deformed centre of the specimen.

## 5.2 Paper B

In this paper, the thermo-mechanical response of a Ti-6242 alloy has been studied by elevated temperature compression tests together with cold and hot sheet metal forming tests for evaluation of the suitability of different cold and hot sheet metal forming processes. The compression tests were designed to function as input for estimation of material model parameters such as the parameters of constitutive equations. Furthermore, results from the forming tests can be used for correlation of finite element (FE) models in predictions of sheet metal forming. Experiments were performed at a broad range of temperatures and strain rates. The compression tests are performed at temperatures ranging from 400-900˚C and strain rates of 0.05-1 $s^{-1}$. The forming tests are performed at 20-1000˚C in both isothermal and non-isothermal forming, at forming velocities of 5 and 10 mm/s. The microstructures of as-received material and deformed specimens were examined using optical microscopy. Experimental results of the compression tests show that initial material hardening was followed by specimen failure where cracks have formed in deformation bands or by flow softening, depending on the temperature. Compressive true strains of 10 to 50% were achieved. The forming tests reveals that optimal forming conditions are a

combination of forming velocity, temperature and holding time. Hence increasing forming temperatures alone does not necessary imply better forming characteristics. A change in springback characteristics occurred at elevated temperatures. It can be concluded that, under the current conditions in this study, Ti-6242 is suitable to form by hot sheet metal forming where the minimal shape deviation occurred for isothermal forming at 400°C applying a holding time of 15 minutes.

## 5.3 Paper C

This paper presents a systematic methodology for the design and manufacturing of deep drawing tools generating high quality components at an extremely short lead time. Prototype tools for five different sheet metal components of the nickel based super alloy Inconel 718 were designed, manufactured and tested in 15 weeks. Two of these prototype tools (A, B) are the topics of this paper. The methodology is based on virtual tool design in which the tool concepts are secured and optimized with respect to sheet metal formability and shape deviation using FE-analyses. Tool surfaces are compensated for springback, if necessary, using the *INTERFACE_COMPENSATED_NEW capability in LS-DYNA v971 (B). The compensated FE tool surfaces are used as reference to generate high quality surfaces suitable for the milling process. Laser scanning was used to determine shape deviation. The CAD-evaluation revealed a minor shape deviation within tolerance of component (A) and a small over-compensation of the final geometry of component (B). The maximum shape deviation was however in the order of the sheet thickness. Rather than stating a new methodology, the work presented in this paper substantiates the idea that it is possible to realize development projects for new applications in Inconel 718 accurately, which is of outmost importance when developing tools at a short lead time. The key is consistent studies according to the systematic methodology in which FE-analyses were used for the virtual tool design and compensation.

## 5.4 Paper D

In the aero engine industry new manufacturing processes for load carrying aero engine structures imply fabrication. The concept of fabrication involves simple forgings, sheet metals and small ingots of e.g. titanium alloys which are welded together and heat treated. In the concept phase of the product development process, accurate evaluations of candidate manufacturing processes with short lead times are crucial. In the design of sheet metal forming processes, the manual die try out of deep drawing tools are traditionally a time consuming, expensive and inexact process. The present work investigates the possibility to

design hot forming tools, with acceptable accuracy at short lead times and with minimal need for manual die tryout, using finite element (FE) analyses of hot sheet metal forming for production of a Ti-6Al-4V component. A rather straight forward and inexpensive approach of material modelling and methods for material characterisation are chosen suitable for evaluations in the concept phase and validated by comparison with data from separate forming experiments performed at moderate elevated temperatures. The computed global force response is shown to be in acceptable agreement with the experiments and the shape deviation is predicted within the sheet thickness. Solutions for the hot forming tool concept regarding heating and regulation, insulation, blank holding and tool material selection are evaluated within the present study.

## 5.5 Paper E

Titanium alloys such as Ti-6Al-4V is commonly used in aerospace applications with moderate operating temperatures, mainly due to the high strength to weight ratio in combination with favourable creep resistance. In the virtual design of suitable hot forming processes for titanium sheet metal components, numerical finite element (FE) analyses are desired to secure forming concepts and study shape deviation. The reliability of the numerical simulations depends on the models and methods used as well as on the accuracy and applicability of the input data. The material model and related property data must be consistent with the conditions of the material in the process of interest. In the present study a set of material tests are performed at temperatures ranging from 20 to 560°C in order to characterise a sheet metal batch of Ti-6Al-4V and generate necessary experimental reference data for calibration of different yield criteria. The criteria are used in FE analyses of cold and hot sheet metal forming of Ti-6Al-4V. This paper functions as a first part to the work presented in paper F.

## 5.6 Paper F

In this work a tool concept for hot forming of a double-curved sheet metal component in the titanium alloy Ti-6Al-4V is proposed. The virtual tool design is based on finite element (FE) analyses of hot sheet metal forming in which two different anisotropic yield criteria are evaluated and compared with an isotropic assumption to predict global forming force, draw-in, springback and strain localisation. The shape of the yield surface was found to be of importance and by including effects of the cooling procedure, the prediction of shape deviation could be improved. The predicted responses show promising

agreement to the corresponding experimental observations using models which account for the anisotropic properties of the material.

# 6. Conclusions and future work

Titanium and its alloys are advanced materials. The material behaviours of different titanium alloys are complex in its nature with anisotropic low elastic modulus and high strength plastic anisotropy, elastic degradation with plastic straining, asymmetric yielding in tension and compression, sensitivity to strain rate and reversed loading direction (Bauschinger effect), low formability at moderate temperatures along with the high temperature behaviour including flow softening. The significant impact of the thermo-mechanical history, initial microstructure, impurities and chemical composition adds to the deviation between different material batches.

However, it has been shown in many research studies that titanium alloys definitely are possible to form into desired sheet metal geometries when performed under favourable circumstances. The FE technique provides with the possibility of performing detailed studies in the design of suitable thermo-mechanical forming procedures for titanium components.

The work performed in this thesis has had multiple purposes and is of multidisciplinary nature. The existing desire from the European aero engine industry has been the driving concern in the research work, stating the alloys of interest and component requirements. The desire concerns the identification of possible sub-suppliers and the development of suitable techniques for production of titanium sheet metal parts for use in complete load carrying aero engine structures. In order to suggest possible forming concepts for the demonstrator prototype components, the structure of the work was defined.

The mechanical properties of foremost Ti-6Al-4V but also of Ti-6242 and the nickel based alloy Inconel 718 were studied to determine necessary model requirements. Naturally, the work was delimited, in this case to include anisotropy and the strength differential effect for Ti-6Al-4V at moderate temperatures assuming isotropic hardening. The course of action in the project has been to perform initial forming tests to experimentally study the forming behaviour and the influence of different process parameters. Experimental values were correlated with FE analyses assuming isotropic hardening and isotropic or anisotropic yield criteria. Great efforts has been put into the short lead time development process of the hot forming tools, performing FE analyses and identifying practical concept solutions for the manufactured tools presented in paper D to F. The predicted responses such as punch force, draw-in, shape deviation and strain localisation show promising agreement with measured observations when applying anisotropic yield criteria. The shape of

the yield surface was found important both to the predicted shape deviation and the occurrence of strain localisation. The isotropic yield surface assumption was found not able to predict the springback distribution. Further, the predicted strain localisation occurred too early in the studied forming concept in paper F.

The ideas for future research work are quite extensive. To be able to further develop the suggested hot forming concepts to function in production, the blank size has to be significantly decreased due to the high material cost. To identify optimal forming procedures for smoothly double-curved geometries with this in mind, several possible design concepts exist. A precise prediction of strain localisation and failure is an area of further interest since it would give the possibility to fully use the material with minimal safety margins. Further on, the temperature is a powerful process parameter. By performing coupled thermo-mechanical analyses the effect of temperature would be possible to study in detail. As illustrated, the benefit from performing such analyses is encouraging considering forming of titanium alloys. Instead of assuming an isotropic yield criterion, anisotropic formulations need to be extended to function in coupled thermo-mechanical analyses.

In order to study sheet metal forming in the higher temperature region, modelling of phase transformations, creep and stress relaxation in which the strain rate is accounted for are of interest. It was found in paper D and F that relaxation occurs in both the elastic and plastic deformation region.

# 7. References


[1] Nemat-Nasser, S., Guo. W.-G., Nesterenko. V.F., Indrakanti. S.S., Gu. Y.-B., Dynamic response of conventional and hot isostatically pressed Ti-6Al-4V alloys: Experiments and modeling, 2001, Mechanics of Materials, Vol. 33, No. 8, August, pp. 425-439, ISSN: 0167-6636.

[2] Belytschko, T., Liu, W.K., Moran, B., Nonliear Finite Elements for Continua and structures, 2000, John Wiley & Sons, New York, ISBN 0-471-98773-4.

[3] Belytschko, T., Mish, K., Computability in non-linear solid mechanics, *International Journal for Numerical Methods in Engineering,* 2001, Vol.52, pp. 3-21.

[4] Adams, V., Askeazi. A., Building Better Products with Finite Element Analysis, On Word Press, 1999, Santa Fee, USA, ISBN 1-56690-160X.

[5] Tekkaya, A.E., State of the art of simulation of sheet metal forming, 2000, *Journal of Materials Processing Technology* Vol. 103, pp. 14-22.

[6] Bathe. K. J., On the state of finite element procedures for forming processes, CP712, 2004, *Materials Processing and Design: Modeling, Simulation and Applications, NUMIFORM 2004,* pp. 34-38. American Institute of Physics.

[7] Boyer, R., Welsch, G., Collings, E.W., 1994, Materials Properties Handbook: Titanium alloys, edition, ASM International.

[8] Lütjering, G., Williams, J.C., Titanium, 2003, Springer-Verlag Berlin Heidelberg.

[9] Semiati,. S.L., Seetharaman, V., Weiss, I., 1998, Materials Science & Engineering A, A243, pp. 1-24.

[10] Ding, R., Guo, Z.X., Wilson, A., Materials Science and Engineering A, Vol. 327, pp. 233-245, 2002.

[11] Ding, R., Guo, Z.X., Qian, M., Computation Materials Science, Vol. 40 (2007), pp. 201-212.

[12] Babu, B., Licentiate Thesis 2008:40, Luleå University of Technology, Sweden, 2008.

[13] Pederson, R., Doctoral Thesis 2004:19, Luleå University of Technology, Sweden, 2004.

[14] Odenberger, E.-L., Licentiate Thesis 2005:63, Luleå University of Technology, Sweden, 2005.

[15] Tuegel, E.J., Pruitt. M.O., Hefti. L.D., Advanced Materials & Processes, Vol. 136, (1989), pp. 36-41.

[16] Peter, N., Journal of Materials Engineering and Performance, Vol. 13, (2004), pp. 660-664.

[17] Wang, G., Zhang, K.F., Wu, D.Z., Wang, J.Z., Yu, Y.D., Superplastic forming of bellows expansion joints made of titanium alloys, Journal of Materials Processing Technology, Vol. 178, Issues 1-3, 14 September 2006, pp. 24-28
[18] Chan, K.S., Koss, D. A., Metallurgical Transactions A, Vol. 14A, n 7, 1983, pp. 1343-1348, ISSN: 0360-2133
[19] Kong, T.F., Chan, L.C., Lee, T.C, Numerical and experimental investigation of preform design in non-axisymmetrical warm forming, Int. J. Adv. Manuf. Technol, Vol. 37, (2008), pp. 908-919.
[20] Lai, C.P, , Chan, L.C., Chow, C.L., Effects of tooling temperature on formability of titanium TWBs at elevated temperatures, J. Materials Processing Technology, Vol. 191, (2007), pp. 157-160.
[21] Lai, C.P, , Chan, L.C., Chow, C.L., Warm forming simulation of titanium tailor-welded blanks with experimental verification, CP908, NIMIFORM ´07, Materials Processing and Design, Simulation and Applications, (2007), pp. 1621-1626
[22] Chen, F.-K, Chiu, K.-H, Stamping formability of pure titanium sheets, J. Mat. Proc. Tech, Vol. 170, (2005), pp. 181-186.
[23] Satoh, J., Gotoh, M., Maeda, Y., Stretch-drawing of titanium sheets, Journal of Materials Processing Technology, Vol. 139, n 1-3 SPEC, Aug 20, 2003, pp. 201-207, ISSN: 0924-0136
[24] Shipton, M.H., Roberts, W.T., Hot deep drawing of titanium sheet, Materials Science and Technology, Vol. 7, n 6, Jun, 1991, pp. 537-540, ISSN: 0267-0836
[25] Hallquist, J. O., LS-DYNA Theoretical Manual, Livermore Software Technology, Livermore, 1998
[26] Bergman, G., Oldenburg, M., A finite element model for thermo-mechanical analysis of sheet metal forming. Int. J. Numer. Methods Eng. Vol. 59, (2004), pp. 1167-1186.
[27] Lewis, R.W., Morgan, K., Thomas, H.R., Seetharamu, K.N.. *The finite element method in heat transfer analysis.* John Wiely & Sons, New York, third edition, 1996. ISBN 0-471-93424-0.
[28] Shapiro, A., LS-DYNA Feutures for Hot Forming, 6th Eouropean LS-DYNA User's Conference, Gothenburg, Sweden, 2007, pp 2.127-2.134.
[29] Lorenz, D., Haufe, A., Recent advances and new developments in hot forming simulation with LS-DYNA, Numisheet 2008, Interlaken, Switzerland, 2008.
[30] Friedman, P.A., Pan, J., Effects of plastic anisotropy and yield criteria on prediction of forming limits, Int. J. Mechanical Science, Vol. 42, 2000, pp. 29-48.
[31] Eggertsen, P.-A., Licentiate Thesis, 2009:05, Chalmers University of Technology, Sweden, 2009.

[32] Lubliner, J., Plasticity theory, 2008, Macmillan, New York.
[33] Ottosen, N.S., Ristinmaa, M., The Mechanics of Constitutive modelling, vol 1 and 2, 1999, Division of Solid Mechanics, Lund University, Sweden.
[34] Barlat, F., Brem, J.C., Yoon, J. W., Chung, K., Dick, R.E., Lege, D.J., Pourboghrat, F., Choi, S.-H., Shu, E.. Plane stress yield function for aluminium alloy sheet – Part1: theory. Int. J. Plasticity. Vol. 19, (2003), pp. 1297-1319.
[35] Cazacu, O., Barlat, F. Orthotropic yield criterion for hexagonal closed packed metals. Int. J. Plasticity. Vol. 22, (2006), pp.1171-1194.
[36] Nemat-Nasser, S., IUTAM Symposium on Micro- and Macrostructural Aspects of Thermoplasticity, Kluwer Academic Publishers, 1999, pp. 101-113.
[37] Wikman, B. and Bergman, G., Technical Report 2000:27, Luleå University of Technology, December 2000.
[38] Åkerström, P., Doctoral Thesis 2006:30, Luleå University of Technology, Sweden, 2006.
[39] Tarantola, A., Inverse Problem Theory – Methods for Data Fitting and Model Parameter Estimation, Elsevier, 1987.
[40] Hill, R., The Mathematical Theory of Plasticity, Clarendon Press, Oxford. (1950).
[41] Jansson, M., Nilsson, L., Simonsson, K., On constitutive modelling of aluminium alloys for tube hydroforming applications, Int. J. Placticity, Vol. 21, 2005, pp. 1041-1058
[42] Lademo, O. G-., Hopperstad, O.S., Langset, M., An evaluation of yield criteria and flow rules for aluminium alloys, Int. J. Plasticity, Vol. 15, (1999), pp. 191-208.
[43] Barlat, F., Lian, J., Plasticity behaviour and strechability of sheet metals Part I: a yield function for orthotropic sheets under plane stress condition. Int. J. Plasticity, Vol. 5, (1989), pp. 51-66.
[44] Hosford, W., On the yield loci of anisotropic cubic metals. 7th North American Metalworking Conf.. SME, Dearborn, MI, (1979), pp. 191-197.
[45] Barlat, F., Aretz, J.C. H., Yoon, W., Karabin, K., Breem, M.E., Dick, R.E., Linear transformation-based anisotropic yield functions, Int. J. Plasticity. Vol. 21, (2005), pp. 1009-1039.
[46] ARAMIS v6: http://www.gom.com, Nov (2009).
[47] Hora, P., Tong, L., Reissner, J., A prediction method for ductile sheet metal failure in FE-simulation, Proceedings of Numisheet'96 Conference, 1996, pp. 252-256.
[48] Karlsson. T., Master's Dissertation, Division of Solid Mechanics, Lund University, 2007, Sweden.

[49] Manual for The Resultant Frequency and Damping Analyser (RFDA) system 23, version 6.3.0, IMCE (2006).
[50] RFDA: http://www.imce.net/, Nov (2009).

# Paper A

# Numerical and Microstructural Evaluation of Elevated Temperature Compression Tests on Ti-6Al-4V

E.-L. Westman, R. Pederson, B. Wikman, M. Oldenburg
Luleå University of Technology, Luleå, Sweden

## Abstract

An investigation of the use of inverse modeling for estimation of material model parameters, of a compression test of forged Ti-6Al-4V, is presented. The compression tests performed on cylindrical specimens indicated that initial material hardening was followed by specimen cracking at lower temperatures while at 700˚C and 900˚C material hardening was followed by flow softening. The alloy was also found to be strain rate sensitive. The ability of three different constitutive models to describe the inelastic thermo mechanical behavior of Ti-6Al-4V has been examined and none of them were found able to describe it satisfactorily. However, it was shown that inverse modeling is a viable way to determine relevant material parameters, if suitable functions are chosen. Changes in the microstructure as a consequence of heat treatment and deformation were also investigated. In general, it was found in cross sections parallel to the loading direction, that the deformation was non-uniform and concentrated in bands going diagonally from one corner to the other. The alpha platelets in the Widmanstätten structure were increasingly broken up going from the less deformed anvil contact region into the more deformed center of the specimen.

# 1. Introduction

Ti-6Al-4V is a commonly used alloy in aerospace applications such as turbine engines and airframes. In industrial applications it is often of great importance to know the thermo-mechanical properties of the material and to be able to predict and detect changes in these properties. Another need for accurate material property data stems from the industrial requirement to perform numerical analyses at different stages in the product development process. This could be simulation of a manufacturing process such as welding or forming, or it could be the function analysis of a component. In order to perform high quality FE-analyses, accurate model input is crucial.

Consequently, the development of appropriate constitutive models for Ti-6Al-4V for various applications is a central issue. It is also essential to emphasize the use of proper routines for efficient application of numerical modeling of industrial processes.

Traditional methods to determine necessary property data in which the material is characterized by several tension and/or compression tests at different temperatures and strain rates is time demanding and expensive and the results are often not in an appropriate form. An alternative route is to obtain material parameters trough force and displacement by inverse modeling [1]. Inhomogeneous stress conditions can be taken into account, which is of great benefit, in contrast to traditional methods where a homogenous stress distribution is assumed. The idea is to create different deformation mechanisms in one test. For the accurate modeling of processes such as forming inverse modeling has [2,3] been shown to generate more accurate material data compared to traditional experiments, and usually requires a reduced number of experiments [2].

# 2 Experimental procedure

The starting material was in the form of cylindrical test specimens of Ti-6Al-4V cut out from a forged jet engine compressor disc. Specimen dimensions were ∅ 4.0 x 5.5 mm or ∅ 6.0 x 8.0 mm (Test 1), the dimensions depending on the desired cooling rate. The microstructure was bimodal consisting of about 34 vol% equiaxed primary alpha ($\alpha_p$) particles and 66 vol% of a Widmanstätten type structure. The chemical composition of the alloy was (in wt%): 6.20 Al, 4.10 V, 0.19 Fe, 0.04 Si, 0.01 Cu, 0.01 C, 0.18 O, 0.005 N, 0.0024 H, <0.001 B, <0.001 Y, and Ti balance.

A Gleeble 1500 thermo mechanical simulator with lengthwise strain control was used to perform axial compression tests. The test specimens were placed between two tungsten carbide anvils, coated with a film of graphite and tantalum to minimize friction and prevent sticking between the anvils and the specimen. Resistance heating of the specimen permitted high temperatures and rapid heating/cooling rates. The temperature was measured using a Pt/PtRh-thermocouple welded onto the surface and at mid height of the specimens. The tests were performed in an evacuated chamber (0.1 torr). During the testing sequence, the axial and radial displacements together with axial compression force and temperature were measured continuously.

Two sets of tests were performed as described in section 2.1 and 2.2. Prior to deformation, all specimens were heated up (10°C/s) to an equilibrium temperature of 950°C and kept there for 20 minutes before cooling down to the

desired test temperature. The main purpose of this heat treatment was both to relieve residual stresses [4], caused by the machining used to produce the specimens, and to reach an equilibrium fraction of alpha and beta phases and thereby avoid time-dependent phase transformation [5]. A rather rapid cooling rate of 25°C/s was chosen.

## 2.1 Isothermal compression tests at different temperatures

Six isothermal tests were performed, all heat-treated as previously described. A schematic temperature history diagram for the isothermal tests is shown in Fig. 1. After the equilibration stage the specimens were cooled to the desired testing temperature, e.g. 900°C (Test 1 in Fig. 1), which was held for 10 seconds (in order to make a few adjustments of the control system). The specimens were then compressed to a final lengthwise true strain of 0.693 at a strain rate of 0.05 $s^{-1}$. Finally, the specimens were cooled down to room temperature (RT, 25°C). The same procedure was applied to Test 2-6, but at test temperatures of 700°C, 500°C, 300°C, 100°C and RT, respectively.

In order to detect strain rate sensitivity, further tests were performed at higher strain rates (0.5 $s^{-1}$ and 5 $s^{-1}$) and at a testing temperature of 500°C (Tests 7 and 8, respectively).

## 2.2 Compression and continuous cooling tests

To receive more information from one single test, compression and continuous cooling tests (C-C) were performed, with the same strain rate and lengthwise strain as in Test 1-6. Two tests were chosen with certain overlaps, Tests 9 and 10. Testing in the lower temperature regime was not conducted due to problems with controlling the desired cooling rate and to fracture of specimens. A schematic temperature history diagram with start and stop temperatures for the C-C tests is shown in Fig. 2 (Test 9: 900-555°C, Test 10: 635-290°C).

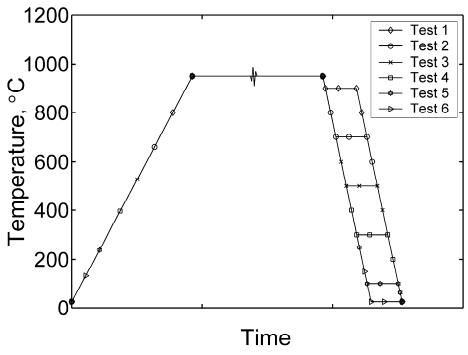


**Figure 1.** Temperature history for isothermal tests.

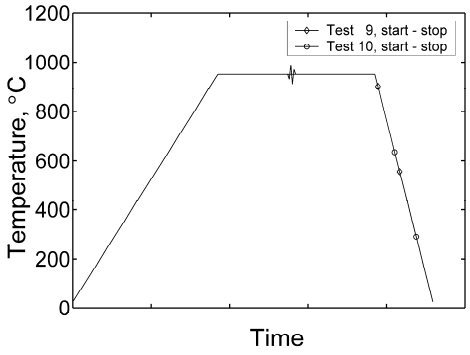


**Figure 2.** Temperature history for C-C tests.

# 3 Experimental results

Experimental results for the isothermal tests are shown in Fig. 3. Initial material hardening was observed followed by specimen cracking at the lower temperatures (Tests 4, 5 and 6). Tests at 700˚C and 900˚C indicated material hardening followed by flow softening while at 500˚C the initial hardening was followed by ideal plastic behavior.

The strain rate dependence of the alloy is shown in Fig. 4; repeated tests were performed to confirm reproducibility of the experiment. It can be seen that for small strains the stress level increased with increasing strain rate, though only marginally from 0.05 to 0.5 $s^{-1}$. For the highest strain rate, flow softening took place after a fluctuating material hardening behavior.

The C-C test results are shown in Fig. 5, which shall be applied in the inverse modeling in future work. The results presented in Fig. 3 to 5 include the elastic strain of the experimental equipment.

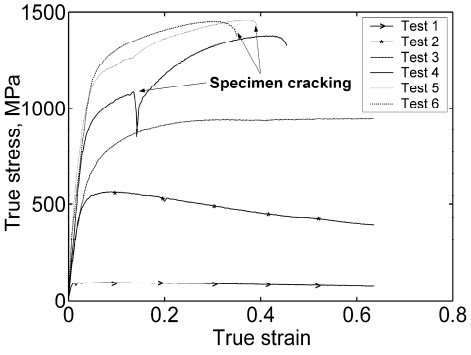


**Figure 3.** True stress-strain curves for isothermal tests, Tests 1-6.

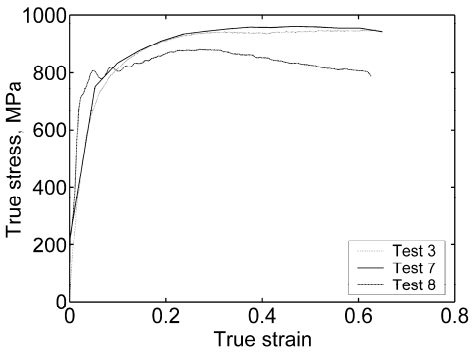


**Figure 4.** Influence of strain rate on stress-strain behaviour at 500°C, Tests 3, 7 and 8.

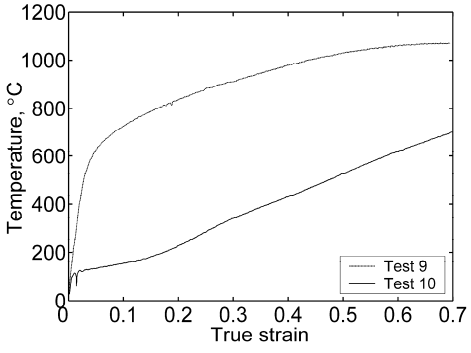


**Figure 5.** True stress-strain curves for C-C tests,Tests 9 and 10..

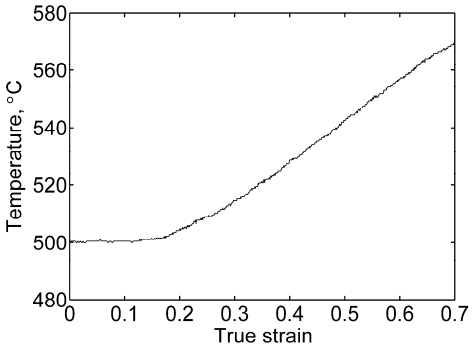


**Figure 6.** Temperature rise during deformation,Test 8.

In order to understand the overall deformation of these samples, it was helpful to examine etched cross sections of deformed samples using both optical microscope and SEM. In general, it was found that in the cross sections parallel to the loading direction, the deformation was non-uniform and concentrated in bands running diagonally from one corner to the other. In three dimensions this can be described as the surfaces of two cones, with their peaks in the center of the sample [6]. The nature of the deformation can be seen in Fig. 7. The alpha platelets in the Widmanstätten structure became increasingly broken up and the primary alpha grains increasingly scattered in going from the less deformed contact surface region into the more deformed center of the specimen. A corresponding computed stress distribution, when going from the surface of the sample into the center, is shown in Fig. 10. In work by others [6] it has been seen that voids/cracks form at the edges of compressed samples and continue to grow along the previously described deformation cone surfaces into the center of the sample. This was also seen in this work, in which the fracture pieces of broken samples were sheared in a diagonal mode to the loading direction.

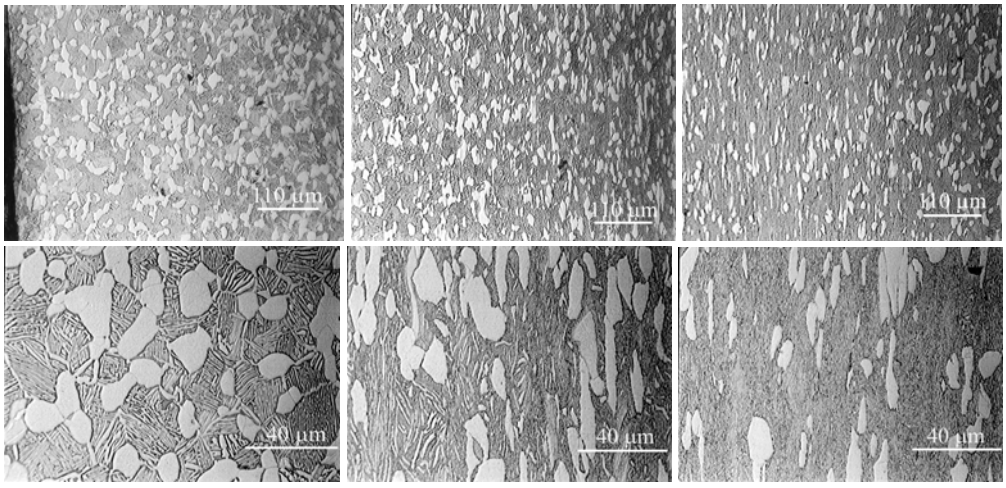


**Figure 7.** Microstructure of sample isothermally compressed at 700°C (Test 2). Left column micrographs are from the surface region close to the pressing tool, mid column is from the region half way to the center of the specimen, and the right column shows the microstructure in the center of the sample. The loading direction is horizontal in the figure.

Metallographic examination of the tested samples revealed a pronounced α stabilized surface region, indicating that the pressure achieved in the chamber was not low enough to avoid oxidation. Micro hardness testing of the cross sections confirmed that the samples had a thin surface layer with an increased hardness, compared to the hardness of the bulk material. This kind of α stabilized structure is usually referred to as α-case, a hard and brittle alpha phase with high concentration of oxygen. The deformed specimens were found

to be non-uniformly recessed at the compression surfaces. A significant temperature rise during the deformation, in Test 8, was also detected (see Fig. 6).

# 4 Numerical procedure

The numerical evaluation was designed to include the inhomogeneous stress development in the specimen during the deformation. Moreover, the Gleeble tests were performed in such a way that they involved simultaneously both thermal effects and deformation mechanisms. By inverse modeling of the actual experiment, material model parameters could be determined by minimizing the difference between the FE-analyses (FEA) and experimental reference data. The general idea of inverse modeling is shown in Fig. 8.

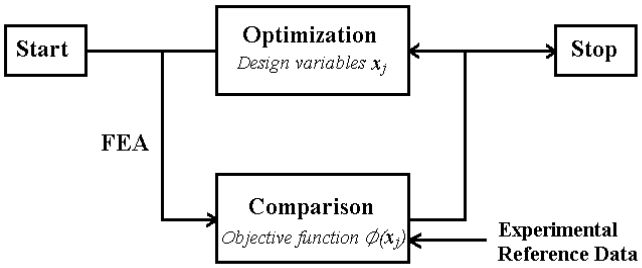


**Figure 8.** Schematic illustration of inverse modeling.

## 4.1 The direct problem

The direct problem consists of solving the FE-problem subjected to variations of material model parameters. In this work the non-linear implicit FE-code MSC.Marc has been used to set up an axi-symmetric model of the Gleeble experiments. The FE-model consists of 150 lower order quadrilateral elements and 176 nodes. Displacement boundary conditions are applied to the rigid anvils corresponding to the desired strain rate and deformation. A homogenous specimen temperature was applied in accordance with the experiment during deformation. The contact between the anvil and the specimen was modeled as a contact interface with a stick-slip friction model. The interface was assumed to be flat with a constant friction coefficient of 0.1. The mesh is shown in Fig. 9.

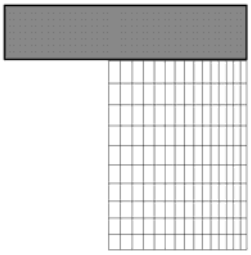

**Figure 9.** Axi-symmetric FE-model of ¼ of the test specimen for Test 3, 150 elements.

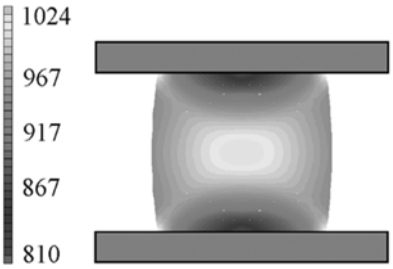


**Figure 10.** Stress field of equivalent von Mises stress at t=6.28 s, estimated parameters Fig. 11b.

Three different constitutive models have been investigated, i.e. the models developed by Johnson-Cook [8], Nemat-Nasser [9] and a polynomial relation described in Reference [2]. In this work, Test 3 was chosen as reference data to evaluate the ability of the material models to describe the inelastic behavior of the alloy.

## 4.2 The inverse problem

The 'Optimization' box in Fig. 8 represents the program INVSYS [10], which is a programming system tailor-made for analysis of inverse problems, the optimization algorithm used is the subspace-searching simplex method [11]. The design variables, $x_j$, the material model parameters, are given appropriate initial values and constraints. The objective function $\phi(x_j)$ is an expression that determines the discrepancy between the computed and measured response, in this work in a least-square sense, normalized according to Equation (1) [7].

$$\phi(x_j) = \frac{1}{2}\sum_{i=1}^{n}\left(\left(\frac{F_i^e - F_i^f(x_j)}{F_i^e}\right)^2 + \left(\frac{D_i^e - D_i^f(x_j)}{D_i^e}\right)^2\right) \qquad (1)$$

where $n$ is the number of sampled values, $F^e_i$ and $F^f_i$ are the compression force from experiment and FEA, respectively. $D^e_i$ and $D^f_i$ are the radial displacement from experiment and FEA, respectively.

In order to evaluate the constitutive models, an estimation of parameters for the experimentally determined hardening function for Test 3 was performed. A material parameter estimation of a reference FE solution was also carried out in order to evaluate the functionality of the inverse modeling programming system, which was found to be successful [7].

# 5 Numerical results

Results of the evaluation of the constitutive models with estimated parameters are presented in Fig. 11. The optimization was performed several times using different initial values of the parameters. It is important to examine the behavior of the objective function in the feasible region in order to find the acceptable minima.

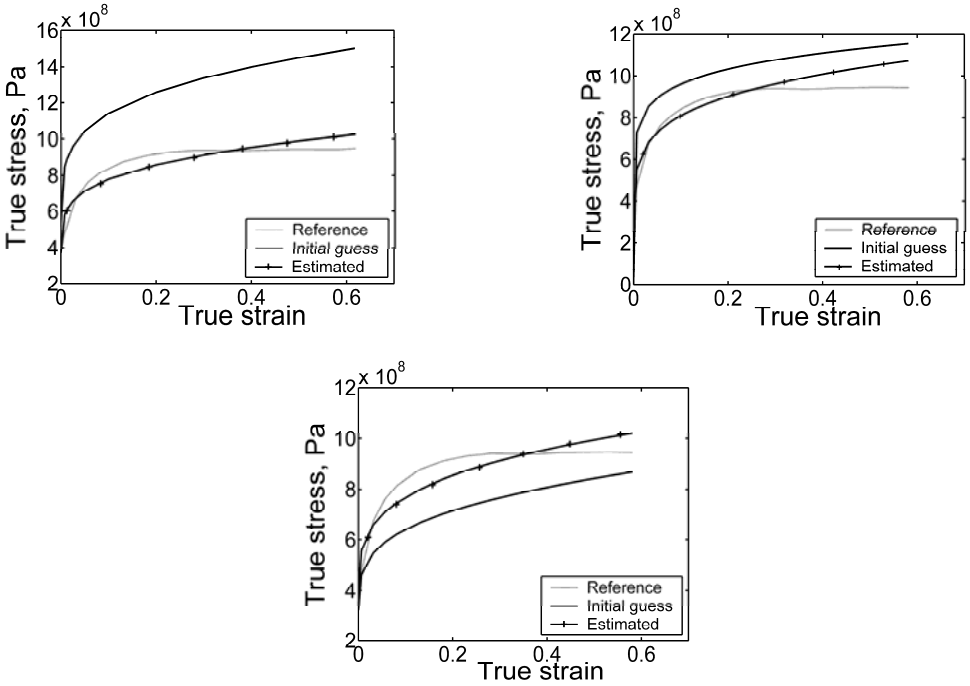


**Figure 11.** Evaluation of Johnson-Cook, Nemat-Nasser and the polynomial relation material models, respectively.

The evaluation shows that none of the three constitutive models describes the inelastic behavior of this specific alloy satisfactorily. The three constitutive models, with estimated parameters, generate functions fairly similar to each other; there are only small differences in the behavior. A mirrored plot showing the von Mises stress of the deformed specimen, with the estimated parameters of the Nemat-Nasser material model presented in Fig. 11b, is shown in Fig. 10.

# 6 Discussion and Conclusions

The samples compressed between RT and 300°C cracked during testing and the cracks leading to fracture were seen to originate at the corners of the samples and to grow in a diagonal mode to the loading direction. This is in well agreement with the simulated stress field occurring in compressed samples during testing (see Fig. 10). It is reasonable to expect that the resistance to crack initiation is reduced because of the observed $\alpha$-case found in the surface regions of the tested samples.

The strain rate sensitivity was examined by applying three different strain rates during isothermal deformation at 500°C, and the resulting stress-strain curves are shown in Fig. 4. No clear difference could be seen between the strain rates of 0.05 $s^{-1}$ and 0.5 $s^{-1}$, but at a strain rate of 5 $s^{-1}$ flow softening seem to occur. This could be explained by heat generation during plastic deformation. Indication of this was found in the recorded temperature during the test (Fig. 6), where the temperature increased by approximately 70°C during the deformation process. If this temperature increase is high enough to cause flow softening is not yet certain, but it is possible that on a local scale (some distance from the thermocouple) the temperature increase could well be significantly higher than that recorded by the thermocouple, due to the variation in the degree of plastic deformation through the sample. The isothermal compression test conducted at 700°C with a strain rate of 0.05 $s^{-1}$ (see Fig. 3) indicated a typical softening behaviour. Thus it is reasonably to suppose that the test performed at 500°C, due to the higher strain rate of 5 $s^{-1}$, could have reached the softening regime observed at 700°C because of local heating in the specimen during deformation. However, it should be pointed out that no similar evidential results of local heating during the compression of Ti-6Al-4V have been found reported elsewhere. Thus, the possibility of an equipment error in the measured temperature rise cannot be ruled out. The slope of the 5 $s^{-1}$ curve seems initially somewhat irregular and also steeper than for the curves at lower strain rates. This serrated form of the curve closely resembles serrated yielding, a phenomenon mainly known to occur in $\alpha$ titanium alloys during plastic deformation at low (cryogenic) temperatures. However, similar compression experiments performed with other materials, with the same Gleeble 1500 equipment as was used in this work, produced similar types of serrated curves when high strain rates were applied. Thus, the serrated form of the curve observed here most likely stems from the equipment.

The three constitutive models that were studied in this work were not able to describe the material hardening behavior satisfactorily. A remaining challenge of future work is therefore to find alternative descriptions for the material behavior. However the estimation performed to check the functionality of the inverse modeling programming system described in Reference [7] shows that inverse modeling is a viable way to determine material model parameters. It shall be mentioned that different sets of parameters can describe the same material behavior. Thus it is important that the error between the reference data and the response generated by the FE-analysis is small. The existence of a minimum for the objective function should be analyzed, since several minima often exist. Another crucial issue to investigate is the stability of the achieved solution. For instance, a flat minimum is considered non-unique, and for this reason the solution may change substantially by even small changes in the data. Thus, it is important to exclude misleading local minima by investigation of different initial guesses. In future work results from the C-C tests are to be used as reference data in order to achieve more accurate data with a reduced number of experiments.

Regarding the FE-model, the friction coefficient between the specimen and the anvils has not yet been investigated but is an important factor. It determines the shape of the billet when deformed and influences the estimated parameters, thus it should be investigated in future work. One possibility is to include the friction coefficient as a design parameter or perform parameter estimations with different friction coefficients. The foil and the recessed area at the compression surfaces of the specimen will cause difficulties in friction modeling. In order to take internal heat generation into account and to determine its effects it may also be justified to perform coupled thermo-mechanical analyses.

# 7 Acknowledgements

The research founding by VINNOVA, grant P22122-1A, and the collaboration with Prof. Pentti Karjalainen and Ph.D. Mahesh Somani at University of Oulu, Finland, are gratefully acknowledged.

# 8 References

1. A. Tarantola, Inverse Problem Theory – Methods for Data Fitting and Model Parameter Estimation, Elsevier, 1987.

2. M. C. F. Eriksson, Doctoral Thesis 2002:19, Luleå University of Technology, Sweden, May 2002.
3. G. Lindkvist, Master Thesis 2001:307, Luleå University of Technology, Sweden, November 2001.
4. Materials Properties Handbook: Titanium alloys, ASM International, 1994, p. 599.
5. R. Pederson, Licentiate Thesis 2002:30, Luleå University of Technology, Sweden, May 2002.
6. A. J. Wagoner Johnson, C. W. Bull, K. S. Kumar, C. L. Briant, Met. Mat. Trans. 34A, 2003, 295-306.
7. E.-L., Westman, Master Thesis 2003:108, Luleå University of Technology, Sweden, February 2003.
8. G. R. Johnson, W. H. Cook in the 7th International Symposium on Ballistics, The Hague, The Netherlands, 1983.
9. S. Nemat-Nasser in the IUTAM Symposium on Micro- and Macrostructural Aspects of Thermoplasticity, Kluwer Academic Publishers,1999, 101-113.
10. B. Wikman and G. Bergman, Technical Report 2000:27, Luleå University of Technology, December 2000.
11. T. H. Rowan, Doctoral Thesis, University of Texas at Austin, Texas, USA, chapter 5, May, 1990.

# Paper B

ELSEVIER

Materials Science and Engineering A 489 (2008) 158–168

MATERIALS SCIENCE & ENGINEERING A

www.elsevier.com/locate/msea

# Thermo-mechanical material response and hot sheet metal forming of Ti-6242

Eva-Lis Odenberger [a,*], Robert Pederson [b], Mats Oldenburg [a]

[a] *Division of Solid Mechanics, Luleå University of Technology, SE-971 87 Luleå, Sweden*
[b] *Volvo Aero Corporation, Materials Technology, 9651RP, SE-46181 Trollhättan, Sweden*

Received 1 March 2007; received in revised form 4 December 2007; accepted 6 December 2007

**Abstract**

The thermo-mechanical response of a Ti-6242 alloy has been studied in elevated temperature compression tests (CT) together with cold and hot sheet metal forming tests (FT) to evaluate the suitability of different cold and hot sheet metal forming processes. The CT are designed to function as input for the estimation of material model parameters such as the parameters of constitutive equations. Furthermore, results from the FT will be used in correlation of finite element (FE) models for the prediction of sheet metal forming. Experiments were performed in a broad range of temperatures and strain rates. In CT at 400–900 °C and strain rates 0.05–1 $s^{-1}$. In FT at 20–1000 °C in both isothermal and non-isothermal forming, at forming velocities of 5 and 10 mm/s. The microstructures of as-received material and deformed specimens were examined using optical microscopy. Experimental results of the CT show that initial material hardening was followed by specimen failure where cracks have formed in deformation bands or by flow softening, depending on the temperature. Compressive logarithmic strains of 10–50% were achieved. The FT reveals that optimal forming conditions are a combination of forming velocity, temperature and holding time. Hence increasing forming temperatures alone does not necessary imply better forming characteristics. A change in spring-back characteristics occurred at elevated temperatures. It can be concluded that, under the current conditions in this study, Ti-6242 is suitable to be formed by hot sheet metal forming.


*Keywords:* Ti-6242; Compression test; Sheet metal forming; Flow stress; Microstructure; Validation test

## 1. Introduction

Titanium alloys are extensively used in aerospace applications such as turbine engines, airframe applications and space shuttles, mainly because of their superior strength to weight ratio. Ti–6Al–2Sn–4Zr–2Mo–0.08Si (hereinafter referred to as Ti-6242) was developed in the late 1960s and is extensively used in turbine-engine applications, mostly for gas turbine components such as compressor blades, disks and impellers but also in form of sheet metal parts, e.g. various "hot" airframe skin applications and in engine afterburner structures. Ti-6242 is a titanium alloy with high temperature stability used for long-term applications and is one of the most creep-resistant titanium alloy, often used when the temperature range do not permit usage of the most widely used α–β titanium alloy Ti–6Al–4V. Ti-6242, sometimes categorized as a near-alpha alloy, has structures that are typically fully transformed or have an equiaxed α in a transformed β matrix. The α-phase has a hexagonal close-packed (hcp) crystal structure and the β-phase has a body-centred cubic (bcc) crystal structure. The fraction of primary α in the structure of sheet products is often of about 80–90%, which tends to be greater than in forgings. The size of the equiaxed α grains in sheet products also tend to be smaller compared to those in forged products. As for other titanium alloys, e.g. Ti–6Al–4V, the microstructure is strongly influenced by the processing and heat treatment history and the mechanical properties are mainly determined by the initial microstructure, the thermo-mechanical loading history and the present impurities together with alloy concentration [1–4].

Titanium alloys are often considered more difficult to form and generally have less predictable forming characteristics than other metallic alloys such as steel and aluminum. This can partly be explained by their high yield stress, $\sigma_y$, and low elastic modulus, $E$, which in combination yields a high degree of spring-back when formed by cold- or hot-forming. The hexagonal crystal structure of the α-phase also possesses anisotropic characteristics that affect its elastic properties. However, if conventional sheet metal forming is performed under favourable circum-

* Corresponding author. Tel.: +46 454 975 45; fax: +46 454 921 21.
*E-mail address:* Eva-Lis.Odenberger@ltu.se (E.-L. Odenberger).

0921-5093/$ – see front matter © 2008 Elsevier B.V. All rights reserved.
doi:10.1016/j.msea.2007.12.047

stances titanium alloys can be successfully formed into complex parts. If forming is followed by a so called hot sizing operation, in which the part is allowed to creep into the desired shape, the difficulties with spring-back can be reduced or even overcome. At the present, components manufactured by super plastic forming (SPF) are available, though it is often reserved for components with a high degree of complexity or when a substantial degree of material stretching is necessary [1,2,5–8]. SPF is an area in which great research efforts have been made. Currently, very limited research is published in the field of direct cold- and hot-forming of Ti-6242. However, research efforts have been made in sheet metal forming of, e.g. Ti–6Al–4V, revealing many interesting forming characteristics of this particular alloy including forming limit diagrams (FLD) [9–14]. For example, Thomas et al. [9] deals with material behaviour models to establish the proper conditions for fabricating titanium alloys, more specifically Ti–6Al–4V, by conventional sheet forming processes. They calculated FLDs and the results indicate that the most critical formability index is the strain rate sensitivity of the material. The forming limits increase with temperature for a given punch speed and with decreasing punch speed for a given temperature. The punch speed was found to be particular important at the investigated temperatures 538 and 677 °C predominantly due to the changes in the strain rate sensitivity of the alloy.

An effort to standardize the description of titanium sheet formability has also been made where a dimensionless index called the minimum bend radius $T_R$ is defined as the ratio between the die radius $R$ and the sheet thickness $H$, such that $T_R = R/H$. Furthermore, extensive experimental results on the compressive deformation behaviour (mostly in the hot forging range) for a broad range of strain rates and temperatures of Ti–6Al–4V are available [3,4,15–19], revealing many different characteristics of this particular alloy. Semiatin and coworkers [20–24] studied the effect on the properties of Ti-6242 in isothermal and non-isothermal hot forging (816–1010 °C). Flow stress behaviour, occurrence of shear bands, chill zones, deformation-induced microstructures and shear cracks were also observed and discussed. For example, it was established that the flow behaviour to a large extent is determined by the starting microstructure. In hot compression it is stated that, for the alloy with an equiaxed α structure, the deformation is stable with a decreasing flow stress with straining due to adiabatic heating. With a transformed β structure, unstable flow was observed and the cause of flow softening was prescribed microstructural modification together with a small adiabatic temperature increase. Criteria for the occurrence of shear bands were established.

In industrial applications it is often of great importance to know the thermo-mechanical properties of the material and also to be able to predict and detect changes in these properties. Further need for accurate material property data descends from the industrial requirement to perform numerical analyses in the product development process to obtain short lead times and efficient manufacturing techniques resulting in high quality components. The computational capacity of today makes precise analyses, such as finite element (FE) analysis, possible. The knowledge of performing numerical analyses to develop and improve industrial processes such as forming is becoming more common. In order to perform high quality FE analyses, accurate model input is crucial. Available material data is often not in an appropriate format and traditional methods of obtaining data are expensive and time consuming.

In the present work we seek to examine experimentally the thermo-mechanical properties of Ti-6242 by elevated temperature compression tests. Sheet metal forming tests are performed in order to determine suitable hot and cold sheet metal forming processes for the alloy. Effects of the temperature, the strain rate and the initial material state on the mechanical properties are studied, spring-back characteristics are detected and metallographic studies are performed. The CT are also designed to function as input for estimation of material model parameters such as the parameters of constitutive equations. A method for identification of material model parameters is inverse modelling. This method, in which the raw data from compression tests are used as experimental reference, has shown to be an effective method requiring a reduced number of experiments with improved accuracy of model parameters compared to traditional methods [25–29]. The experimental data consists of the compression force and diametric displacement, the numerical reference are generated by an FE-analysis of the actual compression test. The improved accuracy in material model parameters can mainly be prescribed (a) that boundary effects can be included in the evaluation by means of FE-analyses, i.e. no assumption of homogeneous stress/strain distribution in the test specimen which the estimated flow curve as direct reference data would imply, (b) compression tests facilitate an easier evaluation at higher strain levels compared to evaluation of tensile tests, after the occurrence of necking, no extrapolation of tensile flow curves for strain levels after necking are needed and (c) compression tests under continuous cooling generate parameters accurate in a desired temperature interval which means that the introduced errors in interpolating between temperatures can be avoided.

Furthermore, the resulting parameter values obtained from the CT will be used in FE simulation for predicting sheet metal forming in future work. The FT will functions as validation tests.

## 2. Experimental procedure

### 2.1. Materials

Specimens for the elevated temperature compression tests (CT) and sheet specimens for the forming tests (FT) were extracted from two different duplex annealed sheet metal plates of Ti-6242. In the compression tests cylindrical specimens with 5 mm diameter and 7 mm height are used. One exception is made for the specimen extracted in thickness direction of the sheet where the height is 5.86 mm. The specimens were machined from a documented alpha case free sheet with thickness 5.86 mm purchased from Industrial Metals International Ltd. (IML), Heat: G-7047. Sheet specimens were machined from a sheet with the mean sheet thickness 1.95 mm purchased from RMI Titanium Company, duplex annealed at 899 °C for 30 min then air-cooled and subsequently at 788 °C for 15 min then air-cooled. The chemical compositions of the two sheet metals are given in

Table 1
Chemical composition of Ti-6242 alloy (wt%)

| Material | Al | Mo | Zr | Sn | Si | Fe | C | O | N | H | Y | Others | Ti |
|---|---|---|---|---|---|---|---|---|---|---|---|---|---|
| CT | 6.27 | 1.98 | 4.09 | 2.07 | 0.07 | 0.02 | 0.02 | 0.11 | 0.01 | 0.0065 | 0.005 | < 0.3 | Balance |
| FT | 5.88 | 1.95 | 3.93 | 2.01 | 0.084 | 0.04 | 0.01 | 0.09 | 0.004 | 24 PPM | <50 PPM | | Balance |

Table 1. The beta transus temperature of the alloy is typically $995 \pm 15\,^{\circ}C$ [1].

### 2.2. Compression tests

The axial compression tests were performed using a Gleeble 1500 thermo-mechanical testing equipment with lengthwise strain control. The test specimens (extracted transverse (T), along (L), in thickness direction or in a 45° mode to the rolling direction) were placed between two tungsten carbide anvils which were coated with a film of graphite and tantalum to prevent sticking and minimize the friction. Resistance heating of the specimens was used to attain the desired temperatures which also permit rapid heating/cooling rates. The temperature in the sample deviates slightly from a uniform distribution along the sample. The $\Delta T$ is estimated to 45 °C at measured 950 °C and is decreasing with temperature. This is based on the observations discussed in Section 3.3.

Prior to deformation, specimens were heated at a rate of 10 °C/s to the desired test temperature after which, in order to make a few adjustments of the control system, a holding time of approximately 15 s was applied. After compression, the specimens were cooled to room temperature at a rate of 25 °C/s. Some isothermal tests, heat treated at 950 °C for 20 min before cooling (25 °C/s) to the desired test temperature, were also performed. Finally compression tests during continuous cooling were performed at a rate of 25 °C/s. The temperature was measured using a Pt/PtRh-thermocouple which was welded onto the surface and at mid-height of the cylindrical specimens. The Gleeble 1500 equipment permits tests to be performed in an evacuated chamber (0.013 kPa) or in a protective gas atmosphere. In the experiments argon gas was used to minimize α-case formation. During the testing sequence the axial compression force, the axial displacement, the diametric increase at mid-height of the specimen and the temperature were measured and logged. The presented flow curves are evaluated using the lengthwise strain gauge.

### 2.3. Forming tests

The sheet metal forming tests were performed using two sets of forming tools. One set with a cold punch and die of tool steel Uddeholm RIGOR, hardness 58–60 HRC and another set with a heated punch and die of tool steel Uddeholm HOTVAR, hardness 57 HRC with a 400 °C-maximum temperature for long time exposure. Both tool materials where purchased from Fr Ramstrom and heat-treated by Bodycote metal technology. The cold punch and die are illustrated in Fig. 1. The heated punch and die are identical to the cold punch and die except that the overall width is 10 mm less and that holes for cartridge heaters are machined. The forming tools are constructed with respect to the theoretical minimum bend radius in room temperature and mounted in a Universal Straining Frame testing machine (DARTEC 250 kN). In these experiments the testing machine was stroke displacement controlled before switching to load controlled displacement at the very end of the forming sequence. The testing machine was calibrated to within ±0.2% of the measured value. Two types of specimens were tested, one type extracted from along the rolling direction (L), the other extracted transverse to and in plane of the rolling direction (T). The dimensions of the sheet specimens were 147 mm × 29 mm × 1.95 mm for tests performed in the cold forming tool and 137 mm × 29 mm × 1.95 mm in tests performed in the forming tool with heating capability. Sheet specimens were ground with abrasive paper of fineness 320 to remove oxide layers, cleaned with ethanol and sprayed with Combat® Boron Nitride Aerosol CC-18 as lubrication, applied in two thin layers.

The T and L sheet specimens were placed and centred in the forming tool after which the forming sequence was carried out. The lower die had a constant velocity of 5 or 10 mm/s. A holding time of 5 s was applied before unloading unless otherwise specified. The sheet specimens were preheated in an oven (NABER 2804 Mod. L51/SR) at temperatures ranging from 400 to 1050 °C before being transferred directly into the forming tool. The temperature of the sheet specimens was continuously measured and logged by three thermocouples (PENTRONIC

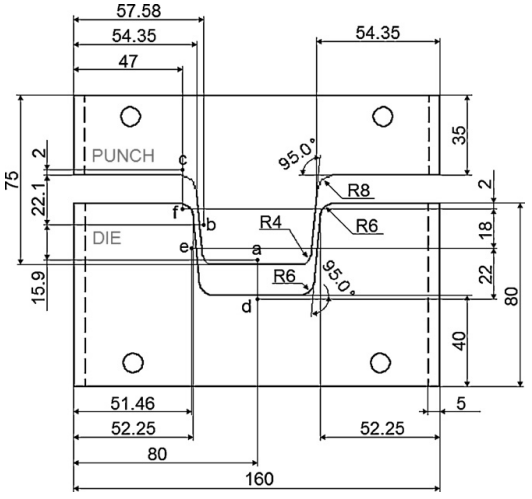


Fig. 1. Mechanical drawing of the cold punch and die (mm). Tool thickness is 29 mm.

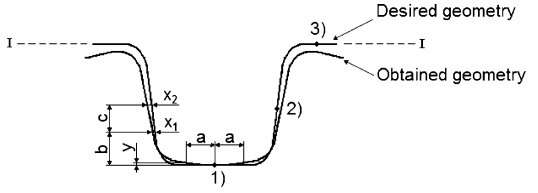


Fig. 2. Illustration of spring-back measurements and location of the three thermocouples welded at the longer edge of rectangular sheet specimens.

type K) welded at the longer edge of the rectangular sheet specimen, labelled (1)–(3), as shown in Fig. 2 (distances from the shorter edge at unformed specimens are 8, 32 and 73.5 mm for tests performed in the cold forming tool and 3, 27 and 68.5 mm in tests performed in the forming tool with heating capability). The temperature of the forming tool was measured by another six thermocouples (PENTRONIC type K) mounted in the centre and as close as possible to the contact surfaces of the forming tool: three in the upper punch labelled a–c in Fig. 1 and three in the lower die labelled d–f in Fig. 1 indicated by the small wholes in the mechanical drawing. The temperature of the forming tool with heating capability was accomplished by the use of three cartridge heaters, one 3/8 in., 250 W with an external length of 2 in. and two 3/8 in., 315 W with an external length of 2.5 in., all purchased from FARNELL. The power was regulated via a computer steered automatic control system using a PID-regulator. The smaller cartridge heater was placed in the centre section of the upper punch and the other two in the centre section of the lower die with an angle of 35° to the horizontal line. The heating of the sheet specimens and the forming tests were performed in laboratory atmosphere. Besides the temperature, the axial stroke displacement and the axial compression force were continuously measured and logged with the sampling frequency of 100 Hz. Further, the spring-back behaviour as shown in Fig. 2 (where $a = 15.0$, $b = 13.05$ and $c = 10.0$ mm) and the material thinning at the sections by thermocouple no. 2 and 3 together with the area just below thermocouple no. 2 of formed sheets were measured.

### 2.4. Metallographic studies

The as-received microstructures of the two sheet metals, the microstructures of specimens from the elevated temperature compression tests and formed sheet plates from the forming tests were examined using optical microscopy. For the as-received microstructures, rectangular samples were extracted in the rolling direction of the sheets. Typical samples of the cylindrical specimens were taken from sections along the compression axis, exact locations are stated with the figures, and samples from the forming tests were taken from the centre section 'I' where the studies have been conducted. These are labelled as 'a–e' where 'a' is at thermocouple (1), 'b' between thermocouple (1) and (2), 'c' at thermocouple (2), 'd' between thermocouple (2) and (3) and 'e' at thermocouple (3) in Fig. 2. The specimens were polished and etched with Kroll's reagent (2% HF, 3% $HNO_3$ and 95% $H_20$).

## 3. Results

### 3.1. Material response observations, compression tests

In Fig. 3, true stress–logarithmic strain relations are presented at the indicated strain rates and temperatures. Fig. 3(a) displays the isothermal stress–strain curves for the strain rate 0.05 $s^{-1}$ at various temperatures. Compression tests with prior heat treatment (HT) for 20 min at equilibrium temperature 950 °C are also presented for comparison. Initial material hardening was observed followed by specimen cracking at the lower temperatures 400–600 °C. Tests at 700–900 °C indicate material hardening followed by flow softening. Peak stresses at certain strains were also observed. The sudden peaks in the flow curves at 600 and 900 °C are however an effect of the measurements and are not related to the material. Flow softening is a well-known phenomenon for Ti-6242 and similar behaviour has been observed for the α–β titanium alloy Ti–6Al–4V. At lower temperatures or at high strain rates formation of microcracks and voids evolve during deformation, see for example [1,4,15,17,20,23]. Compression tests at 600 and 800 °C with the prior heat treatment exhibited higher resistance to deformation

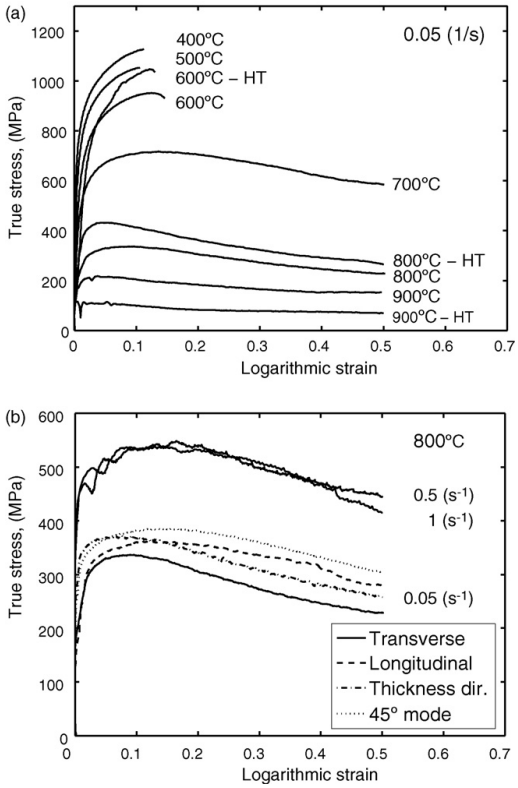


Fig. 3. (a) and (b) True stress–logarithmic strain relations at indicated strain rates, temperatures, heat treatment (HT) and directions to the rolling direction (a) tests on (T)-type specimens.

after heat treatment. The same response is expected at 700 °C. If the cooling rate of 25 °C/s was sufficiently fast, the formation of fine alpha platelets would occur and if these platelets have a smaller size than in the starting material a hardening effect should be observed. The reverse behaviour was observed at 900 °C. The curves in Fig. 3(b) displays the strain rate sensitivity at 800 °C for strain rates from 0.05 to 1 $s^{-1}$. Pronounced hardening due to higher strain rates occurred. However, no significant temperature increase was measured during deformation at any strain rate (a maximum of 7 °C at the maximum strain rate 1 $s^{-1}$). The material has anisotropic properties which also are illustrated in Fig. 3(b), in which results from compression tests on specimens extracted at the indicated directions to the rolling direction are presented. Compressed specimens extracted transverse or along the rolling direction of the sheet became oval during compression due to anisotropy [19]. This was not observed for specimens extracted in thickness direction or with extraction direction in a 45° mode to the rolling direction, these specimens remained circular.

Fig. 4(a) and (b) shows the compression forces versus diametric increase corresponding to the stress–strain results without heat treatment shown in Fig. 3(a) and for compression tests performed under continuous cooling at a rate of 25 °C/s, at the indicated strain rate and start and stop temperatures. The data presented in Fig. 4 provides additional information to the material model parameter estimations by means of inverse modelling [26–28].

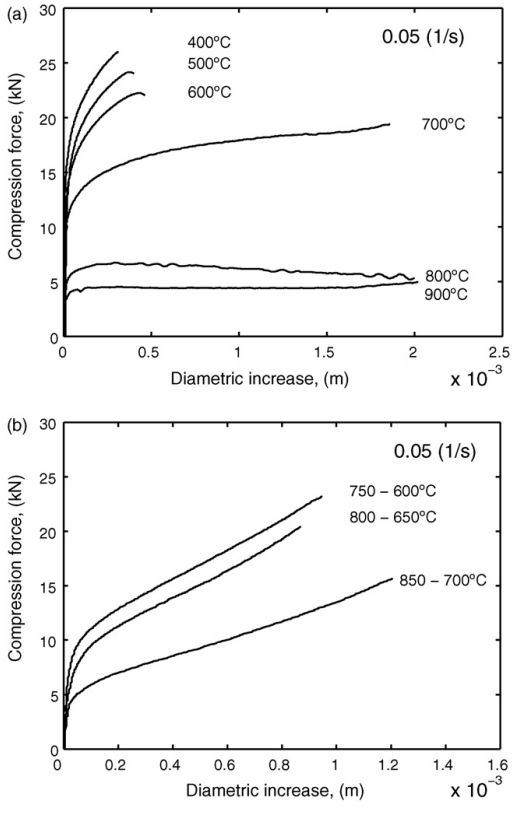


Fig. 4. (a) and (b) Compression force vs. diametric increase at indicated strain rate and temperatures or temperature intervals.

### 3.2. Material response observations, forming tests

Cold forming tests, performed with room tempered (RT) forming tool and sheet plates, could not successfully be performed. The sheet plates broke during the forming process, see Fig. 5(a) in which an abrupt dip in forming force correspond to fracture. When a comparison is made between two forming tests that were performed under identical conditions, with a forming velocity ($\upsilon$) of 5 mm/s, except the extraction direction of the sheet specimens the fractures occurred at different stages in the forming sequence. In the test with the extraction direction along (L) the rolling direction an abrupt fracture occurred above the lower radius of the die, before the critical radius had been reached. The fracture was due to a combined stretching and bending load. The fracture was unsymmetrical, probably due to a small out-of-line placement of the sheet plate in the tool, but local defects such as scratches on the sheet could also have influenced the fracture characteristics. A second fracture occurred at the centre of the opposite lower radius of the die at the very end of the forming sequence. In the other test, where the extraction direction was transverse (T) to the rolling direction, the first fracture occurred comparatively later in the forming process implying that specimens extracted along rolling direction exhibit a higher resistance to plastic deformation. This was previously confirmed by the compression tests shown in Fig. 3(b) and also indicated during the forming test, where a slightly higher forming force was required to deform the sheet plate some time before the first fracture occurred. A test performed with the higher forming velocity 10 mm/s on a T type specimen indicated strain rate sensitivity. When compared to the test performed at forming velocity of 5 mm/s (T), fracture occurred comparatively earlier in the forming sequence. Strain rate sensitivity for Ti-6242 was also confirmed by the elevated temperature compression tests, see Fig. 3(b). Measurements of spring-back and material thinning could not be made due to fracture.

Elevated temperature forming tests, performed with room tempered (RT) forming tools and pre-heated sheet specimens, were successfully performed as shown in Fig. 5(b). The desired start temperatures for all elevated temperature forming tests were 400, 700 and 1000 °C. Forming tests with preheated sheet specimens to a heating temperature of approximately 450, 750 and 1050 °C are presented in Fig. 5(b). The heating time in theses tests was approximately 200 s. Air cooling and contact with the room tempered forming tools imply somewhat lower starting temperatures when formed and substantial lower final temperatures after the 5 s holding time due to the room tempered forming tool. Exact temperatures of the sheets given by the thermocouples labelled (1)–(3), in Fig. 2 and the tools given by the thermocouples labelled ‘a–f’, in Fig. 1 are presented in Table 2 and for one selected test in Fig. 6. The forming tests preheated

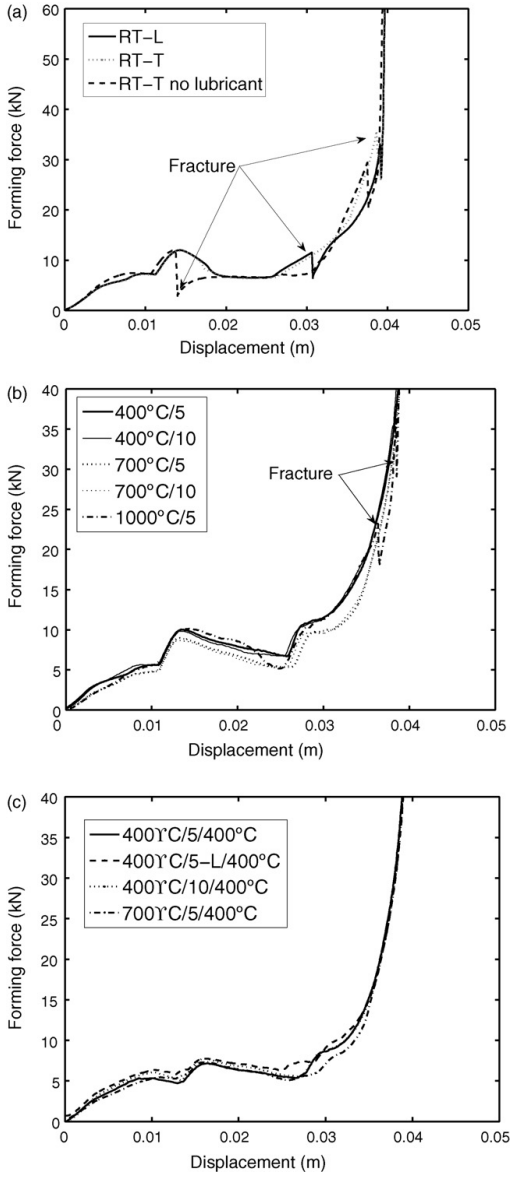


Fig. 5. Compression force vs. stroke displacement (a) at room temperature and extraction directions of sheet specimen (b) at indicated initial temperatures/forming velocities (c) at indicated initial temperatures/forming velocities and extraction directions of sheet specimen/tool temperature.

to about 1050 °C yielded similar magnitudes of forming forces, occasionally even higher, despite the higher forming temperature compared to the other tests shown in Fig. 5(b). Further on, fracture occurred at the end of the forming sequence indicating material embrittlement, caused by an alteration of microstructure into transformed beta with a basket weave structure and

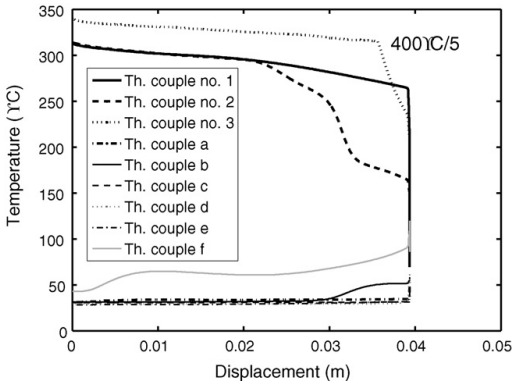


Fig. 6. Temperature history during forming sequence for indicated test and thermo couples.

formation of alpha case, see Fig. 13 which is taken from the outer surface of section 'd'.

Elevated temperature forming tests, with heated forming tools to 400 °C and pre-heated sheet specimens, could successfully be performed. Forming tests are presented in Fig. 5(c) and appertaining temperature history in Table 2. Isothermal forming of a sheet specimen with the extraction direction along the rolling direction indicated noticeable higher resistance to deformation when compared to a sheet specimen with the extraction direction transverse the rolling direction. The strain rate had less influence than extraction direction under isothermal forming at 400 °C, for the tested forming velocities. Forming preheated sheet plates, to approximately700 °C, yielded a slightly decrease in forming force compared to isothermal forming at 400 °C. The reproducibility of the forming tests was confirmed by three repeated tests to within 3.7%.

The use of boron nitride as a lubricant in the forming process was found to be of great importance. When forming in room temperature without lubricants, the friction coefficient increases causing fracture to occur earlier and more abrupt compared to forming with lubricants, see Fig. 5(a). When sheet specimens were pre-heated to 750 °C and room tempered forming tool was used, the forming was successful. However, the evenness and smoothness of the tool surfaces became even more important since existing roughness caused the sheet plate to be more adhesive on one side compared to the other. This caused the sheet plate to slide or stick during the forming process, resulting in a considerable out-of-line placement during forming. No significant material sticking was however observed.

Some material thinning occurred due to material stretching in the forming sequence as can be seen in Table 3. The highest degree of material thinning was observed in the area just below thermocouple no. 2, i.e. between thermocouple no. 2 and 3, for tests with specimens pre-heated to approximately 700 °C and formed with room tempered tools. The higher values than the initial sheet thickness at thermo couple no. 2 is due to a slight bend of the sheet plate which makes accurate measurements with the micrometer precision instrument difficult. The

Table 2
Current temperatures (°C) for hot sheet metal forming tests (temperature sheet/tool velocity (mm/s)/temperature forming tool)

| Test | Thermocouple no. | | | | | | | | |
|---|---|---|---|---|---|---|---|---|---|
| | Heating temperature | | | Starting temperature | | | Final temperature (including 5 s hold time) | | |
| | 1 | 2 | 3 | 1 | 2 | 3 | 1 | 2 | 3 |
| 400/5 | 447 | 441 | 436 | 312 | 314 | 340 | 70 | 85 | 69 |
| 400/10 | 388 | 401 | 409 | 335 | 332 | 338 | 141 | 154 | 148 |
| 700/5 | 697 | 692 | 665 | 553 | 560 | – | 128 | 128 | – |
| 700/10 | 767 | 758 | 705 | 604 | 605 | 587 | 125 | 172 | 110 |
| 700/10-ht2 | 736 | 729 | 709 | 453 | 497 | 560 | 40 | 41 | 41 |
| 400/5/400 | 456 | 458 | 447 | 415 | 425 | 382 | 378 | 396 | 385 |
| 400/5-L/400 | 466 | 469 | 443 | 422 | 432 | 412 | 378 | 401 | 399 |
| 400/10/400 | 465 | 457 | 454 | 412 | 420 | 389 | 379 | 401 | 394 |
| 700/5/400 | 720 | 714 | 688 | 594 | 608 | 604 | 396 | 421 | 451 |

Holding time in forming tool is marked by ht followed by the no. of minutes.

Table 3
Sheet thickness (mean value from five measurements, mm) and spring-back measurements (mean value from six measurements, mm) for forming tests (temperature (°C)/tool velocity (mm/s)/tool temperature (°C))

| Test | Sheet thickness, thermocouple no. | | | Spring-back distance | | |
|---|---|---|---|---|---|---|
| | 2 | Below 2 | 3 | $y$ | $x_1$ | $x_2$ |
| 400/5 | 1.95 | 1.93 | 1.95 | 0.61 | −0.30 | −0.44 |
| 400/10 | 1.96 | 1.93 | 1.94 | 0.47 | −0.06 | 0.18 |
| 700/5 | 1.96 | 1.91 | 1.93 | 0.60 | −0.09 | −1.40 |
| 700/10 | 1.97 | 1.92 | 1.94 | 0.68 | −0.84 | −1.24 |
| 700/10-ht2 | 1.98 | 1.95 | 1.95 | 0.71 | −0.49 | −0.79 |
| 400/5/400 | 1.96 | 1.94 | 1.95 | 0.37 | 0.24 | 0.42 |
| 400/5-L/400 | 1.98 | 1.95 | 1.95 | 0.28 | 0.04 | 0.18 |
| 400/5-ht5/400 | 1.97 | 1.94 | 1.94 | 0.20 | 0.15 | 0.25 |
| 400/5-ht15/40 | 1.97 | 1.94 | 1.95 | 0.25 | −0.04 | 0.00 |
| 400/10/400 | 1.97 | 1.95 | 1.96 | 0.34 | 0.27 | 0.45 |
| 700/5/400 | 1.97 | 1.94 | 1.96 | 0.47 | −0.66 | −1.19 |
| 700/5-ht5/400 | 1.99 | 1.95 | 1.95 | 0.48 | −0.64 | −1.08 |

Holding time in forming tool is marked by ht followed by no. of minutes.

spring-back characteristics of Ti-6242 can be divided into two typical behaviours, schematically illustrated in Fig. 7. Forming with the higher start temperature yields over all a higher degree of spring-back compared to forming conducted at the lower start temperature at the measured sections, see Table 3. The spring-back behaviour in Fig. 7(B), is present in all tests with a start temperature of the sheet greater than the tool temperature. This behaviour can be traced to the thermo-mechanical process, i.e. due to the varying temperature history and corresponding mechanical properties through the thickness in the sheet plate, e.g. the more rapid cooling on the surface area in contact with the tool, in the lower radius of the punch. Similar behaviour has been observed in press hardening of boron steel [27]. The isothermal forming at 400 °C is similar to forming materials at room temperature, where this thermo-mechanical effect is absent, see Fig. 7(A). The degree of spring-back can be reduced by the application of a holding time in the forming tool at the end of the forming sequence. The optimum final geometry was obtained by hot isothermal forming at 400 °C followed by a holding time of 15 min.

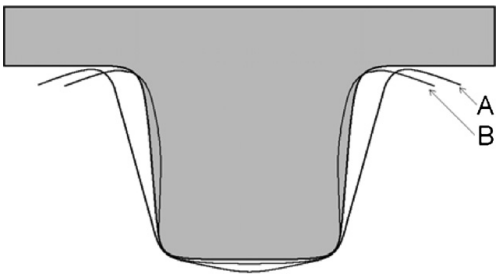


Fig. 7. Schematic illustration of final geometry of formed sheet plates: (A) isothermal test at 400 °C and (B) tests with starting temperature higher than the tool temperature.

Inhomogeneous temperature distribution existed in preheated sheets when formed by room tempered or heated forming tools, except in the isothermal test at 400 °C where the temperature differences were approximately zero. The temperature field varies throughout the sheet and its magnitude therefore depends on location, forming velocity, forming temperature and time. For example in test (700 °C/5/400 °C), the magnitude of the temperature changes vary from only 5 K/s up to 82 K/s (for short time intervals). The rate of temperature change can be even greater in tests with preheated sheets and room tempered forming tools (cooling rates locally up to 200 K/s). This implies that formed

sheet plates have different thermo-mechanical loading histories compared to the compression tests. However, further investigations into this phenomenon was not carried out in the present work.

### 3.3. Microstructural observations

As-received microstructures of the two sheet metals are presented in Fig. 8(a) and (b). The rolling direction is vertical in Fig. 8(a) and horizontal in Fig. 8(b). The microstructure contains alpha grains with some transformed beta in between, typically referred to as the $\alpha + \beta$ microstructure, see for example [22]. The microstructures were oriented containing regions of grains which are highly deformed. The microstructures of the two sheet metals differ with respect to grain size. The sheet metal used in the forming tests possesses a finer structure.

During compression, performed in the temperature range 400–600 °C specimen failure occurred and the fracture pieces of broken samples were sheared diagonal to the loading direction. In the study by Wagoner et al. [15] on compression tests at lower temperatures in Ti–6Al–4V, it was concluded that voids occur in the shear bands which form during the compression. The amount of voids increases with deformation. The voids form in the corners of sectioned specimens and grow into the centre of the specimen, the voids link up to form cracks. These cracks were responsible for the fracture and it was additionally stated that significant crack growth occurred only just before failure occurred. In Fig. 9 shear bands of isothermal compression at 500 °C is presented. Cracks have formed within a shear band in the test conducted at 600 °C.

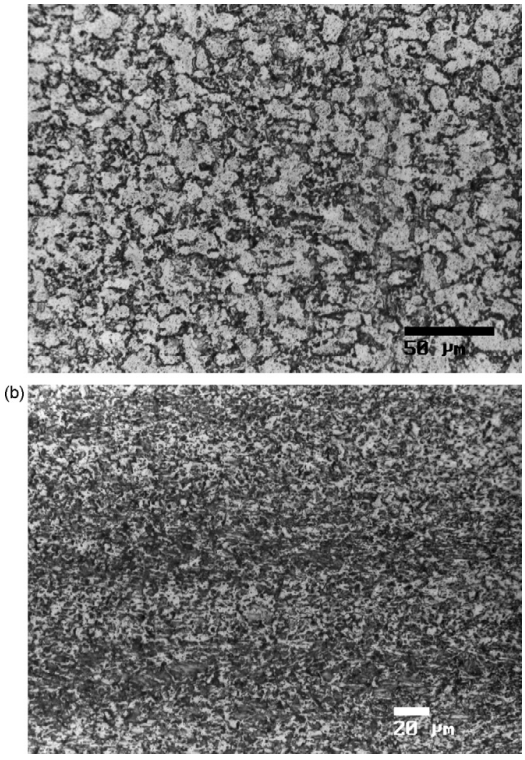


Fig. 8. As-received microstructure of (a) sheet metal for CT, rolling direction are vertical in the figure and (b) sheet metal for FT, rolling direction are horizontal in the figure.

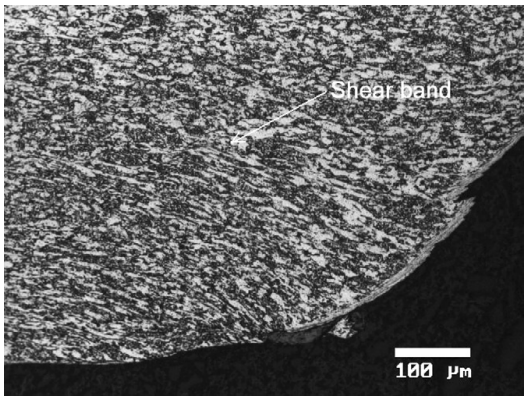


Fig. 9. Microstructure of isothermal compression test at 500 °C, with a strain rate of 0.05 $s^{-1}$. Picture taken from the border of the sample.

In parallel work it has been found that, for Ti–6Al–4V, heating rates of less then ~50 K/s results in close to equilibrium alpha-to-beta transformation up to the beta transus temperature [30]. This means that the applied heating rates in the current work, 10C°/s, should lead to close to equilibrium fraction alpha-to-beta phase for all specimens. The samples tested at temperatures of 600 °C and lower will not have any significant phase transformation at all.

Fig. 10 presents the microstructure of the compression test isothermally deformed at 700 °C, transverse rolling direction, at a strain rate of 0.05 $s^{-1}$ and to a true strain of 0.5. The small sub

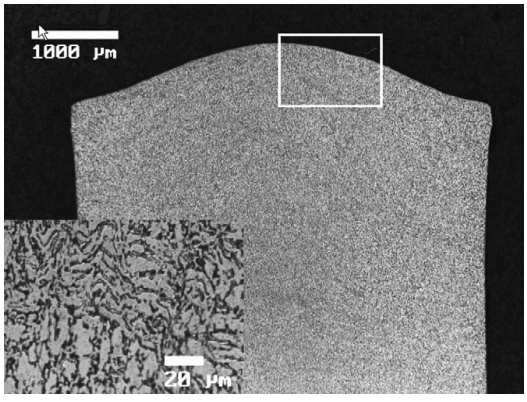


Fig. 10. Microstructure of isothermal compression test at 700 °C with a strain rate of 0.05 $s^{-1}$, to a true strain of 0.5. Shear bands are present in the specimen. Compression direction is horizontal and the rolling direction is vertical in the figures.

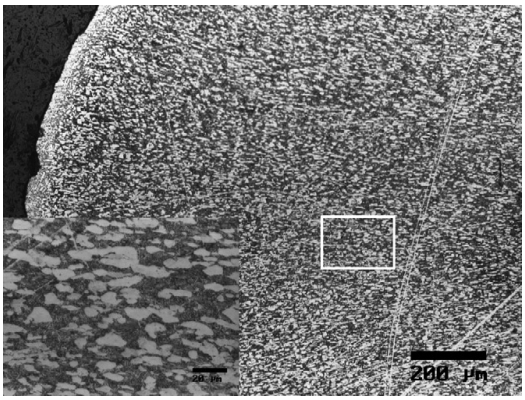


Fig. 11. Microstructure at the free edge of cross-sectioned specimen. Isothermal compression test at 800 °C, prior heat-treated, at a strain rate of 0.05 $s^{-1}$.

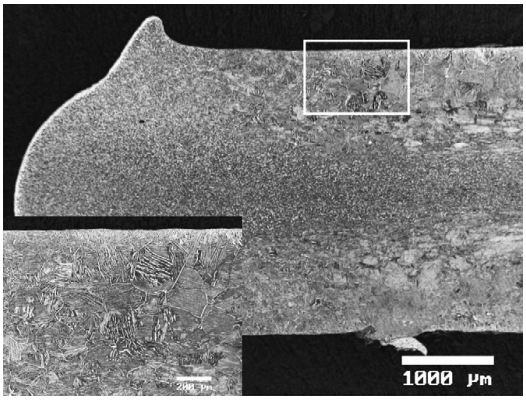


Fig. 12. Microstructure of heat-treated test compressed at 900 °C. The strain rate is 0.05 $s^{-1}$.

figure in Fig. 10 is from within the marked area. The structure becomes more and more deformed going from the anvil contact region into the centre of the specimen. A dead zone exists in the contact region with the anvil in which the structure is visually undeformed. Deformation bands were observed in the structure. The material, when compressed at the higher temperatures 700–900 °C, seems to flow towards the free bulge surface which is observed trough the wave-like deformation bands c.f. Fig. 10. No indication of alpha case was observed, in non-heat-treated specimens. As can be seen in Fig. 11 the microstructure of the heat-treated isothermal compression test at 800 °C was considerably affected. The alpha grains or platelets in the structure have increasingly been broken up and the primary alpha grains increasingly scattered when going from the less deformed contact surface region into the more deformed centre of the specimen. According to Semiatin et al. [3] this breakdown of the microstructure can cause flow softening. Indication of alpha case formation at the free surface of heat-treated specimens, see Fig. 11, indicates that the procedure in which argon gas was supplied to the testing chamber is not sufficient. Leakage occurred in which the specimens were subjected to the laboratory atmosphere. Sheared grains/deformation bands were observed in the structure. In and close to contact regions the microstructure is visually unchanged. The formation of fine alpha platelets, due to the cooling rate, observed in heat-treated compression tests, have a smaller size than in the starting material which probably causes the overall hardening behaviour as previously discussed, in these tests compared to non-heat-treated tests, see Fig. 8(a) and 11. The microstructure of non-heat-treated tests is not visually affected. The pictures are taken from the centre of the sample. The target temperature of the heat treatment was 950 °C. From the metallographic studies of the specimen heat treated for 20 min at 950 °C and compressed at 900 °C it is obvious that the temperature has been at or just above the beta transus temperature, see Fig. 12. The microstructure in the area in contact with the platens consists of fully transformed beta. In the middle of the sample primary alpha grains still exists indicating that the temperature has not exceeded the beta transus temperature, at least not long enough for complete transformation from alpha phase to beta phase. Examination of heat-treated test compressed at 800 °C does not show this fully transformed beta close to the contact region.

The microstructure of formed sheet plates was in general not considerably affected, i.e. no significant phase transformation occurred in the sheet metal forming tests conducted at temperatures up to 700 °C, and thereby no significant microstructural changes exist. However, streaks with grains subjected to a higher degree of deformation were observed. Complete transformed beta microstructure was obtained in the sheet preheated to 1050 °C, see Fig. 13 taken from the outer surface of the sheet at section 'd' in Fig. 2. High and varying temperature changes occurred in the sheet upon cooling by contact with the room tempered forming tool and due to air-cooling. This implies that the sheet was subjected to large temperature variations during the forming process. The microstructure was changed and a transformed beta with a basket weave α-structure was obtained which in combination with the formed alpha case imply less ductility of

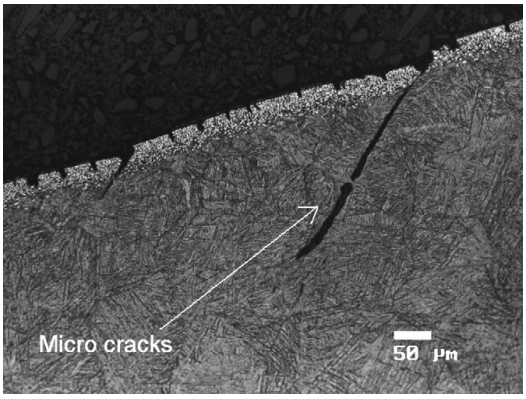


Fig. 13. Forming performed with pre-heated sheet specimen to 1050 °C with room tempered forming tools at section 'd'.

the alloy. It is obvious that alpha case has formed in which micro-cracks form upon loading, especially in bending, which grow with increasing load. The temperature at the fractured section of the sheet may also have been lower compared to other critical sections, implying even less ductility of the material. This, in combination, caused failure to occur during the forming despite the fact that the overall temperature during forming was equal or even higher compared to forming sheet specimens preheated to approximately 700 °C, where the forming was successful. The most frequent and largest micro-cracks could be found at the outer edge in section 'b', close to where fracture occurred and at the outer edge at section 'd'. Indications of micro-cracks were also found in section 'c', but no micro-cracks are visible at section 'e'. The sections labelled 'a–e' are described in Section 2.4.

## 4. Discussion and conclusions

In the present work, the thermo-mechanical response of Ti-6242 was studied in a set of tests with a broad range of temperatures and at different strain rates. By elevated temperature compression tests and sheet metal forming experiments cold and hot sheet metal forming processes for the alloy were evaluated. In future work the experimental data will be used to obtain material model parameters such as those of constitutive equations. Furthermore, results from the hot sheet metal forming tests will be used for correlation of numerical (FE) models in which estimated material model parameters are used for the prediction of sheet metal forming of Ti-6242. Major conclusions from the present work are as follows:

1. Experimental results show that initial material hardening is followed by specimen failure when the alloy was compressed at the lower temperature interval of 400–600 °C and by flow softening when it was compressed at the higher temperature interval 700–900 °C. The fracture pieces of broken samples were sheared diagonal to the loading direction. The material has anisotropic plastic properties. Higher resistance to deformation, with falling magnitude for compression in a 45° mode, in the thickness direction, along and transverse to the rolling direction were observed. Flow curves can be estimated using both a lengthwise strain gauge and a diametrical strain gauge attached to the mid height surface of the specimen. However, the presented flow curves are evaluated using the lengthwise strain gauge which means that mean temperature/strain/stress values are presented. In compression of isotropic materials evaluation of the diametric measurement would imply more accurate values avoiding the temperature and friction effect [31]. However, in compression of anisotropic materials, such as this, the cross sections of the specimens become oval [19]. Since the increase of the diameter is measured at one location only this would introduce an error using the transversal measurement. The study of anisotropic conditions and inhomogeneities are not evaluated in the present work.
2. Microstructural examination reveals that shear bands were formed at the lower temperatures in which cracks may form which as the load increases link up to form macroscopic cracks responsible for the failure. These results correspond to those found by Wagoner et al. [15] and Satish et al. [17]. In the higher temperature interval the structure becomes increasingly deformed from the anvil contact region to the centre of the specimen. A dead zone, at the contact region with the anvil was observed. Deformation bands were observed in the structure, where the material tends to flow towards the free bulging surface. To obtain accurate material model parameters, the inverse modelling technique is suitable since the inhomogeneous stress state can be taken into account [32].
3. Compression tests, that were subjected to the prior heat treatment, exhibit higher resistance to deformation as compared to non-heat-treated isothermal tests at temperatures of 600 and 800 °C. The reverse behaviour is observed at 900 °C.

   Microstructural examination of compression tests, that have been subjected to prior heat treatment, show that the microstructure has been affected. The formations of fine alpha platelets observed in the compressed specimens have a smaller size than in the starting material. This is the main reason for the overall hardening at temperatures below 900 °C, see Fig. 8(a) and 11.

   Since the area close to the platens has been fully transformed into beta phase during the heat treatment, in the test compressed at 900 °C, excessive growth of the prior beta grains has occurred. The temperature has been over the beta transus temperature in this area of the test. It is most likely these large prior beta grains which leads to the decrease in strength compared to the non-heat-treated test. It is obvious that the material deforms and flows in these regions. The material has due to this also flown out and around the edges of the platens. See Fig. 12. This is the main reason for why the strength is slightly lower for the 900 °C specimen as compared with the 900 °C specimen not heat-treated.
4. Sheet metal forming of Ti-6242 at room temperature (cold forming) could not be successfully performed with the present tool geometry. At elevated temperatures, forming was successful. However, when a sheet specimen was subjected to temperatures as high as 1050 °C (above the β-transus temperature) and with high cooling rates, a transformed beta basket weave structure was produced. The structure implies a lower ductility of the material. This, in combination with the brittle alpha case, caused failure to occur during forming. Similar anisotropic behaviour in longitudinal and transverse directions as that seen in the compression tests were observed in the forming tests, i.e. tests with sheet specimens extracted along the rolling direction exhibit higher resistance to deformation. Hardening behaviour was also observed when forming at the higher deformation rate. The examined strain rate had however less influence than extraction direction under isothermal forming at 400 °C.
5. The microstructures of formed sheet plates were not significantly affected. However, streaks with grains subjected to a higher degree of deformation were observed. Pre-heated sheet plates, to 1050 °C, caused failure during the forming despite the fact that the overall temperature during forming was equal to or even higher compared to forming sheet plates pre-heated to about 700 °C.

6. Forming with the higher start temperature (700 °C) yields overall a higher degree of spring-back compared to forming conducted at the lower start temperature (400 °C), in the measured sections. This behaviour can be traced to the thermo-mechanical process, i.e. due to the varying temperature history and corresponding mechanical properties through the thickness in the sheet plate. In isothermal forming this effect is absent. The degree of spring-back could be reduced by application of holding times at the end of the forming sequence. A minimum in shape deviation was obtained by hot isothermal forming at 400 °C followed by a holding time of 15 min.
7. The material thinning was minute in formed sheet plates due to the process itself in witch no binder was used to induce plastic straining. However, the maximum value of material thinning was observed in the test with pre-heated sheet specimens to about 700 °C and formed with room temperature tools.
8. The use of boron nitride as a lubricant in the forming process was found to be important in preventing sheet plates from sticking or sliding causing out of line placement.
9. It can be concluded from the experiments carried out in this study that Ti-6242 is suitable to be formed by hot sheet metal forming. Forming isothermally at 400 °C is to be preferred since it yields a smaller degree of spring-back, especially when holding times are applied. The Gleeble test method is suitable to obtain experimental reference data for estimation of material parameters in constitutive equations by inverse methods. If proper material models are chosen and accurate material model parameters are obtained, FE analyses can be used for the prediction of hot sheet metal forming of Ti-6242. Process parameters and tool geometry can then be studied by means of FE analyses. The final material state can be determined by including the models for phase transformation and microstructure evolution.

   However, it is important to ensure that the data are reproducible. It was found that the procedure, in which the protective atmosphere was generated, is not sufficient to prevent alpha case formation at 950 °C with a holding time of 20 min. The $\Delta T$ at 950 °C also tends to vary which caused different changes in the microstructure and mechanical properties of the alloy.

## Acknowledgements

The research founding by VINNOVA, grant P22122-1A, the collaboration with Prof. Pentti Karjalainen and Ph.D. Mahesh Somani at University of Oulu, Finland, and research assistant Mr. Jan Granström at Luleå University of Technology, Sweden, are all gratefully acknowledged.

## References

[1] R. Boyer, G. Welsch, E.W. Collings, Materials Properties Handbook: Titanium Alloys, ASM International, 1994.
[2] G. Lütjering, J.C. Williams, Titanium, Springer-Verlag, Berlin/Heidelberg, 2003.
[3] S.L. Semiatin, V. Seetharaman, I. Weiss, Mater. Sci. Eng. A A243 (1998) 1–24.
[4] R. Ding, Z.X. Guo, A. Wilson, Mater. Sci. Eng. A 327 (2002) 233–245.
[5] R. Boyer, G. Welsch, E.W. Collings, Materials Properties Handbook: Titanium Alloys, Technical note 5A, Superplastic forming of Titanium Alloys, ASM International, 1994.
[6] E.J. Tuegel, M.O. Pruitt, L.D. Hefti, Adv. Mater. Process. 136 (1989) 36–41.
[7] B.P. Bewlay, M.F.X. Gigliotti, F.Z. Utyashev, O.A. Kaibyshev, Mater. Des. 21 (2000) 287–295.
[8] N. Peter, J. Mater. Eng. Perform. 13 (2004) 660–664.
[9] J.F. Thomas Jr., S.I. Oh, H.L. Gegel, Proceedings of the Conference on Metallurgical Society of AIME, C1982, 1982, pp. 81–100.
[10] M.H. Shipton, W.T. Roberts, Mater. Sci. Technol. 7 (6) (1991) 537–540.
[11] N. Alberti, A. Forcellese, L. Fratini, F. Gabrielli, CIRP Ann. Manuf. Technol. 47 (1) (1998) 217–220.
[12] K.S. Chan, D.A. Koss, Metall. Trans. A 14A (7) (1983) 1343–1348.
[13] A. El-Domiaty, J. Mater. Process. Technol. 32 (1/2) (1992) 243–251.
[14] J. Satoh, M. Gotoh, Y. Maeda, J. Mater. Process. Technol. 139 (1–3) (2003) 201–207 (SPEC).
[15] A.J. Wagoner, C.W. Bull, K.S. Kumar, C.L. Briant, Metall. Mater. Trans. A 34 (2) (2003) 295–306.
[16] V. Seetharaman, L. Boothe, C.M. Lombard, Proceedings of the Symposium on Microstructure Properties Related Titanium Aluminides Alloys Presented 90 TMS Fall Meet, 1991, pp. 605–622.
[17] V.K. Satish, Y.V.R.K. Prasad, S.K. Biswas, Metall. Mater. Trans. A 25A (10) (1994) 2173–2179.
[18] W.-S. Lee, M.-T. Lin, J. Mater. Process. Technol. 71 (2) (1997) 235–246.
[19] S.L. Semiatin, T.R. Bieler, Metall. Mater. Trans. A 32 (7) (2001) 1787–1799.
[20] S.L. Semiatin, G.D. Lahoti, Metall. Trans. A 12A (10) (1981) 1705–1717.
[21] S.L. Semiatin, G.D. Lahoti, Metall. Trans. 13A (2) (1982) 275–288.
[22] S.L. Semiatin, G.D. Lahoti, Metall. Trans. A 14A (1) (1983) 105–115.
[23] P. Dadras, J.F. Thomas Jr., Metall. Trans. A 12A (11) (1981) 1867–1876.
[24] S.L. Semiatin, J.F. Thomas Jr., P. Dadras, Metall. Trans. A 14A (11) (1983) 2363–2374.
[25] A. Tarantola, Inverse Problem Theory—Methods for Data Fitting and Model Parameter Estimation, Elsevier, 1987.
[26] M.C.F. Eriksson, Doctoral Thesis 2002:19, Luleå University of Technology, Sweden, 2002.
[27] P. Åkerström, Doctoral Thesis 2006:30, Luleå University of Technology, Sweden, 2006.
[28] E.-L. Westman, R. Pederson, B. Wikman, M. Oldenburg, Proceedings of the 10th World Conference on Titanium, Ti-2003 Science and Technology, Hamburg, Germany, July 13–18, 2003, pp. 1461–1468.
[29] J. Kajberg. Doctoral Thesis, 2003:35; Luleå University of Technology, Sweden, 2003.
[30] R. Pederson, Doctoral Thesis 2004:19, Luleå University of Technology, Sweden, 2004.
[31] L.X. Li, Y. Lou, L.B. Yang, D.S. Peng, K.P Rao, Mater. Des. 23 (5) (2002) 451–545.
[32] P. Åkerstöm, B. Wikman, M. Oldenburg, Model. Simul. Mater. Sci. Eng. 13 (2005) 1291–1308.

# Paper C

International Deep Drawing Research Group
IDDRG 2008 International Conference
16-18 June 2008, Olofström, Sweden

# A SHORT LEAD TIME METHODOLOGY FOR DESIGN, COMPENSATION AND MANUFACTURING OF DEEP DRAWING TOOLS FOR INCONEL 718

**E.-L. Odenberger[①②], M. Jansson[③], P. Thilderkvist[①], H. Gustavsson[④] and M. Oldenburg[②]**

① Forming Group
Olofström School of Automotive Stamping
Vällaregatan 30, SE-293 38, Olofström, Sweden
E-mail: Eva-Lis.Odenberger@osas.se, Web page: http://www.osas.se

② Division of Solid Mechanics, Luleå University of Technology
SE-971 87 Luleå, Sweden
E-mail: Mats.Oldenburg@ltu.se, Web page: http://www.ltu.se

③ Engineering Research Nordic AB
Garnisonen Brigadgatan 16, SE-581 31 Linköping, Sweden
E-mail: Mikael.Jansson@erab.se, Web page: http://www.erab.se

④ Volvo Aero Corporation
Manufacturing Technology, Fabrication & Simulation, SE-461 81 Trollhättan, Sweden
E-mail: Henrik.Gustavsson@volvo.com, Web page: http://www.volvo.com

**Key words:** Tool Design, Simulation, Springback, Compensation, Validation, Lead Time

**ABSTRACT.** *This paper presents a systematic methodology for the design and manufacturing of deep drawing tools generating high quality components at an extremely short lead time. Prototype tools for five different super alloy Inconel 718 sheet metal components were designed, manufactured and tested in 15 weeks. Two of these prototype tools (A, B) are the topics of this paper. The methodology is based on virtual tool design in which the tool concepts are secured and optimized with respect to sheet metal formability and shape deviation using FE-analyses. Tool surfaces are compensated for springback, if necessary, using the *INTERFACE_COMPENSATED_NEW capability in LS-DYNA v971 (B). The compensated FE tool surfaces are used as reference to generate high quality surfaces suitable for the milling process. Laser scanning was used to determine shape deviation. The CAD-evaluation revealed a minor shape deviation within tolerance of component (A) and a small over-compensation of the final geometry of component (B). The maximum shape deviation was however in the order of the sheet thickness. The work presented in this paper substantiate the idea that it is possible to realize development projects for new applications in Inconel 718 accurately, which is of outmost importance when developing tools at a short lead time. The key is consistent studies according to the systematic methodology in which FE-analyses were used for the virtual tool design and compensation.*

## 1. INTRODUCTION

A successful development project in the modern industry can be characterized by "direct hit" development work, in which the accuracy is high and the lead time is short. The ability to realize successful projects with short lead times has become increasingly important for the forming industry today. To increase the competitiveness of Swedish aerospace industry, alternative manufacturing processes for static load carrying aero engine structures are desired, see Figure 1 for an illustration. Currently, these components are mainly manufactured from large single-part castings delivered by only a few companies. New manufacturing processes imply in this case fabricated components, which mean that components are instead built from simple forgings, sheet metals and small castings. The aerospace industry demands extremely high safety and reliability. Thus, good knowledge is required regarding the effects of the manufacturing process on the material and the influence on the resultant properties through the complete manufacturing chain.

In the design of new products and corresponding tools, considerable costs often arise from the traditional product development process. This is a process which often includes prototype manufacturing and die tryout. If the product fails to fulfill the requirements, the tools have to be re-worked or even re-designed. Today's advanced Finite Element (FE) technology and computer capacity makes precise analyses possible, assuming that proper material descriptions are used. The reliability of numerical analyses depends on chosen models and methods as well as on the accuracy and applicability of the input data. Analyses of sheet metal forming can provide information on formability, shape deviation, resultant mechanical properties and residual stress state. This is important input to analyses of subsequent manufacturing processes such as welding and heat treatment. Numerical methods such as the finite element method are often employed in simulations of manufacturing processes and component functionality, see e.g. [1-5].

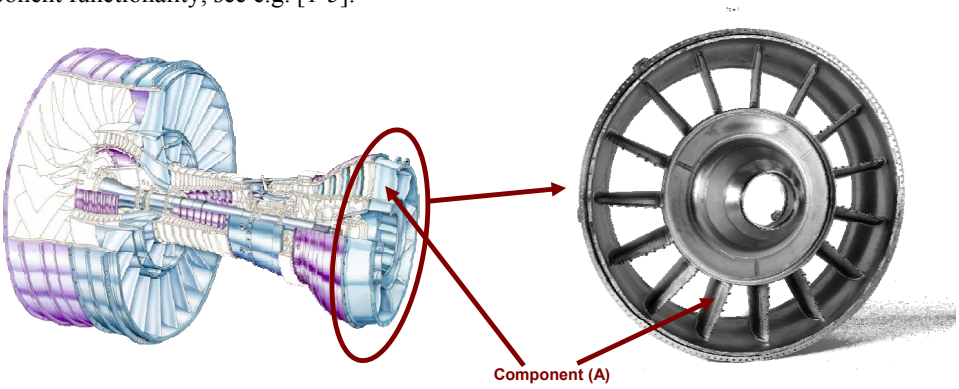


***Figure 1.*** *Illustration of location for static load carrying aero engine structures.*

This paper presents a systematic methodology, a systematic way of working with the design and manufacturing of deep drawing prototype tools generating high quality components at an extremely short lead time. Two of these prototype tools (A, B) are the topics of this paper. The presented methodology comprises material characterization, tool design and tool material selection, analyses of sheet metal forming (FE-analyses), springback compensation, tool manufacturing, choice of lubricant, prototype stamping, laser cutting and laser scanning for shape deviation determination. The procedure is a completely CAE-controlled process, in which time consuming and inexact manual die tryout can be kept at a minimum. In this work, traditional methods to obtain necessary model input data for Inconel

718 were used, i.e. uniaxial tensile tests and a silicon rubber bulge test together with dynamic tests on the Young's modulus. Forming limit tests (FLC) were performed to study strain localization limits.

Rather than stating a "new" methodology, the presented paper contributes to the idea that it is possible to realize development projects for new applications, in this case cold forming of double-curved Inconel 718 components, accurately at a short lead time. In the modern industry, e.g. the automotive industry, long experience using CAE-controlled processes exists and numerous papers are published in the field, see e.g. [6-11] and in references therein.

## 2. MATERIALS

When the lead time is of significant importance, finding time efficient and functional solutions applicable to the process of interest is critical. Concerning sheet metal forming and prototype deep drawing tools, the design, manufacturing and the test stamping procedure are the main time-consuming activities. In order to keep the lead time short a "direct hit" development work is crucial to avoid extensive die tryout. Through material testing and virtual tool design, in which CAD generated forming concepts are evaluated, secured and optimized by means of FE analyses, the best starting position for the tool manufacturing were obtained. Based on the chosen methods and models, the virtual components are within shape and thickness tolerances. Forming concepts are secured and optimized with respect to sheet metal formability, material thinning and shape deviation. The springback of each component are reduced by performing changes in the virtual tool concepts, such as the geometry of the punch and die, punch radii, drawbead geometry and location, draw radii, draw depth and blank holder force. Remaining shape deviation is compensated for, if necessary, with the FE-tool. See figure 2 for a schematic illustration of the tool setup.

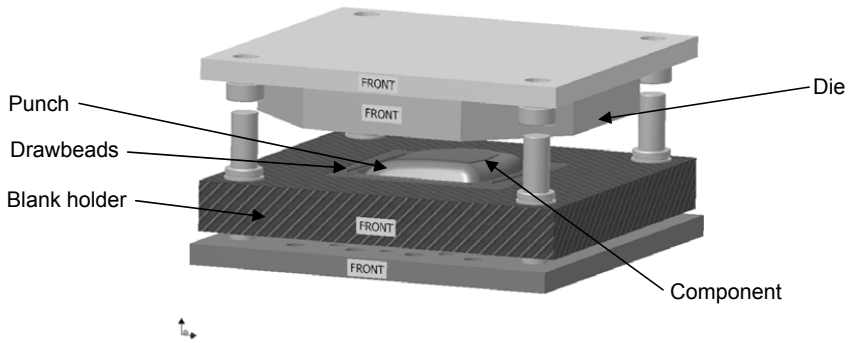


***Figure 2.*** *Schematic illustration of the tool setup.*

The design phase can be divided into four main steps:

i. *Drafting stage* - generation of preliminary forming concepts.
ii. *Evaluation stage* - securing the forming concepts with respect to strain distribution and strain localization limits.
iii. *Improvement stage* - improving the forming concepts to minimize springback and shape deviation. The target is virtual components within thickness tolerance and if possible, also within shape tolerance.
iv. *Compensation stage* - compensating for the remaining shape deviation, if necessary. The target is virtual components within shape and thickness tolerances.

See Figure 3 for a schematic flow chart of the complete design phase and Figure 4 for the compensation stage.

The lead time associated with tool manufacturing is also of great importance. The choice of tool material was therefore made with respect to delivery time, the need for subsequent through-hardening and the machinability. Concurrently, the manufacturing phase was initiated parallel with the design phase, e.g. were certain dimensions frozen early in the project to gain time. During the tool manufacturing and assembly, certain check points were included. Thus, features which were of special importance for the forming procedure were checked and approved during the specific manufacturing process or assembly stage associated to it.

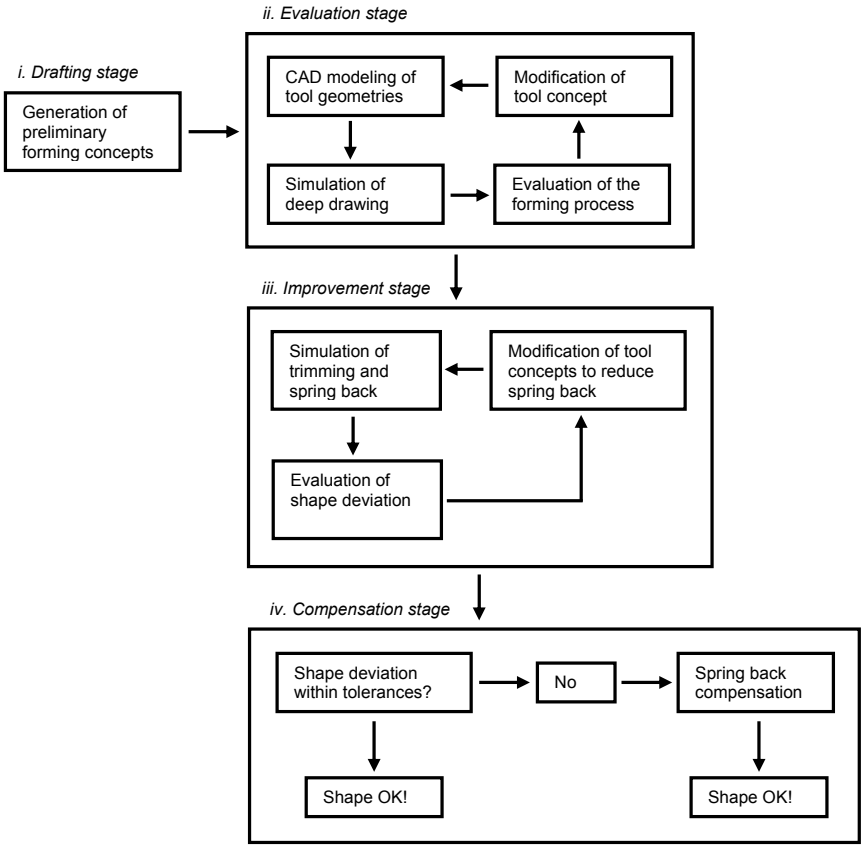


***Figure 3.*** *Schematic flow chart of the design phase.*

## 2.1. Material description of sheet material

A material of interest addressing aero engine structures at high operating temperatures is super alloy Inconel 718. The alloy is an austenitic stainless steel, with an FCC crystal structure [12], which is regarded as advanced high strength steel. The ductile alloy has generally, in sheet metal form, anisotropic properties in combination with high yield strength implying springback characteristics similar to those of high strength steels. Springback is well known to be an issue concerning sheet metal forming in high strength steels. Typical chemical

composition of the alloy together with typical mechanical properties can be found in Table 1 and 2, AMS 5596K [13]. Two different sheet thicknesses were used, a thinner sheet (62.9 % of the thickness for (A)) was used for (B) compared to (A).

***Table 1.*** *Typical chemical compositions of the sheet and the tool material (wt-%). For TOOLOX 44 the phosphorus, sulphur and boron are given in ppm.*

| **Material** | **Chemical composition** | | | | | | | | |
|---|---|---|---|---|---|---|---|---|---|
| Inconel 718 | C | Mg | Si | P | S | Cr | Ni | Mo | Nb |
| | 0.08 | 0.35 | 0.35 | 0.015 | 0.015 | 21.00 | 55.0 | 3.30 | 5.50 |
| | Ti | Al | Co | Ta | B | Cu | Fe | | |
| | 1.15 | 0.80 | 1.00 | 0.05 | 0.006 | 0.30 | reminder | | |
| TOOLOX 44 | C | Si | Mn | P | S | Cr | Mo | V | B |
| | 0.32 | 1.1 | 0.8 | 90 | 15 | 1.35 | 0.8 | 0.14 | 20 |

Methods for the material characterization are described in section 3.

### 2.2. Material description of tool material

The tool material used for the prototype tools was TOOLOX 44. The material is trough-hardened in its delivery condition with hardness of 450 HBW, in combination with ESR-properties [14]. The milling process of the material could be performed fairly time effective with standard milling equipment. Furthermore, the delivery time was short. Typical chemical composition and mechanical properties of TOOLOX 44 can be found in Table 1 and 2.

***Table 2.*** *Typical mechanical properties of the sheet and the tool material.*

| **Material** | **Mechanical properties** | | | | | |
|---|---|---|---|---|---|---|
| | $\rho$ [kg/m$^3$] | E [GPa] | $\upsilon$ | Hardness | $R_{P0,2}$ [MPa] | $R_m$ [MPa] |
| Inconel 718 | 8200 | 200 | 0.29 | 102 HRB | 552 | 965 |
| TOOLOX 44 | 8000 | 210 | 0.3 | 450 HBW | 1300 | 1450 |

### 2.3. Numerical procedure

The tool design, e.g. punch and die geometry, punch radii, binder geometry, drawbead geometry and location, draw radii, and draw depth were designed and optimized to secure the forming process and reduce springback. To obtain components within the specified shape tolerance, springback compensations were performed for one of the components (B). Based on chosen models this procedure implies the best possible starting point for the manufacturing of the tools.

The forming processes in this work are a combination of deep drawing and stretch forming, i.e. moderate draw-in occur during the forming process. The tool concepts were modeled and analysed using LS-DYNA v971 [15, 16]. The general simulation setup consists of a die with physical drawbeads, blank, binder and a punch. Fully integrated shell elements with 7 integration points through the thickness were used. An h-adaptive method of mesh refinement was used to locally increase the mesh density where needed. The tool surfaces were modeled as rigid with a prescribed velocity profile and the contact between the tools and the specimen was included and modeled as a contact interface with a friction model assumed to follow Coulomb's friction law. The friction coefficient was set to 0.125. For the springback analyses, the implicit solver in LS-DYNA was used. Also, the constrained nodes were altered to insure that the obtained shape deviation was not affected by the choice of nodal constraints. See Figure 5 and 6 for definition of shape deviation and the constrained node set (translation).

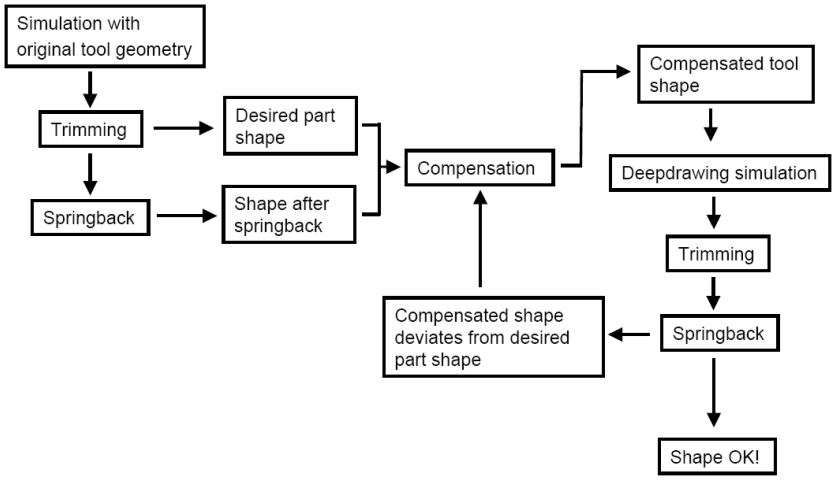


***Figure 4.*** *Schematic flow chart of the compensation stage, the springback compensation.*

The BARLAT_YLD2000 material model [17] was used with eight parameters to describe the yield surface. The yield stress, the hardening and the Lankford parameters were determined in the material characterization by uniaxial tensile tests and a silicon rubber bulge test for the balanced biaxial stress state. The m-parameter was set to a value of 8, which is a typical value for materials with an FCC crystal structure [17].

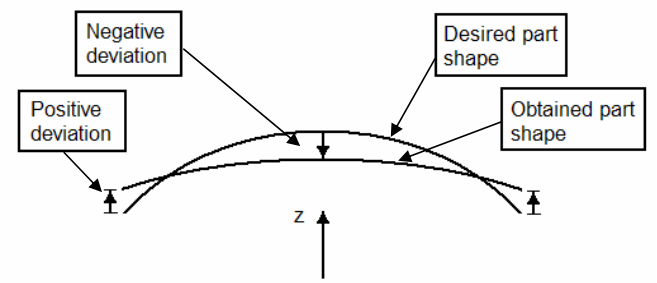


***Figure 5.*** *Schematic illustration of the definition of shape deviation.*

The tool surfaces were compensated for springback, if necessary, using the *INTERFACE_COMPENSATED_NEW capability in LS-DYNA v971 (B). The springback compensation method involves calculation of the deviation from desired part shape and compensating the tool surfaces by a scale factor of the deviation. A scale factor of 1.0 corresponds to a compensation of 100% of the shape deviation. The problem is non-linear. Thus several iterations might be required to obtain a component within shape tolerance. In this case a scale factor of 1.0 was applied for (B) which yielded an FE-component within the specified shape tolerance. The compensated FE tool surfaces were used as input to generate high quality surfaces suitable for the milling process using Tebis Optimizer [18].

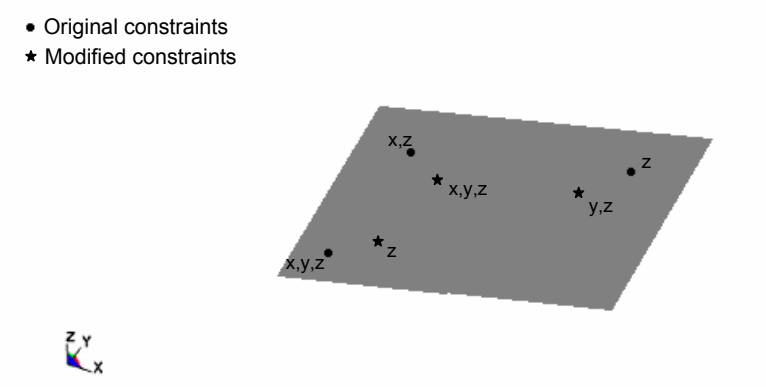


***Figure 6.*** *Schematic illustration of alteration of the nodal constraints for springback analyses.*

## 3. EXPERIMENTAL PROCEDURE

### 3.1. Material characterization

To determine the Young's modulus, dynamic tests were performed using the non destructive impulse excitation technique which is based on the analysis of the vibration of a test sample after excitation by a physical impulse. Using the Resultant Frequency and Damping Analyzer (RFDA) system 23, version 6.3.0, developed and manufactured by IMCE [19], the Young's modulus is determined through the known relationship between the elastic properties of a test specimen and its mechanical resonance frequency. A more detailed description of the procedure can be found in e.g. [19, 20]. Specimens were extracted transverse, along and diagonal to the rolling direction.

Uniaxial tensile tests in three directions to the rolling direction (transverse, along and diagonal) were performed to determine initial yield stress, material hardening and Lankford parameters. A silicon rubber bulge test using ARAMIS optical strain measuring system [21] was performed to determine material hardening and anisotropy in a balanced biaxial stress state. Also, forming limit tests (FLC) using ARAMIS were included in the material test procedure to study strain localization limits.

### 3.2. Test stamping

Test stamping of the prototype tools producing prototype components were performed in order to evaluate shape deviation and compare with predicted values. The area of impact between the punch and the blank was also studied. Two different presses were used for the test stamping due to requirements in blank holder force. For tool (A) a Wemhöner hydraulic press, with a stamping/blank holder force capability of 13000/2000 kN, was used and for tool (B) a Fjellman hydraulic press, with a stamping/blank holder force capability of 7500/3200 kN, was used. Special care was made to, as far as possible, maintain the same conditions in the test stamping procedure as in the simulations. For example, the blank holder force was measured to a maximum of approximately 1850 kN for (A) and to 3.6% higher for (B) of the force used in the simulation. The draw in was measured during the forming and used as an early indicator to observe deviations between obtained and predicted values. Blank materials were coated with a Houghton 500 dry lubricant to reduce friction and prevent wear and scratches to occur, especially in drawbeads.

### 3.3. Evaluation of shape deviation

After forming, addendum material was removed by laser cutting, reference points enabled

laser cutting at correct locations. The reference points were produced at the end of the forming stage. To evaluate shape deviation and material thinning, 3D laser scanning of both sides of the components were made. Best fit evaluations were used as a method to determine the shape deviation from the nominal part geometry. The same definition of shape deviation as in the analyses was used, see Figure 5.

## 4. RESULTS

Measurements revealed an isotropic Young's modulus. The hardening was substantial in Inconel 718. The tensile tests and the bulge test revealed a fairly isotropic behavior in stresses. Figure 7 presents normalized hardening curves for one of the sheet thicknesses in the different directions to the rolling direction, along (L), transverse (T) and diagonal (D).

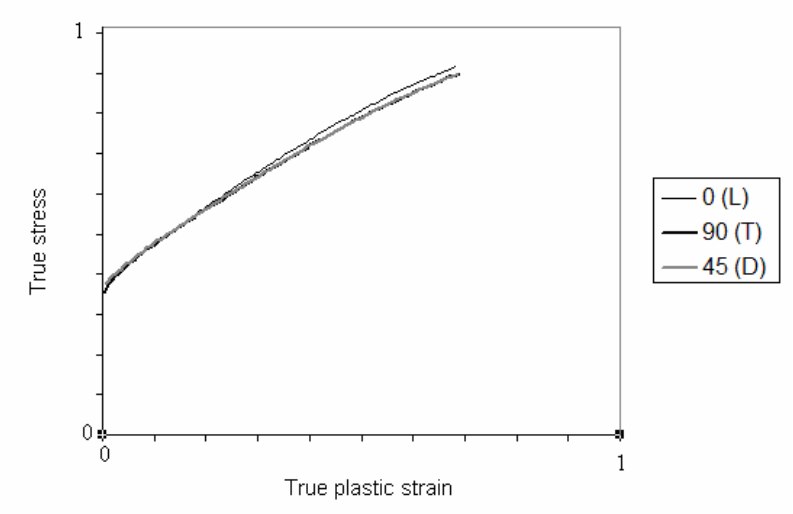


***Figure 7.*** *Normalized hardening curves.*

The uniaxial tensile tests and the balanced biaxial test revealed anisotropic strain properties. The Lankford parameters varied within 69% between the different directions to the rolling direction including the balanced biaxial state. In Figure 8, the shape of the FLC for one of the sheet thicknesses is presented. Five normalized values are presented.

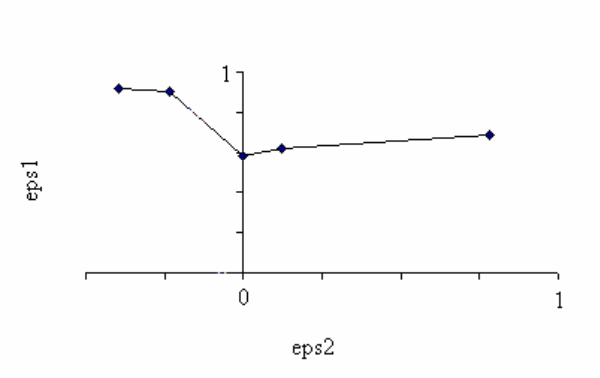


***Figure 8.*** *Shape of the normalized forming limit curve.*

The draw-in was measured with a Vernier caliper during the test stamping to verify the FE-predictions. The measurements revealed values within 12.4-13.2% in one direction and 9.0-20.8% in the other for (A) and 3,3% in one direction and 6,6-18,5% in the other for (B) compared to the calculated ones. See Table 3 for predicted and measured values. It can be concluded that the draw-in was smaller than predicted.

The difference in draw-in can mainly be explained by the friction condition and small differences in draw depth and blank holder force between the FE-models and the manufactured tool setups. The sheet thickness for (A) was 2% larger than then the thickness used in the simulations, which is expected to yield an increased force in the drawbeads that may contribute to a smaller draw-in.

***Table 3.*** *Predicted and measured values of the draw-in during forming (mm).*

| **Component** | **Predicted draw-in** | | | | **Measured draw-in** | | | |
|---|---|---|---|---|---|---|---|---|
| Draw-in direction | $X_1$ | $X_2$ | $Y_1$ | $Y_2$ | $X_1$ | $X_2$ | $Y_1$ | $Y_2$ |
| A | 12.1 | 10.5 | 11.1 | 10.1 | 10.5 | 9.2 | 10.1 | 8.0 |
| B | 12.4 | 12.2 | 17.6 | 18.5 | 10.1 | 11.4 | 18.2 | - |

Results from the laser scanning and best fit evaluation revealed a minor shape deviation, within tolerance, of component (A). After compensating tool surfaces (B) using the *INTERFACE_COMPENSATED_NEW capability in LS-DYNA v971, measurements revealed a small over-compensation of the tool geometry for component (B). See Figure 9 and 11 for sections of the components. The values in the figures are normalized with respect to the sheet thickness in which a value of 1.0 would imply a shape deviation equal to the sheet thickness. The maximum shape deviation was however in the order of the sheet thickness for component (B) and within tolerance for component (A). The material thinning of prototype component (A) is presented in Figure 10, indicating a measured maximum material thinning of 11.9%. The corresponding predicted maximum material thinning was 10.9%. A value of 1.0 corresponds to 100% of the original sheet thickness.

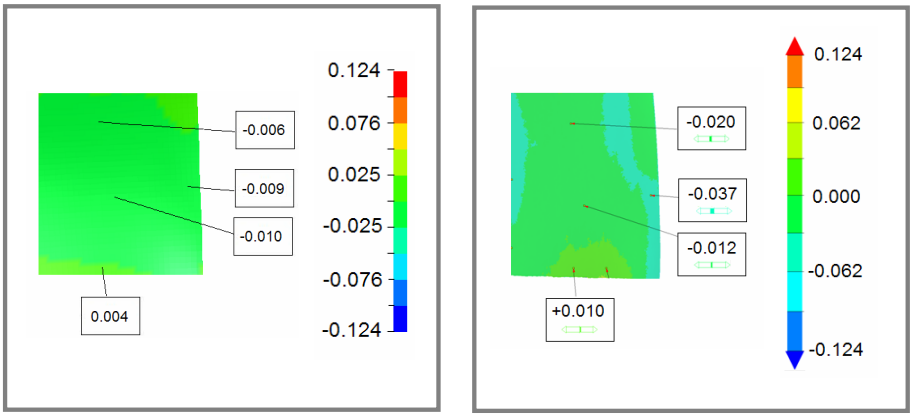


(a) b)

***Figure 9.*** *Shape deviation for section of (A) generated by (a) FE-analysis and (b) laser scanning.*

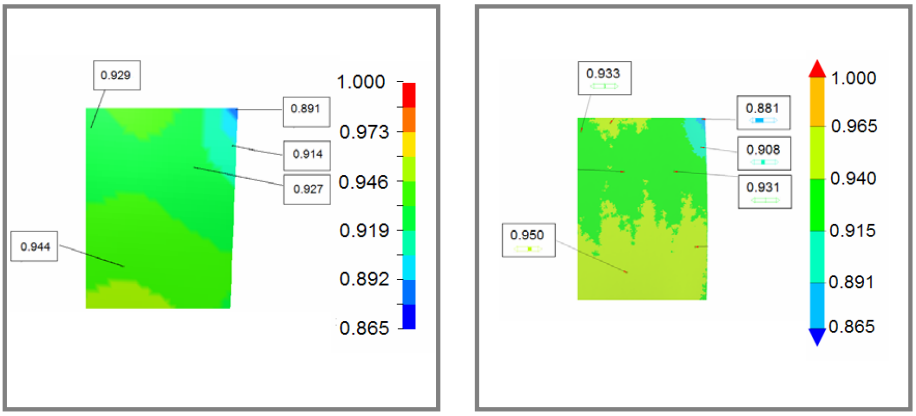


(a) b)

***Figure 10***. *Material thinning for section of (A) generated by (a) FE-analysis and (b) laser scanning*

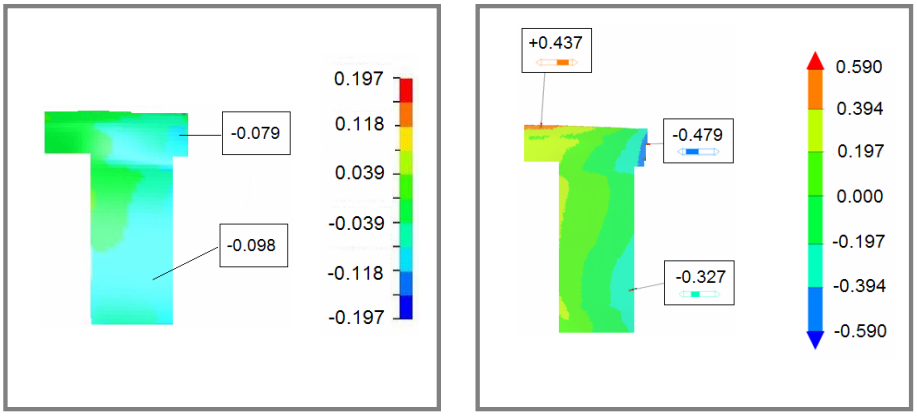


(a) b)

***Figure 11***. *Shape deviation generated by (a) FE-analysis and (b) laser scanning for section of (B).*

## 5. DISCUSSION AND CONCLUSIONS

The work presented in this paper substantiates the idea that it is possible to realize development projects for new applications in Inconel 718 accurately and with minor (B) or no (A) need for modifications of the designed tools. No further need for modifications of the tools for the other three double-curved components not presented here were required. Tool (B) yielded a slightly overcompensated component. The differences in predicted and measured draw-in affect the springback. The shape deviation ought to be improved by obtaining a slightly smaller draw-in according to the measured values and reducing the tool compensation for the springback. A proper choice of compensation magnitude is not straight forward to determine in advance, since it depends on the geometry, the material and the forming process, see e.g. [8, 9]. For one case a compensation which exceeds 110% can be optimal but for other materials much less compensation is applicable, see e.g. [10, 16]. Therefore, test stamping and accurate shape deviation determination is necessary to correlate springback predictions and adjust the tool compensation. The chosen compensation of 100% for (B) was in this case too high. The commercial FE-code, LS-DYNA, in combination with

software to generate high quality surfaces, Tebis Optimizer, were used for the tool compensation in the industrial applications. Despite the simplicity of the method it works remarkably well. The tool was compensated in only one iteration which yielded a virtual component within shape tolerance, see Figure 11 (a). For a more thorough discussion of the possibilities and limitations concerning methods of springback prediction and compensation, see e.g. [6-11] and references therein.

Minimizing the die tryout is of outmost importance when developing tools for short lead times. The key is consistent studies according to the presented systematic methodology in which FE-analyses are used for the tool design and compensation. To obtain equal conditions in the stamping procedure as in the simulation, equal tool geometry and process parameters, correct boundary conditions and proper material descriptions have to be applied. In the design of deep drawing tools for new materials and/or new processes, the FE-technique is a helpful tool in avoiding undesirable effects and improving the tool design which increases the chance of a successful initial tool design.

## 6. ACKNOWLEDGEMENTS

Co-worker Mr. Peter Axelsson at Industrial Development Centre in Olofström AB and tool manufacturer ITE Fabriks AB in Olofström, both located in Sweden, are gratefully acknowledged for their designation to this work and full flexibility.

## 7. REFERENCES

1. T. Belytschko, W.K. Liu, B. Moran, ”Nonliear Finite Elements for Continua and structures”, John Wiley & Sons, New York (2000) ISBN 0-471-98773-4
2. T. Belytschko and K. Mish, ”Computability in non-linear solid mechanics”, *International Journal for Numerical Methods in Engineering* 52 (2001) 3-21.
3. V. Adams and A. Askeazi, ”Building Better Products with Finite Element Analysis”, On Word Press, Santa Fee, USA (1999) ISBN 1-56690-160X.
4. A.E. Tekkaya, ”State of the art of simulation of sheet metal forming”, *Journal of Materials Processing Technology* 103 (2000) 14-22.
5. K. J. Bathe, ”On the state of finite element procedures for forming processes”, In S. Gosh, J.C. Castro and J.K. Lee, editors, CP712, *Materials Processing and Design: Modeling, Simulation and Applications, NUMIFORM* (2004) 34-38. American Institute of Physics.
6. K. Mattiasson, M. Sigvant, ”An evaluation of some recent yield criteria for industrial simulations of sheet forming processes”, *International Journal of Mechanical Sciences* 50 (2008) 774-787.
7. N. Asnafi: ”On springback of double-curved autobody panels”, *International Journal of Mechanical Sciences* 43 (2001) 5-37.
8. T. Meinders, I.A. Burchitz, M.H.A. Bonte, R.A. Lingbeek, ”Numerical product design: Springback prediction, compensation and optimisation”, *International Journal of Machine Tools & Manufacture,* 48 (2008) 499-514 .
9. R. Lingbeek, J. Huétink, S. Ohnimus, M. Petzoldt, J. Weiher, ”The development of a finite elements based springback compensation tool for sheet metal products”, *International Journal of Materials Processing Technology,* 169 (2005) 115-125.
10. T. Dutton, R. Edwards, A. Blowey,”Springback Prediction and Compensation for a High Strenth Steel Side Impact Beam”, In L. S. Smith, F. Pourboghart, J. –W. Yoon and T. B. Stoughton, editors, CP712, *NUMISHEET* (2005) 340-344. American Institute of Physics.
11. S. Ohnimus, M. Petzoldt, B. Rietman, J. Weiher,”Compensating springback in the automotive pratice using MASHAL”, In L. S. Smith, F. Pourboghart, J. –W. Yoon and T. B. Stoughton, editors, CP712, *NUMISHEET* (2005) 322-327. American Institute of Physics.

12. C.T. Sims, N.F. Stoloff, W.C. Hagel, ”Superalloys II”, New York, Weiley, cop. (1987) ISBN 0-471-01147-9.
13. SAE Publications: http://www.sae.org, May (2007).
14. P. Hansson: ”TOOLOX – The Multi-purpose Pre-hardened Tool Steels”, *2nd International Conference on Accuracy in Forming Technology* ICAFT (2006) 183-200.
15. J.O. Hallquist, ”LS-DYNA Theory Manual” Livermore Software Technology Corporation, Livermore (2006).
16. ”LS-DYNA Keyword User´s Manual” Volume 1, v971, Livermore Software Technology Corporation, Livermore (2007).
17. F. Barlat, J.C. Brem, J.W. Yoon, K. Chung, R.E. Dick, D.J. Lege, F. Pourboghrat, S.-H. Choi and E. Chu, ”Plane stress yield function for aluminium alloy sheets – part 1: theory”, *International journal of Plasticity* 19 (2003) 1297-1319.
18. Tebis Optimizer: http://www.tebis.se, April (2008).
19. Manual for The Resultant Frequency and Damping Analyser (RFDA) system 23, version 6.3.0, IMCE (2006).
20. RFDA: http://www.imce.cit.be, April (2008).
21. ARAMIS v6: http://www.gom.com, April (2008).

# Paper D

# Tool development based on modelling and simulation of hot sheet metal forming in titanium Ti-6Al-4V

**E-L Odenberger[1, 2], M Oldenburg[2], P Thilderkvist[1], T Stoehr[3], J Lechler[3], M Merklein[3]**

[1] Forming Group, Olofström School of Automotive Stamping, Industrial Development Centre in Olofström AB, Vällaregatan 30, SE-293 38 Olofström, Sweden

[2] Division of Solid Mechanics, Luleå University of Technology, SE-971 87 Luleå, Sweden

[3] Manufacturing Technology, University of Erlangen-Nuremberg, Egerlandstr. 13, 91058 Erlangen, Germany

E-mail: Eva-Lis.Odenberger@iuc-olofstrom.se

**Abstract**

In the aero engine industry new manufacturing processes for load carrying aero engine structures imply fabrication. The concept of fabrication involves simple forgings, sheet metals and small ingots of e.g. titanium alloys which are welded together and heat treated. In the concept phase of the product development process, accurate evaluations of candidate manufacturing processes with short lead times are crucial. In the design of sheet metal forming processes, the manual die try out of deep drawing tools are traditionally a time consuming, expensive and inexact process. The present work investigates the possibility to design hot forming tools, with acceptable accuracy at short lead times and with minimal need for costly die try out, using finite element (FE) analyses of hot sheet metal forming of the titanium alloy Ti-6Al-4V. A rather straight forward and inexpensive approach of material modelling and methods for material characterisation are chosen, suitable for evaluations in the concept phase and validated by comparison with data from separate forming experiments performed at moderately elevated temperatures. The computed global force response is shown to be in acceptable agreement with the experiments and the shape deviation is predicted within the sheet thickness. Solutions for the hot forming tool concept regarding heating and regulation, insulation, blank holding and tool material selection are evaluated within the present study.

## 1. Introduction

Titanium alloys are often used in aero space applications due to their high strength to weight ratio. For static load carrying aero engine structures titanium alloys are used with running temperatures up to about 350°C. A common alloy for this type of applications is Ti-6Al-4V. Traditionally, these structures mainly consist of large-scaled single castings. Alternative manufacturing processes for static load carrying aero engine structures are developed in order to take advantage of the possibility to reduce weight, and thereby fuel consumption and also product cost. The alternative fabrication process involves simple forgings, sheet metals and small ingots which are welded together and heat treated. Complete titanium structures are often located in the forward part of the aero engine, see figure 1. The

subcomponent consists of sheet metal components (i), ingots (ii) and parts manufactured by metal deposition (iii) which are welded together.

In the chain of manufacturing, the resultant geometry, material thinning and mechanical properties of the parts obtained by sheet metal forming influence the final shape deviation of subcomponents and complete structures upon welding and heat treatment. If results obtained from finite element (FE) analyses of sheet metal forming can be included in analyses of subsequent welding and heat treatment, in an early stage of the product development process, an increased understanding of the incremental shape deviation and suitable methods for compensation can be obtained.

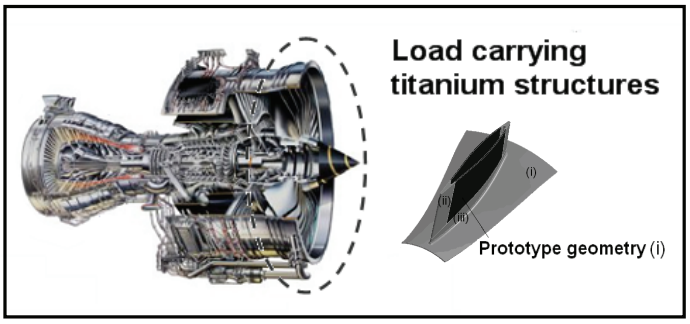


**Figure 1**. Schematic illustration of an aero engine, in which titanium structures often are located in the forward part and a Ti-6Al-4V sub-component with locations of sheet metal components (i).

Sheet metal forming of Ti-6Al-4V is often performed under high temperatures at low strain rates, typically at about 875°C with rates in the order of $10^{-3}$ to$10^{-4}$ $s^{-1}$, referred to as super plastic forming (SPF) [1-5]. In the SPF process, the super plastic properties of the alloy are utilized which imply large formability with minimal springback. SPF is however an advanced process often used for forming of complex geometries. Cold forming or forming at lower elevated temperatures can be applicable for simple geometries, but is limited due to the low formability together with the significant and scattering spring back characteristics of titanium alloys [1, 6-9]. Sheet metal parts in static load carrying aero engine structures have aero-dynamically shaped geometries, which are smoothly single or double-curved. Compensation of significant springback is therefore often not applicable, the forming process benefit from tool designs which minimize the shape deviation. Compensation for the minor remaining springback can be performed by modifying the tool geometries by means of FE analyses, as performed in e.g. [10-12].

The mechanical properties of titanium alloys are mainly determined by the thermo-mechanical loading history, initial micro structure, alloy concentration and existing impurities [1, 2]. In the lower temperature range, Ti-6Al-4V has a hexagonal close packed crystal structure with anisotropic properties and asymmetry in tension and compression. Yield criteria and applications for FE analyses of sheet metal forming in titanium have been proposed by e.g. Cazacu et al. (2006) [13, 14].

In the concept phase of the product development process, accurate evaluations of candidate manufacturing processes at short lead times are crucial. This paper presents an alternative approach to SPF and traditional cold forming or bend-forming. The alternative approach is based on conventional techniques for sheet metal forming, designed for the mechanical properties of Ti-6Al-4V at moderately elevated temperatures. The present work investigates the possibility to design hot forming tools with short lead times and acceptable accuracy were the manual die try out can be kept minimal, by using modelling and FE simulation of sheet metal forming in the titanium alloy Ti-6Al-4V. A rather straight forward and inexpensive approach of material modelling and methods for material characterisation is chosen suitable for evaluations in the concept phase and validated by comparison with data from a separate forming experiment to produce the prototype component at 400°C, see figure 1. The tool concept, material selection and temperature regulation of the hot forming experiment are discussed regarding functionality and suitability for production like conditions.

## 2. Experimental procedures

This section presents the sheet material along with the experimental procedures used in the present work. Test procedures of performed material tests in the characterisation of Ti-6Al-4Al are described, followed by experimental setups for the initial forming tests and a hot forming test performed at 400°C. The hot forming test is used to compare experimental observations with numerical results of punch force and shape deviation.

### *2.1. Material*

Specimens for material testing and the forming experiments have been extracted from annealed or duplex annealed sheet metals of Ti-6Al-4V, all documented alpha case free [1]. A test designation is presented in table 1.

**Table 1.** Test designation.

| Test designation | Type of test | Temperature range |
|---|---|---|
| E | Test on Young's modulus | RT |
| TT | Uniaxial tensile test | Elevated temperature 400°C |
| $TTA_{RT}$ | Uniaxial tensile test evaluated with ARAMIS$^{TM}$ | RT |
| $TTA_{ET}$ | Uniaxial tensile test evaluated with ARAMIS$^{TM}$ | Elevated temperatures 400-560°C |
| IFT | Initial forming tests | Elevated temperatures RT-1050°C |
| HFT | Hot forming test | Elevated temperature 400°C |

A specification of the material used for the different tests, i.e. tests on Young's modulus (E), the uniaxial tensile tests performed in room temperature (RT), ($TTA_{RT}$), elevated temperature tensile tests (TT and $TTA_{ET}$) together with initial forming tests (IFT) and hot forming tests (HFT) can be found in table 2. The chemical compositions are presented in table 3. The beta transus temperature of the alloy is typically 995±15°C [15]. The chemical composition of the tool material, Toolox 44 (TLX), is presented in table 3.

**Table 2.** Specification of Ti-6Al-4V used in the different tests. Thickness in mm.

| | Sheet thickness | Heat treatment | Supplier |
|---|---|---|---|
| TT/E | 1.98 | To AMS 4911, HEAT 8-12-4289-2 | AirCraft Materials UK |
| $TTA_{RT, ET}$, HFT | 2.00 | To AMS 4911, PROD. ANN. 1450°F, 30 MIN A.C. | RTI International Metals, Inc. |
| IFT | 2.03 | - | - |

**Table 3.** Chemical composition of Ti-6Al-4V and TOOLOX 44 (TLX). The phosphorus, sulphur and boron are given in ppm, other elements in weight per cent [wt%].

| | Al | O | N | Fe | C | V | Y | Mn | S | P | Si | B | Mo | Cr | Ti |
|---|---|---|---|---|---|---|---|---|---|---|---|---|---|---|---|
| TT/E | 6.27 | .15 | .008 | .15 | .005 | 3.90 | <.001 | - | - | - | - | - | - | - | Bal |
| TTA/HFT | 6.10 | .15 | .006 | .17 | .009 | 3.80 | .005 | - | - | - | - | - | - | - | Bal |
| TLX | - | - | - | - | .32 | 0.32 | . | .8 | 15 | 90 | 1.1 | 20 | .8 | 1.35 | - |

### *2.2. Material characterisation*

The material characterisation is performed to investigate temperature dependent plastic properties and generate experimental data such as initial yield stress, hardening and Lankford parameters, for use in FE analyses of cold and hot sheet metal forming in the temperature range of 20 to 560°C. Elevated temperature compression test data [16] are used in analyses of hot forming where the temperature exceeds 560°C. The material test procedures are described in the following subsections.

*2.2.1. Tensile tests.* Tensile tests at room temperature, denoted $TTA_{RT}$, are performed in three different directions referenced to the rolling direction, along (L), transverse (T) and diagonal (D). The tests are performed according to SS-EN 10 002-1 using an MTS tensile test equipment with load capacity 100 kN, at a strain rate of 0.003 $s^{-1}$ up to 0.2% engineering strain followed by a strain rate of 0.009 $s^{-1}$. The tests are performed until rupture. During the test procedure the force, the axial and width displacements (using video extensometers) are measured and logged. The tests are also continuously evaluated using ARAMIS$^{TM}$ optical strain measuring system. The evaluation is performed locally within the localised zone to obtain true stress - true strain curves at strain values even after the occurrence of necking. A more detailed description of the procedure can be found in e.g. [17].

*2.2.2. Elevated temperature tensile tests.* Tensile tests at elevated temperatures have been performed using two different setups and evaluation methods, denoted TT and $TTA_{ET}$. Specimens are extracted from different material batches of Ti-6Al-4V according to table 2 and 3. The specimen for the test, TT, is extracted transverse the rolling direction (T) and in two more directions (L) and (D) for the $TTA_{ET}$ tests. The tensile test, denoted TT, is performed at 400°C according to SIS10002-5 using an MTS tensile test equipment with a load capacity of 100 kN, at a strain rate of 0.05 $s^{-1}$ (class 1 accuracy). Heating of the specimen to 400°C is accomplished using inductive heating, 400 kHz inductance coil, applying a holding time of 40 seconds [18]. The test is performed until rupture. During the test, the force, lengthwise displacement (strain extensiometer class 1) and temperature were measured and logged. The temperature was measured using a feedback control system with a thermocouple, type S and axial accuracy of ±5°C.

The conductive hot tensile tests, $TTA_{ET}$, have been carried out at the Chair of Manufacturing Technologies (LFT) of the University of Erlangen-Nuremberg by using a modified Gleeble 1500 system (Dynamic Systems Inc., USA). For a more detailed description of the experimental setup the reader is referred to [19, 20]. The tests are performed at 250, 400 and 560°C at a strain rate of 0.05 $s^{-1}$ following the guideline of the DIN EN 10 002 Part 5. Within the tensile tests the samples have been imposed to the following test program: heating up to the target temperature within 30 seconds, maintaining the samples at the test temperature for additional 10 seconds before subsequently the tensile tests have been carried out. The specimen's geometry is chosen according to the recommendation of EN482-2. To evaluate the direction dependency of the plastic properties, samples with an orientation in, diagonal and transverse to the rolling direction are tested. The deformations of the specimens were observed and computed using the optical measuring system ARAMIS$^{TM}$ by applying a 50 Hz CCD-camera recording images of the progressive elongated samples. Therefore an appropriate stochastic pattern was applied on the samples surface, which is capable to resist high temperatures up to 950°C. The temperature was measured and controlled using Ni/Cr-Ni thermocouples (type K) spot welded onto the sample at half of the length.

For the determination of Lankford parameters as a function of equivalent strain during the hot tensile tests, the analysis of the required strain was followed by [21, 22]. Hereby the optical deformation system calculates the 2-dimensional strain distribution for each facet and node of the rectangular grid drawn by the ARAMIS$^{TM}$ software on top of the taken pictures, respectively. Regarding the final evaluation of the Lankford parameters as function of elongation, only the computed anisotropy values for the column of nodes in the centre of necking area, where the highest strains are localized are taken into account, obtained by averaging the values along this column to reduce the impact of local effects. For an efficient handling of the data a visual basic macro-function was programmed. Following DIN 10130 valid for room temperature characterisation, the Lankford parameters are determined at 20 % homogeneous plastic deformation or at the point of uniform elongation.

*2.2.3. Tests on Young's modulus.* Tests on Young's modulus (E) in room temperature are performed in order to receive elastic data and to study the dependence of rolling direction. Specimens are extracted along (L), transverse (T) and diagonal (D) to the rolling direction. The impulse excitation technique is used, which is based on the analysis of the vibration of a test sample after excited by a physical impulse. Using the Resultant Frequency and Damping Analyzer (RFDA) system 23, version 6.3.0, developed and manufactured by IMCE [23], the Young's modulus is determined through the known relationship between the elastic properties of a test specimen and its mechanical resonance frequency.

A more detailed description of the procedure can be found in e.g. [23, 24]. The main principle of the measurements with the RFDA system is to introduce a small mechanical impulse to the test specimen, the energy of the impulse is dissipated by the material into a vibration. The frequency of this vibration has a spectrum according to its resonant frequencies which depends on the elastic properties of the material, the density and the geometry of the specimen. The vibration is detected by a transducer producing an electrical signal analysed by the signal processor. Each frequency will damp according to the energy absorption of the material. Specimen dimensions are 70x20x1.98 mm, extracted from the same sheet material as for one of the tensile tests (TT).

*2.3. Forming experiments*

Initial forming tests (IFT) at different temperatures are performed with an existing forming tool not originally developed for the purpose of forming titanium sheet metal components with aero engine applications. The tool setup is presented in this section which is used to experimentally study forming and spring back characteristics of the titanium alloy together with alpha case formation and microstructural changes.

Based on the experimental observations, possible forming concepts are virtually generated (CAD). The different forming concepts are then evaluated regarding formability and shape deviation based on numerical FE analyses of hot sheet metal forming. The suggested hot forming concept is manufactured, the hot forming test (HFT), which is used to produce two prototype components. The HFT also provides with measured responses used for correlation with predicted values such as the global forming force, draw-in, temperature and shape deviation. The subcomponent are illustrated in figure 1 (black components) and the prototype geometries in figure 2 and 4, (i) and (ii).

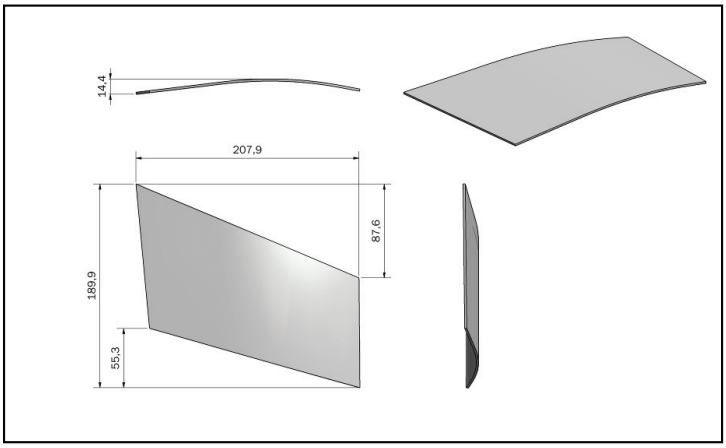


**Figure 2**. Illustration of the prototype geometry.

*2.3.1. Initial forming tests.* The initial forming tests are performed at different temperatures, ranging from RT up to 1050°C. The setup is schematically illustrated in figure 3. The geometry is double curved with the main shape resemble a section of a cylinder. The maximum forming depth at front and back edges, denoted $w_{1\text{-}2}$ respectively in figure 3, is 90.8 mm and 82.2 mm. The blank, with length 500 mm, width 250 mm and thickness 2.03 mm, is heated in an oven to the desired test temperature applying a holding time of 5 minutes, transferred to and located in a room tempered forming tool. During the crash forming operation the punch travels downwards (in negative z-direction) towards the die, without blank holding. The temperature was measured using a thermocouple type K. The punch force, punch velocity and temperatures during forming were not measured whereas the tests provides only with estimations on springback behaviour, alpha case formation and microstructural changes.

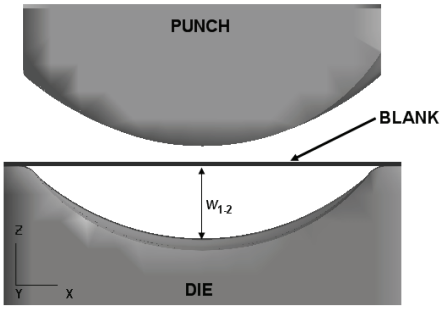


**Figure 3**. Illustration of the forming setup for the initial hot forming tests (IFT).

*2.3.2. Hot forming tests.* The hot forming tests (HFT) are performed at 400 to 560°C, where the isothermal test performed at 400°C is used to correlate experimental values with FE predictions of punch force, draw-in and shape deviation. The tool design and manufacturing was a completely CAE-controlled process, performed using numerical FE analyses of suggested forming concepts are performed to secure the forming concept and minimise springback according to the short lead time methodology described in [10]. The locations of the two prototype components on the blank with size 579x235 mm are illustrated in figure 4, which is smoothly curved.

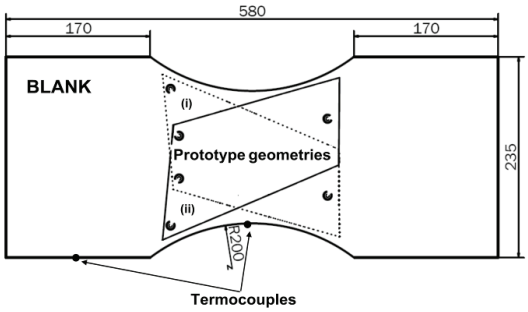


**Figure 4**. Illustration of blank size with locations of the prototype geometries in Ti-6Al-4V.

The final tool concept is illustrated in figure 5, three quarter of the tool is presented for illustrative purpose, which is based on hot inner tool parts assembled inside and insulated from outer inserts. The different inner tool components i.e. the punch, the die parts (*1) - (2*), and the binder (blank holder) are heated to the desired forming temperatures. The elevated temperature tool parts can individually be regulated in the range of RT to 580°C, which is the limit operating temperature for the tool material recommended by the supplier. The tool material used for the prototype tool is TOOLOX 44 (TLX). The material is trough-hardened in its delivery condition with hardness of 450 HBW [25]. The milling process of the material could be performed fairly time effective with standard milling equipment. Typical chemical composition and mechanical properties of TLX can be found in table 3 and 4.

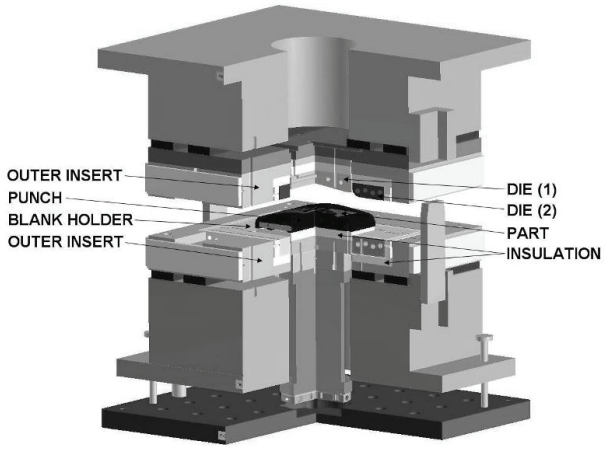


**Figure 5**. CAD-illustration of the tool concept for the hot forming test (HFT) of Ti-6Al-4V.

The heating and maintenance of the temperature in the inner tool components is accomplished by using electrical cartridge heaters, inserted in each component, and regulated via a feedback control system. The control system is based on four compact controllers with program functions, JUMO dTRON 316, one for each inner tool part and six Thyristor units for analogue control, Type TYA-110/3 50A, purchased from JUMO Mät och reglerteknik AB. The location of the cartridge heaters, purchased from Backer BHV, and related power output are presented in figure 5. The temperature is continuously measured at two points in each elevated temperature tool part using mineral-insulated thermocouples (type K) according to DIN 43 710 and EN 60 584. One is used for temperature feedback and regulation, the other is logged during the forming process. The insulation material, rigid laminate micanite (white components in figure 5 and dashed in figure 6, ensure a good insulation which prevent heating of outer inserts and components which facilitate an even distributed tool temperature. Micanite can withstand high compressive loads at high temperatures and is purchased from Elisolation HTM AB. Boron nitride was used as lubricant locally in regions with material transport, such as in the draw radii and over the punch.

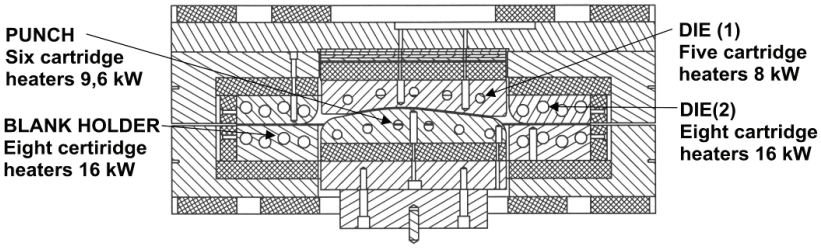


**Figure 6**. Location of cartridge heaters and total power output in the hot forming tool (HFT).

To ensure laser cutting at the correct locations of the prototype components, six reference points are produced in the blank at the end of the forming procedure using fix centre punch geometries mounted in the upper die (1), indicated by the six “dots” in figure 4. A fixture is used for a correct placement during the laser cutting. Laser scanning and best fit CAD evaluation is used as a method to evaluate the shape deviation. The definition of shape deviation is illustrated in figure 7. Two thermocouples, type K, are used on the edge of the blank to measure the temperature during heating, transportation and forming, see figure 4.

The hot forming procedure can shortly be described by the steps below:

i. Tool heating to desired temperatures.
ii. Furnace heating of the blank to desired temperature.
iii. Rapid transportation of the blank to the forming tool at an exact location on the binder, using an ASEA-ERB3000-S3 industrial robot. The binder (blank holder) is placed above the punch.
iv. Hot sheet metal forming of Ti-6Al-4V. The die moves towards the blank holder at a speed of 5 mm/s. A blank holder force of 1850 kN is applied to ensure minimal draw-in during the stretch forming process.
v. A holding time of 15 minutes is applied for one of the tests.
vi. After forming the die moves upwards releasing the formed blank which can be removed and air cooled to RT.
vii. Laser cutting is applied to remove redundant material.

**Table 4.** Typical mechanical properties in room temperature for TOOLOX 44 (TXL). Hardness in HBW.

| Mechanical properties | | | | | |
|---|---|---|---|---|---|
| ρ [kg/m$^3$] | E [GPa] | υ | Hardness | $R_{P0,2}$ [MPa] | $R_m$ [MPa] |
| 8000 | 210 | 0.3 | 450 | 1300 | 1450 |

*2.4. Metallographic studies*

The as-received microstructures of the sheet metal used in the IFT and HFT together with structures after forming are examined using optical microscopy. For the as-received microstructures, rectangular samples were extracted from the sheets. The specimens were polished and etched with Kroll's reagent (2% HF, 3% $HNO_3$ and 95% $H_20$). Specimens from the initial forming tests (IFT) are etched in two steps to evaluate the layer thickness of the alpha case (first step: 1 ml HF, 2 ml $HNO_3$, 100 ml $H_2O$; second step: 2 gr $NH_4HF_2$, 100 ml $H_2O$).

**3. Numerical procedure**

In the present work the explicit FE program LS-DYNA v971 [26, 27] is used for solving the equations of motion. Complex geometries in industrial applications with large deformations, nonlinear materials and contacts can be treated effectively and quickly. In the virtual tool design, different forming concepts, temperatures and tool features are evaluated and modified in a loop of changes using FE analyses of the hot forming procedure. Crash forming without blank holding is compared with forming concepts including blank holding, in which different draw bead geometries are compared with flat binder surfaces. The influences of binder force, punch and die geometry, raw radii and draw depth are evaluated. Available press force capability of 10 000 kN with a binder force of 1800 kN, had to be considered.

The material model used for the analyses is a rate independent elastic-plastic model with isotropic hardening. The nonlinear hardening is defined as tabulated values of yield stress and effective plastic strain. The anisotropic yield criterion proposed by Barlat et al. [28] is applied. The convex isotropic yield function by Barlat et al. is formulated according to equation 1-7.

$$f = \Phi' + \Phi'' - 2\bar{\sigma}_f^{\,m} = 0 \tag{1}$$

where

$$\Phi' = \left|s_1 - s_2\right|^m \tag{2}$$

and

$$\Phi'' = \left|2s_2 - s_1\right|^m + \left|2s_1 + s_2\right|^m \tag{3}$$

$s_1$ and $s_2$ are the principal values of the stress deviator. The exponent *m* is the same parameter as used in the Barlat and Lian (1989) [29, 30] criterion, and is suggested to be equal to 6 for materials with a BCC crystal structure and 8 for materials with an FCC crystal structure. If a value of 2 is applied, the yield surface reduces to the Hill yield surface [31], i.e. to the von Mises yield surface in the isotropic case. With an increasing value of the *m*-parameter, in the isotropic case, the shape of the Barlat tri-component yield surface adopts the shape of the Tresca yield surface.

The anisotropic case is handled by augmenting the occurrence of s in Φ′ and Φ′′ by linear transformations of C′ and C′′, respectively. Equations 2 and 3 becomes

$$\Phi' = \left|X_1' - X_2'\right|^m \tag{4}$$

$$\Phi'' = \left|2X_2'' - X_1''\right|^m + \left|2X_1'' + X_2''\right|^m \tag{5}$$

and in matrix form

$$\left\{X'\right\} = \left[C'\right]\left\{s\right\}, \qquad \left\{X''\right\} = \left[C''\right]\left\{s\right\} \tag{6}$$

assuming an orthotropic behaviour, the most general expressions for the transformation matrices C′ and C′′ are

$$\left[C'\right] = \begin{bmatrix} C_{11}' & C_{12}' & 0 \\ C_{21}' & C_{22}' & 0 \\ 0 & 0 & C_{33}' \end{bmatrix}, \quad \left[C''\right] = \begin{bmatrix} C_{11}'' & C_{12}'' & 0 \\ C_{21}'' & C_{22}'' & 0 \\ 0 & 0 & C_{33}'' \end{bmatrix} \tag{7}$$

containing a total of ten unknown parameters. By the condition $C'_{12}=C'_{21}= 0$ [28], the number of unknowns reduces to eight. The higher order yield function accounts for plastic anisotropy in stress and strain using these eight anisotropy parameters, denoted $\alpha_{1\text{-}8}$, assuming symmetry in tension and compression [28, 30]. The parameters can be determined from standard material tests such as uniaxial tensile tests in different directions referenced to the rolling direction and an equi-biaxial test in which a balanced biaxial stress state is obtained. Although titanium alloys such as Ti-6Al-4V has a hexagonal close packed (hcp) crystal structure, with unsymmetrical properties in tension and compression [13, 14], the BARLAT_YLD2000 yield function is applied for evaluation of its applicability in the concept phase of the tool design. In this study, six parameters are used at room temperature, 400 and 560°C. The m-parameter is assumed equal to 8. Further on, analyses using an isotropic assumption with data from the tensile test transverse (T) the rolling direction at 400°C, $TTA_{ET}$, Lankford coefficients equal to 1 and the m-parameter assumed to a value of 8 are performed for comparative purpose. Fully integrated shell elements with 9 integration points through the thickness are used. The tool surfaces were modelled as rigid with a prescribed velocity profile and the contact between the tools and the specimen was included and modelled as a contact interface with a friction model assumed to follow Coulomb's friction law. A friction coefficient of 0.115 is applied. For the springback analyses, the implicit solver in LS-DYNA was used. Isotropic room temperature elastic properties are applied where the effect of cooling on the shape deviation is not considered.

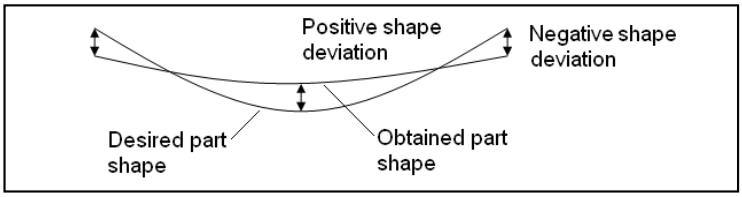


**Figure 7**. Definition of shape deviation.

## 4. Results

The results obtained in the experimental and numerical procedures are presented in this section.

### *4.1. Material characterisation*

The alloy Ti-6Al-4V has anisotropic elastic and plastic properties. The tests on Young's modulus (E) are presented in table 5. The results from the tensile tests performed in room temperature are presented in figure 8, showing true stress – true longitudinal strain curves and the variation of Lankford parameters with plastic strain.

**Table 5.** Elastic properties of Ti-6AL-4V at indicated temperatures. Young's modulus in (GPa).

| Test | Temperature (°C) | Young's modulus (L) | (T) | (D) |
|---|---|---|---|---|
| E | RT | 109 | 130 | 116 |
| TT | 400 | - | 97 | - |

Results from the isothermal tensile tests at 250, 400 and 560°C are presented in figure 9. For the tensile test (TT) the flow curve is extrapolated after the occurrence of necking by a straight line to the final point. The final point is calculated using the actual cross section area and force at failure. Figure 9 also presents the determination of Young's modulus and initial yield stress, $RP_{02}$, at temperature 400°C, indicated by the dot in the figure. A deviation between the flow curves obtained at 400°C (T) (TT, $TTA_{ET}$) with materials from two different material batches of Ti-6Al-4V are observed. The n-value between 2-4 % true plastic strain for the $TTA_{ET}$ test at 400°C (T) is determined to $n_{2\text{-}4}$=0.046. This value is used as a conservative forming limit in plane strain necking [33]. The yield stresses, $RP_{02}$, along with Lankford coefficients chosen for the material model at different temperatures are presented in table 6. Compression tests at high temperatures, see e.g. [16, 32], indicated that peak stresses are followed by flow softening.

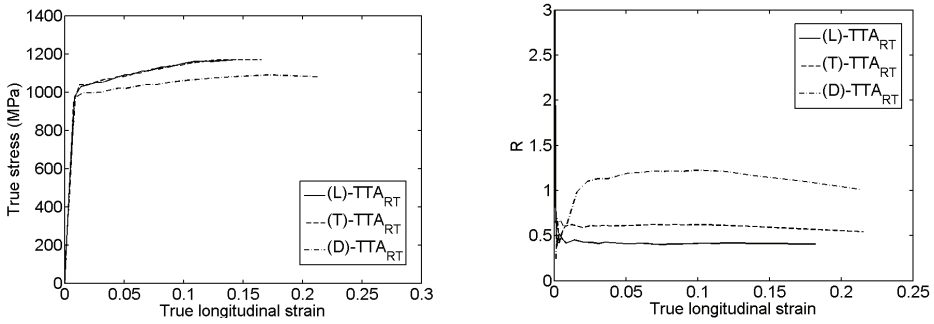


**Figure 8**. True stress – tensile true longitudinal strain – true stress curves at room temperature together with Lankford coefficients.

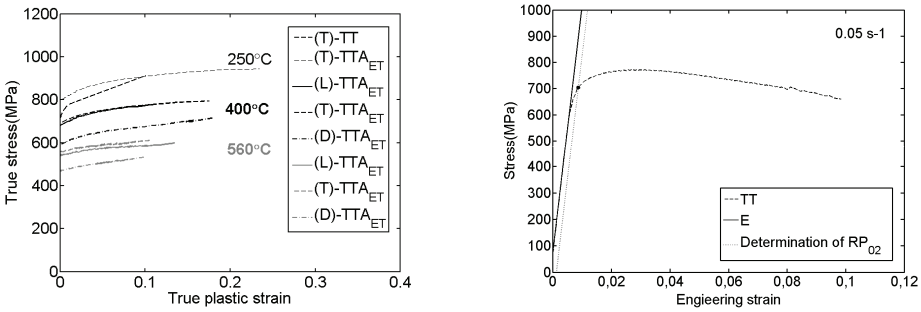


**Figure 9**. True stress – true plastic strain curves obtained by elevated temperature tension tests (TT, $TTA_{ET}$) at different temperatures and determination of Young's modulus and $RP_{02}$ from the tensile test performed at 400°C (TT).

**Table 6.** Parameters used in the analyses of cold and hot sheet metal forming, rolling direction denoted transverse (T), along (L) and diagonal (D).

| Test | Temperature (°C) | Yield stress (MPa) | | | Lankford coefficients | | |
|---|---|---|---|---|---|---|---|
| | | (L) | (T) | (D) | (L) | (T) | (D) |
| $TTA_{RT}$ | RT | 1017.5 | 1020.5 | 985.0 | 0.4 | 0.6 | 1.2 |
| $TTA_{ET}$ | 400 | 681.5 | 691.2 | 591.6 | 0.618 | 0.512 | 1.26 |
| $TTA_{ET}$ | 560 | 564.2 | 559.9 | 468.9 | 0.676 | 0.63 | 1.29 |
| TT | 400 | - | 709.0 | - | - | - | - |

*4.2. Initial forming tests*

The initial forming tests (IFT) established the major springback characteristics of Ti-6Al-4V. Table 7 assembles the initial forming temperatures and related shape deviation, defined as $w_{1\text{-}2}$ in figure 3. Forming at RT results in total springback where no plastic deformation occurs. With increasing temperature, the springback decreases but is still present even with start temperatures of approximately 1050°C. During forming the temperature of the blank decreases, however the temperature is estimated to about 60°C after forming at 1050°C including a holding time (HT) of 5 minutes in the tool. Heating and forming at high temperatures imply alpha case formation, at temperatures above the beta transus temperature, microstructural changes and alpha case formation take place [1, 9, 15, 34], see figures in section 4.4. The rolling direction orientation (X, Y) of the blanks refers to the x and y directions in figure 3. The initial forming tests, along with hot forming tests of Ti-6242 [9], establish the need for a forming concept which minimise the springback by employing elevated temperature tools including blank holding and/or hot sizing.

**Table 7.** Initial forming temperatures (°C) and related springback, $w$, (mm) in the initial forming tests (IFT).

| | Initial forming temperature | Springback measurements $w_1$ | $w_2$ | Rolling direction |
|---|---|---|---|---|
| 1 | RT | 90.8 | 82.2 | Y |
| 2 | 400 | 72.7 | 59.4 | Y |
| 3 | 700 | 35.8 | 32.2 | Y |
| 4 | 900 (HT) | 8.3 | 13.0 | X |
| 5 | 1050 (HT) | -4.4 | 3.9 | X |

*4.3. Hot forming tests and correlation with numerical predictions*

Based on the experimental observations, several possible forming concepts were evaluated using FE analyses of hot sheet metal forming of Ti-6Al-4V. As discussed in section 3, tool geometries, blank holding and draw bead geometries, blank holder force, draw depth and temperatures were modified in a loop of changes to obtain a suitable forming process based on the chosen models.

Considering a forming procedure similar to the crash forming in the IFT with nominal tool geometry, but performed under isothermal conditions with heated tools. FE analyses reveals that it is difficult to obtain plastic straining within the blank, even at 800°C, see figure 10. This implies that the blank will springback totally upon unloading. Isotropic material parameters with true stress- true strain data presented in [16] are applied and used in these analyses. The major driving forces for simulation of relaxation [1, 16] are the development of plastic deformation in combination with holding times under high temperatures. Relaxation or creep forming at elastic strain levels is considered to be a too time consuming forming process. Large springback and thereby major shape deviation is not straight forward to compensate for considering smooth and moderately shaped geometries.

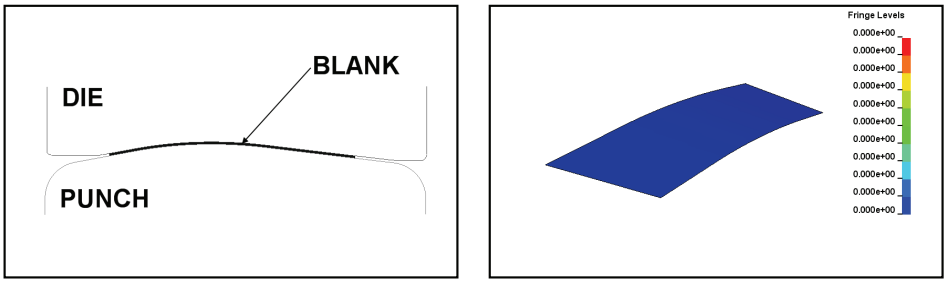


**Figure 10**. Tool concept for hot isothermal crash forming of the prototype component at elevated temperatures and effective plastic strain at 800°C.

The most promising concept (HFT) is instead designed to produce a low plastic strain distribution in the prototype component area without locally high strain levels in the binder area, to minimise the springback and yet possess a good margin to strain localisation, see figure 5 and 11. Further, the geometry of the blank is designed to promote development of plastic straining within the prototype component area. A flat blank holder surface was used to minimize the draw-in and limit locally high strain levels which are common with conventional draw bead geometries. Some limitations regarding the press force capacity and temperature sustainability of the tool material, which should not exceed 580°C [25], had to be considered in the design of the hot forming process. The rolling direction of the blank is in the y-direction in figure 11, transverse the major deformation direction.

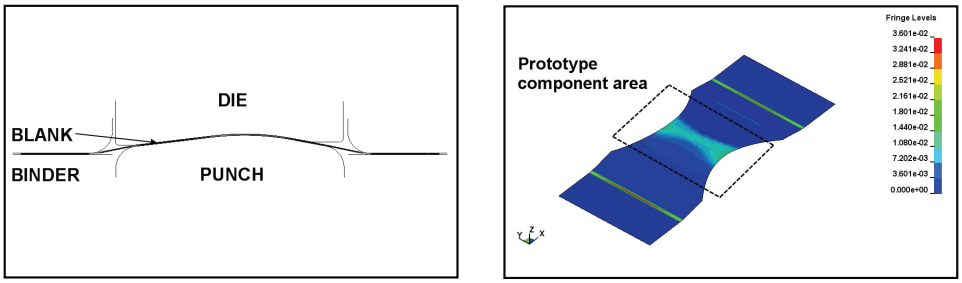


**Figure 11**. Tool concept for hot forming of the prototype component at elevated temperatures and effective plastic strain distribution for isothermal forming at 400°C.

The measured and calculated punch force is presented in figure 12, which indicate a slight deviation at the end of the forming process when forming at 400°C. One repetition test is also presented in the figure, indicating reproducibility. The predicted total draw-in ($x_1 + x_2$) at the end of the forming process is comparable with measured values, as can be seen in table 8, where ($TTA_{ET400°C}$) anisotropic data are used in the analysis. The location $y_1$ corresponds to the draw-in at centre section of the blank and $y_2$ at the edge, according to figure 11. The shape deviation (mm) correlates quite well with measured values, see figure 13. A deviation between predicted shape deviation using isotropic or anisotropic data exists, see figure 14. Isotropic and room temperature elastic properties (T) are used in the springback analyses.

**Table 8.** Measured and predicted draw-in (mm) for the hot forming tests (HFT) at 400°C.

| Location | Predicted draw-in | | | Measured draw-in |
|---|---|---|---|---|
| | $x_1$ | $x_2$ | $x_{tot}$ | $x_{tot}$ |
| $y_1$ | 0.36 | 0.19 | 0.55 | 0.5 |
| $y_2$ | 0.47 | 0.29 | 0.76 | 0.9 |

The predicted punch force when forming at 560°C is also presented in figure 12. The predicted maximum total value of the draw-in is 0.1 mm, which implies a higher degree of material stretching compared to forming at 400°C, and thereby contributes to a higher punch force. The springback analysis indicates that the shape deviation is slightly reduced by increasing the temperature, as expected see figure 15. Considering FE analyses of forming in room temperature with the hot forming concept, the binder force of 1850 kN is found to be too small to prevent major draw-in. No plastic straining develops during forming and the component springback totally upon unloading and removal of binder material. Forming at 400°C and applying a holding time of 15 minutes reduces the shape deviation somewhat, see figure 13 and 15.

The cycle time, including transportation, forming and unloading, is approximately 1 minute. The regulation and insulation of the elevated temperature tool parts functioned very well. The temperatures at the locations of the thermocouples in the punch and inner die are measured and regulated within 10°C. The temperature is even distributed in the blank contact area of the binder. After 8 hours operating temperature at 560°C, the outer inserts located only 30 mm from the inner hot tool parts are approximately 50°C.

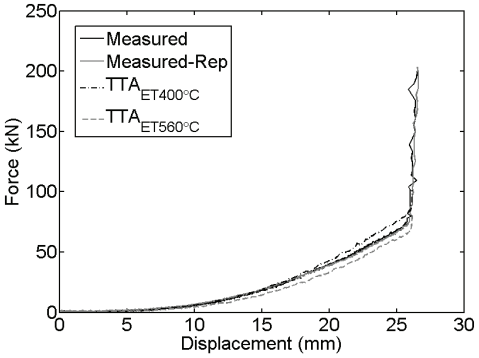


**Figure 12**. Measured and calculated punch force at 400°C isothermal hot forming (HFT).

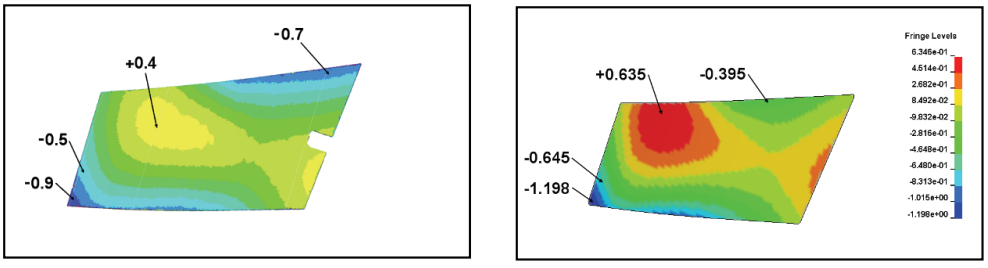


**Figure 13**. Measured and predicted shape deviation of the prototype component formed at 400°C, using anisotropic data.

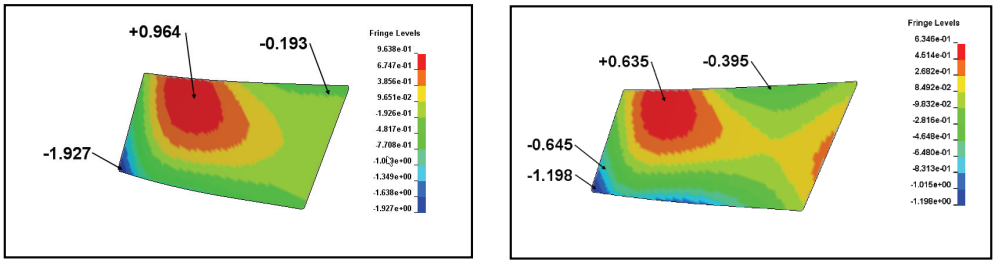


**Figure 14**. Predicted shape deviation at 400°C of the prototype component, using isotropic (T) or anisotropic data.

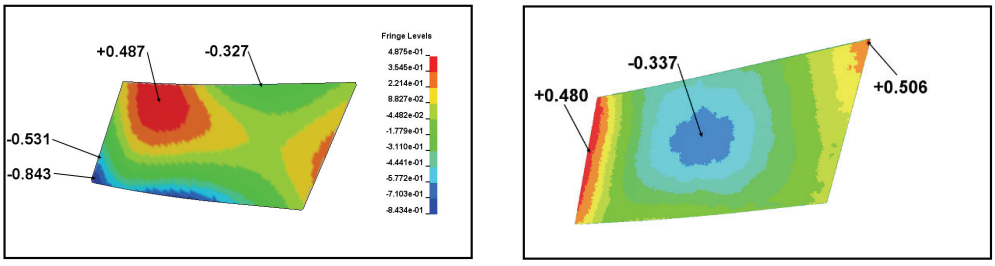


**Figure 15**. Predicted shape deviation when formed at 560°C using anisotropic data and measured shape deviation of the prototype component formed isothermally at 400°C, including a holding time of 15 minutes in the elevated temperature forming tool (reversed direction of the definition of shape deviation).

*4.4. Microstructural observations*

The as-recieved microstructure of the blank material used in the initial forming tests (IFT) is typical that of the equiaxed alpha mill annealed condition. Due the exposure of heating and forming at elevated temperatures, alpha case formation takes place except when forming at 400°C. Forming with initial temperatures of 700, 900 and 1050°C results in a layer of alpha case of 5, 25 and 35 micrometers, respectively. Further, the microstructure of the test with highest initial forming temperature has changed into the azicular transformed beta condition, see figure 16.

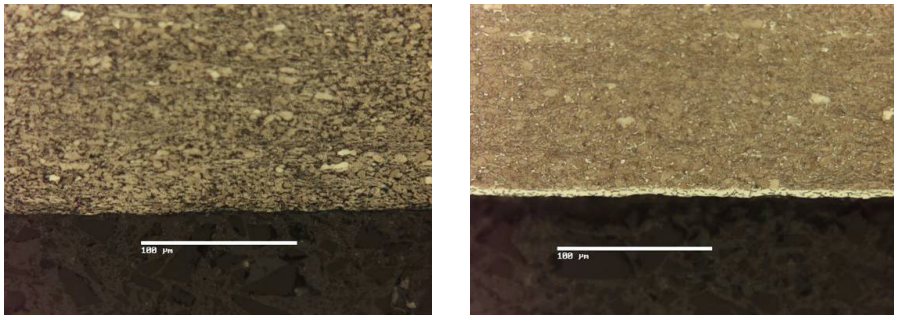

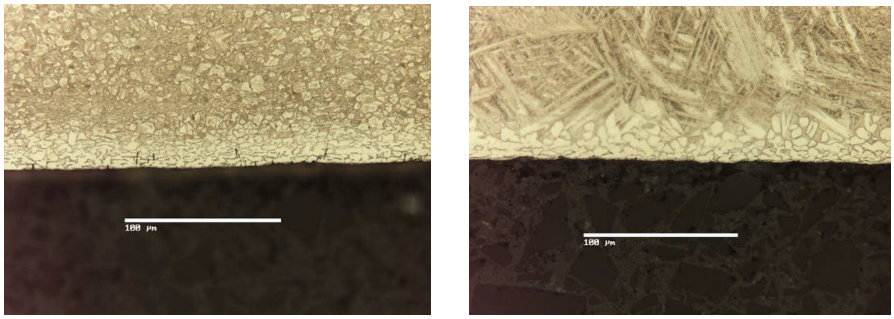


**Figure 16**. Material structures after performing initial hot forming tests (IFT) with initial forming temperatures of 400, 700, 900 and 1050°C, respectively.

The as-received microstructure for the hot forming tests (HFT) consists of equiaxed alpha and elongated alpha in a transformed beta matrix. The forming procedure at 400°C has not affected the structure nor has any alpha case formation occurred, as can be seen in figure 17. The rolling direction is horizontal in the figure.

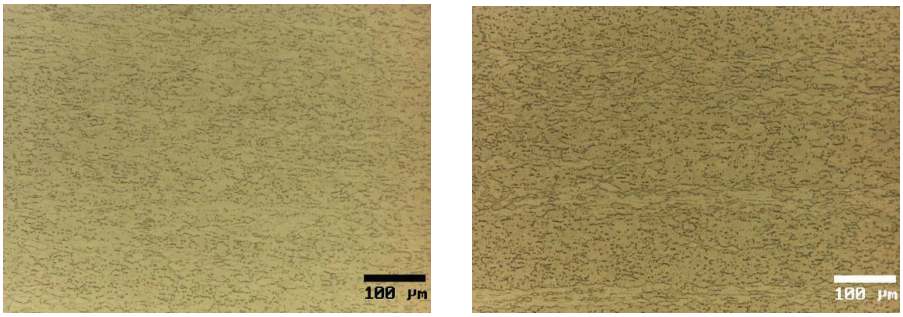


**Figure 17**. As-received microstructure and structure after hot forming (HFT) at 400°C.

**5. Discussion and conclusions**

Considering fabrication as a manufacturing method for static load carrying aero engine structures in which sheet metal parts, simple forgings and small ingots are welded together and heat treated, early FE results of the forming process e.g. material thinning and shape deviation is important input to subsequent analyses of the following manufacturing processes and product functionality. In the current paper, the development of a hot forming procedure for the production of two prototype components using FE analyses of sheet metal forming in Ti-6Al-4V is presented. A rather straight forward and inexpensive approach of material modelling and methods for material characterisation are chosen, based on an anisotropic material model suitable in the medium temperature range, for evaluations early in the concept phase.

The material characterisation consists of tensile tests at room temperature and elevated temperatures together with tests to determine Young's modulus. Numerical predictions are correlated with experimental data using a validation test, the hot forming test (HFT) performed at 400°C. The accuracy is acceptable regarding prediction of punch force, draw-in and shape deviation. One explanation to the slightly higher predicted forming force may originate from the strain rate sensitivity of the alloy. The material testing at elevated temperatures is performed at a higher strain rate (0.05 $s^{-1}$) than obtained in the forming procedure (0.001 $s^{-1}$). When considering the anisotropic properties of Ti-6AL-4V, a more accurate prediction of the shape deviation can be obtained compared to applying an isotropic yield function. The shape deviation is predicted within the sheet thickness, which is possible to compensate for by modifying the punch and die geometries of the tool. Applying a holding time of 15 minutes at 400°C reduced the shape deviation slightly.

The functionality of the tool concept is promising, in which the temperature in the elevated tool components are even distributed and the insulation functionality is satisfying. The tool material was found to function well for prototype studies. In production, a more temperature resistant tool material may be preferable e.g. Inconel 600 or 718. The metallographic study shows that forming at 400°C does not imply alpha case formation, nor microstructural changes. Heating and forming at temperatures of 700°C and above (IFT) cause alpha case formation to occur. Heating and forming above the beta transus temperature is not applicable due to the changed material structure and thereby mechanical properties. With the presented hot forming concept, components with minor shape deviation can be produced at moderate temperatures with a cycle time of approximately 1 minute (excluding heating time of the blank to the desired forming temperature). Considering production, the moderate forming temperatures imply long tool life and good working environment. Further, the need for antioxidation agents, and a second acid pickling procedure to remove alpha case would not be necessary.

Since titanium alloys have asymmetric yielding properties in tension and compression, an interesting extension to the presented work would be to study yield functions which can account for the asymmetry. To perform complementary experimental reference data under equibiaxial loading together with tests to study the *m*-parameter and include the effect of strain rate and mixed hardening laws would be of interest in order to improve the accuracy of predicted responses. Further, altering the individual tool temperatures to improve shape deviation and study forming limits would be most interesting in order to optimize the forming process with respect to shape deviation and blank size due to the high material cost.

**Acknowledgement**
The research founding by VINNOVA, grant 2007-00288, and Volvo Aero Corporation, concerned staff at Industrial Development Centre in Olofström AB and ITE Fabriks AB are gratefully acknowledged.

**References**

[1] G. Lütjering, J. C. Williams, Titanium, Springer-Verlag Berlin Heidelberg, 2003
[2] R. Boyer, G. Welsch, E.W. Collings, Materials Properties Handbook: Titanium alloys, Tachnical note 5A, Superplastic forming of Titanium Alloys, ASM International, 1994.
[3] E.J. Tuegel, M.O. Pruitt, L.D. Hefti, Advanced Materials & Processes, 136 (1989) 36-41.
[4] N. Peter, Journal of Materials Engineering and Performance, 13 (2004) 660-664.
[5] G. Wang, K.F. Zhang, D.Z. Wu, J.Z. Wang, Y.D. Yu, Superplastic forming of bellows expansion joints made of titanium alloys, Journal of Materials Processing Technology, Volume 178, Issues 1-3, 14 September 2006, Pages 24-28
[6] F.-K. Chen, K-H. Chiu, Stamping formability of pure titanium sheets, Metarials Processing Technology, v 170, pp 181-186, 2005.
[7] T. Kong, L. Chan, T. Fee, Numerical investigation of perform design in non-axisymmetric warm forming, Int. J. Adv. Manufacturing Technology, v 37, pp 908-919, 2008.
[8] C.P. Lai, L.C. Chan, C.L. Chow, Warm forming simulation of tailor-welded blanks with experimental verification, CP908, NUMIFORM ’07, Materials Processing and Design: Modelling, Simulation and Applications, pp 1621-1626, 2007.
[9] E-L. Odenberger, R. Pederson, M. Oldenburg. Materials Science and Engineering: A, Volume 489, Issues 1-2, pp158-168, 2008.
[10] E.-L. Odenberger, M. Jansson, P. Thilderkvist, H. Gustavsson, M. Oldenburg, A short lead time methodology for design, compensation and manufacturing of deep drawing tools for Inconel 718, IDDRG 2008 Conference, Best in Class Stamping, pp 697-708.
[11] T. Meinders, I.A. Burchitz, M.H.A. Bonte, R.A. Lingbeek, ”Numerical product design: Springback prediction, compensation and optimisation”, International Journal of Machine Tools & Manufacture, 48 (2008) 499-514 .
[12] T. Dutton, R. Edwards, A. Blowey,”Springback Prediction and Compensation for a High Strenth Steel Side Impact Beam”, In L. S. Smith, F. Pourboghart, J. –W. Yoon and T. B. Stoughton, editors, CP712, NUMISHEET (2005) 340-344. American Institute of Physics.
[13] O. Cazacu, B. Plunkett, F. Barlat, Int. Journal of Placticity, v 22, Issue 7 (2006), pp 1171-1194.

[14] A. S. Khan, R. Kazmi, B. Farrokh, Int. Journal of Placticity, v 23, Issue 7 (2007), pp 931-950.
[15] R. Boyer, G. Welsch, E.W. Collings, Materials Properties Handbook: Titanium alloys, edition, ASM International, 1994.
[16] B. Babu, Licentiate Thesis 2008:40, Luleå University of Technology, Sweden, 2008.
[17] ARAMIS v6: http://www.gom.com, April (2008).
[18] H. Andersson, E. Sjöström, Int. Journal of Fatique, v30, 2008, pp 391-96.
[19] Merklein, M., Lechler, J., Geiger, M., Characterization of the flow properties of the quenchenable ultra high strength steel 22MnB5. Annals of the CIRP 55/1/2006, p. 229.
[20] Merklein, M., Lechler, J., 2006, Investigation of the thermo-mechanical properties of hot stamping steels. In: Metal Forming Conference 2006, Birmingham, 2006, p. 452.
[21] Hoffmann, H., Vogl, Chr., Determination of True Stress-Strain-Curves and Normal Anisotropy in Tensile Test with Optical Deformation Measurement. Annals of CIRP 52/1/2003, p. 217
[22] Hecht, J., Pinato, S., Geiger, M., Determination of mechanical properties for hydroforming of magnesium sheets at elevated temperatures. In: SheMet'05, Germany, p. 763
[23] Manual for The Resultant Frequency and Damping Analyser (RFDA) system 23, version 6.3.0, IMCE (2006).
[24] RFDA: http://www.imce.cit.be, April (2008).
[25] P. Hansson: "TOOLOX – The Multi-purpose Pre-hardened Tool Steels", 2nd International Conference on Accuracy in Forming Technology ICAFT (2006) 183-200.
[26] J.O. Hallquist, "LS-DYNA Theory Manual" Livermore Software Technology Corporation, Livermore (2006).
[27] "LS-DYNA Keyword User´s Manual" Volume 1, v971, Livermore Software Technology Corporation, Livermore (2007).
[28] F. Barlat, J.C. Brem, J.W. Yoon, K. Chung, R.E. Dick, D.J. Lege, F. Pourboghrat, S.-H. Choi and E. Chu, "Plane stress yield function for aluminium alloy sheets – part 1: theory", International journal of Plasticity 19 (2003) 1297-1319.
[29] F. Barlat, J. Lian, Plasticity behaviour and strechability of sheet metals Part I: a yield function for orthotropic sheets under plane stress condition. Int. J. Plasticity, v 5, (1989), 51-66.
[30] M. Jansson, L. Nilsson, K. Simonsson, On constitutive modelling of aluminium alloys for tube hydroforming applications, Int. J. Placticity, v21, 2005, 1041-1058.
[31] R. Hill, The Matematicall, Theory of Plasticity, Clarendon Press, Oxford. (1950).
[32] E.-L. Odenberger, Doctoral Thesis, Luleå University of Technology, Sweden, 2009.
[33] W. F. Hosford, R. M. Caddell, Metal forming – Mechanics and metallurgy, Second edition, PTR Prentice-Hall, Inc.,1993, ISBN: 0-13-588526-4.
[34] G. Lütering, Int. Journal of Materials Science and Engineering, v 243, 1998.

# Paper E

# Thermo mechanical sheet metal forming of aero engine components in Ti-6Al-4V – PART 1: Material characterisation

**E-L. Odenberger[1, 3*], J. Hertzman[1], P. Thilderkvist[1], M. Merklein[2], A. Kuppert[2], T. Stöhr[2], J. Lechler[2] and M. Oldenburg[3]**

[1] Forming Group, OSAS, Industrial Development Centre in Olofström AB, Vällaregatan 30, SE-293 38 Olofström, Sweden

[2] Manufacturing Technology, University of Erlangen-Nuremberg, Egerlandstr. 13, 91058 Erlangen, Germany

[3] Division of Solid Mechanics, Luleå University of Technology, SE-971 87 Luleå, Sweden

* Corresponding author, E-mail: Eva-Lis.Odenberger@iuc-olofstrom.se

**Abstract**

Titanium alloys, such as Ti-6Al-4V are common in aerospace applications with moderate operating temperatures due to their high strength to weight ratio in combination with favourable creep resistance. In the virtual design of suitable hot forming processes for titanium sheet metal components, numerical finite element (FE) simulations are desirable to perform in order to secure the forming concepts with respect to strain localisation and shape deviation. The reliability of the numerical simulations depends on the models and methods used as well as on the accuracy and applicability of the input data. The material model and related property data need to be consistent with the conditions of the material in the process of interest. In the present study a set of material tests are performed at temperatures ranging from room temperature up to 560°C. The purpose is to characterise the material, identify model requirements and generate necessary experimental reference data for model calibration and FE analyses of hot sheet metal forming of Ti-6Al-4V.

## 1. Introduction

In the European aero engine industry, alternative manufacturing methods for load carrying aero engine structures are considered. Traditionally, these structures consist of large scale single castings. By fabrication, the structures are instead built form simple forgings, sheet metal parts and small ingots which are welded together and heat treated in order to reduce product cost and enable weight reduction and thereby fuel consumption. Titanium alloys, such as Ti-6Al-4V are used in aero engine structures where the running temperature is moderate, up to 350°C. In the design phase, numerical methods such as the finite element (FE) method are often employed for evaluation of new manufacturing methods and product functionality [1-6]. In the product development process of complete structures, FE analyses of the welding procedures are utilised, mainly to study shape deviation. In order to increase the accuracy in these predictions and to develop suitable forming procedures for smoothly double curved titanium sheet metal components, accurate analyses of candidate forming processes are desired. The resulting geometry, sheet thickness and residual stress state which are generated

in the sheet metal forming procedure influence the shape deviation of the complete structure in the subsequent welding and heat treatment processes.

The mechanical properties of titanium alloys are sensitive to the thermo-mechanical loading history, initial micro structure, alloy concentration and existing impurities [7-10]. At room temperature and in the low temperature range, Ti-6Al-4V has a *hcp* crystal structure (α-phase, the β-phase has a bcc crystal structure) with anisotropic properties and yielding asymmetry in tension and compression. A large number of studies have been performed in order to understand and model the mechanical behaviour of the alloy under different temperatures and strain rates, see e.g. [9-21]. The mechanical properties depend on the rolling direction, strain rate and temperature and is affected by reversed loading, i.e. asymmetric yielding in tension/compression and the Bauschinger effect. The formability is increased with increasing temperature and typically decreased with an increased strain rate in the lower temperature region. At high temperatures, the compressive flow behaviour is characterised by a peak stress followed by softening, which originates from factors such as temperature rise due to deformation, phase and microstructural changes along with deformation concentration and damage within the specimens.

Numerous anisotropic yield formulations which can account for plastic anisotropy have been formulated the past decades, see e.g. [22-26]. Recent formulations of anisotropic yield criteria developed for metals with cubic crystal structures have been proposed by e.g. Hosford (1979) and Barlat et al. (2003). The formulations can account for plastic anisotropy in yielding and Lankford coefficients assuming symmetry in tension and compression with an increased number of model parameters compared to established models such as the yield criteria developed by Hill (1950) and Barlat's tri-component, Barlat and Lian (1989). The physically based macroscopic formulation by Cazacu et al. (2006) describes both the asymmetry and anisotropy in yielding exhibited by *hcp* materials.

In the present work, the mechanical properties of Ti-6Al-4V is studied by a set of material tests in order to identify model requirements, generate necessary model input and to study failure limits at temperatures ranging from room temperature up to 560°C. Two different material batches of Ti-6Al-4V sheet metals, purchased from different suppliers are evaluated. The obtained results are used as experimental reference data for model calibration and FE analyses in the virtual tool design of hot sheet metal forming intended for the production of a double curved prototype component in Ti-6Al-4V, see [27].

## 2. Material

Specimens for the material testing have been extracted from annealed or duplex annealed sheet metals of Ti-6Al-4V, documented alpha case free. A specification of the materials can be found in table 1 and 2. The beta transus temperature of the alloy is typically 995±15°C [7].

**Table 1.** Specification of Ti-6Al-4V used in the different tests, thickness in [mm].

| | Sheet thickness | Heat treatment | Supplier |
|---|---|---|---|
| Alloy 1 | 1.98 | To AMS 4911, HEAT 8-12-4289-2 | AirCraft Materials UK |
| Alloy 2 | 2.00 | To AMS 4911, PROD. ANN. 1450°F, 30 MIN A.C. | RTI International Metals, Inc. |

**Table 2.** Chemical composition of Ti-6Al-4V, in weight per cent [wt%].

| | Al | O | N | Fe | C | V | Y | Ti |
|---|---|---|---|---|---|---|---|---|
| Alloy 1 | 6.27 | .15 | .008 | .15 | .005 | 3.90 | <.001 | Bal |
| Alloy 2 | 6.10 | .15 | .006 | .17 | .009 | 3.80 | 50 PPM | Bal |

## 3. Experimental procedures

The material characterisation is performed in the temperature range of 20-560°C. A set of material tests are performed in order to study the material behaviour and generate necessary reference data for the calibration of different yield criteria, with application in FE analyses of hot sheet metal forming. For further reading and detailed descriptions references are made to the work performed by Odenberger and Jansson et al. in paper F of [27].

To study the elastic response of Ti-6Al-4V, tests are performed using the non destructive impulse excitation technique, denoted $E_{tmp}$, where *tmp* states the test temperature. Uniaxial tension tests at room temperature (RT), denoted $T_{RT}$, and at elevated temperatures, denoted $T_{tmp}$, are performed to study the anisotropic plastic response and determine initial yield stress, hardening and Lankford parameters (R-values). Uniaxial compression tests, denoted $CT_{tmp}$, are performed to establish the strength differential (SD) in initial yielding between tension and compression. Forming limit curves, denoted $FLC_{tmp}$, are determined experimentally in order to study forming limits. Further on, a viscous bulge test is performed to obtain a balanced biaxial stress state (VBT) and determine the equibiaxial yield stress, $\sigma_b$, and R-value, $R_b$. A uniaxial tension loading-unloading-reloading test (LURL) is performed in order to study the dependence of Young's modulus with plastic straining in room temperature. The different material tests are designated in table 3 and the experimental procedures are presented in the following sections. Heat transfer tests are finally performed to determine the heat transfer coefficient (htc). The tests to determine Young's modulus and uniaxial tension tests at room temperature are performed with material from two different material batches of Ti-6Al-4V in order to detect variations between the two materials.

The conductive hot tension tests, heat transfer tests and the elevated temperature forming limit curve are performed at the Chair of Manufacturing Technologies (LFT), University of Erlangen-Nuremberg, Germany. The other tests are performed at Industrial Development Centre in Olofström, Sweden.

**Table 3.** Test designation.

| Test designation | Type of test | Temperature range [°C] |
|---|---|---|
| $E_{tmp}$ | Non destructive test on Young's modulus | RT-560 |
| $T_{RT}$ | Uniaxial tension test | RT |
| $T_{tmp}$ | Conductive hot uniaxial tension test | 250-560 |
| $CT_{tmp}$ | Uniaxial compression test | RT-400 |
| VBT | Viscous bulge test | RT |
| LURL | Uniaxial loading-unloading-reloading test | RT |
| $FLC_{tmp}$ | Forming limit tests | RT-400 |

### *3.1. Tests to determine the elastic material response*

To study the elastic response in the temperature range of RT to 560°C tests to determine Young's modulus are performed, in three in-plane directions referenced the rolling direction. Specimens are extracted along (00), transverse (90) and in a 45° mode (45) to the rolling direction. The impulse excitation technique is used, which is based on the analysis of the vibration of a test sample after being excited by a physical impulse. The Resultant Frequency and Damping Analyser (RFDA) system 23, version 6.3.0, developed and manufactured by IMCE is used [28]. Young's modulus is determined through the known relationship between the elastic properties of a test specimen and its mechanical resonance frequency. A more detailed description of the procedure can be found in [28, 29]. The main principle of the measurements is to introduce a small mechanical impulse to the test specimen where the energy of the impulse is dissipated by the material into a vibration. The frequency has a spectrum according to its resonant frequencies which depends on the elastic properties of the

material, the density and the geometry of the specimen. The vibration is detected by a transducer producing an electrical signal analysed by the signal processor. Each frequency will damp according to the energy absorption of the material. For the elevated temperature tests a heating time of 5 minutes was applied before performing the excitation and measurements of the test specimens. The specimen dimension is 70x20x2 mm, extracted from the two different material batches of Ti-6Al-4V. The test procedure can shortly be described by the steps below:

i) Sample position
ii) Furnace heating of sample to desired test temperature
iii) Excitation of test sample
iv) Vibration detection
v) Signal processing and analysis

The temperature is measured using a thermo couple (type K) welded onto the surface in the centre of a second specimen of Ti-6Al-4V, not used for the determination of Young's modulus.

*3.2. Room temperature and conductive hot tension tests*

Uniaxial tension tests at room temperature are performed in five different directions referenced to the rolling direction, along (00), in a 22.5° mode (22.5), in a 45° mode (45), in a 67.5° mode (67.5) and transverse (90). The tension tests are performed according to SS-EN 10 002-1 using an MTS tensile test equipment with load capacity 100 kN, at a strain rate of 0.003 $s^{-1}$ up to 0.2% engineering strain followed by a strain rate of 0.009 $s^{-1}$. The tests are performed until rupture. During the test procedure the force, the axial and width displacements (using video extensometers) are measured and logged. The tests are also continuously evaluated using ARAMIS$^{TM}$ optical strain measuring system [30]. A specimen of with 12.5mm and evaluation length of 50 mm was chosen due to a shortage of material, see figure 2. A stochastic speckle pattern is applied, consisting of a white matt base with black graphite powder speckles applied as an aerosol. The camera system take pictures and samples the force and actuator values from the tensile test machine with a frequency of 6 Hz. The evaluation area is the facets were necking occurs, 6 mm in width and 4 mm in height on the unstrained sheet, in order to obtain true stress – strain values even after the occurrence of necking. The Lankford coefficients are presented at 0.05 true longitudinal strain.

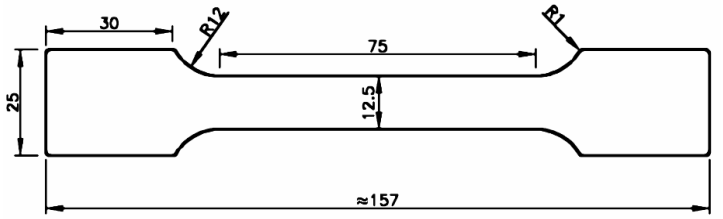


**Figure 2.** Test specimen for the uniaxial tesion tests performed in room temperature [mm].

For the characterization of the flow and the anisotropic properties at elevated temperatures, conductive hot tension tests are carried out by using a modified Gleeble 1500 system (Dynamic Systems Inc., USA). The tests are performed at 250, 400 and 560 °C for a strain rate of 0.05 $s^{-1}$ following the guideline of DIN EN 10 002, Part 5. For a more detailed description of the experimental setup the reader is referred to [31, 32]. During the tension tests, the samples have been imposed to the following test program:

i) Heating up to the target temperature within 30 seconds
ii) Maintaining the samples at the test temperature for additional 10 seconds
iii) Performance of the tension test to failure

The geometry of the specimen is chosen according to the recommendation of EN482-2. To evaluate the direction dependency of the plastic properties, samples with an orientation in the 00, 45 and 90 directions referenced the rolling direction are tested. The deformations of the specimens are observed and computed using the optical measuring system ARAMIS$^{TM}$ by applying a 50 Hz CCD-camera recording images of the progressive elongated samples. Therefore, an appropriate stochastic pattern was applied on the samples surface, which is capable to resist temperatures up to 950°C. The temperature is measured and controlled using Ni/Cr-Ni thermocouples spot welded onto the sample at half of the length. For the determination of the anisotropy coefficient, $R_\alpha$, as a function of rolling direction and equivalent strain during the hot tension tests, the analysis of the required strain follows [31, 32]. The optical deformation system calculates the 2-dimensional strain distribution for each facet and node of the rectangular grid drawn by the ARAMIS$^{TM}$ software on top of the taken pictures, respectively. Only the computed anisotropy values, R-values, for the column of nodes in the centre of necking area are used, where the highest strains are localized. The normal anisotropy is thus obtained by averaging the R-values along this column to reduce the impact of local effects. For an efficient handling of the data, a visual basic macro-function is programmed. Following DIN 10130 valid for room temperature characterization, the anisotropy coefficient R is determined at 20 % homogeneous plastic deformation or at the point of uniform elongation. With respect to a more detailed description of the analyzing method the reader is referred to the literature [33, 34].

*3.3. Uniaxial compression tests*

Uniaxial compression tests at different temperatures are performed in order to determine the strength differential in initial yielding. The tests are performed in the (00) and (90) direction referenced the rolling direction. The specimen geometry has a parallel waist in order to concentrate the compressive strain to a smaller area according to figure 3.

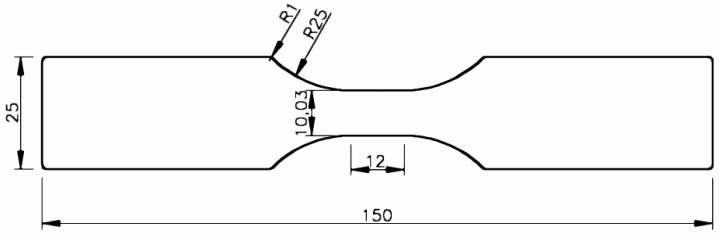


**Figure 3.** Test specimen for the uniaxial compression test, $CT_{tmp}$, [mm].

In order to prevent buckling, a support device is mounted onto the specimen which is coated with lubricants to minimise friction. Teflon is used as lubricants for the room temperature tests and boron nitride at elevated temperatures. An opening is located in the centre of the support device in order to enable strain measurements and evaluation using ARAMIS$^{TM}$. The strain rate in the tests is 0.0029 $s^{-1}$ and performed to approximately 5,5 % true plastic strain, using the MTS equipment. To ensure that the friction between the test specimen and the support device does not influence the results, only data up to the initial yielding are used, where the thickness increase is minute. A thermo couple, type K, is spot welded on the edge

of the test specimen in centre of the evaluation area to control and measure the temperature during heating and testing. A heating time of 5 minutes is applied for the tests performed at 400°C. The temperature is measured during the test to within ± 5°C. The test setup is presented in figure 4. Repetition tests are performed to ensure reproducibility. Similar test setups to determine compressive flow curves in room temperature have been reported in e.g. [35] where a known force is applied to the support device and where a friction and biaxial correction is made to obtain complete compressive flow curves.

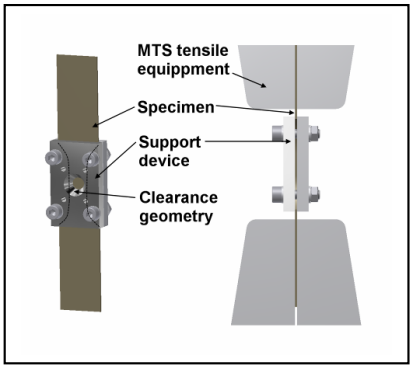


**Figure 4.** Illustration of the test setup for the uniaxial compression tests ($CT_{tmp}$).

*3.3. Loading-unloading-reloading tests*

In order to determine the elastic stiffness degradation due to plastic straining, the unloading behaviour of the titanium alloy is evaluated at different plastic strain levels. To perform the test and determine Young's modulus, a special case of the uniaxial tension test in the (90) direction is performed. The tension test is loaded to about 0.5 % total engineering strain, unloaded to zero force and then loaded again to 1 % total engineering strain. The unloading reloading procedure is repeated to 1.5, 3, 4 and 6 % total engineering strains. The elastic modulus is determined for each unloading by calculating the secant modulus according to the schematic figure 5. The specimen geometry is identical to the one used for the room temperature tension tests, illustrated in figure 2. Elastic degradation with plastic straining has been observed for steels, as presented in e.g. [36].

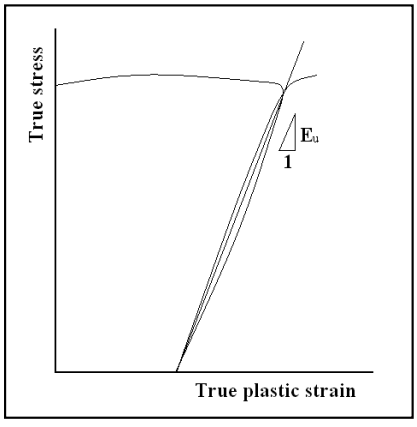


**Figure 5.** Schematic illustration of the unloading-reloading relationship.

*3.5. Viscous bulge test*

A viscous bulge test is performed in room temperature, see e.g. Sigvant et al. [37], to obtain a balanced biaxial stress state. The test is performed in order to produce an experimental biaxial reference point used to determine the equi-biaxial yield stress, $\sigma_b$ , and R-value, $R_b$. The blank with a diameter of 200 mm is formed using a silicon punch to create a uniform pressure on the sheet metal, as illustrated in figure 6. The test uses the same principal tool and test setup as in the forming limit curve tool presented below, in which two cameras are mounted on top of the die. The ARAMIS$^{TM}$ strain measurement system is used to continuously measure surface strains and geometry (radius of the dome) during the test. The pressure is continuously measured by a sensor in the bottom of the silicone rubber punch to determine the biaxial stress according to Equation 1

$$\sigma_b = \frac{p \cdot r_b}{2t_b} \tag{1}$$

where $p$ is the pressure, $r_b$ is the radius of the curvature and $t_b$ is the thickness at the top of the dome. After the test is performed, the biaxial stress-strain curve is determined by a software as a part of the ARAMIS$^{TM}$ system.

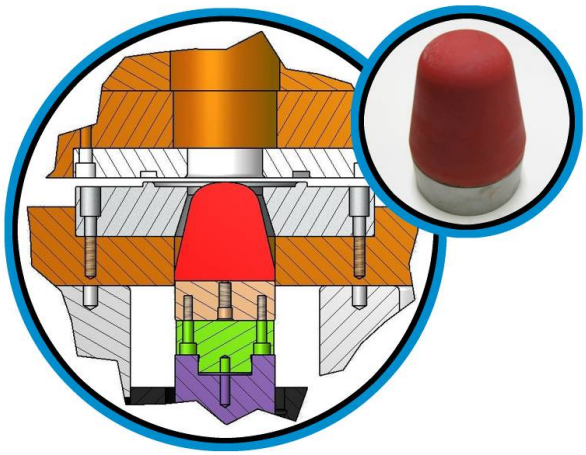

**Figure 6.** Illustration of the test setup for the viscous bulge test (VBT).

*3.6. Forming limit curve (FLC)*

Forming limit curves are determined at room temperature and 400°C, in order to estimate forming limits according to the Nakazima method [38-41]. Three tests geometries at each temperature are performed to generate data with different strain conditions.

The room temperature tests are performed in a tool with a punch diameter of 100 mm and a draw radius of 12 mm. The specimens are locked in the blank holder using flat binder surfaces. In order to maintain low friction between the punch and the specimen, the titanium blank is lubricated by a system of oil, a Teflon film and a PVC-disc at RT. See figure 7, for an illustration of the test setup. A stochastic speckle pattern is applied on the specimens with three blank geometries, I) a diameter of 200 mm, II) a width of 100 mm for the plane strain case and III) a width of 50 mm. The blanks are formed over the hemispherical punch until fracture occurs. Through a hole in the blank holder, the event is recorded using ARAMIS$^{TM}$

camera and strain measurement system with a frequency of 25Hz. The strains are evaluated according to the "ISO-12004 Proposal Version 15-8-2005" [42] in which three strain sections across the crack are plotted. The FLC-strains are achieved, using a macro.


**Figure 7.** Illustration of the test setup for the forming limit tests (FLC).

*3.7. Heat transfer tests*

The values of the heat transfer coefficient (htc) have been determined analytically according to Newton's cooling law from the time-temperature data recording during the quenching tests. A temperature range between 500 and 250 was chosen for the calculation with a Cp value of 607 $JKg^{-1}K^{-1}$ [43]. Three tests at each pressure are performed.During the quenching tests the specimens were imposed to the following test procedure:

i) Furnace heating of the specimen (600 °C) for 5 minutes
ii) Specimens are transferred manually to the quenching tool and subsequently cooled in dependency of various contact pressures (0-40 MPa).

## 4. Results

The tests revealed that the titanium alloy Ti-6Al-4V has anisotropic elastic and plastic properties and yielding asymmetry in tension and compression. The elastic properties of the two material batches are presented in table 4. Alloy 1 has pronounced anisotropic elastic properties at room temperature where Young's modulus vary within 19.3% between the (00) and (90) direction. The elastic anisotropy for alloy 2 is less pronounced. The maximum variation are 2.3% at room temperature, 3.8% at 400°C and 3.9% at 560°C.

**Table 4.** Elastic properties of Ti-6Al-4V. Temperature in [°C] and Young's modulus in [GPa].

| Alloy | Test method | Temperature | Young's modulus | | |
|---|---|---|---|---|---|
| | | | (00) | (90) | (45) |
| 1 | RFDA | RT | 109 | 130 | 116 |
| 2 | RFDA | RT | 118.8 | 119.9 | 117.2 |
| 2 | $T_{RT}$ | RT | 118.6 | 120.8 | 119.9 |
| 2 | RFDA | 250 | 106.7 | 109.0 | 105.9 |
| 1 | RFDA | 400 | - | 97.0 | - |
| 2 | RFDA | 400 | 98.3 | 101.0 | 97.3 |
| 2 | RFDA | 560 | 90.0 | 92.5 | 89.0 |

From the loading-unloading-reloading test the elastic degradation with plastic straining is measured to 5.46 % between 0.0 to 0.031 true plastic strain for alloy 2. See table 5 and figure 7. The elastic modulus is determined for each unloading by calculating the unloading modulus, $E_u$.

**Table 5.** Elastic degradation of Ti-6Al-4V in the 90 direction, determined at different true strain levels in room temperature [GPa].

| Alloy | Test method | The (90) direction, at true plastic strain levels [%] | | | | | |
|---|---|---|---|---|---|---|---|
| | Loading-unloading-reloading | 0 | 0.21 | 0.71 | 1.21 | 2.2 | 3.1 |
| 2 | $E_u$ | 120.8 | 122.0 | 120.7 | 119.3 | 116.7 | 114.2 |

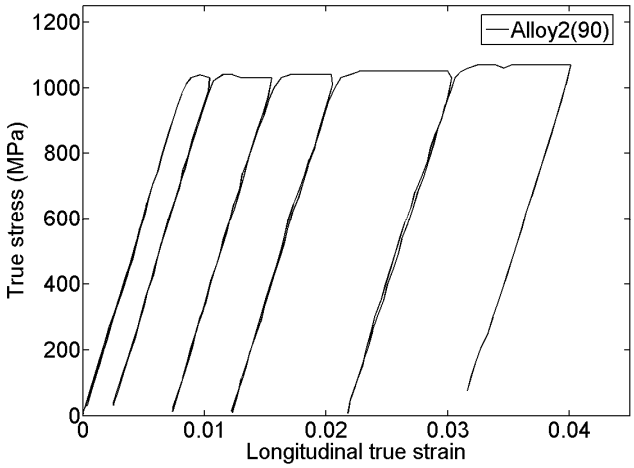


**Figure 7.** True stress - true strain curves under loading-unloading-reloading in room temperature.

Tensile true stress - strain curves for the different alloys, directions and temperatures are presented in figure 8 to 10. The difference in initial yielding and anisotropy between the two material batches of Ti-6Al-4V is obvious. Tension tests with two different strain rates, 0.009 $s^{-1}$ and 0.05 $s^{-1}$ at room temperature are performed for comparative purposes, denoted Alloy2 (90) and Alloy2(90)-HS, respectively,. The tests indicate strain rate sensitivity of the alloy, c.f. figure 8.

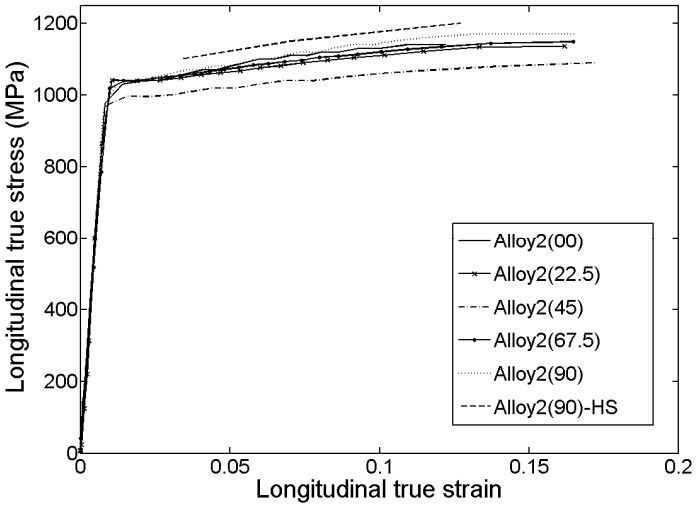


**Figure 8.** Tensile longitudinal true stress - true strain curves at room temperature, alloy 2.

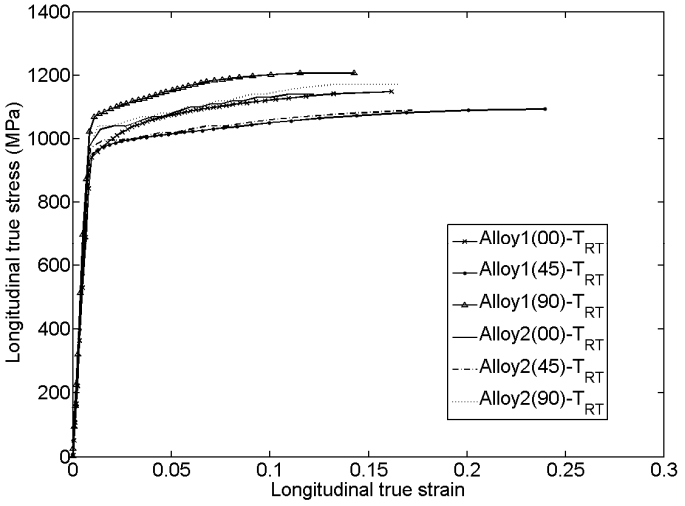


**Figure 9.** Tensile longitudinal true stress - true strain curves at room temperature, alloy 1 and alloy2.

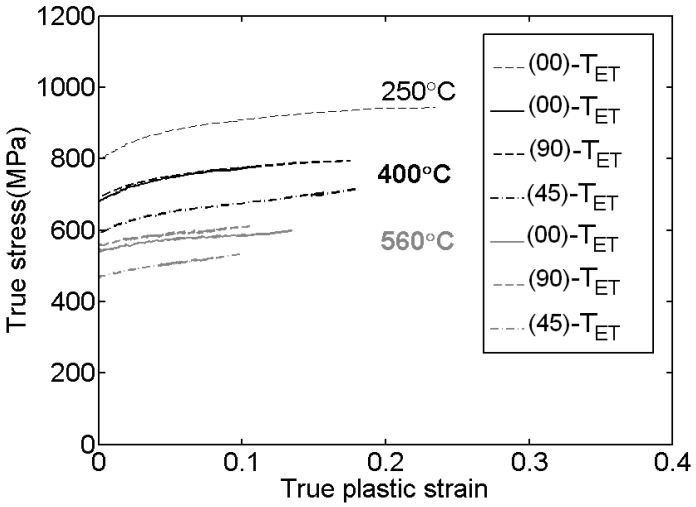


**Figure 10.** Tensile true stress - true plastic strain curves at elevated temperatures.

Results from the uniaxial compression tests at room temperature and 400°C is presented in figure 11 and 12. The uniaxial compression tests are performed at similar strain rates as for the room temperature tension tests of 0.0029 $s^{-1}$ and 0.009 $s^{-1}$, respectively. The tests indicate a strength differential in room temperature.

Due to the comparatively lower strain rate between the uniaxial compression and conductive hot tension tests at 400°C (0.0029 and 0.05 $s^{-1}$, respectively) a complementary test was performed. The complementary test is a tension tests, denoted (CT-T), in which the same geometry and setup as used for the uniaxial compression tests is applied. Theses test results are considered preliminary, in which further investigations are required. However, a different behaviour compared to the room temperature case is observed. In room temperature the compressive initial yield stress is higher than the tensile initial yield stress, as presented in table 6. At 400°C, the strength differential in the (90) direction is minute. The compressive initial yield stress in the (00) direction was found lower compared to the (90) direction.
Table 6 assembles the related initial yield stresses in tension and compression together with Lankford coefficients, in the studied temperature range.

**Table 6.** Initial yielding in tension and compression. Temperature in [°C] and yield stress in [MPa]. (HS) denotes the higher strain rate of 0.05 $s^{-1}$.

| Alloy | Type of test | Temp | Yield stress (00) | (22.5) | (45) | (67.5) | (90) | Lankford parameter (00) | (22.5) | (45) | (67.5) | (90) |
|---|---|---|---|---|---|---|---|---|---|---|---|---|
| 1 | $T_{RT}$ | RT | 940.3 | - | 933.5 | - | 1058.5 | 0.35 | - | 1.6 | - | 1.0 |
| 2 | $T_{RT}$ | RT | 1000.0 | 1025.0 | 972.0 | 1020.0 | 1020.0 | 0.4 | 0.75 | 1.2 | 0.61 | 0.61 |
| 2 | $T_{RT(HS)}$ | RT | - | - | - | - | 1062.8 | - | - | - | - | 0.55 |
| 2 | $C_{tmp}$ | RT | 1106.3 | - | - | - | 1075.0 | - | - | - | - | - |
| 2 | $T_{tmp}$ | 250 | - | - | - | - | 912.8 | - | - | - | - | 0.53 |
| 2 | $T_{tmp}$ | 400 | 681.0 | - | 591.0 | - | 691.0 | 0.618 | - | 1.26 | - | 0.512 |
| 2 | $CT_{tmp}$ | 400 | 596.0 | - | - | - | 648.0 | - | - | - | - | - |
| 2 | CT-T | 400 | - | - | - | - | 635.0 | - | - | - | - | - |
| 2 | $T_{tmp}$ | 560 | 564.2 | - | 468.9 | - | 559.9 | 0.676 | - | 1.29 | - | 0.63 |

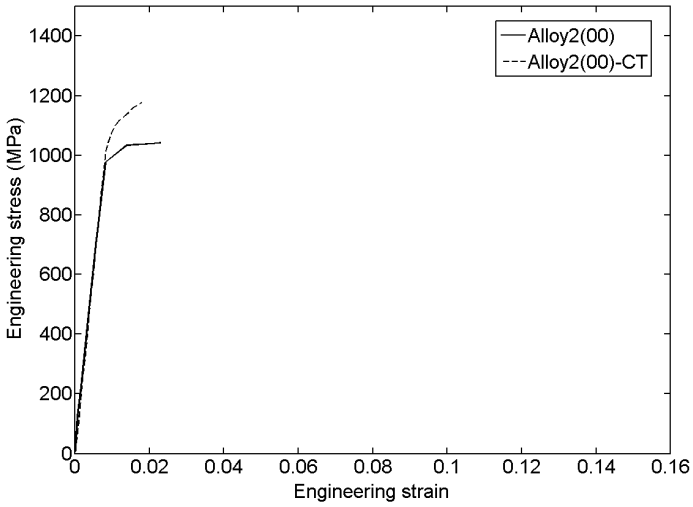


**Figure 11.** Tensile and compressive engineering stress - strain curves in room temperature.

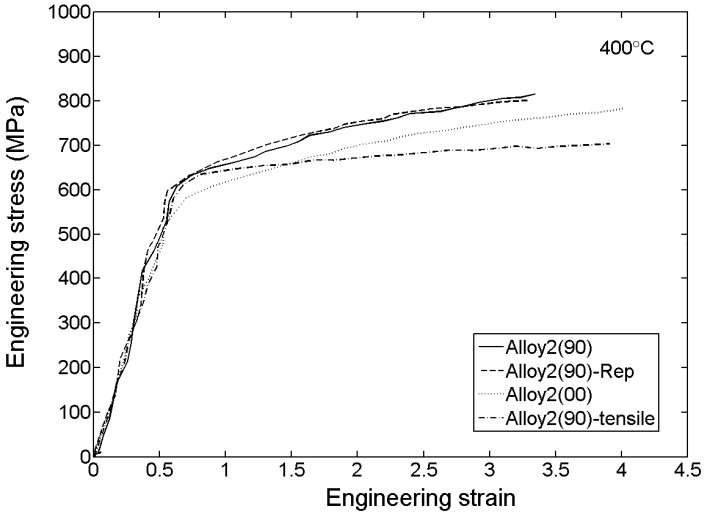


**Figure 12.** Tensile and compressive engineering stress - strain curves at 400°C with respect to the rolling direction.

The biaxial true stress – thickness strain curve obtained from the viscous bulge tests and the biaxial $R_b$-value is presented in figure 13 and 14. The tension test in the 00 direction is presented as a reference. The experimental biaxial reference point for the determination of the biaxial initial yield stress is chosen according to (2) and the biaxial R-value is equal to 1.02.

$$REF(\sigma, -\varepsilon_t) = (1136.0, 0.075) \quad (2)$$

Figure 15, illustrates the deformed specimen used in the viscous bulge test. Due to the formability of Ti-6AL-4V, fracture occurred in the draw radius during the test procedure. Further on, a pressure level close to the maximum available in the test setup was obtained at the occurrence of fracture.

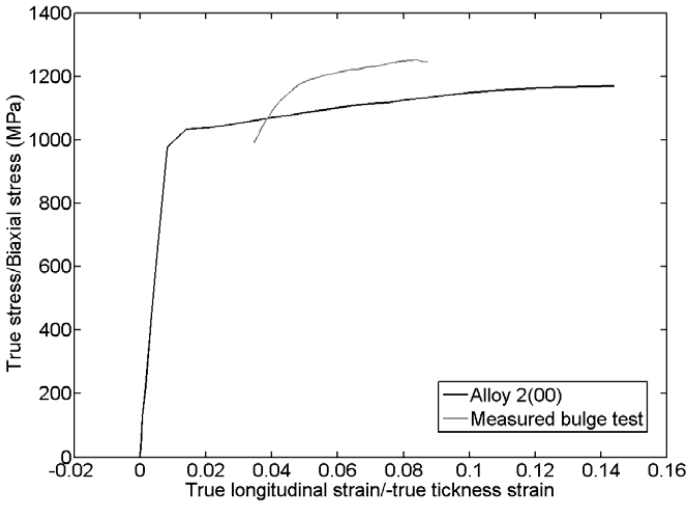


**Figure 13.** Flow curve for the tension test (00) and the balanced biaxial stress state at room temperature, alloy 2.

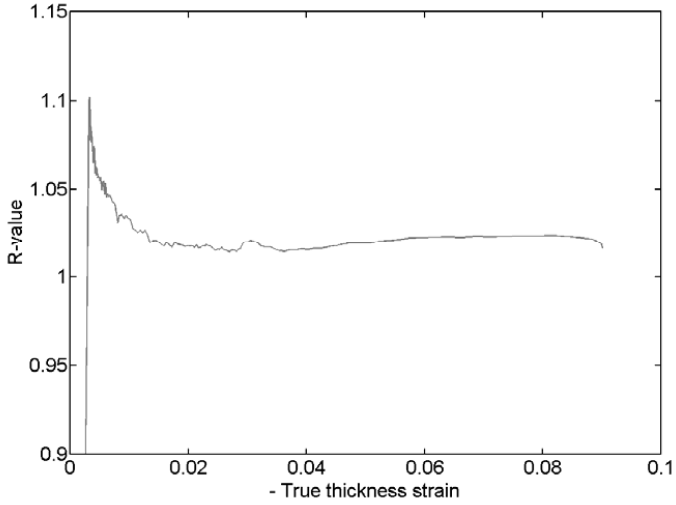


**Figure 14.** R-value for the balanced biaxial stress state at room temperature, alloy 2.

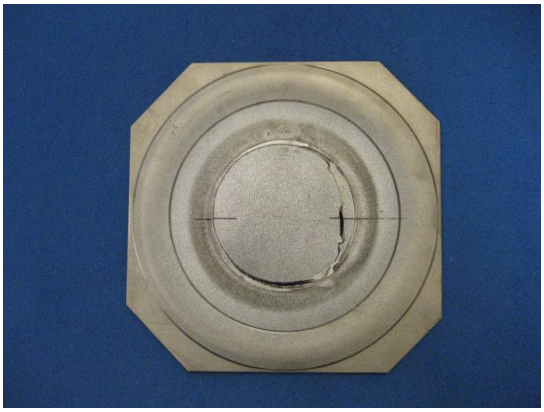

**Figure 15.** Picture of the blank deformed in the viscous bulge test at room temperature. Fracture occurred in the draw radius.

The results from the experiments performed to determine the forming limits curves of Ti-6Al-4V are presented in figure 16.

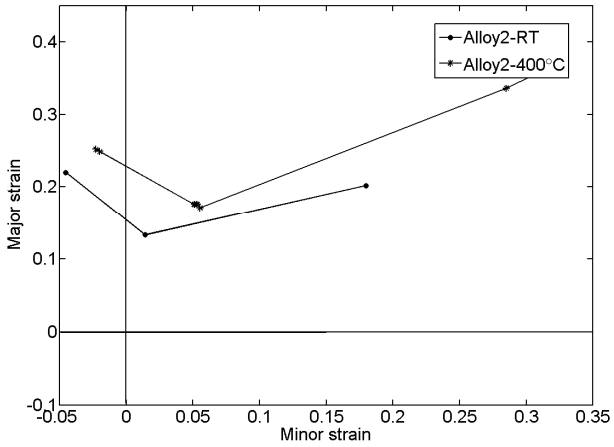


**Figure 16.** Forming limit curves (true strain). Experimental values for alloy 2 in room temperature and at 400°C.

The three different blank geometries formed at room temperature are illustrated in figure 17, the rolling direction is horizontal in the figure. From the biaxial test on the right hand side in the figure, facture has occurred in the rolling direction (00) of the blank. This suggest that the blank possess a lower formability in the rolling direction (00) compared to transverse (90) the rolling direction, at room temperature.

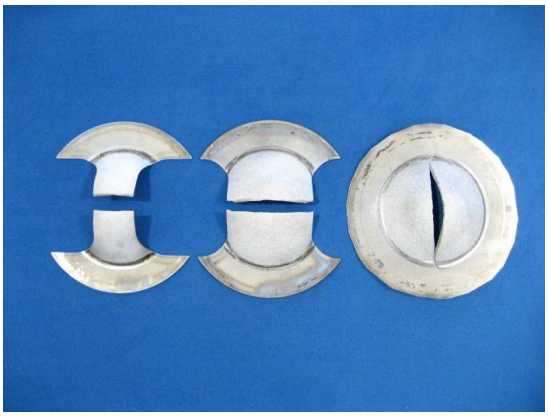

**Figure 17.** Formed blank geometries for the room tempered forming limit tests (FLC). From left to right, Ø 50, Ø 100 and Ø 200 mm, respectively.

The determined values of the heat transfer coefficient are presented in figure 18. A mean value of 2000 $Wm^{-2}K^{-1}$ is suggested for use in coupled thermo mechanical FE analyses. The standard deviation is presented in table 7 and indicated in figure 18.

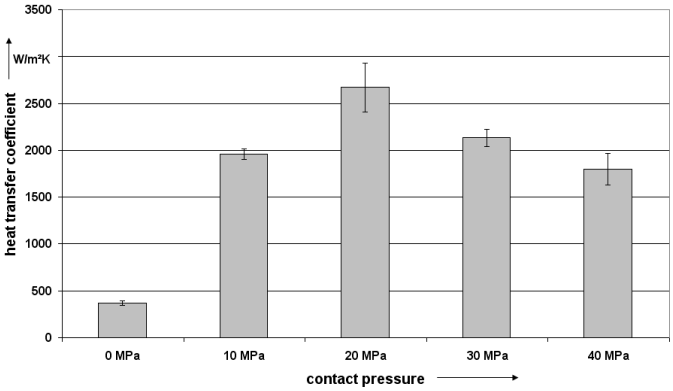


**Figure 18.** Determined heat transfer coefficient with contact pressure.

**Table 7**. Standard deviation for the heat transfer tests.

| Alloy | Contact pressure [MPa] | Standard deviation [$Wm^{-2}K^{-1}$] |
|---|---|---|
| 2 | 0 | 26.5710793 |
| 2 | 10 | 56.1249406 |
| 2 | 20 | 263.144354 |
| 2 | 30 | 90.5973722 |
| 2 | 40 | 171.648041 |

## 5. Discussion and conclusions

The performed tests in the material characterisation show the elastic and plastic anisotropy of Ti-6Al-4V. Young's modulus, initial yielding and anisotropy coefficients vary with the in-plane direction. The studied properties of the two material batches of Ti-6Al-4V do not coincide, i.e. the properties deviate between the two alloys. Since the deviation is quite significant, it is of importance to obtain experimental reference data from the same batch of Ti-6Al-4V as used in the application of interest. The influence of different material batches on the manufacturing process of interest is important to determine. By performing parameter studies or analyses of robustness, the influence on predicted FE results such as shape deviation and material thinning in sheet metal forming can be obtained.

The second batch of Ti-6Al-4V, Alloy 2, has unsymmetrical initial yielding properties in tension and compression at room temperature. Further on, the alloy is sensitive to elastic degradation with plastic straining. By using the optical system for strain evaluation, ARAMIS$^{TM}$, true stress - true strain curves could be obtain for values after the occurrence of necking by performing strain evaluations locally within the necking area.

The tests performed to study forming limits indicate that the alloy can be formed to higher strain values at 400°C than at room temperature before fracture occurs. In practice, safety margins with respect to the measured values are applied. Based on experience, the safety margin may be assumed to values of about 40 % to avoid strain localisation [44]. The large value of safety margin originates from different aspects such as, 1) the definition of "incipient" necking which occur much earlier than failure, 2) the subjectivity in test procedures and test evaluation, 3) applied tool geometry, process parameters and friction conditions and 4) the effect of changed strain path on the FLC. See e.g. [38-42]. In this work the strains are evaluated according to the "ISO-12004 Proposal Version 15-8-2005" in which the purpose is to reduce the subjectivity in the determination method.

An interesting extension to the present work would be to increase the experimental study in order to further evaluate the strength differential, strain rate and to study cyclic loading in order to investigate the Bauschinger effect for a proper choice of hardening law for FE analyses, even at elevated temperatures. By performing tests in different in-plane directions referenced the rolling direction, the direction dependence on studied material response can be obtained.

## References


[1] R.D. Cook, D.S. Malkaus, M.E. Plesha. *Concepts and applications of finite element analysis.* John Wiely & Sons, New York, third edition, 1989. ISBN 0-471-50319.

[2] T. Belytschko, W.K. Liu, B. Moran. *Nonlinear finite elemens for continua and structures.* John Wiely & Sons, New York, third edition, 2000. ISBN 0-471-98774-3.

[3] V. Adams and A. Askeazi, "Building Better Products with Finite Element Analysis", On Word Press, Santa Fee, USA (1999) ISBN 1-56690-160X.

[4] A.E. Tekkaya, "State of the art of simulation of sheet metal forming", Journal of Materials Processing Technology 103 (2000) 14-22.

[5] K. J. Bathe, "On the state of finite element procedures for forming processes", In S. Gosh, J.C. Castro and J.K. Lee, editors, CP712, Materials Processing and Design: Modeling, Simulation and Applications, NUMIFORM (2004) 34-38. American Institute of Physics.

[6] R.W. Lewis, K. Morgan, H.R. Thomas, K.N. Seetharamu. *The finite element method in heat transfer analysis.* John Wiely & Sons, New York, third edition, 1996. ISBN 0-471-93424-0.

[7] R. Boyer, G. Welsch, E.W. Collings, Materials Properties Handbook: Titanium alloys, edition, ASM International, 1994.

[8] G. Lütjering, J. C. Williams, Titanium, Springer-Verlag Berlin Heidelberg, 2003
[9] S.L. Semiatin, V. Seetharaman, I. Weiss, Materials Science & Engineering A, A243 (1998) 1-24.
[10] R. Ding, Z.X. Guo, A. Wilson, Materials Science and Engineering A, 327 (2002) 233-245.
[11] P. S. Follansbee, G.T. Grey III, An analysis of the low temperature, low and high strain.rate deformation of Ti-6Al-4V. Metall. Trans. A 20A (5), (1989), 863-874.
[12] S. Nemat-Nasser, W.-G. Guo, V.F. Nesterenko, S.S. Indrakanti, Y.-B. Gu, Dynamic response of conventional and hot isostatically pressed Ti-6Al-4V alloys: Experiments and modeling, Mechanics of Materials, v 33, n 8, August, 2001, p 425-439, ISSN: 0167-6636.
[13] R. C. Picu, A. Majorell, Mechanical behaviour of Ti-6Al-4V at high and moderate temperatures – Part II: constitutive modelling. Mater. Sci. Eng. A326, (2002), 306-316.
[14] W. S. Lee, M. T. Lin, The effects of strain rate and temperature on the compressive deformation behavior of Ti-6Al-4V alloy. J. Mater. Proc. Tech. v71, (1997), 235-246.
[15] A. S. Khan, Y. S. Suh, R. Kazmi, Quasi-static and dynamic loading responses and constitutive modeling of titanium alloys, Int. J. Plast., V20, (2004), 2233-2248.
[16] A. S. Khan, R. Kazmi, B. Farrokh, Multiaxial and non-proportional loading responses, anisotropy and modelling of Ti-6Al-4V titanium alloy over a wide ranges of strain rates and temperatures, Int. J. Plast., V23, (2007), 931-950.
[17] R. Ding, Z.X. Guo, M. Qian, Computation Materials Science, 40 (2007) 201-212.
[18] A.J. Wagoner, C.W. Bull, K.S Kumar, C.L. Briant, Metallurgical and Materials Transactions A, v 34, n 2 (2003) 295-306.
[19] Lee. Woei-Shyan, Lin. Ming-Tong, Journal of Materials Processing Technology, v 71, n 2 (1997) 235-246.
[20] S.L. Semiatin, T.R. Bieler, Metallurgical and Materials Transactions A, v 32, n 7 (2001) 1787-1799.
[21] B. Babu, Licentiate Thesis 2008:40, Luleå University of Technology, Sweden, 2008.
[22] R. Hill, The Matematicall, Theory of Plasticity, Clarendon Press, Oxford. (1950).
[23] F. Barlat, J. Lian, Plasticity behaviour and strechability of sheet metals Part I: a yield function for orthotropic sheets under plane stress condition. Int. J. Plasticity, v 5, (1989), 51-66.
[24] W. Hosford, On the yield loci of anisotropic cubic metals. 7th North American Metalworking Conf.. SME, Dearborn, MI, (1979), 191-197.
[25] F. Barlat, J.C. Brem, J. W. Yoon, K. Chung, R.E. Dick, D.J. Lege, F. Pourboghrat, S.-H. Choi, E. Shu. Plane stress yield function for aluminium alloy sheet – Part1: theory. Int. J. Plasticity. v 19, (2003), 1297-1319.
[26] O. Cazacu, F. Barlat. Orthotropic yield criterion for hexagonal closed packed metals. Int. J. Plasticity. v 22, (2006), 1171-1194.
[27] E.-L. Odenberger, Doctoral Thesis, Luleå University of Technology, Sweden, 2009.
[28] Manual for The Resultant Frequency and Damping Analyser (RFDA) system 23, version 6.3.0, IMCE (2006).
[29] RFDA: http://www.imce.net/, Oct (2009).
[30] ARAMIS v6: http://www.gom.com, Oct (2009).
[31] H. Hoffmann, Chr. Vogl, Determination of True Stress-Strain-Curves and Normal Anisotropy in Tensile Test with Optical Deformation Measurement. Annals of CIRP 52/1/2003, p. 217
[32] J. Hecht, S. Pinato, M. Geiger, Determination of mechanical properties for hydroforming of magnesium sheets at elevated temperatures. In: SheMet'05, Germany, p. 763

[33] H. Hoffmann, Chr. Vogl, Determination of True Stress-Strain-Curves and Normal Anisotropy in Tensile Test with Optical Deformation Measurement. Annals of CIRP 52/1/2003, p. 217
[34] J. Hecht, S. Pinato, M. Geiger, Determination of mechanical properties for hydroforming of magnesium sheets at elevated temperatures. In: SheMet'05, Germany, p. 763
[35] R.K. Boger, R.H. Wagoner, F. Barlat, M.G. Lee, K. Chung, Continuous, large strain, tension/compression testing of sheet material, Int. J. Plasticity, Vol. 21, 2005, pp. 2319-2343.
[36] P.-A. Eggertsen, Licentiate Thesis, 2009:05, Chalmers University of Technology, Sweden, 2009.
[37] M. Sigvant, K. Mattiasson, H. Vegter, P. Thilderkvist, A viscous pressure bulge test for the determination of a plastic hardening curve and equibiaxial material data, Submitted for publication.
[38] K. Nakazima, T. Kikuma, K. Hasuka, Yamata Tecnical Report, v 264, 1968, pp. 141-154.
[39] S.P. Keeler, Determination of forming limit in automotive stamping, Soc. Of. Automotive Engineering, 1965, Nr 650 535, pp 1-9,
[40] P. Hora et al., A prediction method for ductile sheet metal failure using FE-simulation, NUMISHEET, Dearborn, MI, USA, 1996, pp 252-256.
[41] L. Tong, P. Hora, J. Reisser, Prediction of Forming Limit with nonlinear Deformation Paths using Modified Maximum Force Criterion, NUMISHEET 2002.
[42] Draft International Standard, ISO/DIN 12004-2, "Metallic materials-Sheet and strip-Determination of forming limit curves–Part 2: Determination of forming limit curves in laboratory.
[43] VDI-Wärmeatlas, Springer Verlang, 2002, ISBN: 3-540-41200
[44] M.Sigvant, K. Mattiasson, M. Larsson, The definition of incipient necking and its impact on experimentally or theoretically determined forming limit curves, IDDRG 2008 Conference, Olofström, Sweden, pp. 207-218.

# Paper F

# Thermo mechanical sheet metal forming of aero engine components in Ti-6Al-4V – PART 2: Constitutive modelling and validation

**E-L Odenberger[1, 3*], M Jansson[2], M Oldenburg[3]**

[1] Forming Group OSAS, Industrial Development Centre in Olofström AB, Vällaregatan 30, SE-293 38 Olofström, Sweden

[2] Engineering Research Nordic AB, Garnisonen, Brigadgatan 16, SE-581 31 Linköping, Sweden

[3] Division of Solid Mechanics, Luleå University of Technology, SE-971 87 Luleå, Sweden

* Corresponding author, E-mail: Eva-Lis.Odenberger@iuc-olofstrom.se

**Abstract**

In this work a tool concept for hot forming of a double-curved sheet metal component in the titanium alloy Ti-6Al-4V is proposed. The virtual tool design is based on finite element (FE) analyses of hot sheet metal forming in which two different anisotropic yield criteria are evaluated and compared with an isotropic assumption to predict global forming force, draw-in, springback and strain localisation. The shape of the yield surface was found to be of importance and by including the cooling procedure, the accuracy of predicted shape deviation could be improved. The predicted responses show promising agreement to the corresponding experimental observations when the anisotropic properties of the material are considered.

## 1. Introduction

Titanium alloys are common in aero space applications, mainly due to their high strength to weight ratio. Ti-6Al-4V is a frequently used titanium alloy in aero engine components such as for load carrying structures, fan frame structures and compressor blades with moderately elevated running temperatures. Alternative manufacturing technologies for static load carrying aero engine structures are desired in order to reduce product cost and enable weight reduction and thereby fuel consumption. Traditionally, these structures consist of large-scale single castings. By fabrication sheet metal parts, small ingots and simple forgings are instead welded together and heat treated in order to produce complete structures. The fabrication process implies the need for time and cost efficient methods for evaluation of candidate manufacturing techniques early in the product development process.

One challenge in fabricating such structures within tolerance lies in accurate prediction and compensation for springback and shape deviation, which occurs in the different processes of the manufacturing chain. The aero dynamic geometries of included sheet metal parts are generally smoothly double-curved and the resultant geometry, thickness, residual stress state and mechanical properties obtained in the forming procedure influence the shape deviation of the complete structure upon welding and heat treatment. Accurate predictions of and compensation for springback in sheet metal forming processes by means of finite element (FE) analyses, is therefore one key subject considering fabrication of complete titanium

structures. A schematic example of a static load carrying aero engine structure is illustrated in figure 1, in this case consisting of materials such as nickel based alloys.

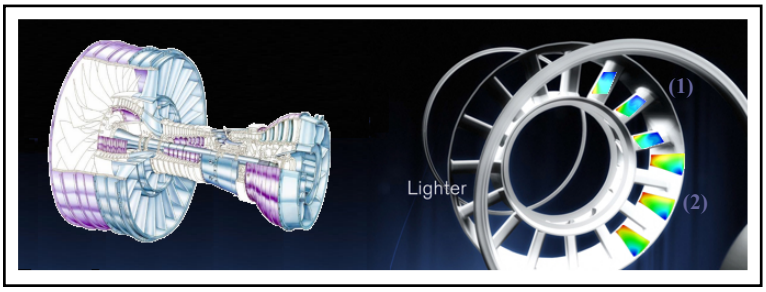


**Figure 1**. An example of a static load carrying aero engine structure containing sheet metal parts, ingots and forgings (nickel based alloys). FE analyses of shape deviation for sheet metal components.

The mechanical properties of the titanium alloy Ti-6Al-4V are mainly determined by the initial microstructure, the thermo-mechanical loading history and the present impurities together with alloy concentration [1-4]. At room temperature (RT) and medium elevated temperatures the common structure consists of equiaxed α and elongated α (*hcp* crystal structure) in a minor volume content β-matrix (*bcc* crystal structure). In the form of thin sheet metals, the mechanical properties are sensitive to the rolling direction. The alloy has anisotropic elastic and plastic properties and asymmetric yielding in tension and compression. A large number of studies have been performed in order to understand and model the mechanical behaviour of the alloy under different temperatures and strain rates, see e.g. [3-14]. Numerous anisotropic yield formulations which can account for plastic anisotropy have been formulated the past decades. E.g. Hill's yield criterion (1950) [15], which is an extension of the von Mises isotropic yield criterion to cover anisotropy, commonly applied in FE analyses of sheet metal forming. The criterion contains four anisotropy coefficients in the plane stress condition, which have to be determined experimentally. Since only four parameters are available, the criterion is not able to capture together the observed anisotropy in yield stress and Lankford coefficients [16, 17]. Barlat and Lian's (1989) tri-component criterion [18] presented a yield criterion for plane stress conditions in which, as for the Hill's criterion, four anisotropy parameters are used to describe the yield surface. In this model the material parameter $m$, is proposed which is suggested to be equal to 6 for materials with a *bcc* crystal structure and 8 for materials with an *fcc* crystal structure. If a value of 2 is applied, the yield surface reduces to the Hill yield surface i.e. to the von Mises yield surface in the isotropic case. With an increasing value of $m$, in the isotropic case, the shape of the Barlat tri-component yield surface adopts the shape of the Tresca yield surface. The anisotropic yield criteria developed for cubic metals by e.g. Hosford [19] and Barlat and co-workers (2003, 2005) [20, 21] accounts for plastic anisotropy with an increased number of parameters. The anisotropy coefficients are determined from experimental reference data in order to calibrate the yield criteria with respect to both yield stress and Lankford coefficients. Examples of applicable material tests are uniaxial tension tests in three in-plane directions referenced to the rolling direction in combination with a test to produce a balanced biaxial stress state. These models assume symmetry in tension and compression. The physically based macroscopic formulation by Cazacu et al. (2006) [22] describes both the anisotropy and asymmetry in yielding exhibited by *hcp* materials.

Sheet metal forming of Ti-6Al-4V is often performed under high temperatures at low strain rates, typically at about 875°C with rates in the order of $10^{-3}$ to $10^{-4}$ $s^{-1}$, referred to as super plastic forming (SPF) see e.g. [2, 23, 24]. In the advanced SPF process, the super plastic

properties of the alloy are utilized which imply large formability with minimal springback often used for forming of complex geometries. Sheet metal forming of titanium alloys in room temperature or at lower elevated temperatures is generally limited due to quite low formability in combination with the scattering and major springback behaviour. Published work with applications of sheet metal forming procedures in the lower temperature region is quite limited, see e.g. [25-30].

In the present study a tool concept for hot forming in the medium temperature range of a double-curved titanium sheet metal component is suggested. The component is included in a Ti-6Al-4V subcomponent for a static load carrying aero engine structure, schematically illustrated as part (2) in figure 1. The virtual tool design, choice of process parameters and manufacturing are based on CAD modelling and evaluations by FE analyses of hot sheet metal forming in Ti-6Al-4V. Two different anisotropic yield criteria are compared with an isotropic assumption for the prediction of the forming procedure and related shape deviation, i.e. the yield criteria developed by Barlat et al. (2003) and Cazacu et al. (2006). The material characterisation presented in paper E in [31] is used as experimental reference to calibrate the yield criteria and determine the shape of the yield surfaces, in the temperature range of 20-560°C. The global calculated responses such as the punch force, draw-in and shape deviation are compared with measured values obtained by hot forming at 400°C.

## 2. Material

The material used in the hot forming tests is from the same batch of Ti-6Al-4V, alloy 2, as used in the material characterisation presented in paper E in [31]. A specification of the chemical composition can be found in table 1. The beta transus temperature of the alloy is typically 995±15°C [24].

**Table 1.** Chemical composition of Ti-6Al-4V, in weight per cent [wt%].

| | Al | O | N | Fe | C | V | Y | Ti |
|---|---|---|---|---|---|---|---|---|
| Alloy 2 | 6.10 | .15 | .006 | .17 | .009 | 3.80 | 50 PPM | Bal |

## 3. Experimental procedures

The experimental procedures used in this work are presented in this section.

The procedures constituting the material characterisation at temperatures ranging from room temperature up to 560°C consists of different test methods, as presented in [31]. Experimental data are produced in order to study forming limits but foremost to determine the shape of the yield surface of Ti-6Al-4V, in which different yield criteria are evaluated. To produce the prototype component and generate measured values used for correlation with numerical predictions, a hot sheet metal forming concept referred to as the validation test (VT) is developed and manufactured. The validation test is presented in this section.

The plastic anisotropy of materials implies different inelastic properties along different axes. This could be the result of a cold rolling process but also due to the crystal structure of the material itself, especially considering hcp materials such as titanium where anisotropy also pertain the elastic properties. Typical for sheet metals are that the blank possesses orthotropic properties i.e. the properties vary in the rolling direction (longitudinal), transverse and in the through-thickness direction. The plastic anisotropy is characterised by a difference in yield stress and plastic flow relative to the rolling direction, defined by the Lankford coefficient, $R_\alpha$, assuming plastic incompressibility:

$$R_\alpha = \frac{\varepsilon_w^p}{\varepsilon_t^p} = plastic\ incomp. = -\frac{\varepsilon_w^p}{\varepsilon_w^p - \varepsilon_l^p} \tag{1}$$

where α is the angle from the rolling direction, *w*, denotes the plastic strain in the width direction, *t*, the thickness and, *l*, longitudinal direction.

*3.1. Material Characterisation*

As a summary of the experimental observations made in the material characterisation, uniaxial tension test results at different temperatures are presented in figure 2 and 3. From these tests the initial yield stress, plastic hardening and Lankford coefficients were determined, depending on the angle to the rolling direction.

The uniaxial loading-unloading-reloading tension test indicated elastic degradation, i.e. the elastic modulus decrease with plastic straining, see section 4.1.2. Alloy 1, is presented in [31].

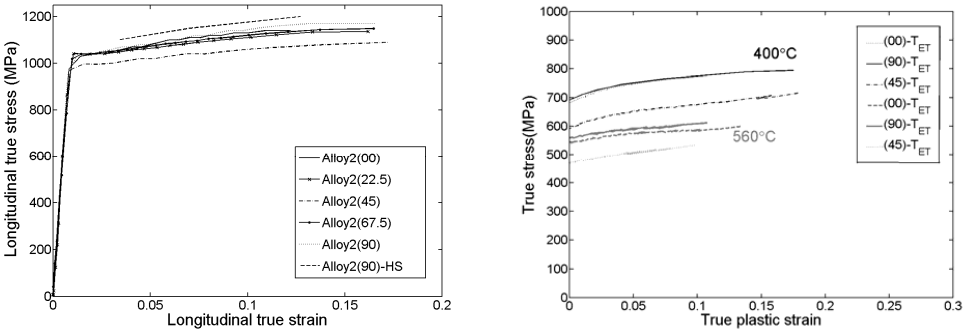


**Figure 2**. Hardening curves for Ti-6Al-4V at room temperature and at elevated temperatures, respectively. The strain rate in the elevated temperature tests is 0.05 $s^{-1}$ [31].

To determine the asymmetry in yielding between tension and compression (strength differential) uniaxial compression tests were performed. The initial compressive yield stress in room temperature along the rolling direction (00) was determined to 1106.3 MPa, which is higher compared to the initial yield stress in tension of 1000.0 MPa. The viscous bulge test was used to produce a balanced biaxial stress state and determine the initial biaxial yield stress, $\sigma_b$, and R-value, $R_b$, from an experimental reference point ($\sigma$, $-\varepsilon_t$). Forming limit tests were performed to determine forming limit curves, at room temperature and at 400 °C as illustrated in figure 3.

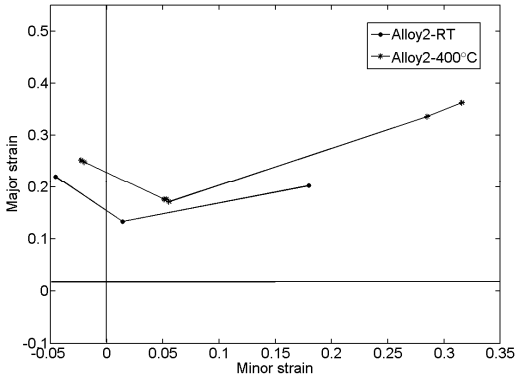


**Figure 3.** Forming limit curves (true strain), experimental values for alloy 2 in room temperature and at 400°C.

*3.2. Validation test*

A validation test (VT), the hot forming test, is performed at 400°C which is used to correlate FE predictions of punch force, draw-in, shape deviation and the occurrence of strain localisation. Further on, a hot sizing test (HST) at 560°C is performed in order to evaluate such a procedure and the resultant shape deviation. The geometry of the sheet metal part which is produced by hot forming is smoothly double-curved, as illustrated in figure 4. The prototype component is used as a part of subcomponents in the fabrication process for static load carrying aero engine structures. The tool design and manufacturing is a completely CAE-controlled process, performed using FE analyses to secure the forming concept with respect to strain localisation limits and minimise the springback according to the short lead time methodology presented in [32]. The hot forming process is a stretch forming procedure in which a minor draw-in is desired, designed to produce a fairly low level plastic strain distribution in the blank. A combination of flat binder surfaces and edge bending features are applied. The tool concept is illustrated in figure 5, where three quarter of the tool is presented for illustrative purposes.

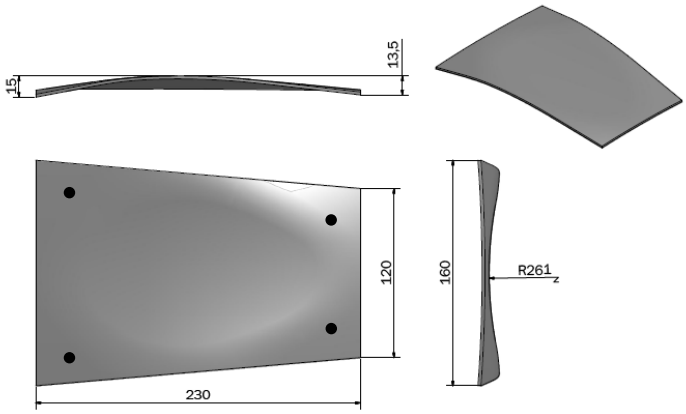


**Figure 4**. Geometry of the double curved Ti-6Al-4Vsheet metal component [mm].

The tool concept is based on heated inner tool parts which are assembled inside and insulated from outer inserts. The different inner tool components i.e. punch, die parts (*1) - (2*), and the binder (blank holder) are heated to the desired forming temperatures using electrical cartridge heaters, inserted in each tool component. Each component can be regulated individually, in the range of room temperature up to 580°C using a feedback control system. The temperature 580°C is the upper limit operating temperature for the tool material, TOOLOX 44, recommended by the supplier. Typical chemical composition and mechanical properties of TOOLOX 44 can be found in e.g. [33]. A substantially higher temperature can however be obtained due to the total power output of the cartridge heaters of 65 kW. The temperature is continuously measured at two points in each elevated temperature tool part using mineral-insulated thermocouples (type K) according to DIN 43 710 and EN 60 584. One thermocouple is used for temperature regulation and the other is measured and logged during the forming test. The insulation material, rigid laminate micanite (white components in figure 5), ensures good insulation which prevent heating of outer inserts and components and facilitate a fairly even distributed tool temperature (within 10°C at 400°C for the measured locations). Boron

nitride was used as a lubricant locally in regions over the punch and draw radius to minimise friction yet accomplish a minor draw-in.

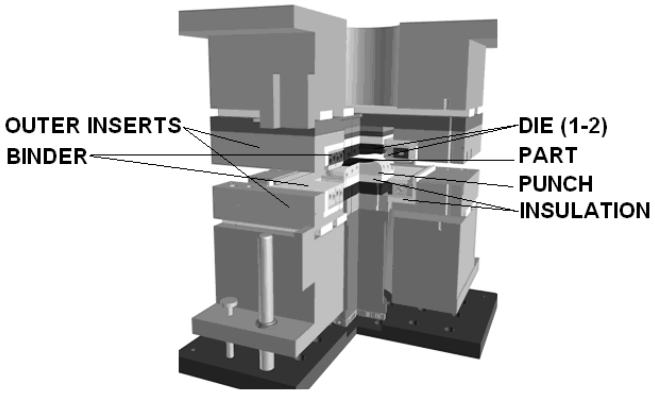


**Figure 5**. CAD-illustration of the hot tool concept for the validation test (VT).

The hot forming procedure can shortly be described by the steps below:

i. Tool heating to desired temperatures.
ii. Furnace heating of the blank to desired temperature.
iii. Transportation of the blank to the forming tool.
iv. Hot forming of Ti-6Al-4V. The die moves towards the blank holder at a speed of 5 mm/s. A blank holder force of 1850 kN is applied.
vi. After forming the die moves upwards releasing the formed blank which are removed and air cooled to room temperature.
vii. Laser cutting is applied to remove redundant material.

In the hot sizing test (HST), a cold blank geometry with size of the prototype geometry including 10 mm addendum material is placed onto the hot punch in the forming tool. The component is crash formed without blank holding at a temperature of 560°C applying a forming force of 1500 kN and a holding time of 15 minutes.

To ensure laser cutting of the prototype component at the correct location, four reference points are produced onto the blank at the end of the forming procedure using fix centre punch geometries mounted in the upper die (1), indicated by the dots in figure 4. A fixture is used for a correct placement during the laser cutting. Laser scanning and best fit CAD evaluation is used as a method to evaluate the shape deviation. Two thermocouples, type K, are used on the edge of the blank to measure the temperature during heating, transportation and forming.

## 4. Yield surface parameter identification

In this section, the studied yield criteria and model calibration are presented. An isotropic yield description is also applied using the Barlat et al. (2003) criterion for comparative purpose.

In this work, the shape of the yield surfaces are determined using a material testing and material identification scheme which minimise the objective function in a least square sense. The experimental reference data at different temperatures ranging from room temperature up to 560°C consist of data from uniaxial tension tests performed in the 00 (along), 45 and 90 (transverse) directions referenced to the rolling direction such as the initial yield stress, hardening, and Lankford coefficients. Further on, the balanced biaxial yield stress, $\sigma_b$, and the

biaxial R-value, $R_{b,}$ are used which are obtained using the experimental biaxial reference point measured during biaxial tension ($\sigma_{11} = \sigma_{22}$) in the viscous bulge test according to

$$REF(\sigma, -\varepsilon_t) = (1136.0, 0.075) \tag{2}$$

where the biaxial R-value was determined to 1.02 according to

$$R_b = \frac{\varepsilon_{22}^p}{\varepsilon_{11}^p} \tag{3}$$

The biaxial yield stress, $\sigma_b$, is determined by calibrating the considered yield surface to obtain the experimental reference point response in equation (2) by applying a biaxial tension to an element using FE analyses.

The uniaxial compressive yield stress is used in the material parameter identification of the Cazacu et al. (2006) yield criterion. The compressive and biaxial data are transformed to 400°C assuming the same behaviour as in room temperature.

*4.1. The Barlat et al. yield criterion*

Barlat et al. (2003) propose an anisotropic yield criterion which is composed of two convex functions formulated as

$$f = \Phi' + \Phi'' - 2\bar{\sigma}_f^m = 0 \tag{4}$$

where

$$\Phi' = \left|X_1' - X_2'\right|^m \tag{5}$$

and

$$\Phi'' = \left|2X_2'' - X_1''\right|^m + \left|2X_1'' + X_2''\right|^m \tag{6}$$

where $X'_{1,2}$ and $X''_{1,2}$ are the principal values of the linearly transformed stress deviator matrices $\{s\}$,

$$\left\{X'\right\} = \left[C'\right]\{s\} \tag{7}$$

$$\left\{X''\right\} = \left[C''\right]\{s\} \tag{8}$$

The exponent *m* is the same parameter as in the Barlat's tri-component criterion, [18], which can be seen as a material parameter of its own. For an *m*-value equal to two, the yield surface reduces to Hill yield surface, i.e. von Mises yield surface in the isotropic case. With increasing value of *m* for the isotropic case, the Barlat et al. yield surface adopts the shape of the Tresca yield surface. The matrices C' and C'' can be expressed in terms of eight anisotropy coefficients $\alpha_i$, which all reduces to unity in the isotropic case, see [20].

To determine the anisotropy coefficient $\alpha_1$ to $\alpha_8$, eight material tests need to be performed. In this work, the initial yield stresses $\sigma_{00}$, $\sigma_{45}$, $\sigma_{90}$, and the Lankford coefficients $R_{00}$, $R_{45}$, $R_{90}$

are determined from uniaxial tension tests. The viscous bulge test is used to determine the biaxial yield stress, $\sigma_b$, and biaxial R-value, $R_b$. The yield stress data and Lankford coefficients used in the calibration are presented in table 2 and the resulting anisotropy coefficients in table 3. The rolling direction of the Ti-6Al-4V blank is used as reference in the calibrations. The resulting yield surfaces at 400°C is shown in figure 6, for different amount of shear stress $\sigma_{12}/\bar{\sigma}$. In figure 7 and 8 the predicted initial yield stress $\sigma_Y$ and R are compared with measured values, assuming an *m*-value 8 for different temperatures and angle directions (α) referenced to the rolling direction (0). The rolling direction is the reference direction, denoted 11.

**Table 2.** Calibration data for Ti-6Al-4V at different temperatures. Initial yield stress, $\sigma_\alpha$, in (MPa).

| | $\sigma_{00}$ | $\sigma_{45}$ | $\sigma_{90}$ | $\sigma_b$ | $R_{00}$ | $R_{45}$ | $R_{90}$ | $R_b$ |
|---|---|---|---|---|---|---|---|---|
| RT | 1000.0 | 972.0 | 1020.0 | 1093.8 | 0.4 | 1.19 | 0.61 | 1.02 |
| 400°C | 681.0 | 591.0 | 691.0 | 744.9 | 0.6 | 1.26 | 0.512 | 1.02 |
| 560°C | 545.0 | 461.0 | 560.0 | 596.1 | 0.65 | 1.325 | 0.63 | 1.02 |

**Table 3.** Barlat et al. parameter values for Ti-6Al-4V at different temperatures.

| | $\alpha_1$ | $\alpha_2$ | $\alpha_3$ | $\alpha_4$ | $\alpha_5$ | $\alpha_6$ | $\alpha_7$ | $\alpha_8$ |
|---|---|---|---|---|---|---|---|---|
| RT | 0.7713 | 1.021 | 0.8272 | 0.9666 | 0.9889 | 0.7464 | 1.024 | 1.151 |
| 400°C | 0.9828 | 0.8534 | 0.7874 | 0.9764 | 0.986 | 0.7878 | 1.132 | 1.426 |
| 560°C | 0.9748 | 0.8883 | 0.8199 | 0.9647 | 0.9756 | 0.7851 | 1.162 | 1.486 |

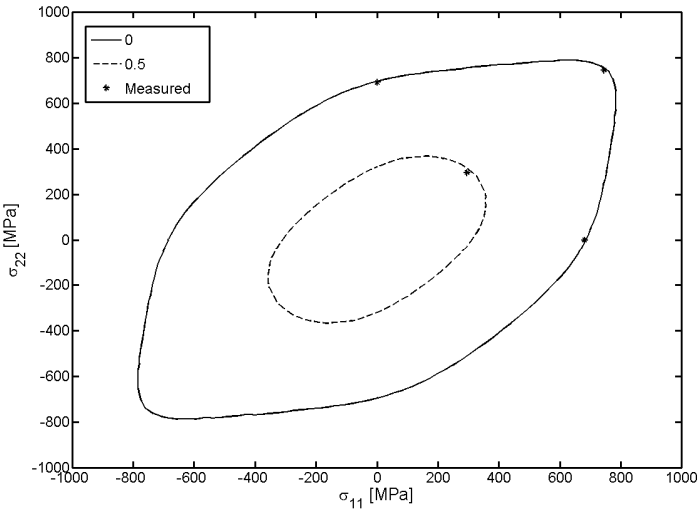


**Figure 6**. Titanium alloy Ti-6Al-4V yield surface at 400°C determined with 8 parameters for equal amounts of shear stress $\sigma_{12}/\bar{\sigma}$. The biaxial yield stress is assumed to follow the room temperature properties.

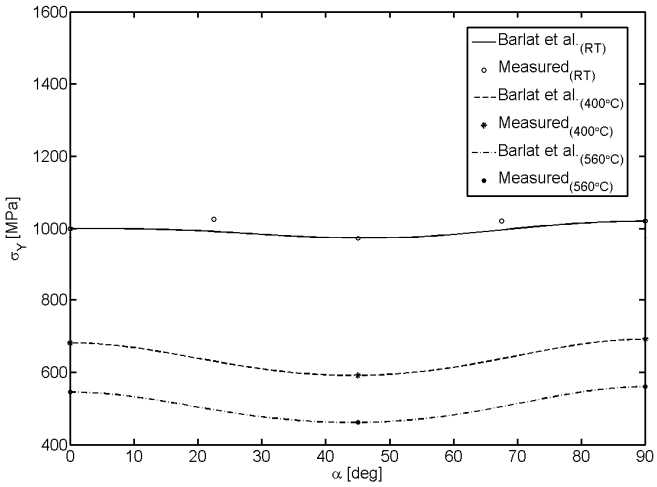


**Figure 7**. $\sigma_Y$ predicted and measured with eight parameters at indicated temperatures.

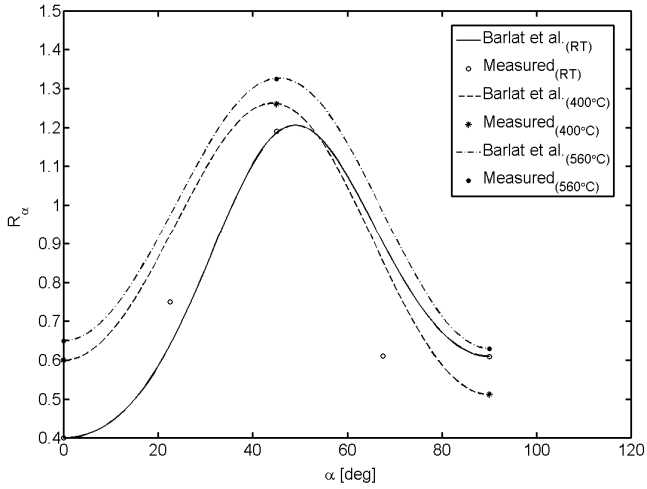


**Figure 8**. $R_\alpha$ predicted and measured with eight parameters at indicated temperatures.

*4.2. The Cazacu et al. yield criterion*

The orthotropic yield criterion proposed by Cazacu et al. (2006), consider both the tension/compression asymmetry and the anisotropic behaviour of hcp metals and alloys. The authors introduced an isotropic yield criterion of the form

$$\left(|S_1| - kS_1\right)^a + \left(|S_2| - kS_2\right)^a + \left(|S_3| - kS_3\right)^a = F \tag{9}$$

where $S_i$, $I = 1,\ldots,3$ are the principal values of the stress deviator. The exponent $a$, is a positive integer and $k$ is a material constant. The ratio of tensile to compressive uniaxial yield stress is given by

$$\frac{\sigma_T}{\sigma_C} = \left\{ \frac{\left(\frac{2}{3}(1+k)\right)^a + 2\left(\frac{1}{3}(1-k)\right)^a}{\left(\frac{2}{3}(1-k)\right)^a + 2\left(\frac{1}{3}(1+k)\right)^a} \right\}^{\frac{1}{a}} \tag{10}$$

or

$$k = \frac{1 - h\left(\frac{\sigma_T}{\sigma_C}\right)}{1 + h\left(\frac{\sigma_T}{\sigma_C}\right)} \tag{11a}$$

with

$$h\left(\frac{\sigma_T}{\sigma_C}\right) = \left[ \frac{2^a - 2\left(\frac{\sigma_T}{\sigma_C}\right)^a}{\left(2\frac{\sigma_T}{\sigma_C}\right)^a - 2} \right]^{\frac{1}{2}} \tag{11b}$$

If $k = 0$ and $a = 2$, the criterion reduces to the von Mises yield criterion. From equation 11b, it follows that for different values of the exponent $a$, $k$ is restricted in order to be real [22]. The isotropic formulation is extended to orthotropy by a linear transformation on the deviatoric stress tensor, S:

$$\Sigma = C[S] \tag{12}$$

where C is a constant 4th-order tensor. Thus, the orthotropic criterion is

$$\left(|\Sigma_1| - k\,\Sigma_1\right)^a + \left(|\Sigma_2| - k\,\Sigma_2\right)^a + \left(|\Sigma_3| - k\,\Sigma_3\right)^a = F \tag{13}$$

For the 3-D stress condition the orthotropic criterion involves 9 independent anisotropy coefficients together with $a$ and $k$. For $k \in [-1,1]$ and any integers $a \geq 1$, the anisotropic yield function is convex in the variables $\Sigma_1$, $\Sigma_2$, $\Sigma_3$ (principal transformed stresses).

The yield stress data in tension, compression and for the balanced biaxial stress state together with Lankford coefficients used in the calibration are presented in table 5. The seven identified anisotropy parameters along with $a$ and $k$, for the plane stress condition, are presented in table 6. The resulting yield surfaces at 400°C are shown in figure 9 and 10, for different values of $a$ and amount of shear stress $\sigma_{12}/\bar{\sigma}$. In figure 11 and 12 the predicted initial yield stress $\sigma_Y$ and R-values are compared with measured values, for different angle directions referenced the rolling direction ($\alpha$).

**Table 5.** Calibration data for Ti-6Al-4V at different temperatures. Initial yield stress, $\sigma_a$, in [MPa]

| | $\sigma_{00}$ | $\sigma_{45}$ | $\sigma_{90}$ | $\sigma_b$ | $\sigma_{C00}$ | $R_{00}$ | $R_{45}$ | $R_{90}$ | $R_b$ |
|---|---|---|---|---|---|---|---|---|---|
| RT | 1000.0 | 972.0 | 1020.0 | 1093.8 | 1106.3 | 0.4 | 1.19 | 0.61 | 1.0 |
| 400°C | 681.0 | 591.0 | 691.0 | 744.9 | 753.4 | 0.6 | 1.26 | 0.512 | 1.0 |

**Table 6.** Cazacu et al. parameter values for Ti-6Al-4V at 400°C.

| | $C_{11}$ | $C_{22}$ | $C_{33}$ | $C_{12}$ | $C_{13}$ | $C_{23}$ | $C_{44}$ | $a$ | $k$ |
|---|---|---|---|---|---|---|---|---|---|
| 400°C | 1.7268 | 1.74 | 1.849 | 0.762 | 0.653 | 0.663 | 1.321 | 2 | -0.255 |
| 400°C | 1.959 | 1.837 | 1.955 | 0.684 | 0.48 | 0.451 | 1.88 | 8 | -0.085 |

The elastic degradation i.e. the decreasing elastic modulus with plastic straining, is accounted for applying values according to table 7 when applying the Cazacu et al. (2006) yield criterion in the FE analyses of the validation test (VT).

**Table 7.** Elastic degradation of Ti-6Al-4V in the (90) direction, determined at different true plastic strain levels in room temperature [31].*Scaled from room temperature data.

| Alloy | Temperature [°C] | Direction | Young's modulus [GPa] at true plastic strain level [%] | | | | |
|---|---|---|---|---|---|---|---|
| | | | 0 | 0.71 | 1.21 | 2.2 | 3.1 |
| 2 | 20 | (90) | 120.8 | 120.7 | 119.3 | 116.7 | 114.2 |
| 2 | 400* | (00) | 98.30 | 98.22 | 97.08 | 94.96 | 92.93 |

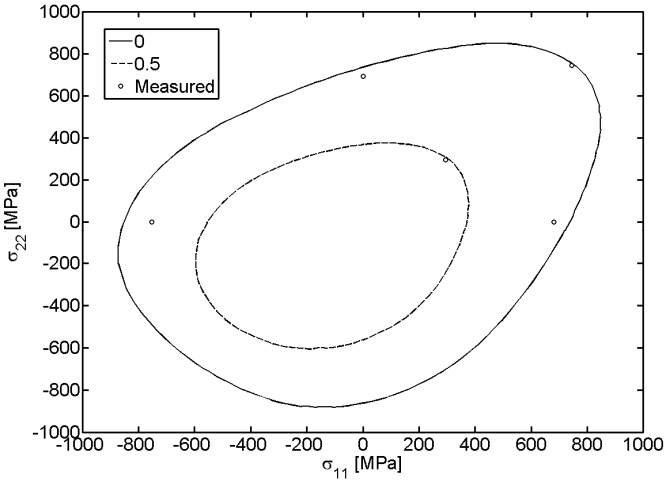


**Figure 9**. Titanium alloy Ti-6Al-4V yield surface at 400°C determined with seven anisotropy parameters together with $k$ and $a = 2$, with the Cazacu et al. criterion, for equal amounts of shear stress $\sigma_{12}/\bar{\sigma}$ .

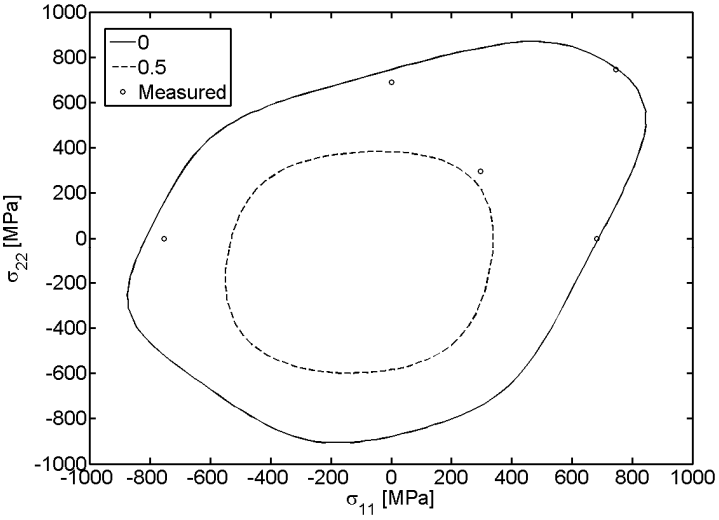


**Figure 10**. Titanium alloy Ti-6Al-4V yield surface at 400°C determined with seven anisotropy parameters together with $k$ and $a$ = 8, with the Cazacu et al. criterion, for equal amounts of shear stress $\sigma_{12}/\bar{\sigma}$ .

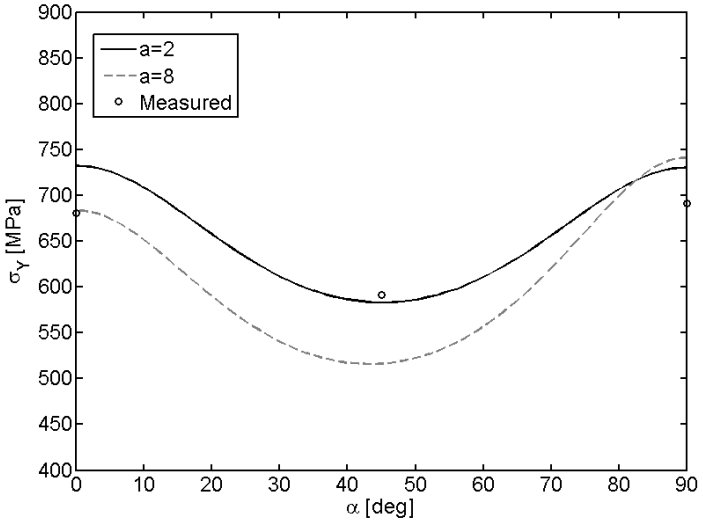


**Figure 11**. $\sigma_Y$ predicted and measured with seven parameters and indicated values of $a$.

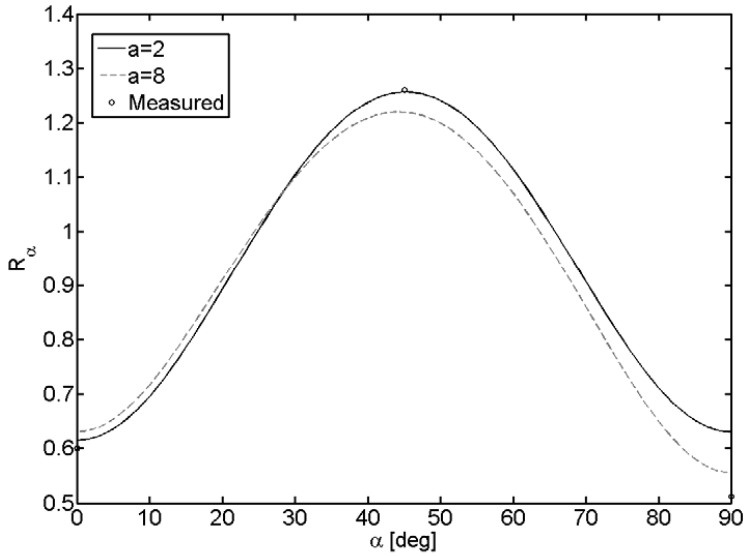


**Figure 12**. $R_\alpha$ predicted and measured at 400°C with seven anisotropy parameters and for different values of *a*.

*4.3. The isotropic assumption*

For the isotropic assumption, the Barlat et al. (2003) yield criterion is applied, using the initial yield stress in the (00)-direction along with R-values equal to 1. The *m*-parameter is chosen to 2 and 8 obtaining the von Mises yield surface and a more Tresca-like yield surface, see figure 13.

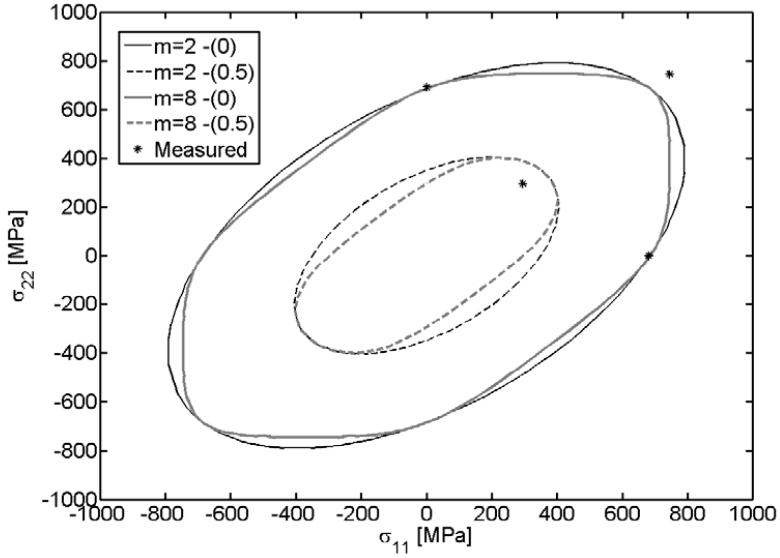


**Figure 13**. Titanium alloy Ti-6Al-4V yield surface at 400°C determined with an isotropic assumption for different values of the parameter *m* and equal amounts of shear stress $\sigma_{12}/\bar{\sigma}$ .

## 5. FE analyses of hot sheet metal forming

In this work, the explicit FE program LS-DYNA v971 [34, 35] is used for solving the equations of motion. Complex geometries in industrial applications with large deformations, nonlinear materials and contacts can be treated effectively and quickly. The material model used for the FE analyses of the hot sheet metal forming of Ti-6AL-4V is a rate independent elastic-plastic model with isotropic hardening. The anisotropic plastic behaviour is described using the presented yield criteria, proposed by Barlat et al. (2003) or Cazacu et al. (2006). The nonlinear hardening is defined as tabulated values of yield stress and effective plastic strain. Isotropic elastic properties are assumed in the analyses of forming, cooling, trim and springback. The general simulation setup consists of a die and binder with physical edge bending features, a blank, and a punch according to figure 14. The tool is designed in such a way that the draw depth is easily adjusted. Fully integrated shell elements with 9 integration points through the thickness are used. An h-adaptive method of mesh refinement is used to locally increase the mesh density where needed. The tool surfaces are modelled as rigid with a prescribed velocity profile and the contact between the tools and the specimen is included and modelled as a contact interface with a friction model assumed to follow Coulomb's friction law. A friction coefficient of 0.25 is applied.

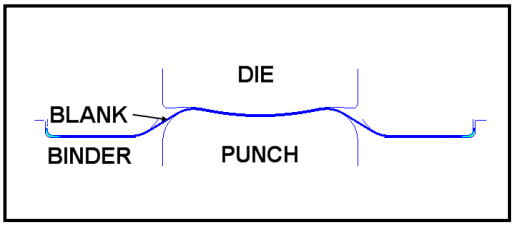


**Figure 14**. FE setup for analyses of hot forming to produce the prototype component (2) at elevated temperatures.

The constrained nodes in the springback analyses were altered to insure that the obtained shape deviation is not affected by the choice of nodal constraints. The definition of shape deviation is illustrated in figure 15.

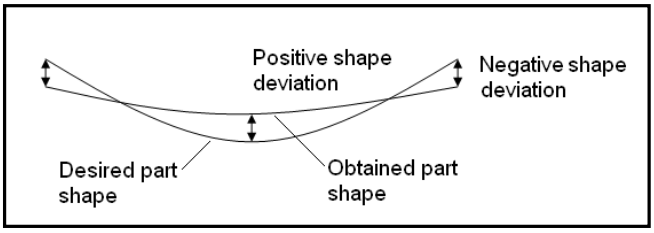


**Figure 15**. Definition of shape deviation.

## 6. Results

The experimental material characterisation revealed the anisotropic properties and asymmetry in yielding between tension and compression of the Ti-6Al-4V blank. To obtain accurate predictions of strain localisation and shape deviation, the use of suitable material descriptions that are able to describe the elastic and inelastic properties is of utmost importance.

Failure in sheet metal forming processes can occur in different ways, such as strain localisation, fracture, wrinkling and shape distortion. The shape of the yield surface in

combination with a correct description of the slope of the hardening curve is of significance for the prediction of strain localisation [36].

The validation test performed at 400°C provide with experimental values of punch force, draw-in and shape deviation. In addition, strain localisation occurred during the forming procedure. In this section, the numerical predictions are compared with experimental measurements and observations.

*6.1. Strain localisation*

The validation test is used to suggest a suitable choice of the *m*- and *a*-parameters for the Barlat et al. (2003) and Cazacu et al. (2006) yield criteria, respectively. Measured values of punch force, draw-in and strain localisation are compared with predicted values in which the identified anisotropy coefficients are applied. The strain localisation which occurred in the hot forming procedure is visible in figure 16, where the blank is photographed after forming and laser cutting.

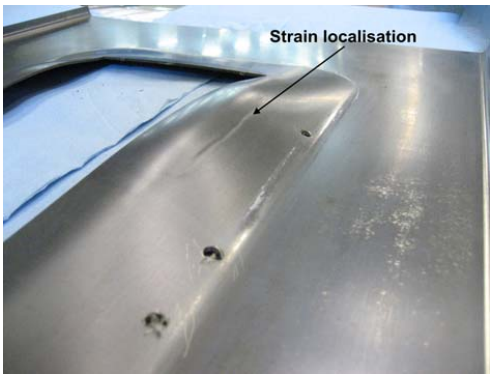


**Figure 16**. Photograph of the strain localisation which occurred in the hot forming procedure of the Ti-6AL-4V sheet metal component.

To evaluate the ability of the studied yield criteria to predict the hot forming procedure, FE analyses are performed. The different yield criteria are applied, in which the identical FE model is used. Predicted and measured values of draw-in, the occurrence of strain localisation or fracture, punch force and springback are compared. See table 8 to 9 and figure 20, for the Barlat, Cazacu and the isotropic assumption in which different *m* and *a* parameter values are applied. The shape deviation is presented in the next section.

**Table 8.** Predicted and measured occurrence of strain localisation. The applied yield criteria with different values of the *m*- and *a*-parameters, assuming a friction coefficient of 0.25.

| Yield criterion | Parameter | Occurrence of strain localisation | Occurrence of fracture |
|---|---|---|---|
| Barlat et al. | $m = 2$ | (x) | |
| Barlat et al. | $m = 8$ | | |
| Cazacu et al. | $a = 2$ | x | |
| Cazacu et al. | $a = 8$ | | |
| Isotropic ass. | $m = 2$ | x | x |
| Isotropic ass. | $m = 8$ | | x |

**Table 9.** Predicted and measured draw-in [mm]. The applied yield criteria with different values of the *m*- and *a*-parameters, assuming a friction coefficient of 0.25.

| Yield criterion | Parameter | Predicted draw-in | Measured draw-in |
|---|---|---|---|
| Barlat et al. | $m = 2$ | 1.61 | 2.0 |
| Barlat et al. | $m = 8$ | 1.63 | 2.0 |
| Cazacu et al. | $a = 2$ | 1.97 | 2.0 |
| Cazacu et al. | $a = 8$ | 2.39 | 2.0 |

To determine if strain localisation occurs, the FLC plot is evaluated. The elevated temperature forming limit diagram is considered with a safety factor of 40% [37]. It is obvious if strain localisation occurs since the strain path changes to plane strain upon localisation. This is also observed in the validation test, in which a considerable material thinning has occurred in the localised region. See figure 18 for an example. It was found that the Barlat et al. (2003) yield criterion do not fully capture the strain localisation observed in the validation test. For an m-value of 2, an initial localisation may be observed. The magnitude of the strain values does not enter the safety region, illustrated as the yellow are within the FLC plot in figure 18. The predicted draw-in is smaller than the measured, see table 9. A smaller draw-in imply an increased straining of the blank compared to a larger draw-in. Thus, a smaller draw-in promotes strain localisation to occur.

Applying the Cazacu et al (2006) yield criterion with a low *a*-value ($a = 2$), a close prediction of the occurrence and location of the observed strain localisation is predicted. See figure 18. A high value of the *a*-parameter does not result in any strain localisation. The predicted draw-in applying a value of the *a*-parameter equal to 2, gives the closest match to the measured value cf. table 9.

When the isotropic assumption is applied, strain localisation leads to failure. This was not experimentally observed. As expected, the strain localisation occurs earlier with a high value of the *m*-parameter compared to a low value in the isotropic case, see figure 19. The measured and predicted punch forces are presented in figure 20.

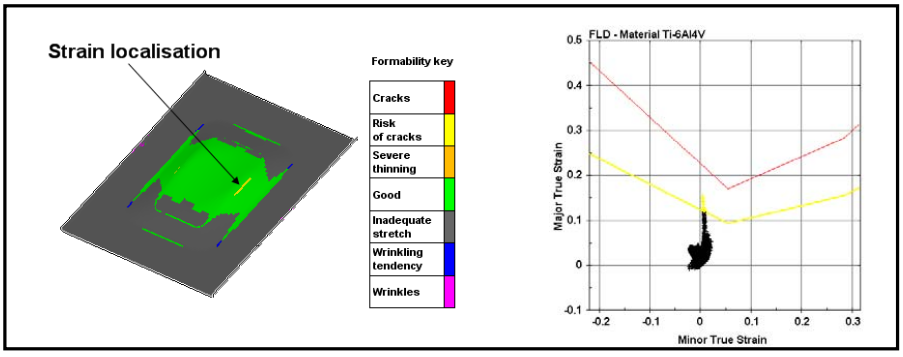


**Figure 18**. Formability and FLC plot for the forming test performed isothermally at 400°C, with the Cazacu et al. yield criterion assuming a value of *a* equal to 2.

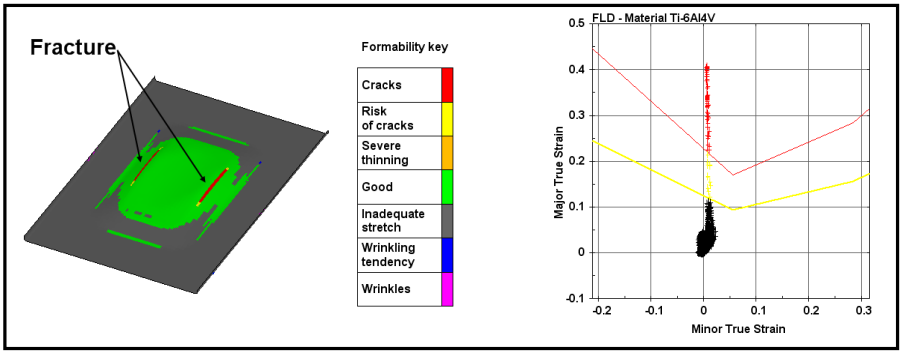


**Figure 19**. FLC plot for the forming test performed isothermally at 400°C, with an isotropic yield surface assumption and an m-value of 8.

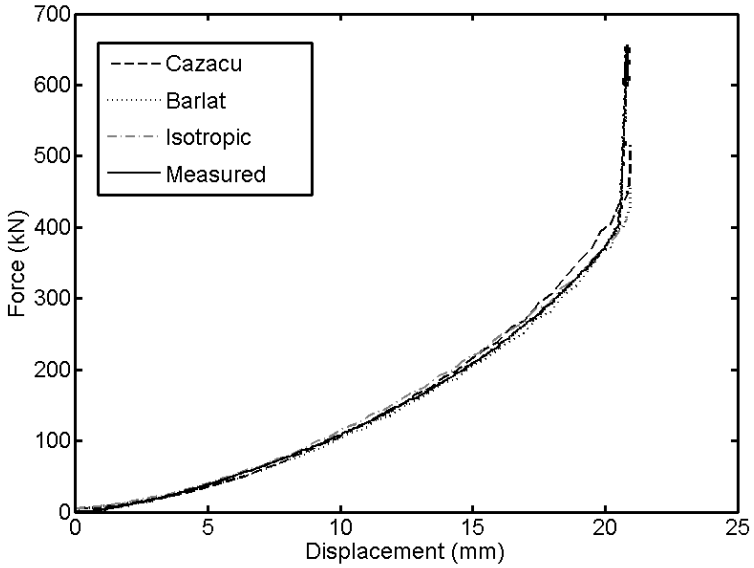


**Figure 20**. Measured and predicted punch force for the studied yield criteria, *m* and *a* equal to 2.

*6.2. Springback*

The measured shape deviations of the validation test (VT) and the hot sizing test (HST) are presented in figure 21, respectively. The measured maximum shape deviation is determined to (-0.626/+0.2) mm, excluding the corner at the upper left hand side of +0.75 mm for the validation test and to (-1.85/+1.74) mm for the hot sizing test. It is obvious that relaxation occur with time during the elastic deformation at 560°C. However, the hot sizing procedure cause a quite large shape deviation compared to the nominal part geometry presented in figure 4. Further on, the forming procedure is time consuming due to the holding time of 15 minutes. The shape deviation and necessary holding times ought to be reduced with increasing temperature.

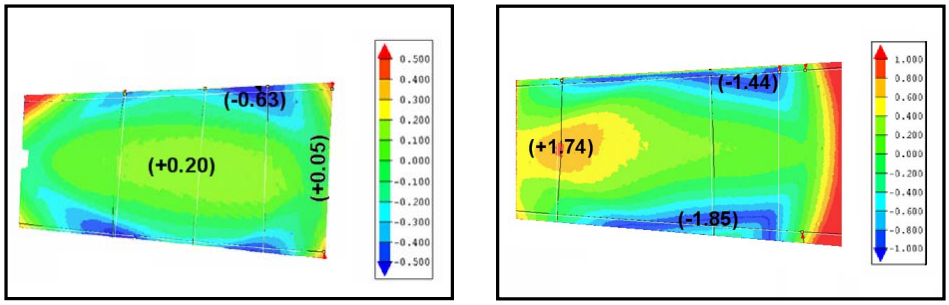


**Figure 21**. Measured shape deviation of the prototype component formed at 400°C (VT) and crash formed at 560°C including a holding time of 15 minutes (HST), respectively.

The corresponding predicted shape deviations for the validation test (VT), depending on the used yield criterion and values of the *m*- or *a*- parameters, are presented in table 10. The effect of the cooling procedure, in which the development of thermal straining is included in the FE analysis, is of importance for the magnitude of the shape deviation. The predicted shape deviations are comparative to the measured values, considering the Barlat et al. (2003) yield criterion, with the exception of the measured deviating corner on the upper left hand side, cf. figure 21 and 22. The predicted shape deviation is in close match with the measured values, using the Cazacu et al. (2006) yield criterion, see figure 23. Note that the shape deviation distribution correlates well with the measured, again with the exception of the upper left hand corner.

**Table 10.** Predicted and measured shape deviation [mm] of the prototype component, neglecting or including the effect of the cooling procedure. The applied yield criteria with different values of the *m*- and *a*-parameters.

| Yield criterion | Parameter | Predicted shape deviation | Predicted shape deviation including the cooling procedure | Measured shape deviation |
|---|---|---|---|---|
| Barlat et al. | $m = 2$ | +0.15/-0.55/-0.13 | +0.30/-0.54/-0.05 | +0.20/-0.63/+0.05 |
| Barlat et al. | $m = 8$ | +0.07/-0.53/+0.15 | +0.16/-0.52/+0.24 | +0.20/-0.63/+0.05 |
| Cazacu et al. | $a = 2$ | +0.09/-0.63/-0.18 | +0.17/-0.62/-0.10 | +0.20/-0.63/+0.05 |
| Cazacu et al. | $a = 8$ | +0.20/-0.63/+0.00 | +0.26/-0.60/-0.19 | +0.20/-0.63/+0.05 |

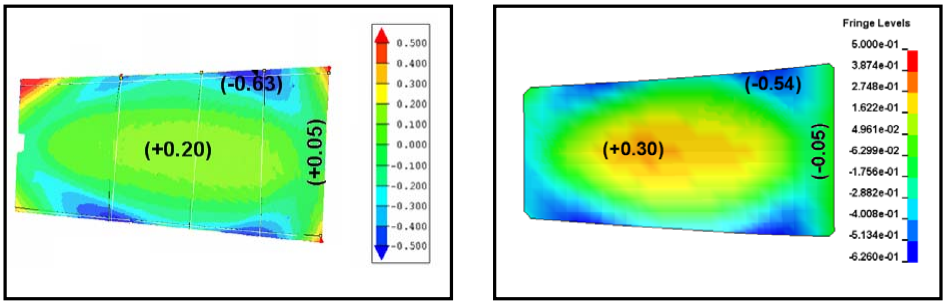


**Figure 22**. Measured and predicted shape deviation, respectively, using the Barlat et al. (2003) yield criterion ($a$=2).

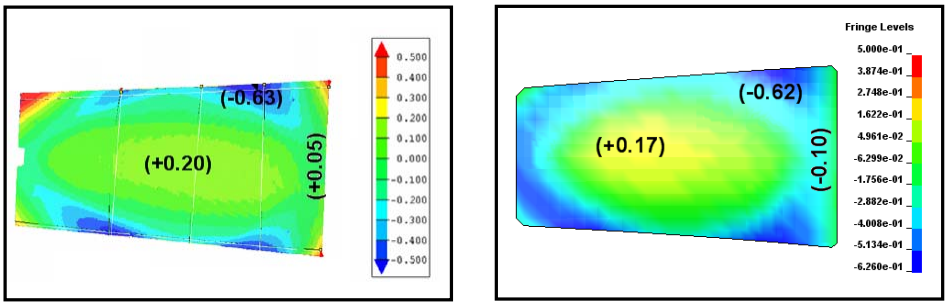


**Figure 23**. Measured and predicted shape deviation, respectively, using the Cazacu et al. (2006) yield criterion ($a$=2).

Based on the accurate prediction of draw-in, strain localisation, punch force and shape deviation for the Cazacu et al. (2006) yield criterion assuming an $a$-value equal to 2, a low value of the parameter is preferable to a higher $a$ value. Hence, a value of the $a$-parameter equal to 2 is assumed to be a suitable value for Ti-6AL-4V under the present forming conditions.

## 7. Discussion and conclusions

In the present work, a tool concept for hot sheet metal forming of a double-curved Ti-6Al-4V component is suggested. The predicted responses of punch force, draw-in, strain localisation and shape deviation show promising agreement with experimental values when formed at 400°C and applying an anisotropic yield criterion.

Draw-in, strain localisation and shape deviation are predicted accurately when applying the yield criterion proposed by Cazacu et al. (2006). Seven anisotropy coefficients along with $k$ and the $a$-parameter equal to 2 are used to determine the shape of the yield surface.

The shape deviation is predicted quite well when applying the yield criterion proposed by Barlat et al. (2003). Eight anisotropy coefficients assuming an $m$-value equal to 2 or 8 are used to determine the shape of the yield surface. The prediction of strain localisation is however not satisfactory and the draw-in is smaller than the measured. For both yield criteria the effect of the cooling procedure was found to be of significance to the prediction of shape deviation.

Considering an isotropic assumption, the shape of the yield surface is not able to coincide with the experimental values, as expected. Strain localisation causing fracture is predicted but was not observed during the validation test.

The predicted punch forces are in close agreement with the measured. A slight deviation can be observed between the different yield criteria.

The present work is limited to studies of different yield criteria based on the assumption of isotropic hardening and isotropic elastic properties. Further, the FE model does not include the influence of strain rate and stress relaxation or models for phase changes. Based on the observations, an interesting extension to the present work would be to optimise hot sheet metal forming procedures such as for the studied components by extending an anisotropic yield criterion to function in coupled thermo-mechanical FE analyses. This, in order to study the temperature as an important process parameter. The Cazacu et al. (2006) yield criterion is considered to be a suitable choice. The von Mises isotropic yield criterion is commonly applied in thermo-mechanical coupled analyses of sheet metal forming, an assumption that may provide inaccurate predictions of strain localisation and springback [31]. In addition, constitutive equations accounting for the strain rate is of importance. Considering hot forming

in the higher temperature region, models for phase transformation and creep/stress relaxation are necessary for numerical predictions with high accuracy.

**References**


[1] Materials Properties Handbook: Titanium alloys, ASM International, 1994, 483-636.
[2] Lütjering, G., Williams, J. C., Titanium, Springer-Verlag Berlin Heidelberg, 2003.
[3] Semiatin, S.L., Seetharaman, V., Weiss, I., Materials Science & Engineering A, A243 (1998) 1-24.
[4] Ding, R., Guo, Z.X., Wilson, A., Materials Science and Engineering A, 327 (2002) 233-245.
[5] Follansbee, P.S., Grey III, G.T., An analysis of the low temperature, low and high strain.rate deformation of Ti-6Al-4V. Metall. Trans. A 20A (5), (1989), 863-874.
[6] Nemat-Nasser, S., Guo, W.-G., Nesterenko, V.F., Indrakanti, S.S., Gu, Y.-B., Dynamic response of conventional and hot isostatically pressed Ti-6Al-4V alloys: Experiments and modeling, Mechanics of Materials, v 33, n 8, August, 2001, p 425-439, ISSN: 0167-6636.
[7] Picu, R.C., Majorell, A., Mechanical behaviour of Ti-6Al-4V at high and moderate temperatures – Part II: constitutive modelling. Mater. Sci. Eng. A326, (2002), 306-316.
[8] Lee, W.S., Lin, M.T., The effects of strain rate and temperature on the compressivedeformation behavior of Ti-6Al-4V alloy. J. Mater. Proc. Tech. v71, (1997), 235-246.
[9] Khan, A.S., Suh, Y.S., Kazmi, R., Quasi-static and dynamic loading responses and constitutive modeling of titanium alloys, Int. J. Plast., V20, (2004), 2233-2248.
[10] Khan, A. S., Kazmi, R., Farrokh, B., Multiaxial and non-proportional loading responses, anisotropy and modelling of Ti-6Al-4V titanium alloy over a wide ranges of strain rates and temperatures, Int. J. Plast., V23, (2007), 931-950.
[11] Ding, R., Guo, Z.X., Qian, M., Computation Materials Science, 40 (2007) 201-212.
[12] Wagoner, A.J., Bull, C.W., Kumar, K.S, Briant, C.L., Metallurgical and Materials Transactions A, v 34, n 2 (2003) 295-306.
[13] Lee. W.-S., Lin. M.-T., Journal of Materials Processing Technology, v 71, n 2 (1997) 235-246.
[14] Semiatin, S.L., Bieler, T.R., Metallurgical and Materials Transactions A, v 32, n 7 (2001) 1787-1799.
[15] Hill, R., The Mathematical Theory of Plasticity, Clarendon Press, Oxford. (1950).
[16] Jansson, M., Nilsson, L., Simonsson, K., On constitutive modelling of aluminium alloys for tube hydroforming applications, Int. J. Placticity, v21, 2005, 1041-1058
[17] Lademo, O. G-., Hopperstad, O.S., Langset, M., An evaluation of yield criteria and flow rules for aluminium alloys, Int. J. Plasticity, v15, (1999), 191-208.
[18] Barlat, F., Lian, J., Plasticity behaviour and strechability of sheet metals Part I: a yield function for orthotropic sheets under plane stress condition. Int. J. Plasticity, v 5, (1989), 51-66.
[19] Hosford, W., On the yield loci of anisotropic cubic metals. 7th North American Metalworking Conf. SME, Dearborn, MI, (1979), 191-197.
[20] Barlat, F., Brem, J.C., Yoon, J. Chung, W., K., Dick, R.E., Lege, D.J., Pourboghrat, F., Choi, S.-H., E. Shu. Plane stress yield function for aluminium alloy sheet – Part1: Theory. Int. J. Plasticity. v 19, (2003), 1297-1319.
[21] Barlat, F., Aretz, J.C. H., Yoon, W., Karabin, K., Breem, M.E., Dick, R.E., Linear transformation-based anisotropic yield functions, Int. J. Plasticity. v 21, (2005), 1009-1039.

[22] Cazacu, O., Barlat, F., Orthotropic yield criterion for hexagonal closed packed metals. Int. J. Plasticity. v 22, (2006), 1171-1194.
[23] Hamilton, C.H., Superplacticity and superplastic forming, Warrendale: TMS-AIME, 1989.
[24] Materials Properties Handbook: Titanium alloys, ASM International, 1994, 483-636.
[25] Kong, T.F., Chan, L.C., Lee, T.C, Numerical and experimental investigation of preform design in non-axisymmetrical warm forming, Int. J. Adv. Manuf. Technol, v 37, (2008), 908-919.
[26] Lai, C.P, , Chan, L.C., Chow, C.L., Effects of tooling temperature on formability of titanium TWBs at elevated temperatures, J. Materials Processing Technology, v 191, (2007), 157-160.
[27] Lai, C.P, , Chan, L.C., Chow, C.L., Warm forming simulation of titanium tailor-welded blanks with experimental verification, CP908, NIMIFORM ´07, Materials Processing and Design, Simulation and Applications, (2007), 1621-1626
[28] Chen, F.-K., Chiu, K.-H., Stamping formability of pure titanium sheets, J. Mat. Proc. Tech, v 170, (2005), 181-186.
[29] Satoh, J., Gotoh, M., Maeda, Y, Stretch-drawing of titanium sheets, Journal of Materials Processing Technology, v 139, n 1-3 SPEC, Aug 20, 2003, p 201-207, ISSN: 0924-0136
[30] Shipton, M.H., Roberts, W.T., Hot deep drawing of titanium sheet, Materials Science and Technology, v 7, n 6, Jun, 1991, p 537-540, ISSN: 0267-0836
[31] Odenberger, E.-L., Concepts for hot sheet metal forming of titanium alloys, Doctoral thesis, Luleå University of Technology, Sweden, 2009.
[32] Odenberger, E.-L., Jansson. M., Thilderkvist, P., Gustavsson, H., Oldenburg, M., A short lead time methodology for design, compensation and manufacturing of deep drawing tools for Inconel 718, IDDRG 2008 Conference, Best in Class Stamping, pp 697-708.
[33] Hansson, P., ”TOOLOX – The Multi-purpose Pre-hardened Tool Steels”, 2nd International Conference on Accuracy in Forming Technology ICAFT (2006) 183-200.
[34] Hallquist, J.O., ”LS-DYNA Theory Manual” Livermore Software Technology Corporation, Livermore (2006).
[35] LS-DYNA Keyword User´s Manual, Volume 1, v971, Livermore Software Technology Corporation, Livermore (2007).
[36] Friedman, P.A., Pan, J., Effects of plastic anisotropy and yield criteria on prediction of forming limits, Int. J. Mechanical Science, Vol. 42, 2000, pp. 29-48.
[37] Sigvant, M., Mattiasson, K., Larsson, M., The definition of incipient necking and its impact on experimentally or theoretically determined forming limit curves, IDDRG 2008 Conference, Olofström, Sweden, pp. 207-218.